VNIVERSITAT ID VALÈNCIA

PhD program in Biomedicine and Biotechnology

INTERNATIONAL PhD THESIS

Rescue of ovarian function:
stem cells and regenerative factors

Author:

Maria Marchante Cuevas

Bachelor's Degree in Biotechnology

Master's Degree in the Biotechnology of Assisted Human Reproduction

Supervised by:

Prof. Antonio Pellicer

Dr. Sonia Herraiz

Valencia, December 2022

El **Prof. Antonio Pellicer Martínez**, Catedrático en Ginecología, Doctor en Medicina y Cirugía, Profesor titular del Departamento de Pediatría, Obstetricia y Ginecología de la Facultad de Medicina de la Universidad de Valencia, fundador del Instituto Valenciano de Infertilidad y presidente de la Fundación IVI.

CERTIFICA:

Que el trabajo de investigación titulado: "**Rescue of ovarian function: stem cells and regenerative factors**" ha sido realizado íntegramente por Maria Marchante Cuevas bajo mi dirección. Dicha memoria está concluida y reúne todos los requisitos para su presentación y defensa como TESIS DOCTORAL ante un tribunal.

Y para que así conste a los efectos oportunos, firmo la presente certificación en Valencia a 12 de diciembre de 2022.

Fdo. Dr. Antonio Pellicer Martínez

VNIVERSITAT
ⒺE VALÈNCIA

La **Dra. Sonia Herraiz Raya**, Doctora en Biología, Investigadora principal del área de Rejuvenecimiento ovárico y Preservación de la fertilidad en Fundación IVI (FIVI) y miembro del grupo de Investigación en Medicina Reproductiva del Instituto de Investigación Sanitaria (IIS) La Fe.

CERTIFICA:

Que el trabajo de investigación titulado: "**Rescue of ovarian function: stem cells and regenerative factors**" ha sido realizado íntegramente por Maria Marchante Cuevas bajo mi dirección. Dicha memoria está concluida y reúne todos los requisitos para su presentación y defensa como TESIS DOCTORAL ante un tribunal.

Y para que así conste a los efectos oportunos, firmo la presente certificación en Valencia a 12 de diciembre de 2022.

Fdo. Dr. Sonia Herraiz Raya

ACKNOWLEDGEMENTS

Cuando la gratitud es tan absoluta, las palabras se quedan cortas.

Gracias a mis directores por la oportunidad que me dieron de trabajar y aprender junto a ellos, por formarme y guiarme durante esta etapa.

Porque si hoy estoy aquí es gracias a vosotros.

Gracias Sonia y Profesor Pellicer.

Gracias a los IPs, a todos mis compañeros y amigos de Fundación IVI y de la Universidad de Valencia, por su ayuda, por su generosidad, por escucharme, por animarme, por hacerme reír, por los viajes y congresos, por los viernes de despacho.

Porque sois lo mejor que me llevo de esta etapa.

Gracias a TODOS.

Gracias a mi madre, por darme la vida y todo lo que tengo, por su amor infinito, por su apoyo incondicional, por su valentía, por su fuerza y coraje.

Porque eres mi referente. Ojalá algún día llegue a ser como tú.

Gracias Mamá.

Gracias a mi hermana, por no soltarme nunca de la mano, por sus ganas de sumar siempre, por ayudarme a ser mejor persona.

Porque eres mi mitad y lo mejor que tengo en el mundo.

Gracias Lourdes.

Gracias a mis ángeles, por guiarme y acompañarme desde el cielo.

Porque sois mi luz y mi esperanza.

Gracias Papá y abuelos, Félix, Justa y Alfonso.

Gracias a toda mi familia, por lo valores que he recibido de ellos, por enseñarme el significado del esfuerzo, trabajo y sacrificio, pero también del amor, de la gratitud, de la honestidad, y de lo verdaderamente importante.

Porque sois mi mayor Tesoro.

Gracias primas, primos, tías, tíos y abuela María.

Gracias a mi amor, por acompañarme en cada paso que doy, por aceptarme y quererme tal y como soy, por llenar mis días de alegría, por ayudarme a ver el lado bueno y positivo de las cosas.

Porque eres mi gran suerte.

Gracias Marc.

Gracias a todos mis amigos, a los de siempre, a los del pueblo, a los de la ciudad, a las biotecH, a las flamencas, a todos los que están a mi lado, por entenderme, por respetarme, por ayudarme a desconectar, por hacerme disfrutar de la vida.

Porque sois fundamentales para mí.

Gracias a TODOS.

Y, por último, gracias a ti también, por el trabajo duro, por el esfuerzo, por no rendirte, por hacer todo lo posible, por hacer el bien, por ser siempre tú misma.

Gracias, María.

La memoria del corazón es el agradecimiento, y a todos y cada uno de vosotros os llevaré siempre conmigo.

¡OS QUIERO!

The top of one mountain is the bottom of the next

so, keep climbing.

CONTENTS

LIST OF FIGURES

INTRODUCTION

MATERIALS AND METHODS

LIST OF TABLES

INTRODUCTION

MATERIALS AND METHODS

RESULTS

ABBREVIATIONS

4-HNE   4-hydroxy-2-nonenal

ACN   Acetonitrile

AFC   Antral follicle count

AKT   Protein kinase B

AMA   Advanced maternal age

AMH   AntiMüllerian hormone

ASCOT   Autologous stem cell ovarian transplant

ATM   Ataxia telangiectasia mutated

ATP   Adenosine triphosphate

BAX   Bcl2 associated with X activity

Bcl2   B-cell lymphoma 2

BMDSCs   Bone marrow-derived stem cells

BPs   Biological processes

BRCA1   Breast cancer susceptibility gene 1

BRCA2   Breast cancer susceptibility gene 2

BSA   Bovine serum albumin

Bu   Busulfan

CaCl$_2$ Calcium choride

CCs   Cellular components

ChT   Chemotherapy

COS   Gonadotropin-controlled ovarian stimulation

Cy   Cyclophosphamide

DAPI   4´,6-diamidino-2-fenilindol

DEPs   Differential protein expression

DMSO   Dimethyl sulfoxide

DNA	Deoxyribonucleic acid
DOR	Diminished ovarian reserve
DSBs	Double-strand breaks
EGF	Epidermal growth factor
FA	Formic acid
FC	Fold change
FGF	Fibroblast growth factor
FGF-2	Fibroblast growth factor-2
FOXO3a	Forkhead box O3
FSH	Follicle stimulating hormone
GCs	Granulosa cells
G-CSF	Granulocyte-colony stimulating factor
GDF-9	Growt/differentiation factor 9
GnRH	Gonadotropin-releasing hormone
GO	Gene Ontology
H&E	Hematoxylin-eosin
H2AX	Histone protein family member X
hCG	Human chorionic gonadotropin
HGF	Hepatocyte growth factor
HR	Homologous recombination
HRP	Horseradish peroxidase
HSCs	Hematopoietic stem cells
IB4	Isolectin B4
IGF	Insulin-like growth factor
IL-6	Interleukin

LH	Luteinizing hormone
MFs	Molecular functions
MII	Metaphase II
MSCs	Mesenchymal stem cells
mtDNA	mitochondrial DNA
MVD	Microvessel density
nDNA	nuclear DNA
PB	Peripheral blood
PBS	Phosphate Buffered Saline
PDGF	Platelet-derived growth factor
PDK1	Phosphoinositol-dependent kinase-1
PFA	Paraformaldehyde
PI3K	Phosphatidylinositol 3OH-Kinase
PMSG	Pregnant mare serum gonadotropin
POI	Premature ovarian insufficiency
POR	Poor ovarian response
PRP	Platelet-rich plasma
PTEN	Phosphatase and tensin homolog
RT-qPCR	Real-time quantitative polymerase chain reaction
RT	Room temperature
RIPA	Radioimmunoprecipitation assay
RNA	Ribonucleic acid
ROS	Reactive oxygen species
RPA	Replication protein A
SCs	Stem cells

SDF-1	Stromal-derived factor-1
TBST	Tris-buffered saline
TFA	Trifluoroacetic acid
TGF	Transforming growth factor-beta
THSP-1	Thrombospondin-1
TUNEL	Transferase-mediated dUTP nick-end labeling
UCB	Umbilical cord blood
VEGF	Vascular endothelial growth factor
α-SMA	Alpha-smooth muscle actin

SPANISH SUMMARY

1. INTRODUCCIÓN

1.1 El ovario

El ovario es un órgano altamente organizado formado por células germinales (ovocitos) y células somáticas (células de la granulosa (CG), estroma y células de la teca). Entre las funciones principales del ovario se encuentran la oogénesis y la secreción de hormonas esteroideas necesarias para mantener la fertilidad femenina y la homeostasis endocrina.

Las interacciones entre las células germinales y somáticas establecen la formación de la unidad funcional del ovario, denominada folículo ovárico, que contiene el ovocito. Los ovocitos se forman a partir de células germinales primordiales durante el desarrollo fetal, y tras un proceso de mitosis para aumentar su número, comienzan la meiosis, deteniéndose en la misma. Una vez formado, este conjunto de folículos quiescentes constituye la reserva ovárica, que es limitada y no renovable.

Los folículos en la primera fase de desarrollo se denominan folículos primordiales y están rodeados por varias células somáticas aplanadas, denominadas células preganulosa. Los folículos primordiales pueden tener uno de estos cuatro destinos: permanecer inactivos en la fase quiescente; activarse, pero luego sufrir atresia; activarse, desarrollarse, madurar y finalmente ovular; o morir directamente desde el estado quiescente.

Foliculogénesis

El desarrollo de los folículos ováricos desde el estadio primordial hasta su etapa final, la ovulación, se conoce como foliculogénesis. A medida que el proceso continúa, en el ovario pueden coexistir diferentes tipos de folículos: primordiales, primarios, secundarios, preantrales, antrales y preovulatorios. Tras diferentes procesos en los que intervienen tanto señales externas como reguladores paracrinos y autocrinos intrafoliculares, un folículo preovulatorio dominante ovula y libera un ovocito maduro para su fecundación. A continuación, el folículo residual sufre una luteinización y se convierte en un cuerpo lúteo, responsable de la secreción de progesterona y de la preparación del endometrio para la implantación en caso de fecundación.

El desarrollo folicular puede clasificarse, en función de la necesidad de gonadotropinas, como desarrollo folicular independiente de gonadotropinas o dependiente de gonadotropinas. En el primero de ellos, se produce la transición de folículo primordial a primario y posteriormente a secundario. La comunicación paracrina entre el ovocito y las células somáticas controla el reclutamiento del folículo primordial. Esta comunicación está mediada por factores de crecimiento secretados, y el ovocito controla las vías de señalización, incluyendo rutas como la fosfatidil inositol 3-OH-quinasa (PI3K)-AKT-FOXO3a.

Los acontecimientos significativos durante la etapa del folículo primario incluyen la expresión de los receptores hormonales como la hormona folículo estimulante (FSH) y el crecimiento y la diferenciación del ovocito. En este periodo, el ovocito aumenta su diámetro, desarrolla la zona pelúcida y aumenta el número de capas de células de la granulosa que los rodean, así como de células de la teca, importantes para la producción de hormonas esteroideas.

Durante la fase dependiente de gonadotropinas, la hormona liberadora de gonadotropinas (GnRH) es segregada de forma pulsátil por el hipotálamo y estimula la secreción de la hormona estimulante del folículo (FSH) y la hormona luteinizante (LH) por la hipófisis. Estas hormonas actúan en el ovario, regulando el crecimiento y la maduración folicular y desencadenando la ovulación.

1.2. Envejecimiento

Envejecimiento ovárico

El envejecimiento celular se define como un deterioro gradual de la integridad fisiológica, que deteriora la función y aumenta la susceptibilidad a la muerte. En la actualidad, uno de los retos importantes para los investigadores es entender y descifrar el proceso de envejecimiento para prevenir o revertir esta patología fisiológica, dado el aumento de la esperanza de vida en nuestra sociedad. Esto es de máxima prioridad en el caso de las mujeres, que sufren un proceso de envejecimiento acelerado conocido como envejecimiento ovárico.

El sistema reproductor femenino envejece aproximadamente diez años antes que otros sistemas orgánicos que experimentan una reducción funcional relacionada con la edad. El envejecimiento reproductivo se ha convertido en una de las principales preocupaciones en el campo de la fertilidad, ya que actualmente las mujeres siguen retrasando su edad de maternidad debido a los cambios en las circunstancias socioeconómicas.

La fertilidad femenina se correlaciona negativamente con la edad, con notables descensos de la reserva ovárica hasta la menopausia, consecuencia natural del envejecimiento ovárico fisiológico, marcado por la disminución de la cantidad de ovocitos. A medida que aumenta la edad de la mujer, la calidad de sus ovocitos también disminuye. Este descenso es más significativo a partir de los 35 años, cuando se considera que la mujer tiene una edad materna avanzada (AMA), y la capacidad de quedarse embarazada con sus propios ovocitos disminuye.

Mecanismos subyacentes al envejecimiento ovárico

Las aberraciones cromosómicas durante la meiosis femenina, la disfunción mitocondrial, el estrés oxidativo y los daños en el ADN, entre otros, han sido identificados como mecanismos responsables de la disminución de la calidad de los ovocitos relacionada con la edad.

La falta de segregación cromosómica durante la meiosis femenina ha sido descrita como la principal causa de pérdida de embarazos e infertilidad humana. Para evitar la aneuploidía, los mecanismos que garantizan una división meiótica y una segregación cromosómica precisas son esenciales durante el desarrollo de los ovocitos. Sin embargo, se ha demostrado que, con el envejecimiento, se producen alteraciones en la dinámica de separación de cromátidas, tanto por fallos en los microtúbulos, como por cambios en las proteínas relacionadas con los cromosomas (como los cinetocoros y las cohesinas).

En el caso de la función mitocondrial, esta se encuentra directamente relacionada con la calidad ovocitaria. Dado que, en la meiosis, la fecundación y el desarrollo embrionario se consume una gran cantidad de ATP, se sugiere que la disminución de la producción de ATP debida a un deterioro de la función mitocondrial da lugar a una disminución de la calidad de los ovocitos. Además, los errores en la replicación del ADN mitocondrial

(ADNmt) se han correlacionado con el envejecimiento, al generarse mutaciones que afectan a la funcionalidad de estos orgánulos. Del mismo modo, el envejecimiento afecta a el número de copias del ADNmt, que disminuye debido a las especies reactivas de oxígeno (ROS) producidas en la matriz mitocondrial. Estudios recientes han relacionado un menor número de copias de ADNmt con una peor calidad de los ovocitos, y también han empleado el número de copias como marcador de calidad.

Las ROS se generan constantemente en las mitocondrias, pero también son eliminadas por las enzimas antioxidantes manteniendo así el equilibrio redox y la homeostasis. En condiciones fisiológicas normales, las ROS son importantes en diferentes procesos celulares. Sin embargo, debido al envejecimiento el equilibrio redox se pierde al generarse un exceso de ROS o reducirse la capacidad antioxidante. La acumulación de ROS disminuye la calidad ovocitaria, induce la apoptosis y conduce a la atresia folicular. Además, genera daño en el ADN, peroxidación lipídica y degradación de proteínas. De hecho, algunos productos intermediarios de las ROS como el 4-hidroxi-2-nonenal (4-HNE) se han descrito como los responsables del daño oxidativo.

Los daños en el ADN se producen en todas las células y pueden deberse a causas endógenas (ya comentado previamente), pero también al estrés genotóxico exógeno, como el inducido por tratamientos quimioterapéutico o por radiación. Los folículos primordiales, que constituyen la reserva ovárica, están detenidos en meiosis durante mucho tiempo hasta ser activados y son muy susceptibles a la acumulación de daños en el ADN. Las células disponen de mecanismos eficientes para reparar los daños en el ADN y evitar así las aberraciones cromosómicas y las mutaciones. Sin embargo, cada vez hay más pruebas de la asociación entre el daño al ADN, la capacidad de reparación de los ovocitos y la edad materna. En los ovocitos, esto podría conducir a una mala calidad, a la apoptosis y, en última instancia, a la infertilidad.

Alteraciones de la fertilidad femenina

Existen condiciones en las que la función ovárica está alterada o el proceso de envejecimiento ovárico se acelera, independientemente de la edad.

Entre ellas se encuentran la reserva ovárica disminuida (DOR), un proceso fisiológico causado por la reducción del número de folículos. Sin embargo, algunas mujeres pueden

sufrir una DOR patológica cuando su reserva ovárica disminuye antes de lo habitual, y posteriormente se vuelven infértiles de forma prematura. Estas pacientes suelen tener ciclos menstruales regulares pero una baja respuesta a los regímenes de estimulación ovárica y valores de reserva ovárica anormales, denominándose pacientes con baja respuesta ovárica (POR).

Por otro lado, la insuficiencia ovárica prematura (POI) es un defecto ovárico caracterizado por la ausencia de menarquia o por el agotamiento prematuro de los folículos ováricos antes de los 40 años. Las mujeres con POI primaria no tienen desarrollo puberal, mientras que, en la POI secundaria, suele haber una pubertad normal con la consiguiente desaparición de los ciclos menstruales. Entre sus causas se incluyen anomalías cromosómicas, cirugías ováricas, enfermedades autoinmunes, infecciones, trastornos metabólicos y terapias oncológicas.

1.3. Estrategias para mejorar el potencial reproductivo de las pacientes con función ovárica comprometida

Los cambios socioeconómicos que ha experimentado nuestra sociedad en los últimos años han retrasado el momento en que muchas mujeres desean tener hijos. Por ello, la edad de las pacientes es una de las principales causas de infertilidad. Además, también ha aumentado el número de pacientes que presentan una alteración de la función ovárica, como la DOR o POI. Estas pacientes representan un reto clínico porque, aunque existen diversas intervenciones terapéuticas destinadas a aumentar su potencial reproductivo, estas intervenciones tienen una eficacia limitada y poco reproducible.

Técnicas de reproducción asistida basadas en la estimulación ovárica controlada

Estas estrategias incluyen el aumento de las dosis de FSH, la administración de FSH en la fase lútea, el uso de FSH recombinante en lugar de FSH urinaria purificada, la modificación de los protocolos de desensibilización hipofisaria, el pretratamiento con estrógenos o anticonceptivos orales combinados y el pretratamiento con andrógenos. Sin embargo, debido al bajo número de folículos antrales susceptibles de estimulación, estas estrategias no suelen producir buenos resultados.

Por lo tanto, la única alternativa clínica disponible para estas mujeres es la donación de ovocitos/óvulos, que permite a las mujeres lograr la maternidad independientemente de la edad o del estado de los ovocitos. Sin embargo, no es una opción adecuada en todos los casos, ya sea por razones éticas, religiosas, normativas e incluso económicas.

Células madre derivadas de la médula ósea (BMDSC)

Estudios recientes han demostrado que existen folículos residuales en el ovario de pacientes con POI que pueden ser activados mediante tratamientos de activación y fragmentación *in vitro*, dando lugar a ovocitos maduros y al nacimiento de niños sanos. Este enfoque podría ayudar a mejorar el potencial reproductivo de las mujeres sometidas a tratamientos quimioterapéuticos u otras condiciones de baja reserva ovárica, en las que, aun cuando el ovario pierde su función y capacidad de ovular, un pequeño grupo de folículos es susceptible de ser rescatado.

Con el desarrollo de la medicina regenerativa, se está considerando cada vez más el uso de células madre para mejorar el potencial reproductivo de las pacientes con una función ovárica deteriorada. Aunque se han identificado numerosas células madre, una de las más estudiadas para rescatar la fertilidad han sido las células madre derivadas de la médula ósea (BMDSCs). De hecho, se ha sugerido que las BMDSCs pueden ser las responsables de rescatar los folículos primordiales residuales y la fertilidad tras el trasplante de médula ósea en pacientes oncológicos, proponiendo las terapias basadas en BMDSCs como un tratamiento alternativo para estas pacientes.

La terapia celular con BMDSCs presenta ciertas ventajas que hacen que sea de especial interés. En primer lugar, su seguridad ha sido probada mediante estudios en los que se realiza su trasplante o infusión para el tratamiento de diferentes enfermedades. En segundo lugar, su facilidad de obtención en sangre periférica tras la movilización, lo que las convierte en una fuente accesible de células madre autólogas.

Los estudios realizados por nuestro grupo en modelos animales de DOR y POI inducidos por quimioterapia (ChT) confirman los efectos regenerativos de las BMDSC en la restauración de la producción hormonal, la reactivación de la foliculogénesis y la mejora del estado del estroma ovárico. Además, estos efectos positivos también fueron validados en tejido ovárico humano de pacientes POR. Nuestro grupo también

comprobó el potencial terapéutico de dicho tratamiento en un estudio piloto prospectivo en mujeres con POR. El trasplante ovárico autólogo de células madre (ASCOT) mejoró los biomarcadores de la función ovárica y se lograron embarazos y nacimientos vivos en mujeres de mal pronóstico, donde la donación de ovocitos era previamente la única opción clínica.

Recientemente, se ha propuesto que la señalización paracrina, a través de la secreción de citocinas, quimiocinas y factores de crecimiento podría ser el principal mecanismo por el que las células madre adultas ejercen sus efectos regenerativos. Las BMDSC secretan citoquinas y factores esenciales en la angiogénesis, la inflamación, la inmunomodulación, la apoptosis y la proliferación, mejorando así el microambiente para promover la recuperación del tejido dañado. Este mecanismo paracrino podría explicar la correlación observada entre la respuesta ovárica positiva de las pacientes POR tras el ASCOT, y la concentración de FGF-2 y trombospondina-1 (THSP-1) en el plasma de aféresis de las pacientes de ASCOT.

Tratamientos con plasma

En base al mecanismo paracrino comentado anteriormente y de los efectos observados en los estudios con células madre, se ha planteado que la administración de proteínas específicas o de factores plasmáticos segregados por las células madre podría ser una alternativa al uso de las células. De este modo, se ha propuesto la inyección de plasma joven enriquecido con factores de crecimiento, plasma de sangre de cordón umbilical (UCB) o proteínas específicas del plasma en organismos dañados y envejecidos para estimular la regeneración y reparación del tejido nervioso. En el contexto de la medicina reproductiva, se ha evaluado la inyección intraovárica de plasma rico en plaquetas (PRP) como estrategia de reactivación ovárica. El PRP es el componente de la sangre que queda tras la separación de glóbulos rojos y blancos, compuesto por plaquetas sanguíneas, citoquinas, factores de crecimiento y pequeñas moléculas. Numerosos autores han estudiado el efecto del PRP en la mejora de la fertilidad femenina desde diferentes perspectivas. Sin embargo, los protocolos no están estandarizados y pocos se centran en comprender los mecanismos de acción que subyacen a los efectos regenerativos observados.

1.4. Modelos animales de envejecimiento ovárico, y condiciones de DOR y POI.

Se necesitan modelos animales apropiados para comprender el envejecimiento ovárico y encontrar nuevas estrategias para retrasar o revertir las condiciones de DOR y POI. Entre los diferentes modelos empleados, *Mus musculus* es el más utilizado debido a su similitud genética con los humanos y a la similitud en las características reproductivas.

Los modelos de ratón establecidos por deleción génica y ChT se han utilizado para estudiar el envejecimiento y los fenotipos comparables a DOR y POI en humanos. Por un lado, la ingeniería genética permite estudiar los efectos de las alteraciones genéticas en el envejecimiento ovárico, como las anomalías cromosómicas y las mutaciones genéticas. Sin embargo, los modelos knockout han presentado algunas limitaciones, por ejemplo, no imitan los sistemas reproductivos de los seres humanos. Además, estos modelos son caros y complejos de generar, lo que lleva a utilizar los modelos inducidos por ChT. Los fármacos quimioterapéuticos se han empleado tradicionalmente para establecer modelos de daño ovárico, generado desde un daño parcial que reduce la fertilidad hasta la destrucción de la reserva folicular y la atrofia tisular.

Sin embargo, aunque estos modelos permiten estudiar las características derivadas del envejecimiento y los fenotipos de las condiciones DOR y POI, no representan un modelo murino de envejecimiento progresivo y fisiológico. Por lo que es necesario desarrollar y caracterizar un modelo animal apropiado, económico y reproducible, que muestre la mayoría de las características ováricas de las diferentes etapas de la vida reproductiva de la mujer.

2. HIPÓTESIS

Las células madre adultas derivadas de la médula ósea son capaces de recuperar la función ovárica promoviendo el desarrollo folicular y la regeneración del estroma mediante la secreción de factores solubles y citoquinas que actúan de forma paracrina en el ovario dañado. Por lo tanto, el plasma rico en factores secretados por las células madre podría ser una terapia adecuada para mejorar el potencial reproductivo de pacientes con la función ovárica deteriorada.

3. OBJETIVOS

3.1 Objetivo principal

El objetivo principal de esta tesis doctoral es evaluar si la administración de plasma rico en factores secretados por las células madre puede ser una terapia alternativa para mejorar la función ovárica de pacientes con DOR y POI o mujeres con problemas de fertilidad relacionados con la edad.

3.2. Objetivos secundarios

Para alcanzar el objetivo principal, el trabajo se dividió en diferentes fases

A) EFECTO REGENERATIVO DE DIFERENTES FUENTES DE PLASMA RICO EN FACTORES DE CRECIMIENTO EN MODELOS MURINOS DE DAÑO OVÁRICO INDUCIDO POR QUIMIOTERAPIA

1. Evaluar la capacidad de diferentes fuentes de plasma ricas en factores secretados por diferentes tipos de células madre, como las células madre de la médula ósea (BMDSC), y las células madre de la sangre del cordón umbilical (UCB), para promover el desarrollo folicular, la ovulación y la fecundación en los modelos DOR y POI.

2. Analizar el efecto de los plasmas de BMDSC y UCB en la tasa de gestación y el tamaño de la camada.

3. Evaluar los efectos de la inyección de estos plasmas en el nicho ovárico: análisis de la vascularización, proliferación, degeneración y apoptosis.

4. Evaluar si la activación de los plasmas, para liberar el contenido de las plaquetas, mejora los efectos regenerativos.

5. Caracterizar la composición de los diferentes plasmas para entender los mecanismos subyacentes a los tratamientos.

6. Estudiar las vías de reparación del ADN en un modelo *in vitro* de daño ovárico inducido por la quimioterapia.

B) EVALUACIÓN DEL EFECTO DEL PLASMA MÁS BENEFICIOSO EN TEJIDO OVÁRICO HUMANO

1.	Validar los efectos regenerativos del plasma BMDSC activado (aBMDSC) en tejido ovárico humano de pacientes de POR empleando un modelo de xenotransplante, analizando el desarrollo de los folículos y la regeneración del estroma.

2.	 Dilucidar los mecanismos responsables de los efectos regenerativos del plasma aBMDSC en el tejido ovárico humano.

C) DESARROLLO Y VALIDACIÓN DE UN MODELO ANIMAL DE ENVEJECIMIENTO OVÁRICO FISIOLÓGICO.

1.	Caracterizar un modelo murino de envejecimiento reproductivo fisiológico que muestre la mayoría de las características ováricas de las diferentes etapas de la vida reproductiva de la mujer.

2.	Evaluar diferentes variables reproductivas (reserva ovárica y estroma, número de ovocitos y embriones, calidad de los ovocitos MII, desarrollo embrionario *in vitro*, disfunciones mitocondriales y perfil proteómico ovárico) para determinar si el modelo puede utilizarse para probar terapias para mujeres con problemas de fertilidad relacionados con la edad.

D) ADMINISTRACIÓN INTRAOVÁRICA DEL PLASMA MÁS BENEFICIOSO EN UN MODELO MURINO DE ENVEJECIMIENTO FISIOLÓGICO

1.	Evaluar la capacidad del plasma rico en plaquetas activado (aPRP) y la combinación de factores secretados por las BMDSC y contenidos en las plaquetas (aBMDSC) para promover la activación y el desarrollo folicular en un modelo de envejecimiento ovárico fisiológico mediante una única inyección intraovárica.

2.	Analizar el efecto de la inyección intraovárica de aPRP y aBMDSC sobre la tasa de ovulación, la calidad de los ovocitos y el desarrollo embrionario.

3.	Analizar los efectos del plasma en el estroma ovárico mediante el estudio de la proliferación y la vascularización.

4. Estudiar la disfunción mitocondrial, el daño oxidativo y la apoptosis tras la administración intraovárica de plasma.

5. Evaluar si existen cambios a nivel proteómico tras la administración de plasma y estudiar las vías biológicas diferenciales implicadas.

4. MATERIALES Y MÉTODOS

A) EFECTO REGENERATIVO DE DIFERENTES FUENTES DE PLASMA RICO EN FACTORES DE CRECIMIENTO EN MODELOS MURINOS DE DAÑO OVÁRICO INDUCIDO POR QUIMIOTERAPIA

Estudio de la administración sistémica de plasma humano en modelos de daño ovárico inducido por quimioterapia.

Para evaluar los posibles efectos regenerativos de los plasmas en el tejido ovárico murino, empleamos dos modelos animales previamente establecidos de daño ovárico inducido por ChT: DOR y POI.

Las condiciones de DOR y el POI se indujeron en ratones NOD/SCID inmunodeficientes de 8 semanas de edad, mediante inyección de Ciclofosfamida (Cy) y Busulfán (Bu). Se empleó una dosis estándar (12 mg/Kg de Bu - 120 mg/Kg de Cy) o reducida (1,2 mg/Kg de Bu - 12 mg/Kg de Cy), respectivamente. Una semana después, cuando se estableció el daño ovárico, los animales DOR y POI fueron asignados (n = 11 por grupo) en siete grupos experimentales que recibieron inyecciones de: (1) solución salina (ChT); (2) plasma de sangre periférica de mujeres POR (plasma PB); (3) plasma PB activado (plasma aPB); (4) plasma rico en factores secretados por BMDSCs (plasma BMDSC); (5) plasma activado de BMDSC (plasma aBMDSC); (6) plasma rico en factores secretados por células madre del cordón umbilical (plasma UCB); o (7) plasma UCB activado (plasma aUCB). Para proporcionar valores de referencia para las distintas variables del estudio, se utilizaron hembras NOD/SCID sin ningún tipo de tratamiento (n=11, grupo wild-type).

El plasma PB se obtuvo de la sangre periférica de las mujeres POR. El plasma BMDSC se obtuvo de la aféresis de 10 pacientes POR tras movilización de células madre mediante un tratamiento farmacológico de 5 días con el factor estimulante de colonia de

granulocitos (G-CSF). La sangre del cordón umbilical de los recién nacidos se recogió de pacientes sanas que dieron a luz en el Hospital La Fe. Las fracciones de plasma se aislaron mediante una centrifugación a 1600 x g durante 10 minutos a 4ºC y se almacenaron a -80ºC hasta su uso. Las fracciones de plasma activado (aPB, aBMDSC y aUCB) se obtuvieron utilizando CaCl$_2$ 0,1M al 5%, para liberar factores de crecimiento y otras moléculas de señalización encerradas en gránulos-α antes de la inyección.

Los tratamientos se administraron en días alternos durante 2 semanas mediante una inyección en la vena de la cola (100 uL/día). Tras el tratamiento, los ratones se sometieron a una estimulación ovárica controlada (EOC) basada en una inyección de 10 UI de gonadotropina sérica de yegua preñada (PMSG) y 48 horas (h) después, 10 UI de gonadotropina coriónica humana (hCG) antes del cruce con machos. A continuación, se sacrificó a una parte de las hembras (n= 7 / grupo) y se recuperaron los ovarios y oviductos para analizar los efectos a corto plazo, realizándose recuentos foliculares y estudio del número de ovocitos metafase-II (MII) y embriones en estadio de 2-células. También se estudió el estado estroma ovárico, analizando la proliferación celular y la vascularización mediante inmunohistoquímica, y la apoptosis por Western Blot.

Los animales restantes (n = 4 / grupo) se utilizaron para evaluar los efectos a largo plazo sobre el rendimiento reproductivo, realizando cruces sucesivos durante tres meses en los que se registró el número de gestaciones y el tamaño de las camadas por cruce.

En esta misma fase del estudio, se realizó la caracterización proteómica de los diferentes plasmas utilizados para comprender los mecanismos subyacentes, mediante análisis SWATH-MS y estudio de las proteínas diferencialmente expresadas (DEPs).

Estudio *in vitro* para analizar los efectos del plasma en el daño y la reparación del ADN

Teniendo en cuenta el análisis proteómico del plasma, decidimos evaluar el efecto de los tratamientos en la promoción de la reparación del ADN en un modelo de daño ovárico inducido por ChT.

Se aislaron ovarios de ratones CD1 de doce semanas de edad, se cultivaron durante 24 h y luego se asignaron aleatoriamente a los grupos (n=6/grupo) 1) Grupo ChT: tratado con 1,2 µM de 4-hidroperoxi Cy + 0,12 µM de Bu; 2) Grupo PB: tratado con ChT y plasma

PB; 3) Grupo BMDSC: tratado con ChT y plasma BMDSC; y 4) Grupo UCB: tratado con ChT y plasma UCB; 5) Grupo control: sin ChT ni tratamiento con plasma. Los ovarios se recogieron a las 12 o a las 24 h y se agruparon por grupos para analizar el daño en el ADN mediante western blot (H2AX, Bax, Bcl2 y caspasa-3 escindida) y la reparación del ADN (ATM, p53, Rad51, Apex1) mediante reacción en cadena de la polimerasa cuantitativa en tiempo real (RT-qPCR). La mayoría de estos genes y proteínas se seleccionaron en función de su papel en la reparación de la rotura de la doble cadena, el sistema de daño y reparación del ADN más común en los ovocitos.

Análisis del agotamiento folicular inducido por la quimioterapia

De forma paralela se realizó un experimento para establecer la dinámica del agotamiento folicular inducido por ChT, con el fin de comprender mejor cómo los tratamientos podrían aumentar el número de folículos, considerando que la reserva folicular es finita y no renovable.

Para ello, se emplearon hembras CD1 de ocho semanas de edad a las que se les administró vía intraperitoneal una dosis estándar de ChT (12 mg/Kg Bu - 120 mg/Kg Cy, n = 12) o vehículo (DMSO, n = 8). Se recogieron las muestras ováricas a los 2, 7, 14 y 21 días después de la inyección, se realizaron recuentos foliculares.

B) EVALUACIÓN DEL EFECTO DEL PLASMA MÁS BENEFICIOSO EN TEJIDO OVÁRICO HUMANO

Debido a las diferencias funcionales entre el tejido ovárico murino y el humano, se evaluó el tratamiento más eficaz en el tejido ovárico humano.

Seis hembras NOD/SCID ovariectomizadas fueron xenotrasplantadas con fragmentos de corteza ovárica humana de pacientes POR. Una semana después, los animales fueron asignados en dos grupos experimentales, recibiendo solución salina (grupo de control) o plasma BMDSC activado (grupo aBMDSC) a través de la vena de la cola, en días alternos durante 2 semanas. A continuación, se recuperaron los fragmentos (n = 4 grupo control; n = 6 grupo aBMDSC) para evaluar los efectos del plasma en el desarrollo folicular y el nicho ovárico, realizando recuentos foliculares y estudiando la proliferación y vascularización del estroma ovárico mediante inmunohistoquímica. Además, se realizó

el estudio proteómico del tejido para dilucidar los mecanismos responsables de los efectos regenerativos.

C) DESARROLLO Y VALIDACIÓN DE UN MODELO ANIMAL DE ENVEJECIMIENTO OVÁRICO FISIOLÓGICO.

Para evaluar adecuadamente los efectos de nuevas terapias en el tratamiento de la infertilidad relacionada con la edad, se necesitan estudios preclínicos en modelos animales adecuados. Por lo tanto, nos propusimos caracterizar un modelo murino de envejecimiento ovárico fisiológico, representando diferentes etapas de la vida reproductiva de la mujer.

Se emplearon doce ratones hembra NOD/SCID de 8, 28 y 36-40 semanas de edad para imitar diferentes fenotipos ováricos reproductivos humanos: jóvenes (~18-20 años), edad materna avanzada (AMA, ~36-38 años) y mujeres añosas (>45 años), respectivamente.

Una vez que los animales alcanzaron la edad apropiada, fueron estimulados, cruzados y sacrificados para recuperar ovarios, ovocitos MII y embriones de 2-células. A continuación, se evaluó la tasa de ovulación, la calidad de los ovocitos mediante inmunofluorescencia y microscopia confocal, así como el desarrollo *in vitro* de los embriones hasta estadio de blastocisto. También se recogieron los ovarios para estudiar el desarrollo folicular mediante recuentos foliculares, el estado del estroma ovárico analizando la proliferación celular y la vascularización mediante inmunohistoquímica. Además, se evaluaron las disfunciones mitocondriales considerando el número de copias de ADNmt, el daño oxidativo y la apoptosis, analizadas mediante RT-qPCR, inmunohistoquímica y ensayo TUNEL, respectivamente.

D) ADMINISTRACIÓN INTRAOVÁRICA DEL PLASMA MÁS BENEFICIOSO EN UN MODELO MURINO DE ENVEJECIMIENTO FISIOLÓGICO

Para comprobar si el plasma rico en factores secretados por las BMDSCs y las plaquetas puede recuperar la función ovárica en la infertilidad relacionada con la edad, empleamos el modelo de envejecimiento ovárico fisiológico caracterizado previamente, En este estudio, comparamos el efecto del tratamiento más beneficioso (aBMDSC) frente al aPRP.

Además, los plasmas se administraron mediante una única inyección intraovárica, en un intento de acercar la administración del tratamiento a la práctica clínica.

Ratonas NOD/SCID jóvenes, AMA y viejas (n=12/edad) fueron asignadas al azar para recibir una única inyección intraovárica en ambos ovarios (10 µl/ovario) de solución salina (grupo control), PRP activado de sangre periférica (grupo aPRP), o plasma activado rico en factores secretados por las BMDSCs y plaquetas (grupo aBMDSC).

Una semana después de los tratamientos, los animales fueron sometidos a una EOC y apareados. A continuación, las ratonas fueron sacrificadas para recuperar los ovocitos MII ovulados y los embriones de 2-células del oviducto. También se recuperaron los ovarios para analizar el crecimiento folicular, el estroma, la función mitocondrial y los perfiles proteómicos a diferentes edades.

5. RESULTADOS Y DISCUSIÓN

A) EFECTO REGENERATIVO DE DIFERENTES FUENTES DE PLASMA RICO EN FACTORES DE CRECIMIENTO EN MODELOS MURINOS DE DAÑO OVÁRICO INDUCIDO POR QUIMIOTERAPIA.

Diferentes fuentes plasmáticas, enriquecidas en factores secretados por células madre, promovieron el desarrollo de folículos en modelos murinos de daño ovárico inducido por quimioterapia.

En el modelo DOR, el tratamiento con aBMDSC y aUCB redujo parcialmente el agotamiento folicular inducido por la ChT. Este rescate puede estar impulsado en gran medida por la conservación de los folículos primordiales, con valores similares a los observados en el grupo wild-tipe. Además, ambos plasmas activados aumentaron el número de folículos preantrales tardíos por encima de los niveles de wild-type, pero sólo el aBMDSC restauró el número de folículos antrales tempranos. De hecho, los tratamientos con aBMDSC y aUCB aumentaron el número de ovocitos MII y embriones.

En el modelo POI, el plasma aBMDSC y el aUCB rescataron la pérdida de folículos inducida por ChT, recuperando los valores al aumentar las poblaciones de folículos primordiales, secundarios y preantrales tardíos, siendo el aBMDSC también capaz de

aumentar el número de folículos en fase antral. Además, se observó un ligero aumento de las poblaciones primordiales, secundarias y preantrales tardías tras la administración de aPB, aunque no fue tan significativo como el efecto inducido por aBMDSC y aUCB. La administración de UCB, aUCB y aBMDSC también tuvo efectos positivos sobre el número de ovocitos MII.

Dado que la reserva folicular es limitada y no renovable, nuestra hipótesis es que el plasma rescata los folículos primordiales dañados antes de que sufran atresia. De hecho,el análisis paralelo realizado para comprender el proceso de agotamiento folicular tras la administración de ChT, indicó que se producen una oleada inmediata de muerte folicular a los dos días de la exposición, mientras que la segunda no se produce hasta los siete días, finalizando al veintiuno. Por tanto, una semana después del tratamiento con ChT, quedan folículos primordiales susceptibles de ser reparados y rescatados por factores solubles del plasma.

La fertilidad a largo plazo fue rescatada por la terapia basada en factores secretados por células madre

Las hembras DOR de todos los grupos de tratamiento lograron gestaciones y dieron a luz a crías en tasas similares. Sin embargo, tanto UCB como BMDSC aumentaron el tamaño de las camadas siendo más significativo cuando se utilizaron formas activadas, especialmente para el grupo aUCB.

En el modelo POI, los animales de los grupos de control ChT y PB no lograron gestación tras varios intentos de apareamiento. Sin embargo, el 40% de las ratonas tratadas con BMDSC y UCB obtuvieron la gestaciones y nacimiento de crías sanas. El uso de aBMDSC y aUCB aumentó las tasas de gestación al 80% y 67% respectivamente. El plasma aPB también permitió las gestaciones y nacimientos, aunque su efecto fue del 40%.

Los plasmas ricos en factores solubles de células madre regeneraron el estroma ovárico

Los plasmas BMDSC y UCB aumentaron drásticamente la proliferación celular en el tejido ovárico en ambos modelos. Los plasmas aBMDSC y aUCB tuvieron efectos más potentes sobre la proliferación que las formas no activadas en los modelos DOR. El plasma aPB aumentó en menor medida la proliferación celular.

Además, en comparación con la solución salina, todos los tratamientos con plasma promovieron la formación de nuevos vasos en los ratones DOR. Sin embargo, en la condición POI, el aumento fue más leve para los plasmas PB y aPB, y muy alto tras el tratamiento con BMDSC, aBMDSC, UCB y aUCBa, que aumentaron la vascularización a niveles del grupo wild-type. Cuando se evaluó la apoptosis en los ratones DOR, el plasma de BMDSC fue el único tratamiento que disminuyó los niveles de proteína caspasa 3-escindida. En el modelo POI, la apoptosis se redujo tras el tratamiento con BMDSC, aBMDSC, UCB y aUCB.

La evaluación proteómica de las diferentes fuentes de plasma reveló proteínas y vías relacionadas con el rescate ovárico.

Se cuantificó un total de 293 proteínas para identificar las DEPs asociadas al tipo de plasma y/o al estado de activación. La comparación de las muestras de BMDSC y UCB con el plasma de control arrojó un alto porcentaje de DEPs implicadas en el ciclo celular, la expresión génica, la reparación del ADN y en las vías relacionadas con las RhoGTPasas, los receptores de muerte y la HIPPO en la muestra de BMDSC. Las reguladas al alza en el plasma UCB estaban relacionadas principalmente con el metabolismo, la hemostasia, el transporte mediado por vesículas, la organización de la matriz extracelular y la señalización por GPCRs, integrinas y la familia MAPK. A continuación, se compararon las fracciones activadas, y la fracción aBMDSC mostró el mayor porcentaje de proteínas sobreexpresadas relacionadas con expresión génica, la reparación del ADN y la señalización por RhoGTPasas, receptores nucleares, NOTCH, PDGF y WNT. Las proteínas de la fracción aUCB estaban implicadas en los mismos procesos enriquecidos en la fracción no activada, lo que indica que la activación tiene un efecto mucho menor en este tipo específico de plasma.

El reconocimiento y la reparación del daño en el ADN fueron promovidos por el plasma BMDSC en un modelo *in vitro*.

La expresión de los genes de reconocimiento de daños en el ADN (ATM y p53) y de reparación (Rad51, Albkh2 y Apex1) aumentó tras el tratamiento con el plasma BMDSC y de forma menos dramática con el tratamiento con UCB a las 12 h de la exposición. La activación de estas vías de señalización se correlacionó con una disminución de la

relación pro-apoptótica BAX/Bcl2. A las 24 h, tanto el grupo BMDSC como el UCB mostraron una reducción de la expresión del marcador de daño en el ADN H2AX, de la proporción pro-apoptótica BAX/Bcl2 y de la caspasa 3 escindida. Asimismo, la expresión de los genes de reconocimiento y reparación del daño en el ADN fue menor en los grupos tratados con BMDSC y UCB que en el grupo ChT a las 24 h.

B) EVALUACIÓN DEL EFECTO DEL PLASMA MÁS BENEFICIOSO EN TEJIDO OVÁRICO HUMANO

El plasma aBMDSC promovió el desarrollo folicular y la regeneración del estroma en la corteza ovárica humana.

El plasma aBMDSC fue el tratamiento más eficaz en los modelos animales y, por tanto, prometedor para ser validado en el tejido ovárico humano.

Al comparar la densidad folicular y el recuento total de folículos, no se detectaron diferencias, lo que pone de manifiesto la homogeneidad de las muestras incluidas en ambos grupos. No obstante, en los fragmentos tratados con aBMDSC se observó una disminución de los folículos primordiales, junto con un aumento de las poblaciones primarias y secundarias, lo que indica una promoción del crecimiento folicular. De hecho, sólo se detectaron folículos secundarios en los trasplantes humanos que recibieron aBMDSC. Además, el aBMDSC indujo una mejora en la proliferación celular y vascularización en comparación con el control.

Para profundizar en el análisis de los efectos beneficiosos del plasma aBMDSC en el tejido ovárico humano, se estudiaron los perfiles proteómicos de los trasplantes. Se cuantificaron un total de 1.224 proteínas, siendo 17 de ellas DEPs en los fragmentos del grupo aBMDSC en comparación con los controles. El 35% de estas proteínas estaban implicados en la síntesis y el procesamiento de proteínas en el retículo endoplásmico, el 24% en la autofagia y el 18% en la angiogénesis. Además, varias de las proteínas más reguladas mostraron una función específica en el ovario con un papel clave en la foliculogénesis o en la atresia folicular.

C) DESARROLLO Y VALIDACIÓN DE UN MODELO ANIMAL DE ENVEJECIMIENTO OVÁRICO FISIOLÓGICO.

El desarrollo folicular y el potencial reproductivo disminuyó en el modelo fisiológico de envejecimiento ovárico.

La reserva ovárica se vio globalmente mermada a medida que aumentó la edad de los ratones en el modelo de envejecimiento, con una disminución del número de folículos primordiales y primarios especialmente en los ratones viejos en comparación con los grupos jóvenes y AMA. También se observó un número reducido de folículos en crecimiento en diferentes etapas de desarrollo, siendo estas disminuciones reflejadas en el número total de folículos. Además, el número de cuerpos lúteos fue menor en los ovarios más viejos. Este fenómeno fue acompañado de una menor activación de los folículos primordiales por extrusión nuclear de FOXO3 tanto en los ratones AMA como en los viejos en comparación con los controles jóvenes.

Tras la EOC, se recuperaron menos ovocitos MII de los ratones AMA en comparación con el grupo joven, siendo este descenso mayor en el grupo viejo donde el 67,5% de los ovocitos se encontraron fragmentados como consecuencia de una calidad reducida. De hecho, el análisis de la calidad ovocitaria mediante inmunofluorescencia, mostró una disminución del área del huso y un ensamblaje anormal del mismo tanto en los ovocitos AMA como en los viejos. Estos grupos también presentaron un aumento en el número de ovocitos con los cromosomas desalineados.

En el momento del sacrificio, el número de embriones de 2-células recuperados fue menor en los ratones AMA en comparación con los ratones jóvenes, y el posterior cultivo *in vitro* reveló un deterioro de las tasas de formación de blastocistos. En el caso de los ratones viejos, la peor condición de envejecimiento ovárico, no se recuperaron embriones viables.

El estroma ovárico se deterioró en los ratones envejecidos.

También se observaron deficiencias relacionadas con la edad en el estroma ovárico, ya que la proliferación celular disminuyó significativamente en los ovarios AMA y viejos en comparación con los jóvenes. De hecho, el porcentaje de folículos primarios

proliferativos y secundarios fue menor en estos grupos, todo ello junto con una menor vascularización en los ratones más envejecidos.

El envejecimiento ovárico afectó la función mitocondrial y aumentó el daño oxidativo.

Cuando se analizaron el número de copias de ADNmt como marcador de disfunción mitocondrial, se detectó un número menor en los ratones AMA y viejos en comparación con los jóvenes. En el grupo de los ratones más envejecidos, la reducción de las copias mitocondriales también se asoció a un mayor nivel de 4-HNE, marcador de peroxidación lipídica y daño oxidativo, y a un mayor número de células apoptóticas.

Los efectos observados como consecuencia del envejecimiento fueron corroborados a nivel proteómico.

El análisis de regresión ElasticNet de las muestras identificadas mediante SWATH-MS, detectó 30 DEPs entre las condiciones de joven, AMA y viejo. La agrupación jerárquica dividió estos DEPs en dos categorías principales: una con el grupo de ratones viejos y otra que incluía los grupos de jóvenes y AMA, que a su vez se clasificaron en dos subgrupos distintos. Al estudiar el número de proteínas reguladas al alza y a la baja, observamos un mayor número de proteínas reguladas a la baja en el grupo de ratones envejecidos.

A continuación, se estudiaron las vías reguladas por las DEPs, realizando un análisis Gene Ontology (GO) para comprender mejor el proceso biológico subyacente, la función molecular y los componentes celulares. El GO reveló procesos biológicos relacionados con la regulación de los procesos metabólicos, la expresión génica, el transporte de lípidos y la angiogénesis, además de las vías implicadas en la actividad mitocondrial, como la respuesta al estrés, los procesos metabólicos del ATP o la cadena respiratoria de transporte de electrones. También se enriquecieron diferentes componentes celulares y funciones moleculares relacionadas con dichos procesos. Y un análisis GOchord destacó los genes más significativos y comunes en los procesos biológicos.

D) ADMINISTRACIÓN INTRAOVÁRICA DEL PLASMA MÁS BENEFICIOSO EN UN MODELO MURINO DE ENVEJECIMIENTO FISIOLÓGICO

El tratamiento local con aBMDSC promovió la activación y el crecimiento folicular

Una única inyección intraovárica de aBMDSC activó los folículos latentes en todos los grupos de edad, como indica el mayor porcentaje de folículos primordiales con extrusión nuclear de FOXO3, en comparación con los grupos de control y de tratamiento con aPRP. La activación folicular también se confirmó por una reducción del número de folículos primordiales tanto en los ratones jóvenes como en los AMA. Estos cambios en la dinámica folicular se asociaron a un mayor número de poblaciones en crecimiento (primarias, antrales y cuerpos lúteos) en los ratones jóvenes, AMA y, en menor medida, en los viejos. Por último, el tratamiento con aPRP también produjo efectos positivos sobre la activación primordial y el número de folículos primarios tanto en los ratones AMA como en los viejos.

La inyección de aBMDSC mejoró la cantidad y la calidad de los ovocitos en el modelo de envejecimiento fisiológico

Tras la EOC, se recuperaron un número mayor de ovocitos MII de los ratones jóvenes tratados con aBMDSC que del control. Además, no se observaron diferencias en el porcentaje de ovocitos MII fragmentados, lo que sugiere que la inyección de aBMDSC no produce efectos deletéreos al ser administrado a ovocitos jóvenes.

En el grupo AMA, el plasma aBMDSC aumentó el número de MII y redujo el porcentaje de ovocitos fragmentados hasta un nivel comparable al de los ratones jóvenes. Al evaluar la calidad de los ovocitos de los ratones AMA, observamos que el tratamiento aBMDSC aumentó el área del huso, mejoró el ensamblaje y redujo la desalineación cromosómica. A pesar de que los ratones viejos mostraban los peores resultados iniciales, se observaron efectos beneficiosos tras la inyección de aBMDSC con un mayor número de MII, una menor fragmentación ovocitaria y una mejor alineación cromosómica. Los beneficios del tratamiento aPRP también se reflejaron en el modelo AMA, en la cantidad y calidad de los ovocitos, aunque en menor medida que con aBMDSC.

El plasma aBMDSC mejoró el desarrollo y la competencia embrionaria.

En el momento del sacrificio, se recuperaron más embriones de 2-células en los ratones jóvenes, AMA y viejos tratados con aBMDSC que en el control. El posterior cultivo *in vitro* mostró que el tratamiento con aBMDSC favoreció la formación de blastocistos especialmente en los ratones AMA y viejos. El aPRP también mejoró la tasa de formación de blastocistos en la condición AMA y permitió obtener embriones en los ratones viejos. Sin embargo, este tratamiento no tuvo mejoras significativas en el posterior desarrollo embrionario en ninguno de los grupos de edad.

El tratamiento local con aBMDSC promovió la regeneración del estroma ovárico.

El plasma aBMDSC aumentó significativamente la proliferación celular en el estroma ovárico de los ratones jóvenes, AMA y viejos, mientras que el aPRP mejoró la proliferación sólo en los grupos jóvenes y AMA. Se observaron más folículos primordiales, primarios y secundarios proliferativos tras el tratamiento con aBMDSC en los grupos AMA y viejos.

Ninguno de los tratamientos mejoró la vascularización en los ratones jóvenes. Sin embargo, la densidad de microvasos en los ratones AMA y viejos aumentó hasta niveles comparables a los encontrados en los ratones jóvenes tras la inyección de aBMDSC. El tratamiento con aPRP sólo aumentó la vascularización en los ratones más envejecidos.

La inyección de plasma aBMDSC mejoró la función mitocondrial, mitigando el daño oxidativo y la muerte celular en los ratones envejecidos.

No se observaron diferencias en los ratones jóvenes tras el tratamiento. Sin embargo, el plasma aBMDSC aumentó el número de copias de ADNmt en los grupos de ratones AMA y viejos, mientras que el plasma aPRP solo tuvo efecto en este último.

El efecto positivo del plasma aBMDSC se reflejó también en los niveles de daño oxidativo, detectado una menor peroxidación lipídica y apoptosis en los ratones más viejos.

El análisis de proteómica funcional puso de manifiesto los efectos de los tratamientos plasmáticos a diferentes edades.

El análisis de regresión ElastiNEC mostró 26 DEPs en los ratones jóvenes tratados con plasmas. La agrupación jerárquica dividió estas DEPs en dos categorías principales: una

formada por el grupo control, y otra que incluía los grupos aPRP y aBMDSC. Las muestras tratadas con plasma tenían un mayor número de proteínas reguladas al alza en comparación con el grupo control. Del mismo modo, identificamos 30 DEPs en ratones AMA y 27 DEPs en ratones viejos. En estos casos, el clustering jerárquico clasificó y discriminó un cluster compuesto por las muestras aBMDSC y otro por los grupos aPRP y control. Además, encontramos respectivamente un mayor número de proteínas reguladas a la baja en los grupos AMA y viejo tratados con aBMDSC con respecto a sus correspondientes grupos de control.

A continuación, se estudiaron las vías reguladas por las DEPs. En los ratones jóvenes, las DEPs se asociaron principalmente con funciones relacionadas con las mitocondrias. En los ratones AMA, se identificaron vías enriquecidas relacionadas con la regulación, organización y proliferación de la actina, además de procesos metabólicos de ROS, regulación de la proliferación celular y de la angiogénesis. Por último, en el grupo de ratones viejos, el análisis funcional identificó procesos relacionados con la oxidación, el metabolismo y la modificación de lípidos, así como del transporte de electrones mitocondrial y la regulación del ensamblaje del huso.

6. CONCLUSIONES

De esta tesis se pueden extraer las siguientes conclusiones:

1. La administración sistémica de plasma humano enriquecido en factores secretados por células madre (plasmas BMDSC y UCB) rescata el desarrollo folicular y la fertilidad, induciendo la formación de microvasos y la proliferación celular, y reduciendo la apoptosis en modelos de ratón de DOR y POI.

2. La activación de los plasmas BMDSC y UCB potenció los efectos positivos sobre la fertilidad en modelos murinos de daño ovárico.

3. Los análisis proteómicos e *in vitro* indican que los efectos del plasma pueden estar mediados por factores solubles relacionados con el ciclo celular/apoptosis, la expresión génica, la transducción de señales, la comunicación celular, la respuesta al estrés y la reparación del ADN.

4. El tratamiento más eficaz, el plasma aBMDSC, promovió el desarrollo folicular y regeneró el estroma en el tejido ovárico humano de las mujeres POR, corroborando los efectos observados en los modelos DOR y POI.

5. Los plasmas BMDSC y UCB podrían ser tratamientos eficaces para aumentar los resultados reproductivos en mujeres con deterioro de la función ovárica debido a diversas causas. Sin embargo, la combinación de los beneficios de los factores de crecimiento secretados por las células madre y por las plaquetas podría mejorar y acelerar los efectos regenerativos en los ovarios. El plasma activado de BMDSC es el tratamiento más prometedor debido a sus potentes efectos restauradores.

6. Se estableció un modelo murino de envejecimiento fisiológico, que representa diferentes perfiles de fertilidad de la mujer, como la edad materna avanzada y añosa. Este modelo representa una herramienta para descifrar el proceso de envejecimiento ovárico y probar futuros tratamientos potenciales para frenar o revertir los efectos del envejecimiento ovárico.

7. Una única inyección intraovárica que combina factores secretados por células madre y plaquetas (aBMDSC) mejoró los resultados reproductivos en un modelo murino de envejecimiento fisiológico, promoviendo la activación y el desarrollo de los folículos y regenerando el estroma ovárico.

8. Los efectos del plasma aBMDSC en los resultados de fertilidad se asociaron positivamente a la función mitocondrial, con el tratamiento aumentando el número de copias de ADN mitocondrial y reduciendo el daño oxidativo y la apoptosis.

9. La mejora del potencial reproductivo tras la inyección de aBMDSC se acompañó de cambios a nivel proteómico, con proteínas implicadas en los mecanismos de reorganización del huso ovocitario, la regulación de la proliferación y la apoptosis, y las funciones mitocondriales.

10. Una única inyección intraovárica de plasma aBMDSC parece un tratamiento prometedor para mejorar los resultados reproductivos de las mujeres con infertilidad relacionada con la edad.

I. INTRODUCTION

I. INTRODUCTION

1. The ovary

1.1 Physiology and anatomy of the ovaries

1.1.1 Ovarian function and structure

The ovary is a highly organized organ formed by germ cells (oocytes) and somatic cells (granulosa cells (GCs), stromal and theca cells). The interactions between germ and somatic cells dictate the formation of the functional unit of the ovary, called the ovarian follicle, which contains the oocyte.

Among the primary functions of the ovary are oogenesis, and secretion of steroid hormones necessary for maintaining female fertility and endocrine homeostasis. The hypothalamic-pituitary axis controls both functions through the hypothalamic hormone (gonadotropin-releasing hormone, GnRH), and pituitary hormones (follicle stimulating hormone (FSH) and luteinizing hormone (LH)). These hormones act on the ovaries to stimulate follicular development, ovulation, and the secretion of steroid hormones[1].

Three structural zones or regions can be differentiated in the ovary: epithelium, cortex, and medulla (Figure 1). The distribution of follicles in the ovary is determined by collagen concentration. The ovarian cortex is the outer part of the ovary, covered by the epithelium, and the most rigid region of the ovary, which contains the follicles in the first stage of follicle development. The medulla is the central part, which contains connective tissue, nerves and blood and lymphatic vessels. This is where growing follicles can be found[2,3].

3
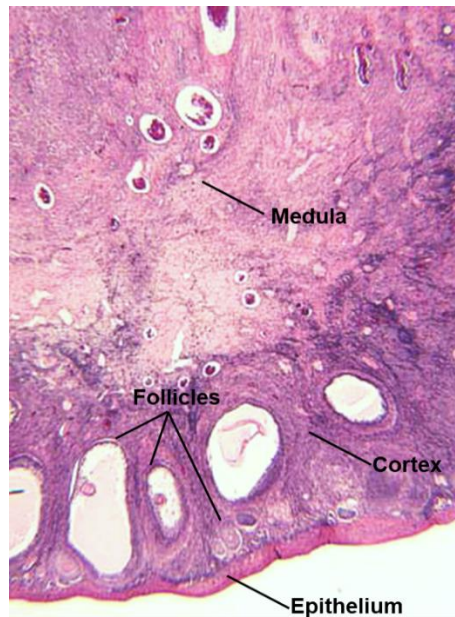
Figure 1.Structure of the ovary. Histological section of a human ovary in which the three structural parts of the ovary can be distinguished: epithelium, cortex with follicles, and medulla in the innermost part.

1.1.2 Ovarian reserve

Oocytes are formed from primordial germ cells that migrate from the endoderm of the yolk sac to the genital ridge[4,5] and initiate a period of rapid mitosis to increase their number[6,7]. Subsequently, some continue to divide, others enter programmed cell death (apoptosis), and others begin meiosis, arresting in the diplotene phase of meiosis. Once formed, this pool of dormant follicles constitutes the ovarian reserve, which is limited and non-renewable[8,9] (Figure 2). These follicles first appear in human fetuses at around 15 to 20 weeks pregnancy[10]. The total number of oocytes drops radically from a peak of 6 to 7 million at 20 weeks pregnancy, to less than 1 million at birth[11], with approximately 300 000 to 400 000 remaining per ovary[7].
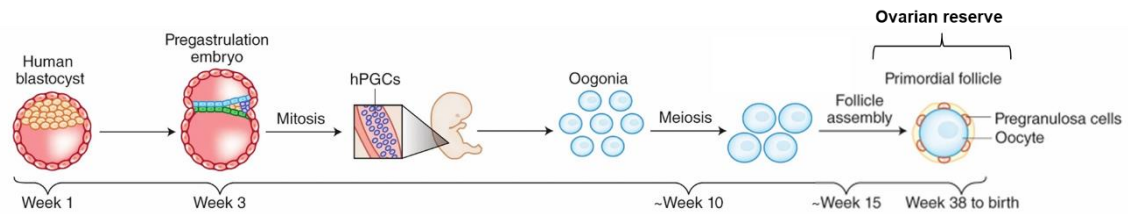
Figure 2. Ovarian reserve origin. In humans, oogonial development starts during weeks 6 to 10 of pregnancy. The primordial follicles are formed between week 15 and birth. Image modified from Stringer and Western, 2019[12].

Follicles at the first stage of development are called primordial follicles and are surrounded by several flattened somatic cells, called pre-granulosa cells. Oocytes that are not enclosed in the primordial follicles are lost due to apoptosis[13,14].

The primordial follicles can have one of four fates: remain inactive in the quiescent stage; activate but then undergo atresia; activate, develop, mature, and finally ovulate; or die directly from the quiescent state[15,16].

1.1.3 Folliculogenesis

Folliculogenesis refers to the development of ovarian follicles from primordial follicles to their final stage, ovulation. It is a very lengthy process which is regulated and controlled in a coordinated manner by growth factors, hormones, receptors, and enzymes[17–19].

Folliculogenesis begins with the recruitment of a primordial follicle into the group of growing follicles and ends with ovulation or death by atresia[20]. As the process of follicular development continues, different follicle types can co-exist in the ovary at any one time: primordial follicles, primary follicles, secondary follicles, preantral follicles, antral follicles, and preovulatory follicles. After different processes involving both extra-ovarian signals and intra-follicular paracrine and autocrine regulators, a dominant preovulatory follicle ovulates and releases a mature oocyte for fertilization. Then, the residual follicle undergoes luteinization and becomes a corpora lutea, which is responsible for

progesterone secretion and for preparing the endometrium for implantation in the event of fertilization[15] (Figure 3).
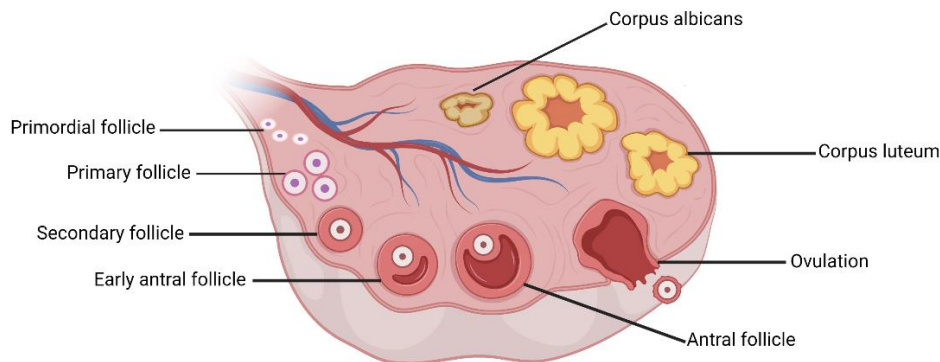
Figure 3. Folliculogenesis. When the follicles are activated, they go through various stages of growth and maturation until one of them releases an oocyte (ovulation), after which this follicle becomes a corpora luteum and then albicans. Image created with biorender.com

When a woman is of reproductive age, the process of folliculogenesis happens every month. The primordial follicle starts to grow, proliferating the surrounding pre-granulosa cells, which develop from a few flattened cells to multiple cuboidal GCs[17]. Then, the ovarian follicle is enclosed by a layer of GCs, which provide nutrients to the growing oocyte. The oocyte and surrounding GCs are separated from the interstitial tissue (stroma) by a membrane known as the basal lamina. As a result of GCs proliferation and differentiation, the follicle reaches the secondary or preantral stage, defined by several layers of GCs around the oocyte. In addition, in developing secondary follicles, a layer of specialized cells, the theca cells, appear around the outer layer of granulosa cells. The theca cells are essential for follicular growth, implementing a vascular system that allows communication with the hypothalamic-pituitary axis during the reproductive cycle, and allows for the release of nutrients essential for this process[21]. Subsequently, the antral cavity (or antrum) is formed by accumulating follicular fluid in the granulosa layer. Of all the follicles recruited in each menstrual cycle, only one reaches the preovulatory stage, and the rest enter atresia (mainly in the antral stage) (Figure 4).

During follicular development, the follicle grows from 40 µm to 15-22 mm in diameter. The process of folliculogenesis in humans requires more than 200 days for a primordial follicle to grow and develop to the ovulation stage[12].
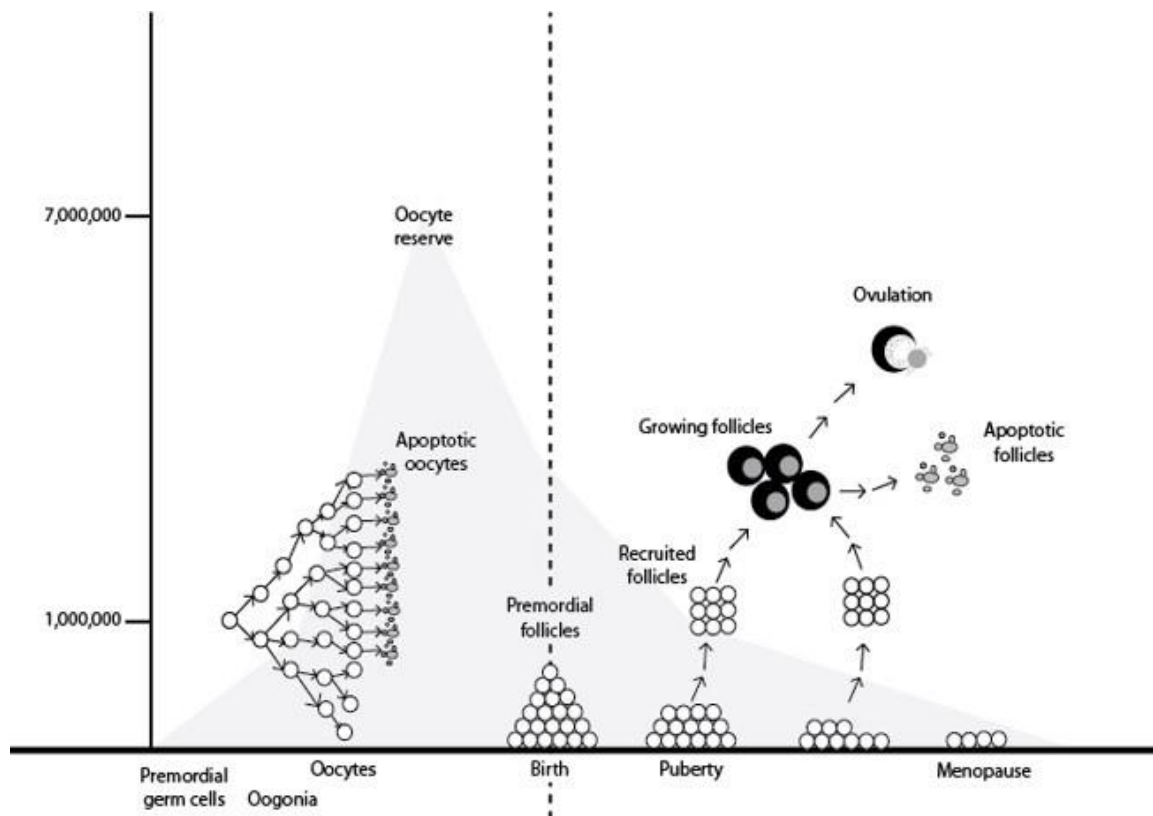
Figure 4. Evaluation of the ovarian reserve. From puberty to menopause, every month a pool of dormant follicles is activated and acts as a source of developing follicles and oocytes. One of the oocytes will be ovulated each month. Image modified from McGee and Hsueh, 2000[17].

1.2 Regulation of folliculogenesis

Follicular development can be classified, based on the requirement for gonadotropins, as either gonadotropin-independent or gonadotropin-dependent follicle development[17] (Figure 5).
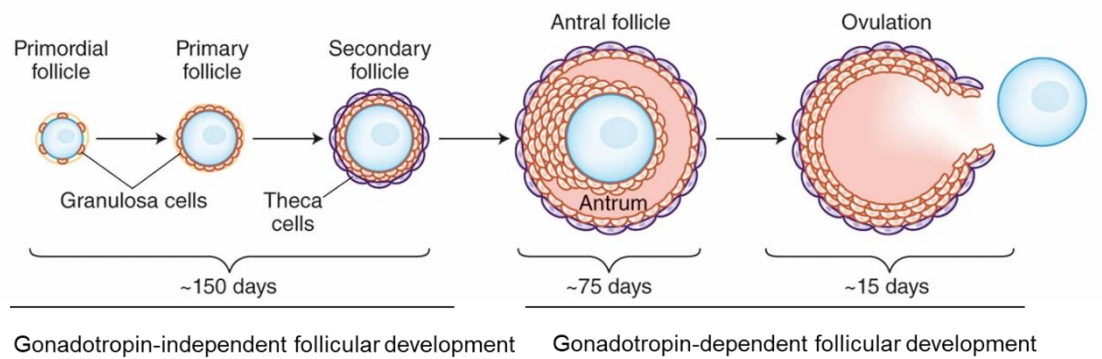
Figure 5. Regulation of follicular development. The stages of folliculogenesis can be differentiated according to the response of follicles to gonadotropins (independent or dependent). Follicle development, oocyte maturation, and ovulation occur after birth and take ~240 days in total. Image modified from Stringer and Western, 2019[12].

1.2.1 Gonadotropin-independent follicular development

a. Primordial to primary transition

The mechanisms that control the ovarian reserve and the activation of the primordial follicles determine the duration of a woman's fertility. Studying this process is difficult due to the slow growth of many small follicles over a prolonged period[22]. During folliculogenesis, only a small number of dormant oocytes become activated in the phase of rapid growth, during which oocyte volume, ribonucleic acid (RNA) content[23], and protein synthesis increase[24].

Paracrine communications between the oocyte and somatic cells control primordial follicle recruitment. This communication is mediated by secreted growth factors, including members of the transforming growth factor-beta (TGF) superfamily.

The oocyte controls the signaling pathways that regulate follicular growth[25]. Phosphatidyl inositol 3-OH-kinase (PI3K)-AKT-FOXO3a signaling is responsible for restraining follicle activation, by preventing the primordial-primary transition[10]. In this pathway, PI3K phosphorylates phosphatidylinositol-4,5-bisphosphate (PIP2), generating phosphatidylinositol-3,4,5-triphosphate (PIP3), which acts as a second messenger recruiting different proteins with lipid binding groups, namely phosphoinositol-dependent kinase-1 (PDK1) and Akt, into the cytoplasm. PDK1 then phosphorylates Akt, activating its function. Once active, Akt phosphorylates FOXO3a, promoting its nuclear

exclusion (from the nucleus to the ooplasm) and culminating in a global primordial follicle[26] (Figure 6).

Different studies have demonstrated the importance of PTEN (phosphatase and tensin homolog), a lipid phosphatase that inhibits signaling by the PI3K pathway. The loss of PTEN in oocytes generates global activation of primordial follicles, suggesting that PTEN-mediated inhibition of PI3K signaling is required to prevent follicle activation[27]. Similarly, FOXO3a knockout mice undergo global primordial follicle activation[28]. Thus, a principal physiologic role of the PI3K pathway is to control primordial follicle activation via FOXO3.

In addition to these signaling pathways, chemokines and factors such as stromal-derived factor-1 (SDF-1) are secreted by oocytes to regulate follicle activation[29].

b. Primary to secondary transition

The significant events during the primary follicle stage include FSH receptor expression and oocyte growth and differentiation. In this period, the oocyte increases in diameter from ~25 μm to ~120 μm and develops its surrounding extracellular matrix, the zona pellucida. This growth happens because of the reactivation of the oocyte genome[30]. During the growth phase, the oocyte is highly transcriptionally active. It must generate sufficient proteins and mRNA transcripts to support its growth and future critical oocyte maturation, fertilization, and early embryo development.

Secondary follicle development begins with acquiring a second layer of granulosa cells. It involves a change in the arrangement of the GCs from simple cuboidal epithelium to stratified columnar epithelium (Figure 6).

The transcription factors FIGLA (Folliculogenesis Specific BHLH Transcription Factor) and NOBOX (NOBOX Oogenesis Homeobox) regulate the zona pellucida proteins, and the growth factors GDF-9 (Growth/Differentiation Factor 9) and BMP-15 (Bone-

Introduction

Morphogenetic Protein-15)[31,32]. These growth factors play an essential role in stimulating granulosa cell proliferation and theca development[33].

The Kit ligand signaling pathway is crucial for oocyte growth and follicle development. Kit ligand is generated by GCs and required for oocyte growth[34]. In addition, the Kit ligand is also essential for organizing theca cells around the growing follicle.

As secondary follicle development proceeds, two primary layers of theca appear. An inner theca layer that is closest to the granulosa cells (theca interna), which contains the endocrine cells that produce the steroid hormones, and an outer theca that is a connective tissue layer derived from fibroblast-like cells (theca externa), which produce extracellular matrix factors, such as collagen[35]. The formation of small blood vessels through angiogenesis also accompanies theca development. Consequently, blood can then circulate within the follicle, providing nutrients and gonadotropins, and expelling waste and secretory products from the developing follicle.
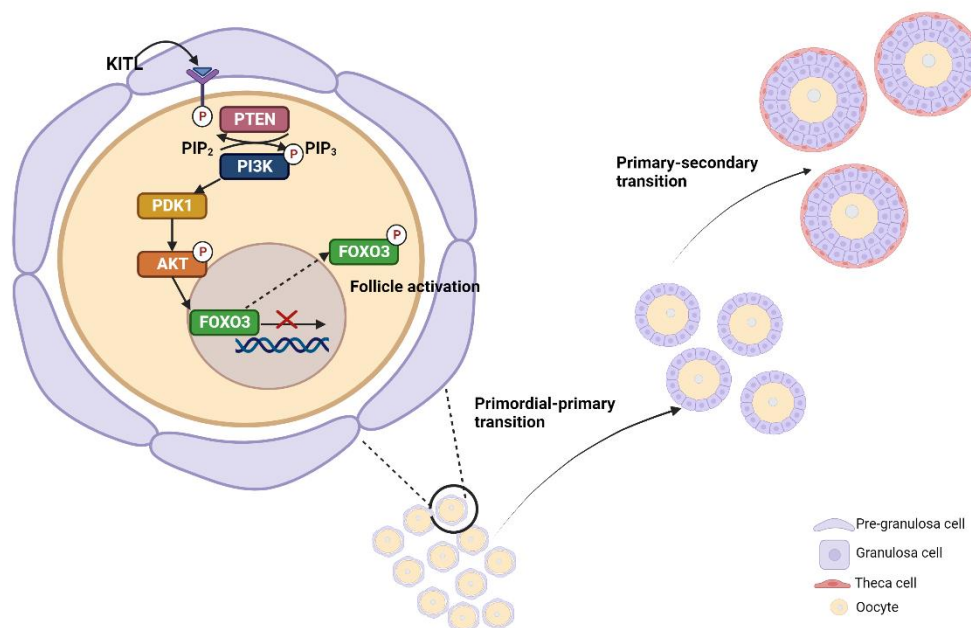
Figure 6. Gonadotropin-independent follicular development. (PI3K)-AKT-FOXO3a signaling is required to restrain follicle activation and prevent the primordial to primary transition. Extraction of FOXO3 from the nucleus to the ooplasm of the oocyte activates the primordial follicle. After activation, the primary stage follicle begins to increase in size, with granulosa cells' division and theca cells' development until the secondary stage. Image created with biorender.com.

1.2.2 Gonadotropin-dependent follicular development

During follicular development, dormant primordial follicles are activated, and develop until they form an antral cavity. Subsequently, the antral follicles grow until they reach the preovulatory stage. This occurs under cyclic stimulation by GnRH.

GnRH is secreted in a pulsatile manner by the hypothalamus and acts on the pituitary gland, inducing the secretion of FSH and LH. FSH plays a key role in developing the antral follicle and, in combination with LH, stimulates preovulatory follicular growth[17,36] (Figure 7).
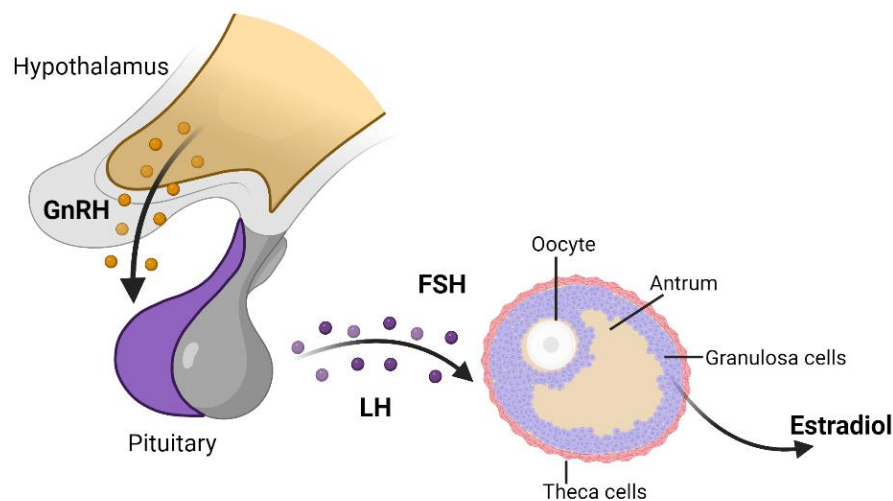
Figure 7. Gonadotropin-dependent follicular development. Gonadotropin-releasing hormone (GnRH) is secreted in a pulsatile manner by the hypothalamus and stimulates the secretion of follicle-stimulating hormone (FSH) and luteinizing hormone (LH) by the pituitary. These hormones act on the ovary, regulating follicular growth and maturation and triggering ovulation. Image created with biorender.com.

FSH also stimulates the production of estradiol by the GCs. The estradiol acts in an autocrine and paracrine manner, favoring granulosa cells' proliferation and the LH receptor's expression[37].

In each female cycle, one of the developing antral follicles increases its response to estradiol and causes a decrease in FSH secretion[36,38], leading to atresia of the remaining antral follicles. Thus, in each ovulation cycle, there is only one dominant follicle[39]. Finally, in response to the secreted estradiol, there is a peak in LH secretion by the pituitary. This

LH peak triggers ovulation and causes the oocyte of the dominant follicle to complete meiosis and generate a haploid gamete ready for ovulation and subsequent fertilization[40].

2. Aging

Cellular aging is defined by a gradual deterioration of physiological integrity, which impairs function and increases susceptibility to death[41]. This physiological process is one of the significant risk factors for multiple different human pathologies, including cancer, diabetes, cardiovascular problems, and neurological illnesses.

Different studies have aimed to elucidate the mechanisms responsible for this progressive deterioration, highlighting genomic instability, telomere attrition, epigenetic alterations, loss of proteostasis, deregulated nutrient-sensing, mitochondrial dysfunction, cellular senescence, stem cell exhaustion, and altered intercellular communication[42] (Figure 8).
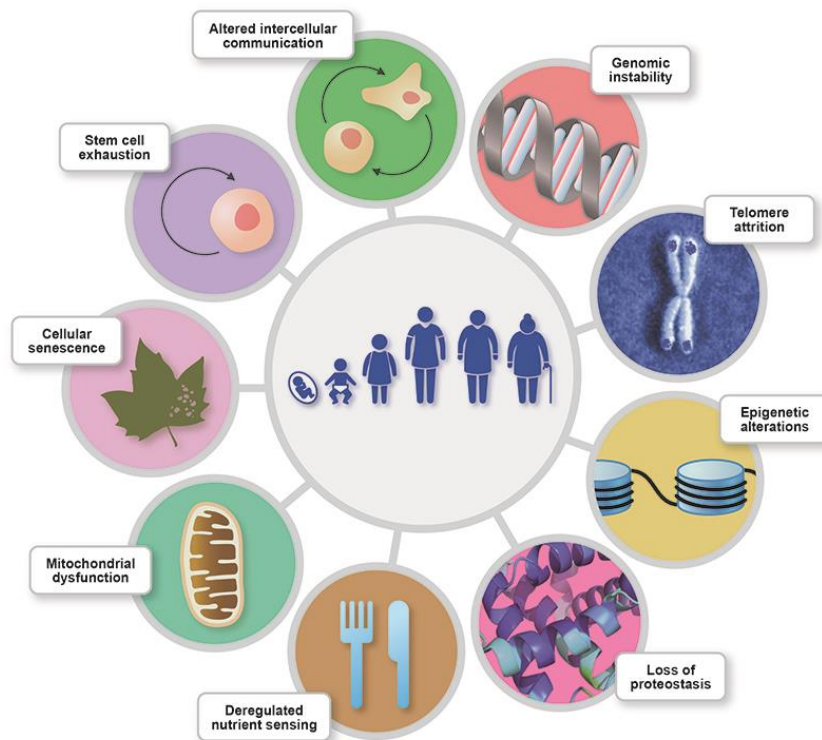
Figure 8. The hallmarks of aging. Image modified from López-Otín et al., 2013[42].

2.1 Physiological ovarian aging

Nowadays, one of the significant challenges for researchers is to understand and decipher the aging process, in order to prevent or reverse this pathophysiology, given the increase in life expectancy in our society[43]. This is of utmost priority in the case of women, who suffer from an accelerated ovarian aging process [44].

The female reproductive system ages approximately ten years before other organ systems naturally experience age-related functional reduction. Reproductive aging has gradually become a primary health concern, as nowadays women continue delaying their age of childbearing due to changes in socio-economic circumstances and cultural norms[45].

Female fertility is negatively correlated with age, with noticeable declines in ovarian reserve until menopause, which is a natural consequence of physiological ovarian aging marked by the quantity of oocytes falling below 1000[46–49]. As the age of a women increases, the quality of her oocytes also decreases (Figure 9). This decline is most significant from age 35, when women are considered to be of advanced maternal age (AMA), and a woman's ability to fall pregnant with her own oocytes decreases[50,51].
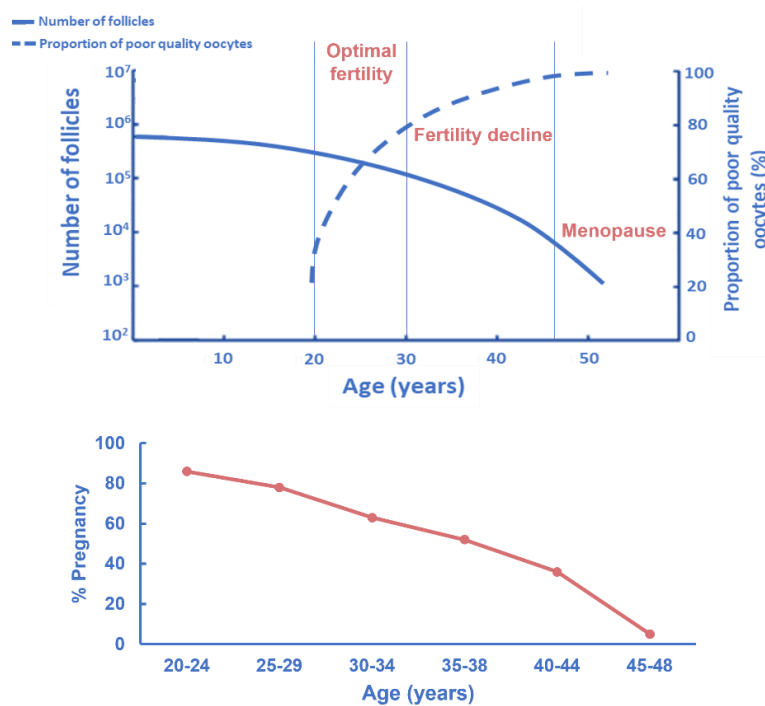
Figure 9. The decline of ovarian reserve with age. Oocyte quantity and quality decline from the late thirties in humans until they reach menopause. As a woman's age increases, the ability to fall pregnant decreases. Image modified from Li et al., 2012[49].

The menopausal transition period, which includes the final menstrual cycle, starts, on average, at age 46 (but can start at any age between 34 and 54), with the final menopause reached at an average age of 51. The first symptomatic indications of advanced reproductive aging[52] are shortening and irregularity of menstrual cycles, and a decrease in follicles. Ovarian reserve markers such as the antral follicle count (AFC) and serum anti-Müllerian hormone (AMH) levels allow assessment of the ovarian reserve to estimate the remaining reproductive life.

2.2 Mechanisms underlying the ovarian aging process

Chromosomal aberrations during female meiosis, mitochondrial dysfunction, oxidative stress, and DNA damage, among others, have been identified as the significant underlying etiologies of age-related decline of oocyte quality[53,54] (Figure 10).
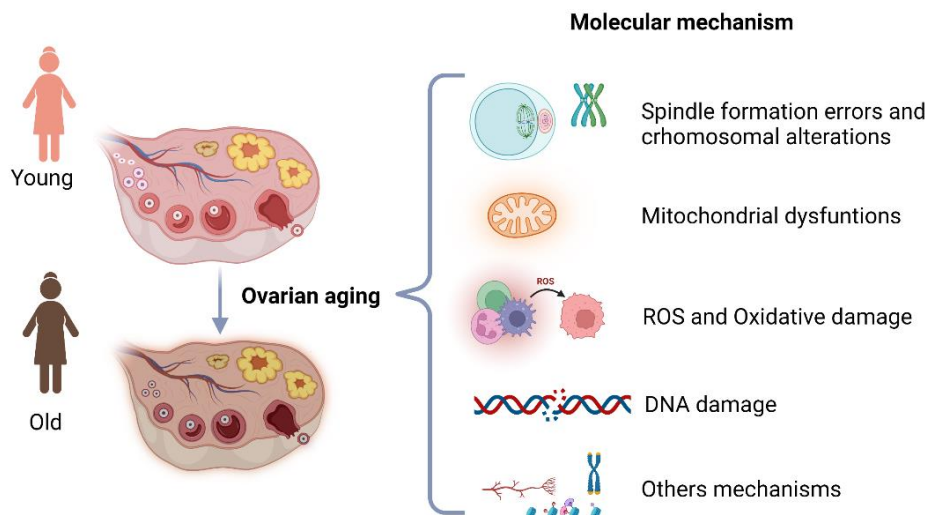
Figure 10. Mechanisms underlying ovarian aging. Image created with biorender.com.

2.2.1 Spindle formation error and chromosomal alterations

Chromosome missegregation during female meiosis is the leading cause of pregnancy loss and human infertility. To prevent aneuploidy, mechanisms that ensure accurate meiotic division and chromosome segregation are essential during oocyte development. Chromosome separation is driven by the interaction between spindle microtubules and kinetochores. Studies with aging mouse oocytes showed that altered spindle microtubule dynamics result in mistakes during sister chromatid separation[55], giving rise to embryo aneuploidies.

These mistakes in meiosis during ovarian aging are not only attributed to cytoplasmic defects in the microtubule cytoskeleton but also to changes in chromosome-related proteins (such as kinetochores and cohesins), which can lead to chromosome separation[56].

Centromere chromatin, which is also responsible for the chromosomal anomaly, disappears with increasing maternal age. Fragmented kinetochores are abnormally attached to spindle microtubules, affecting the oocyte quality[57]. Studies in mice and humans have shown that with increasing female age, chromosomal cohesion in oocytes naturally deteriorates.[58,59] Decreased cohesion leads to increased chromosome segregation errors, premature chromatid separation, and aneuploidy[60].

2.2.2 Mitochondrial dysfunctions

Mitochondria are essential organelles that produce energy by aerobic respiration. Human mitochondrial genetic material (mtDNA) is approximately 16.6 kb long, double-stranded, circular, and lacks histones. It contains 37 genes encoding 2 mitochondrial rRNAs, 22 tRNAs, and 13 protein subunits of oxidative phosphorylation complexes (OXPHOS) I, III, IV, and V. The rest of the mitochondrial proteome, consisting of about 1,500 proteins, is encoded in the nuclear DNA (nDNA)[61,62].

The mtDNA is maternally inherited and is redundant, present in multiple copies in each mitochondrion. Each animal cell contains between 100 and 10,000 copies of mtDNA. However, this number varies significantly according to cell type, tissue stage of development, as well as in various pathological conditions and during the aging process[62]. In the case of oocytes, mitochondria are the most abundant organelle in the cytoplasm. However, their concentration varies depending on the developmental stage of the egg. Dormant oocytes in primordial follicles contain fewer than 10,000 mitochondria[63], and metaphase II (MII) oocytes at mid-ovulation may have up to 1.5 million[64]. Mature oocytes have the highest mitochondrial content in human cells, which may be due to the enormous energy demands of oocyte fertilization and early embryo development[65.] In oocytes, mitochondria are closely related to the decline in oocyte quality with age[66].

Since a large amount of ATP is consumed in meiosis, fertilization, and embryonic development, it is a likely that decreased ATP production due to impaired mitochondrial function results in reduced oocyte quality[67]. In addition, this decreased ATP production in the oocyte may be responsible for spindle misassembly during meiosis.

Errors in mtDNA replication have been linked to aging, causing mutations and depletions in the mitochondrial genome[68]. The mtDNA is vulnerable and easily mutated due to its proximity to the reactive oxygen species (ROS)-producing respiratory chain, lack of protective histones, and the deficiency of efficient repair mechanisms[69]. Mutations of mitochondrial genes, in turn, lead to reduced mitochondrial function[70].

During aging, the mtDNA copy number decreases due to ROS produced in the mitochondrial matrix. In this regard, several reports have shown that aging causes

mtDNA damage and dysfunction[71–73]. In these cases, the quantification of mtDNA damage and mtDNA copy number may be promising biomarkers for disease progression and therapy development[74]. In non-pathological or aging-related conditions, mtDNA quantification is also a good indicator of mitochondrial mass. Since mtDNA levels remain almost constant in a normal/healthy physiological state, the assessment of mtDNA copy number can be a good indicator of the mitochondrial mass in a diseased state. Recent studies have linked lower mtDNA copy numbers to poorer oocyte quality, and thus employed copy number as a marker of quality[75–77].

Mitochondrial fusion and fission also play a critical role in maintaining mitochondrial activity. Genes such as mitofusin 1 and 2 mediate these processes, and associated deficiencies due to aging could affect oocyte quality. Specific deletion of these genes in oocytes results in severely reduced oocyte quality, with elevated ROS levels[78,79].

2.2.3 Reactive oxygen species and oxidative damage

ROS are highly reactive molecules containing oxygen with unpaired electrons. ROS are constantly generated in the mitochondria of aerobic organisms but are also removed by antioxidant enzymes in the mitochondria, thus maintaining redox balance and homeostasis[80]. Under normal physiological conditions, ROS mediate several responses, including cell differentiation, migration, and proliferation[81]. However, redox balance is lost when excessive ROS are generated, or antioxidant capacity is reduced due to aging. ROS accumulates, inducing apoptosis, associated follicular atresia, and a decline in oocyte quality[82]. Therefore, excess ROS harms ovarian aging, affecting different processes such as deterioration of mitochondria and spindle formation error but also DNA damage, lipid peroxidation and protein degradation[83,84] (Figure 11). Reactive molecules not only attack DNA to cause DNA damage and adduct formation (i.e., DNA double-strand breaks, 8-hydroxy-2-deoxyguanosine/8-oxo-dG) but also lead to protein oxidation and lipid peroxidation[85].

Some secondary intermediates of ROS, such as 4-hydroxy-2-nonenal (4-HNE) are responsible for oxidative damage[86]. Moreover, 4-HNE is employed as a biomarker of oxidative stress and identified as one of the most formidable reactive aldehydes[87]. In

ovarian aging, lipid peroxidation, and its electrophilic product 4-HNE, affect folliculogenesis and oocyte meiosis[88], contributing to the accumulation of spindle assembly defects, chromosome misalignments, and aneuploidy[89].
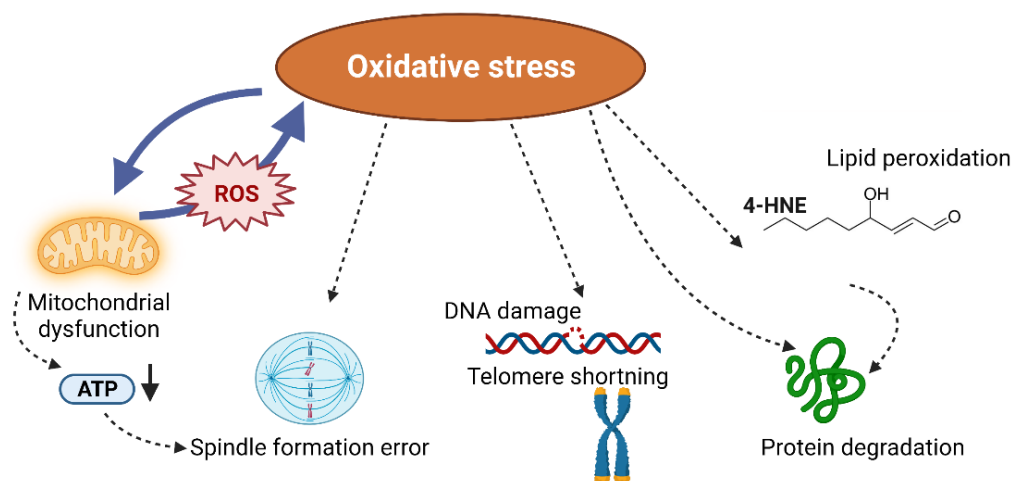
Figure 11. Effect of oxidative stress. Reactive oxygen species (ROS) in dysfunctional mitochondria produce oxidative stress in ovaries, generating spindle oocyte mistakes, DNA damage, lipid peroxidation, and protein degradation. Image modified from Sasaki et al., 2019 with biorender.com.

2.2.4 DNA Damage

DNA damage, especially double-strand breaks (DSBs), occurs constantly in all cells and can be due to endogenous causes such as the ROS-induced oxidative stress (discussed above), but also due to exogenous genotoxic stress, such as chemotherapeutic treatment or radiation[90].

The primordial follicles, which constitute the ovarian reserve, are arrested in prophase meiosis for a long time until they are activated and are therefore very susceptible to the accumulation of endogenous and exogenous DNA damage. Indeed, follicles cannot be replaced, making them the longest-lived cells in the female body, and therefore potentially vulnerable to DNA damage[91].

Cells have efficient mechanisms to repair DNA damage and thus prevent chromosomal aberrations and mutations. However, there is increasing evidence of an association between DNA damage, oocyte repair capacity, and maternal age. Different studies have

shown that the efficiency of the mechanisms involved in DNA repair are affected by age, leading to the accumulation of mutations over time[92,93]. In oocytes, this could lead to poor quality, apoptosis, and ultimately infertility[94].

There are different repair pathways: base excision repair, nucleotide excision repair, mismatch repair, non-homologous end joining, and homologous recombination (HR)[95].

The HR pathway occurs in the oocyte at all stages of folliculogenesis[96] [97]. The HR pathway starts with the detection and recognition of DNA DSBs by the meiotic recombination 11-Rad50-Nijmegen (MRE11-RAD50-NBS1) break syndrome 1 (MRN) complex, which triggers phosphorylation of ataxia telangiectasia mutated (ATM). Activation of ATM results in phosphorylation of several DNA damage response kinases, such as histone protein H2A family member X (H2AX), checkpoint kinase 2 (Chk2), and p53 (TAp63α in primordial oocytes). Mediator DNA damage checkpoint protein 1 (MDC1) binds to γH2AX via breast cancer susceptibility gene 1 (BRCA1) and forms foci that co-localize with γH2AX. HR activation generates single-stranded DNA in multiple steps, requiring a specific factor, the replication protein A (RPA). The RPA complex of the ssDNA-binding protein in oocytes is replaced by Rad51, and meiotic cDNA1 (DMC1) breast cancer susceptibility gene 2 (BRCA2), which repairs the DNA[98] (Figure 12A).
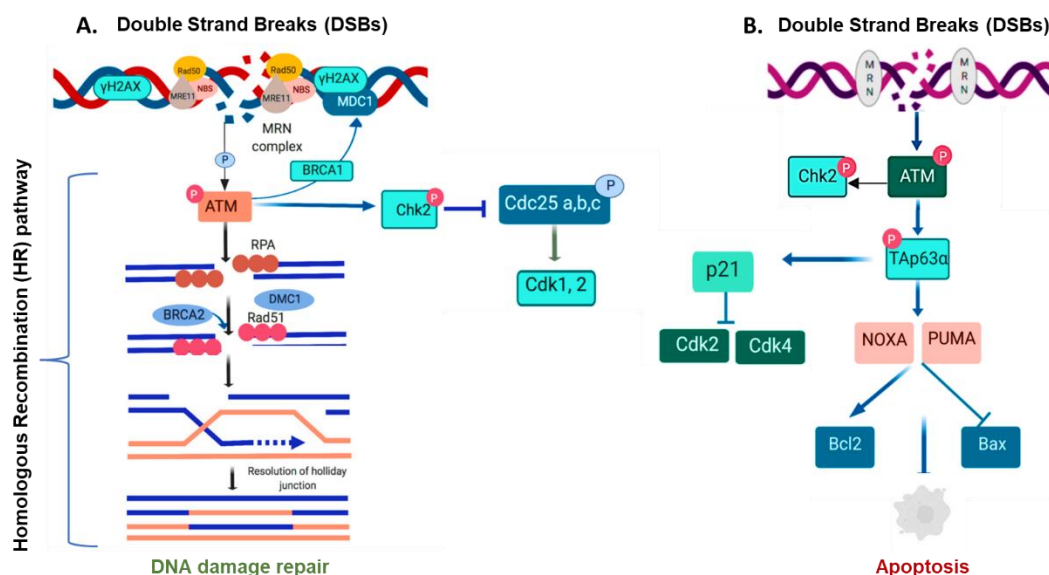
Figure 12. DNA double-strand breaks response pathway. (A) Homologous recombination (HR) repair pathway to combat DNA DSBs and repair. (B) Apoptosis pathway to respond to excessive or irreparable DNA damage. Image modified from Maidarti et al., 2020[98].

Alternatively, TAp63 can induce an apoptotic signaling pathway in response to excessive or irreparable DNA damage. Induction of p53 upregulates the modulator of apoptosis (PUMA) and NOXA[99]. Apoptosis is then controlled by the balance between anti-apoptotic B-cell lymphoma 2 (Bcl2) protein and proapoptotic Bcl2 associated with X activity (BAX) protein[100] (Figure 12B).

2.2.5 Other mechanisms

The condition of the ovarian stroma is affected by age, with decreased blood vessels, hyaluronic acid, and cell proliferation and increased fibrosis and apoptosis over time. An impaired ovarian stroma is characterized by a decrease in the number and quality of eggs and may affect follicular development and oocyte quality[101–103].

Inappropriate epigenetic modifications in the DNA of reproductive cells [104] and telomere shortening[105,106] also play a critical role during the aging process of oocytes.

2.3 Alterations of female fertility

There are conditions in which ovarian function is impaired or the process of ovarian aging accelerated, irrespective of age.

2.3.1 Diminished ovarian reserve

Diminished ovarian reserve (DOR) is a physiological process caused by reduced follicle number. As mentioned above, this process begins at 30 years old and is exacerbated until menopause[44]. However, some women may suffer from pathological DOR when their ovarian reserve decreases earlier than usual, and they subsequently become prematurely infertile. These patients usually have regular menstrual cycles but a low response to ovarian stimulation regimens and abnormal ovarian reserve values[107].

In assisted reproduction, 10-25% of treatment patients exhibit an inadequate response to gonadotropin-controlled ovarian hyperstimulation (COS) and are referred to as Poor Ovarian Response (POR) patients[108].

Regardless of the cause of DOR, up to one-third of these patients experience a POR to COS, leading to cycle cancellation and a reduced chance of a live birth[109]. The most critical limitation in treating these patients is the heterogeneity of the population included in this definition, which is given by grouping women with different biological characteristics and, therefore, different prognoses.

2.3.2 Premature ovarian insufficiency

Premature ovarian insufficiency (POI) is an ovarian defect characterized by the absence of menarche (primary amenorrhea) or premature depletion of ovarian follicles before the age of 40 years (secondary amenorrhea)[110]. This disorder affects approximately 1 % of women under 40 years of age and 0.1 % under 30[111]. Women with primary POI have no pubertal development, whereas, in secondary POI, there is usually normal puberty with subsequent disappearance of menstrual cycles. Secondary POI is characterized by the absence of menses for at least four months, in combination with low levels of gonadal hormones (estrogens and inhibin), and high FSH levels (greater than 25IU/L), occurring before the age of 40 years (Figure 13).

The causes of POI include chromosomal abnormalities, ovarian surgeries, autoimmune diseases, infections, metabolic disorders, and oncologic therapies[112].

Women with POI have a very low spontaneous pregnancy rate[113], and therefore new strategies to improve their reproductive potential are required.
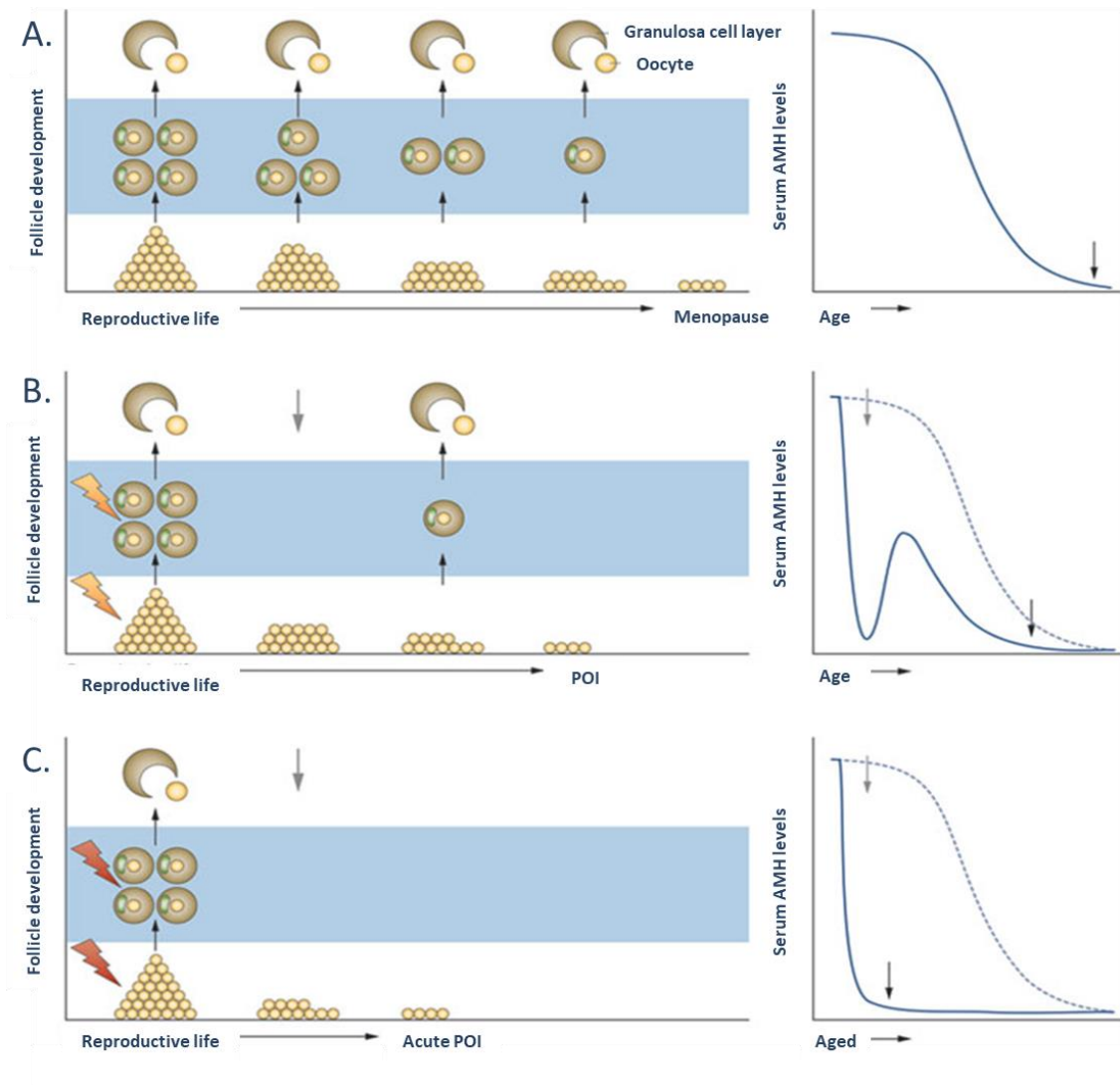
Figure 13. Effects of ovarian aging on ovarian reserve and AMH levels. (A) Typical physiological ovarian aging, which is characterized by a progressive decline in follicle number and anti-Müllerian hormone (AMH) levels with increasing biological age. (B) An altered normal ovarian function profile (e.g., Diminished ovarian reserve (DOR)) characterized by follicle count and AMH levels decreasing earlier than usual. (C) Premature ovarian insufficiency (POI) profile, where no antral follicles are produced, and AMH levels are almost undetectable. In all cases, when ovarian function is lost, residual primordial follicles remain. Image modified from Visser et al., 2012[114].

3. Strategies to improve the reproductive potential of patients with compromised ovarian function

As we have described above, age is one of the leading causes of infertility[115]. Thus, age-related infertility and low ovarian reserve represent a clinical challenge because, although various therapeutic interventions are aimed at increasing their reproductive potential[116,117], all these interventions have limited and poorly reproducible efficacy.

3.1 Assisted reproductive techniques based on controlled ovarian stimulation

Among the options available to these patients are therapies based on the hormonal stimulation process. These strategies include increasing FSH doses, administering FSH in the luteal phase, using recombinant FSH instead of purified urinary FSH, modifying pituitary desensitization protocols, pre-treatment with estrogens or combined oral contraceptives, and pre-treatment with androgens[118–120]. However, due to the low number of antral follicles susceptible to stimulation, these strategies generally do not produce good outcomes.

Therefore, the only clinical alternative available to such women is oocyte/egg donation, which allows women to fall pregnant regardless of age or oocyte status. However, it is not a suitable option in all cases, as it may be unacceptable to a patient depending on ethical, religious, regulatory, and even economic reasons.

3.2 Bone marrow-derived stem cells (BMDSCs)

Recent studies have shown that there are residual follicles in the ovaries of POI patients that can be activated by *in vitro* activation and fragmentation treatments, resulting in mature oocytes, and giving rise to successful pregnancies and healthy children[121–124]. This approach could help to improve the reproductive potential of women undergoing chemotherapeutic treatments or other conditions of low ovarian reserve, in which, even when the ovary loses its function and capacity to ovulate, a small group of follicles is susceptible to rescue.

With the development of regenerative medicine, various stem cells (SCs), including adult SCs[125], are increasingly being considered to improve the reproductive potential of patients with impaired ovarian function. Adult SCs are present in different tissues, where they act as a reservoir to replace damaged and senescent cells[126]. Although numerous somatic SCs have been identified, one of the most studied to rescue fertility are the bone marrow-derived stem cells (BMDSCs). Indeed, years ago it was suggested that BMDSCs may be responsible for rescuing residual primordial follicles and fertility after bone marrow transplantation in oncologic patients[127–131], suggesting the potential of BMDSC-based therapies as an alternative treatment to recover fertility.

3.2.1 Characteristics of BMDSCs

Bone marrow is rich in SCs, including hematopoietic stem cells (HSCs) that can give rise to all blood cell types, and mesenchymal stem cells (MSCs), which have the ability to differentiate into various cell types, including osteocytes, chondrocytes, adipocytes, hemocytoblasts, mast cells, and fibroblasts[132,133] (Figure 14).
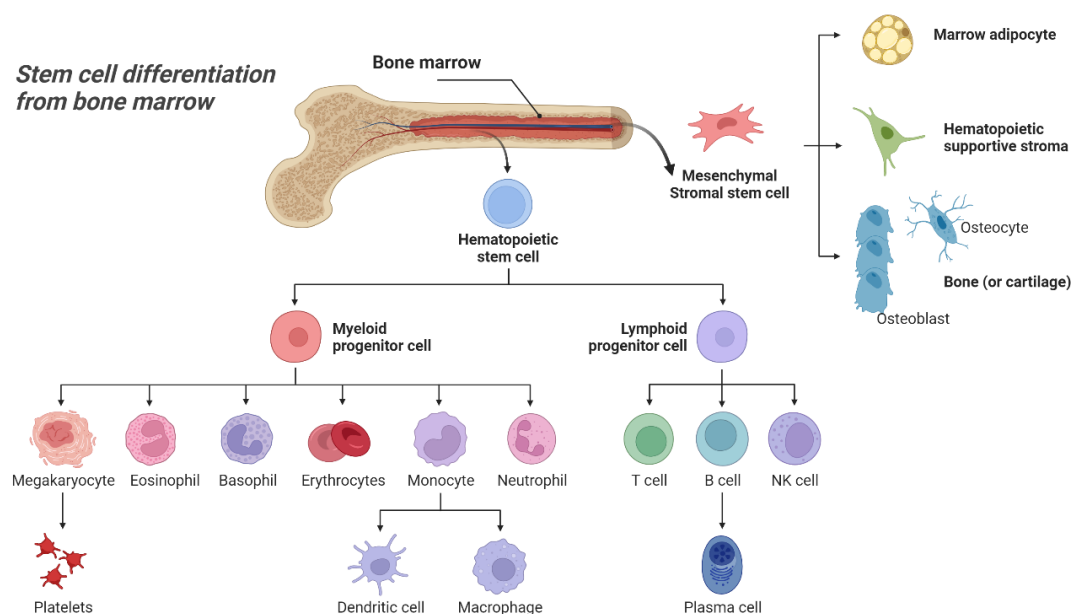
Figure 14. Stem cell differentiation from bone marrow. Within the bone marrow, we can distinguish between two major stem cell populations: hematopoietic stem cells (HSCs), which can give rise to all cell types of the hematopoietic lineage, and mesenchymal stem cells (MSCs). Image adapted from "Stem Cell Differentiation from Bone Marrow" by BioRender.com.

Cell therapy with BMDSCs presents certain advantages that make these therapies of particular interest. Firstly, their safety is supported by data obtained after transplantation or infusion in treating different diseases[134,135]. Secondly, improved collection protocols from peripheral blood after mobilization or by iliac crest puncture make them an attractive and ethically robust source of autologous SCs[136].

Mobilization of SCs from bone marrow to peripheral blood through pharmacological treatments has become the gold-standard for autologous transplantation, as this avoids invasive iliac crest puncture and technical difficulties[137]. The most utilized mobilization treatment in clinical practice is granulocyte-colony stimulating factor (G-CSF) administration. G-CSF is a hematopoietic growth factor that modulates hematopoiesis and the immune system. It is widely used in the clinic to increase hematopoietic cell proliferation and differentiation and to activate neutrophil functions[138]. Once mobilized, SCs can be isolated from peripheral blood by apheresis and subsequent density gradient centrifugation[139]. The product of this centrifugation contains HSCs, MSCs, and cells committed to a cell lineage at various stages of maturation.

3.2.2 BMDSC-based therapies to restore ovarian function

Studies performed by different groups in animal models of ovarian failure confirm the regenerative effects of BMDSCs in restoring hormone production, reactivating folliculogenesis, and improving ovarian stromal status[140–144]. Similarly, clinical trials have been conducted wherein BMDSCs restore menstruation, improve ovarian reserve markers, and allow pregnancies and births.

Previously, our group aimed to evaluate whether BMDSCs infusion promoted follicular growth in a murine model of DOR and POI induced by chemotherapy[145] (Figure 15). In this study, BMDSCs reached the ovarian niche, settling mainly near vessels and follicles. They promoted follicular growth to the preovulatory stage, increased vascularization and cell proliferation, and inhibited apoptosis in chemotherapy-damaged mouse ovaries. In addition, BMDSCs infusion restored the estrous cycle, which had been previously disrupted due to chemotherapy treatments. Ovulation capacity was also improved in the

two chemotherapy doses studied, increasing the number of MII oocytes and embryos retrieved.
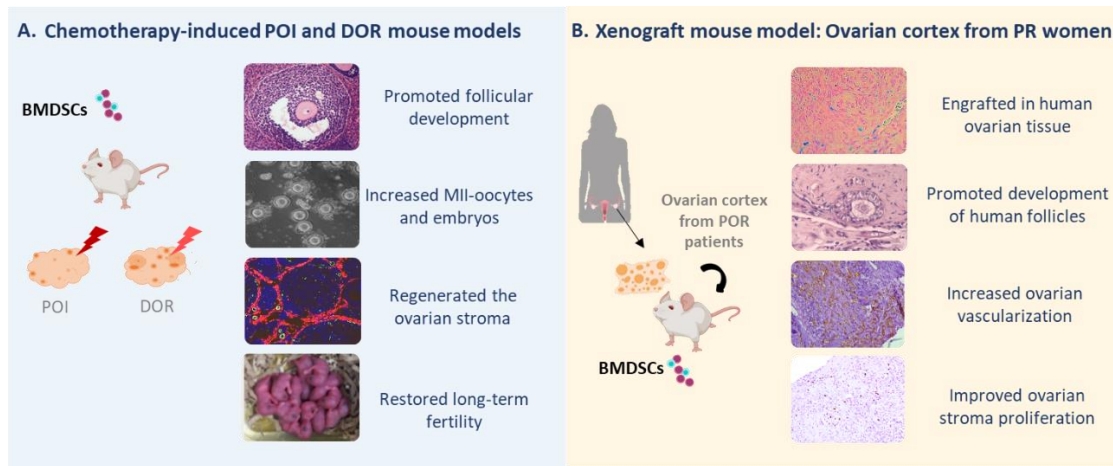
Figure 15. Effects of BMDSCs in animal models. (A) Regenerative effects of bone morrow-derived stem cells (BMDSCs) in mouse models of diminished ovarian reserve (DOR) and premature ovarian insufficiency (POI). (B) Corroboration of the BMDSCs positive effects in human ovarian tissue from poor ovarian response (POR) patients by employing a xenotransplant model. Image created by Herraiz et al. 2018[145].

Furthermore, these positive effects were also validated in human ovarian tissue from POR patients[145] (Figure 15). In this case, BMDSCs were able to rescue residual primordial follicles. In addition, they stimulated vascularization and proliferation of the ovarian stroma, thus generating an appropriate niche to support growth of activated follicles.

Following this, the therapeutic potential of such treatment was tested in a prospective pilot study in POR women[146]. In that study, autologous stem cell ovarian transplant (ASCOT) improved ovarian function biomarkers in 81.3% of women, as measured by antral follicle count and/or serum anti-Müllerian hormone. BMDSCs also allowed pregnancies and live births in poor-prognosis women, where oocyte donation was previously the only clinical option. A total of six pregnancies were achieved (3 by IVF and 3 spontaneous conceptions), and three healthy babies were born after BMDSC administration.

3.2.3 Mechanisms of action of BMDSCs

Different mechanisms have been proposed by which SCs could exert their regenerative effects in damaged or aged tissues. Regarding BMDSCs, it was initially proposed that the primary mechanisms underlying their therapeutic action were transdifferentiating into tissue-derived and vascular lineage cells[147]. However, the paracrine signaling, through secretion of cytokines, chemokines, and growth factors with crucial functions in tissue repair, has recently been proposed as the primary mechanism by which adult SCs exert their regenerative effects[148–151].

BMDSCs secrete cytokines and factors such as vascular endothelial growth factor (VEGF), fibroblast growth factor-2 (FGF-2), insulin-like growth factor (IGF), hepatocyte growth factor (HGF), and interleukin (IL)-6, among others[152]. This paracrine signaling is essential in angiogenesis, anti-inflammation, immunomodulation, anti-apoptosis, and proliferation, thus improving the microenvironment to promote the recovery of damaged tissue (Figure 16).
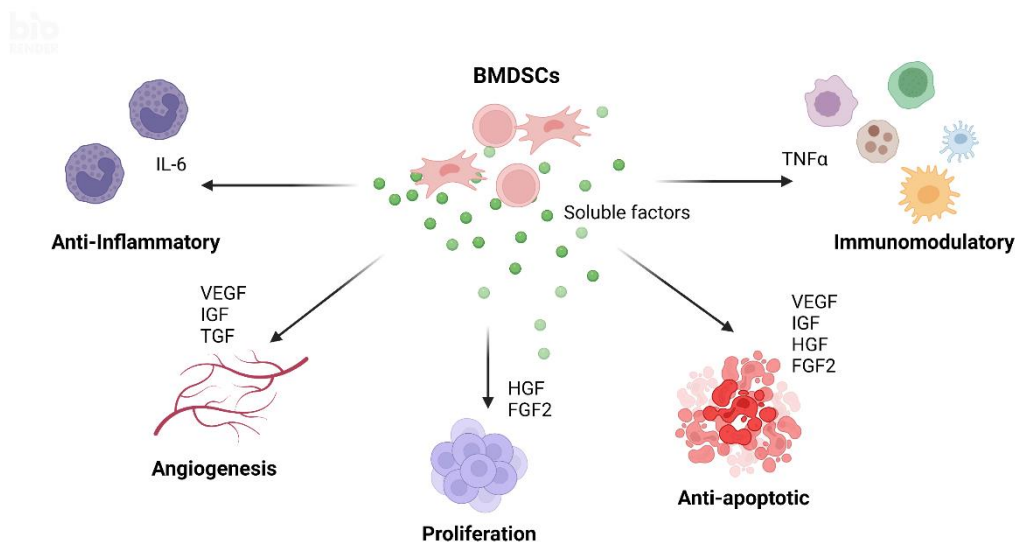
Figure 16. Paracrine mechanism of action of BMDSCs. Bone marrow-derived stem cells (BMDSCs) can exert their effects by secreting soluble factors such as chemokines and cytokines, which are involved in processes such as anti-inflammation, angiogenesis, proliferation, anti-apoptotic functions, and modulation of the immune response. Image created with biorender.com.

Indeed, a direct effect of SCs on tissue repair is unlikely as the number of cells present in damaged tissues after the infusion is too low to explain the functional improvement

observed[145,151,153,154]. Moreover, exposure to stem cell-conditioned media causes the same positive effects as cellular infusion upon the injured ovary [155].

This paracrine mechanism could explain the correlation observed between the positive ovarian response of POR patients after ASCOT, and the increased plasma levels of FGF-2 and thrombospondin-1 (THSP-1) into the plasma of apheresis[146].

3.3 Plasma-based treatments

Based on the paracrine mechanisms discussed above and the effects observed in stem cell studies, the administration of specific proteins or plasma-containing factors secreted by SCs has been proposed as an alternative therapy to the use of SCs.

3.3.1 Young blood

The human umbilical cord was first successfully tested as a source of MSCs for cell therapy[156], and its potential as an alternative therapeutic option for chemotherapy-induced POI was evaluated[141,157–159]. However, the low survival rate and uncertain efficacy of these SCs after transplantation still limit their clinical application.

Recently, the injection of young, growth factor-enriched plasma, umbilical cord blood (UCB) plasma, or plasma-specific proteins into damaged and aged organisms has been proposed to stimulate nervous tissue regeneration and repair[160–162]. In these studies, UCB is shown to have a rejuvenating effect and stimulate neurogenesis, which improves hippocampal functioning, cognitive function, learning ability, and memory in old mice. Castellano et al. (2017) showed that UCB plasma contained plasticity-enhancing proteins of high translational value for targeting aging- or disease-associated hippocampal dysfunction.

Other studies have demonstrated that the regenerative effects observed after UCB plasma administration could be mediated by cytokines and growth factors present in plasma[163,164]. Romanov et al. (2019) determined the content of biologically active molecules, cytokines, and growth factors in UCB samples to confirm the paracrine

mechanisms of action. This study showed that UCB plasma is a rich source of cytokines and growth factors with pronounced anti-inflammatory, angiogenic, and anti-apoptotic effects.

3.3.2 Platelet-rich plasma

Intraovarian injection of platelet-rich plasma (PRP) has been proposed among the strategies for ovarian reactivation. PRP is a component of blood that remains after *in vitro* removal of red and white blood cells, which contains platelets, cytokines, growth factors, and small molecules[165]. Indeed, PRP is mainly composed of growth factors such as platelet-derived growth factor (PDGF), fibroblast growth factor (FGF), VEGFs, epidermal growth factor (EGF), and transforming growth factor β-1 (TGF-β1), among others.

In human reproductive medicine, one of the first research groups to use PRP was Callejo et al. (2013). They implanted cryopreserved human ovarian tissue into the peritoneum using PRP as a proangiogenic and proliferative agent, leading to live birth[166]. Subsequently, numerous authors have studied the effect of PRP in improving female fertility from different perspectives. The largest cohorts published to date and the main findings are shown in Table 1.

Table 1. The largest human clinical studies of platelet-rich plasma (PRP) intraovarian injection to rescue fertility.

Authors	Characteristics of the study population			Methods		Fertility outcomes
	Number (n)	Age (Years old)	Ovarian condition	PRP treatment	Key measurements	
Cakiroglu et al. (2020)	311	24-40	POI	Intraovarian injection of 2 to 4 ml of PRP (non-activated) in each ovary.	-Serum levels of FSH, AMH, and AFC after PRP therapy. -Pregnancies (IVF cycle or spontaneous)	-AMH levels and AFC improved after PRP treatment. -Spontaneous pregnancy was achieved in 23 of 311 women, and 16 resulted in sustained implantation or live birth. -201 patients attempted IVF. 57 of the 82 women who developed embryos underwent embryo transfer, 9 resulted in sustained implantation or live birth[167].
Jackman et al. (2020)	140	42-44	DOR	Intracortical injection of 200 μL of PRP (non-activated).	AFC before and after PRP injection (once a week for a total of 6 weeks).	-AFC increased significantly in both ovaries after PRP treatment[168].
Melo et al. (2020)	83	39-44	DOR	Intracortical injection of 200 μL of PRP (activated by calcium chloride) in each ovary monthly for three consecutive cycles.	-Serum levels of FSH and AMH, and AFC before and after PRP therapy. -IVF cycle.	-A significant increase in FSH, AMH and AFC was observed after PRP treatment. -PRP increased the pregnancy rates. There was no difference between groups (PRP and control) between first-trimester miscarriage and live birth rates[169].
Sfakianoudis et al. (2020)	120	36-50	POI POR Premenopausal Menopausal	Intraovarian injection of 4 ml of PRP (activated by calcium gluconate).	-In POR women, AMH levels and AFC in POI, perimenopausal and menopausal women, restoration of the menstrual cycle and FSH levels before and after PRP therapy. -Pregnancies and live births (IVF cycle and spontaneous).	-Menses was restored for POI patients (18 of 30) after PRP. AMH and AFC improved significantly, with 3 spontaneous pregnancies and live births. -For POR women, there was an improvement in pregnancy rates after ICSI cycles. -For perimenopausal women, PRP improved hormone levels and AFC, with

Authors	Characteristics of the study population			Methods		Fertility outcomes
	Number (n)	Age (Years old)	Ovarian condition	PRP treatment	Key measurements	
						four spontaneous pregnancies and three live births noted. -13 of 30 menopausal patients responded positively to PRP treatment, with one spontaneous pregnancy and live birth noted[170].
Sillls et al. (2020)	182	39-51	DOR	Intraovarian injection of 1 mL of PRP (activated by calcium gluconate).	-Serum levels of FSH, estradiol and AMH every two weeks for three months.	-PRP injection increased the levels of AMH in 51 patients at different ages[171].
Parvanov et al. (2022)	66	34-46	POR	Intraovarian injection of 0.5 mL of PRP (activated by calcium gluconate) in each ovary in two subsequent menstrual cycles.	-Serum levels of FSH and AMH, and AFC before and after PRP treatment. -IVF cycle.	-PRP injections decreased the FSH levels, and increased AMH and AFC. -The number and quality of oocytes, the fertilization rate and number of blastocysts were higher after PRP[172].
Cakiroglu et al. (2022)	510	30-45	POR	Intraovarian injection of 4 mL PRP (non-activated) into at least one ovary.	-Serum levels of FSH and AMH, and AFC before and after PRP treatment. -Pregnancies and live births (IVF cycle and spontaneous).	-PRP treatment decreased the FSH levels and increased the AMH and AFC. -22 women conceived spontaneously. -Among women who attempted IVF (474), 312 generated embryos and underwent embryo transfer, achieving 83 pregnancies and 54 sustained implantation and live birth[173].

Introduction

As shown in Table 1, some trials also include a plasma activation phase[169,174,175]. The term activation refers to the degranulation of platelets to release additional growth factors contained in platelets[176]. Different activation protocols are employed, although the most common is by adding calcium chloride ($CaCl_2$).

However, in other studies, PRP is injected without activation[166,177,178], suggesting that spontaneous platelet activation will occur after administration. The automatic mechanism by which platelets are activated is complicated by the involvement of numerous receptors. Spontaneous platelet activation is driven by "outside-in" signaling, initiated through a broad repertoire of G protein-coupled receptors, integrins, and glycoprotein channels on the platelet surface[179], including, among others, thrombin, collagen, adenosine diphosphate (ADP), thromboxanes, serotonin, oxidized LDL, and extracellular divalent cations[179–182] (Figure 17).
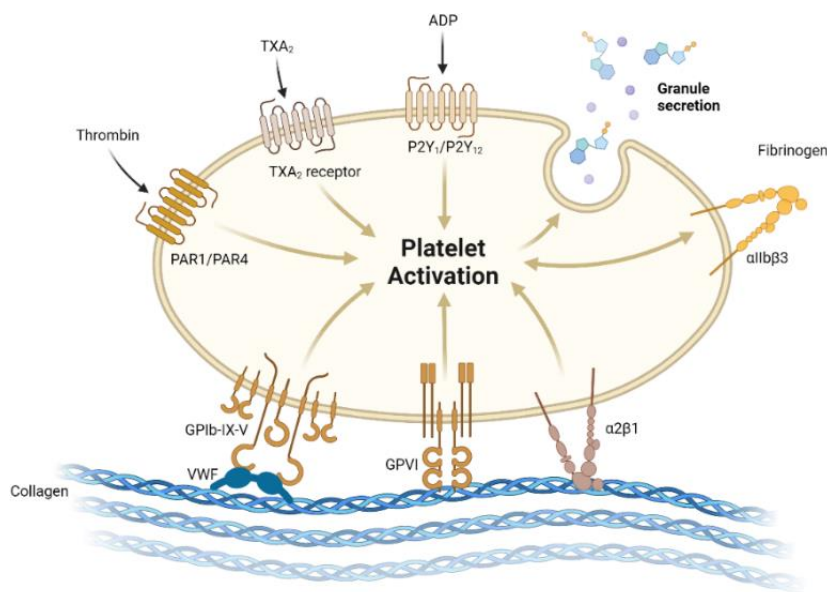
Figure 17. Natural process of platelet activation. Image adapted from "Platelet activation" by BioRender.com.

Recent studies have shown that PRP from resting platelets differs from that containing activated platelets[183].

Numerous clinical trials are investigating PRP as a therapy for improving impaired ovarian function, with encouraging results. However, the protocols and study groups employed vary, and few focus on understanding the mechanisms of action underlying the observed

regenerative effects[184]. Thus, further mechanistic research and preclinical studies[185–188] are still required.

4. Animal models of ovarian aging, DOR, and POI conditions.

Appropriate animal models are needed to understand ovarian aging and find new strategies to delay or reverse DOR and POI conditions[189]. Among the different models employed, *Mus musculus* is the most widely used due to its genetic similarity to humans[190] and similarity in reproductive characteristics[191].

Mouse models established by gene deletion and chemotherapy (ChT) have been used for studying aging and phenotypes comparable to DOR and POI in humans[192].

On the one hand, genetic engineering allows us to study the effects of gene alterations on ovarian aging, such as chromosomal abnormalities and genetic mutations. Brca2 receptor deficiency[193], follicle-stimulating hormone receptor depletion[194], loss of pigment epithelium-derived factor[195], or deletion of mitochondrial genes[76], are knockout models employed to decipher potential mechanisms of ovarian aging, and to study the phenotype of POI women. However, these models have presented some limitations. For example, the ovaries of animals are damaged and affected from the early stages of development and do not mimic reproductive systems in humans. In addition, these models are expensive and complex to generate, which leads to using other animal models such as those induced by ChT.

Clinically, the effect of cytotoxic treatments on the ovary can range from partial damage that reduces fertility, to the destruction of the follicular pool and tissue atrophy, leading to POI and a loss of fertility[196]. The degree of gonadotoxicity differs depending on the ChT drugs and dose, with alkylating drugs carrying the highest risk of ovarian failure[197]. Therefore, these ChT drugs are often employed to establish a mouse model of ovarian damage. Most studies employ high doses of chemotherapy, representing the worst ovarian condition, POI[198,199]. However, our group also developed an animal model to represent less severe conditions such as DOR, using reduced doses of chemotherapy[200].

The mechanisms of action of the ChT drugs are believed to be the induction of DNA damage[201,202], inducing chromosomal aberrations, sister chromatid exchange, DNA adducts, single-strand breaks, and the formation of double DNA crosslinks[203]. In mice, primordial follicles, growing follicles and GCs are the most sensitive to chemotherapy-induced ovarian damage[204]. Thus, these mouse models of ovarian damage allow us to study the effects of ChT on fertility measures, like follicle loss and oocyte death, and are crucial to finding therapies to protect or rescue fertility.

Although knockout and chemotherapy-induced models enable the study of characteristics derived from aging and phenotypes of DOR and POI conditions, they do not represent a progressive and physiological aging mouse model. In this sense, to evaluate potential therapies to slow down or reverse the physiological aging process, it is necessary to develop and characterize an appropriate, economic, and reproducible animal model, displaying most of the ovarian characteristics of different stages during women's reproductive life.

II. HYPOTHESIS

II. HYPOTHESIS

Adult stem cells derived from bone marrow can repair damaged mouse and human ovarian tissue by promoting follicular development and stromal regeneration, through the secretion of soluble factors and cytokines in a paracrine manner. Therefore, plasma rich in factors secreted by stem cells could be a suitable therapy to improve the reproductive potential of patients with impaired ovarian function.

Hypothesis

III. OBJECTIVES

III. OBJECTIVES

1. Main objective

The main objective of this doctoral thesis is to evaluate whether the administration of plasma rich in factors secreted by stem cells presents an alternative therapy to improve the ovarian function of DOR and POI patients, or women with age-related fertility problems.

2. Secondary objectives

To achieve the main objective, the work was divided into different phases:

A) REGENERATIVE EFFECT OF DIFFERENT PLASMA SOURCES, RICH IN GROWTH FACTORS, IN MOUSE MODELS OF OVARIAN DAMAGE INDUCED BY CHEMOTHERAPY

1. To assess the ability of different plasma sources rich in factors secreted by different stem cell types, such as bone marrow stem cells (BMDSC plasma), and umbilical cord blood (UCB plasma) stem cells, to promote follicular development, ovulation, and fertilization in DOR and POI models.
2. To analyze the effect of BMDSC and UCB plasmas on pregnancy rate and litter size.
3. To evaluate the effects of the injection of these plasmas on the ovarian niche: analysis of vascularization, proliferation, degeneration, and apoptosis.
4. To evaluate whether the activation of plasmas in order to release platelet contents improves regenerative effects.
5. To characterize the composition of the different plasmas to understand the mechanisms underlying treatments.
6. To study DNA repair pathways in an *in vitro* model of chemotherapy-induced ovarian damage.

B) EVALUATION OF THE MOST BENEFICIAL PLASMA TREATMENT ON HUMAN OVARIAN TISSUE

1. To validate the regenerative effects of activated BMDSC plasma (aBMDSC) in human ovarian tissue from POR patients by employing a xenotransplant model and analyzing follicle development and stroma regeneration.

41

Objectives

2. To elucidate the mechanisms responsible for the regenerative effects of aBMDSC plasma in human ovarian tissue.

C) DEVELOPMENT AND VALIDATION OF A MOUSE MODEL OF PHYSIOLOGICAL OVARIAN AGING

1. To characterize a physiological reproductive aging mouse model displaying most ovarian characteristics of different stages during women's reproductive life.

2. To evaluate different reproductive variables (ovarian reserve and stroma, number of oocytes and embryos, MII oocyte quality, *in vitro* embryo development, mitochondrial dysfunctions, and ovarian proteomic profile) to determine if the model can be used to test therapies for women with age-related fertility problems.

D) INTRAOVARIAN ADMINISTRATION OF THE MOST BENEFICIAL PLASMA TREATMENT IN A PHYSIOLOGICAL AGING MOUSE MODEL

1. To assess the ability of a single intraovarian injection of activated platelet-rich plasma (aPRPa) and the combination of factors secreted by BMDSCs and contained in platelets (aBMDSC), to promote follicular activation and development in a physiological ovarian aging model.

2. To analyze the effect of intraovarian injection of aPRP and aBMDSC on ovulation rate, oocyte quality, and embryo development.

3. To analyze the effects of plasma on ovarian stroma by studying proliferation and vascularization.

4. To study mitochondrial dysfunction, oxidative damage, and apoptosis after intraovarian administration of plasma.

5. To evaluate if there are changes at the proteomic level after plasma administration and to study the differential biological pathways involved.

IV. MATERIAL AND METHODS

IV. MATERIAL AND METHODS

In the Ph.D. thesis work herein, we first evaluated the potential of systemic administration of different plasma sources, rich in factors secreted by bone marrow-derived stem cells (BMDSC plasma) or umbilical cord stem cells (UCB plasma), to recover the ovarian function of chemotherapy-induced DOR and POI murine models. Moreover, we also assessed the additional effect of plasma activation, i.e., the release of factors contained in platelets, on reproductive outcomes (Phase A). We also characterized the protein profile of different plasmas tested to establish the potential mechanisms underlying the observed regenerative effects. Based on these results, we studied the role of plasmas in DNA repair, by performing an additional in vitro experiment with mice ovaries exposed to chemotherapy. Then, due to the functional differences between murine and human ovaries, we evaluated the most beneficial treatment in human ovarian tissue (Phase B). Plasma combining factors secreted by both bone marrow derived stem cells and platelets (aBMDSC) was tested in human ovarian tissue from POR patients xenografted into immunodeficient mice.

Finally, given the increasing number of patients with age-related ovarian infertility requiring novel therapeutic approaches, we developed a physiological aging mouse model, displaying most of the ovarian characteristics of different stages during women's reproductive life (Phase C). This model allowed us to evaluate the regenerative effects of aBMDSC as a therapy for treating age-related infertility (Phase D). Their effects were compared with platelet-rich plasma (aPRP), and both plasmas were administered by a single intraovarian injection to bring the treatment's administration closer to clinical practice.

A) REGENERATIVE EFFECT OF DIFFERENT PLASMA SOURCES, RICH IN GROWTH FACTORS, IN MOUSE MODELS OF OVARIAN DAMAGE INDUCED BY CHEMOTHERAPY

1. Ethical approval

Material and Methods

All study procedures were approved and conducted according to the Institutional Review Board of Hospital Universitario y Politécnico La Fe, Valencia, Spain (2014/0147) and the Institutional Review Board and the Ethics Committee from University of Valencia, Valencia, Spain (A1510574679987).

2. Animal housing

The animal experimentation was carried out in the authorized animal house of the Faculty of Medicine of the University of Valencia, by current regulations and respecting the handling and euthanasia procedures recommended by the Spanish and European legislation (Royal Decree 1201/2005, B.O.E. 252, October 10, 2005, and the European 2005 and the European Convention 1-2-3, March 18, 1986).

During the experiment, mice were housed in a specific pathogen-free area under constant temperature (23ºC) and humidity (60–70%), with a 12-h light/dark cycle and free access to the standard rodent diet and water.

3. Experimental design

3.1 Study of the systemic administration of different human plasma sources in chemotherapy-induced ovarian damage models.

To assess the potential regenerative effects of plasmas on mouse ovarian tissue, we employed two previously established animal models of chemotherapy-induced ovarian damage: DOR and POI models[200]. DOR and POI were induced in immunodeficient NOD/SCID mice by reduced and standard ChT regimens, respectively. One week later, when ovarian damage was established, DOR and POI animals were allocated (n = 11 per group) into seven experimental groups receiving injections of: (1) saline (ChT); (2) peripheral blood plasma from women with POR (PB plasma); (3) activated PB plasma from women with POR (aPB plasma); (4) Plasma rich in factors secreted by BMDSCs (BMDSC plasma); (5) activated BMDSC plasma (aBMDSC plasma); (6) plasma rich in factors secreted by umbilical cord stem cells (UCB plasma); or (7) activated UCB plasma (aUCB plasma). Treatments were administered every other day for 2 weeks though tail

vein injection (100 uL/day). Following treatment, mice underwent ovarian hyperstimulation before mating with fertile males. Then, some of the females (n= 7 / group) were euthanized, and ovaries and oviducts recovered to analyze the short-term effects of plasma administration. The remaining animals (n = 4 / group) were not sacrificed and were used to assess the long-term effects on breeding performance.

To provide reference values for the different study variables, NOD/SCID females without chemotherapy and plasma treatment (n= 11, wild-type group) were used (Figure 18).
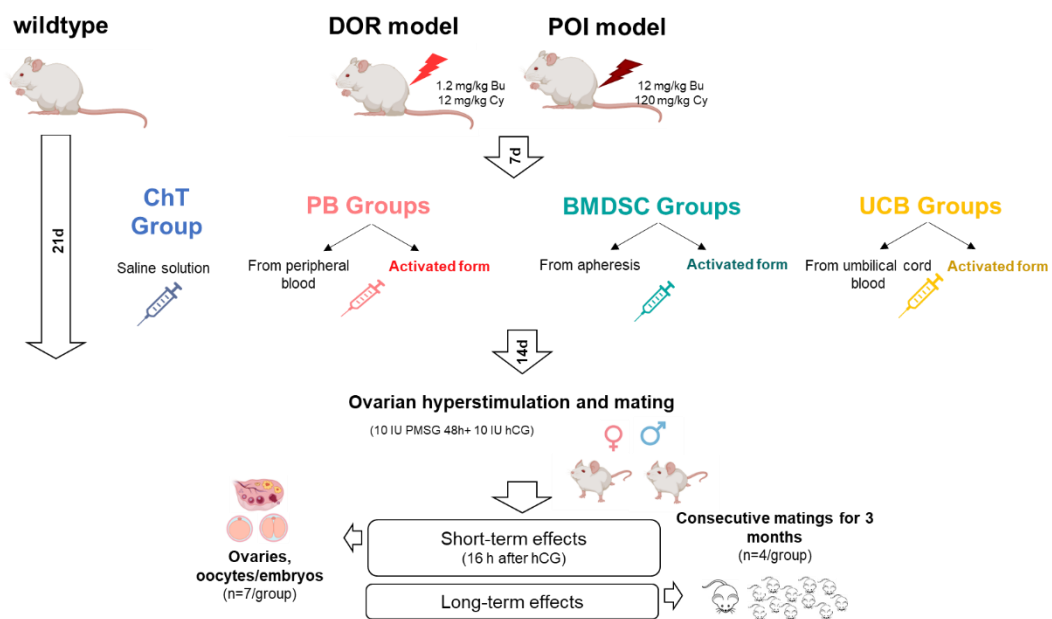
Figure 18. Experimental design to test different plasma sources in mouse models of ovarian damage induced by chemotherapy. The conditions of diminished ovarian reserve (DOR) and premature ovarian insufficiency (POI) were induced by a reduced and standard dose of cyclophosphamide (Cy) and busulfan (Bu), respectively. One week later, the different plasmas were administered every other day for two weeks through tail vein injection. After ovarian stimulation and mating, the effects on short (sacrifice after stimulation) and long-term effects (successive mating for three months) on fertility were assessed. A group without chemotherapy and plasma treatment was included as a wild-type control.

Proteomic characterization of the different plasmas was also carried out to understand the mechanisms underlying treatments. Moreover, additional experiments to evaluate the effect of proposed treatments on DNA repair (section 3.2) and to understand the depletion of ovarian reserve associated with our mouse model (Section 3.3), were included.

3.2 *In vitro* study to analyze the plasma effects on DNA damage and repair

An additional experiment was performed to evaluate treatment effects on promoting DNA repair in a model of ChT-induced ovarian damage.

Twelve-week-old CD1 mouse ovaries were isolated, cultured for 24h and then randomized to the following groups (n=6/group): 1) ChT group: treated with 1.2 µM 4-hydroperoxy cyclophosphamide (Cy) + 0.12 µM busulfan (Bu); 2) PB group: treated with ChT and PB plasma; 3) BMDSC group: treated with ChT and BMDSC plasma; and 4) UCB group: treated with ChT and UCB plasma; 5) Control group: without chemotherapy or plasma treatment. Ovaries were collected at 12h or 24h and pooled by group to analyze DNA damage by western blot (*H2AX, Bax, Bcl2* and *Cleaved caspase-3*) and DNA repair (*ATM*, *p53*, *Rad51*, *Apex1*) by real-time quantitative polymerase chain reaction (RT-qPCR) (Figure 19). The majority of these genes and proteins (Table 2) were selected based on their role in repairing DSBs, the most common DNA damage and repair system found in oocytes[205–207].
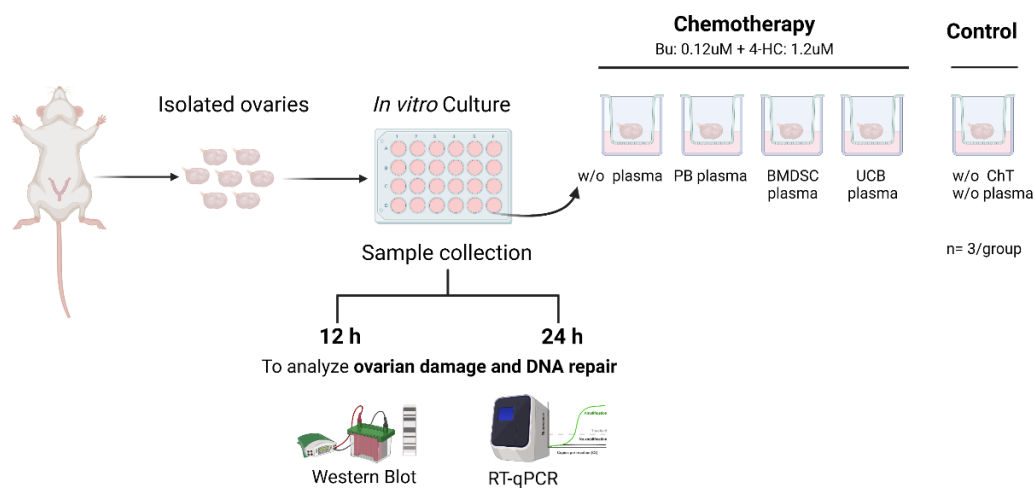
Figure 19. *In vitro* study to analyze the effects of plasma treatments on DNA damage and repair. Isolated mouse ovaries were cultured with chemotherapy (ChT) and plasmas treatment for 12 and 24 h. Then, the ovaries were pooled by group to analyze to analyze ovarian damage and DNA repair by Western Blot and RT-qPCR. Image created with biorender.com

Table 2. Glossary of the genes and proteins employed to study the DNA damage and repair.

Gene ID	Gene name	Role
11920	Ataxia telangiectasia mutated (*ATM*)	DNA damage recognition
22059	Transformation related protein 53 (*p53*)	DNA damage recognition
19361	RAD51 recombinase (*Rad51*)	DNA repair
231642	AlkB homolog 2, alpha-ketoglutarate dependent dioxygenase (*Alkbh2*)	DNA repair
11792	Apurinic/apyrimidinic endonuclease 1 (*Apex1*)	DNA repair
Protein ID	**Protein name**	**Role**
P27661	H2AX variant histone (H2AX)	DNA damage marker
P10417	B cell leukemia/lymphoma 2 (Bcl2)	Anti-apoptotic protein
Q07813	BCL2 associated X, apoptosis regulator (Bax)	Pro-apoptotic protein
P70677	Cleaved caspase 3	Apoptotic regulator

3.3 Analysis of follicle depletion induced by chemotherapy

As the ovarian reserve is formed by a non-renewable pool of follicles[14], a further experiment to establish the dynamics of ChT-induced follicular depletion was performed to better understand how the treatments might affect follicle numbers.

To this end, eight-week-old female CD1 mice (Charles River Laboratories, Saint-Germain-sur-l'Arbresle, France) were intraperitoneally injected with a standard ChT dose (12 mg/Kg Bu – 120 mg/Kg Cy, n = 12) or vehicle (DMSO, n = 8). Ovarian samples were harvested at 2, 7, 14, and 21 days after injection. Samples were processed and follicles counted as described below.

4. Plasma collection

PB plasma was obtained from peripheral blood of POR women. BMDSC plasma was obtained from the apheresis of 10 POR patients undergoing stem cell mobilization by a

5-day pharmacological treatment with G-CSF as previously described[145]. This treatment consisted of a daily subcutaneous injection of 10µg/kg G-CSF for five days. On the fifth day, plasma was obtained in those patients who reached a CD34+ cell threshold ≥10 cells/µL[208]. aBMDSC collection was performed with standard apheresis procedures employing continuous flow in an OPTIA cell separator (Cardian, Denver, USA). Apheresis samples were also analyzed by flow cytometry for confirmation. Umbilical cord blood from newborn babies was collected from healthy patients delivered at Hospital La Fe (Figure 20).

Apheresis and blood samples were collected in EDTAK$_2$ BD Vacutainer® tubes (BD Diagnostics, Madrid, Spain) and plasma fractions isolated by a 280 x g centrifugation for 10 min at 4ºC and stored at -80º C until use.
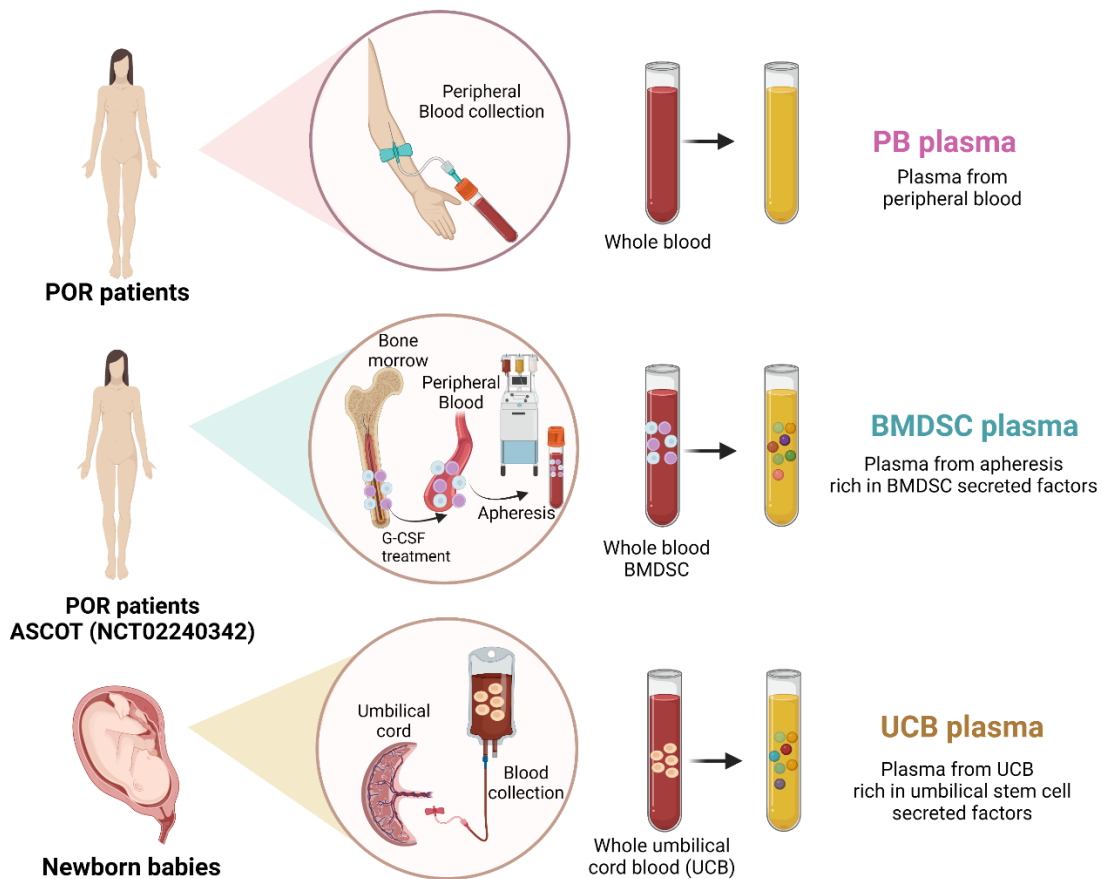
Figure 20. Plasma collections. Plasma from peripheral blood (PB plasma) from poor ovarian response (POR) patients without mobilization. Plasma rich in bone-marrow derived stem cell secreted factors (BMDSC plasma) after mobilization with granulocyte stimulating factor (G-CSF). Plasma rich in umbilical cord stem cell secreted factors (UCB) from newborn babies. Image created with biorender.com.

Fractions of three plasma types (PB, BMDSC, and UCB plasmas) were activated (aPB, aBMDSC, aUCB plasmas) using 5% $CaCl_2$ 0.1M (Sigma-Aldrich, St. Louis, US). Activation induces platelet degranulation which allows the release of growth factors and other signaling molecules enclosed in α-granules[176] before injection.

5. DOR and POI models induced by chemotherapy

DOR and POI were induced in seventy-seven 8-week-old female NOD-SCID mice (Charles River Laboratories, Saint-Germain-sur-l'Arbresle, France) by Cy and Bu. Mice were administered a standard (12 mg/Kg Bu – 120 mg/Kg Cy) or a reduced (1.2 mg/Kg Bu – 12 mg/Kg Cy) dose was employed, respectively. We used these drugs because they are frequently employed for the treatment of breast cancer and hematological malignancies, such as leukemia and lymphomas, which are the cancers that most affect women's fertility[209]. Moreover, by using immunosuppressed NOD/SCID mice, who do not develop T and B lymphocytes and have impaired natural killer cell functionality, human origin treatments can be tested.

To prepare the standard dose, 48 mg of Cy and 4.8 mg of Bu were dissolved in 2 mL of DMSO (all Sigma-Aldrich, St Louis MI). Then, the above solution was diluted 1:10 dilution in DMSO, obtaining the reduced dose of chemotherapy. Both solutions were filtered using a 0.45 μm pore size filter (VWR International Eurolab, S.L., Barcelona, Spain) and used immediately after preparation. The solutions were prepared under sterile conditions in a laminar flow cabinet.

A single intraperitoneal injection was used to administer ChT in the abdominal area. For injections, 1 mL syringes (VWR International Eurolab, S.L., Barcelona, Spain) and 27G-gauge Sterican® hypodermic needles (Braun Vetcare, S.A., Barcelona, Spain) were used.

6. Plasma administration and ovarian stimulation

First, the grouping of animals was randomized using the virtual tool random.org into seven experimental groups. The plasma infusion was performed via tail vein injection using 1 mL syringes (VWR International Eurolab, S.L., Barcelona, Spain) and 27G-gauge

Sterican® hypodermic needles (Braun Vetcare, S.A., Barcelona, Spain) every other day for two weeks. The volume and duration of plasma treatments was established based on previous animal studies[161,210,211], and considering our previous results with BMDSC infusion[145,146], in a similar experimental set up.

Ovarian stimulation consisted of an injection of 10 IU of pregnant mare serum gonadotropin (PMSG, Sigma-Aldrich, St. Louis, MO, USA) to induce follicle growth and maturation, and 48 h later, 10 IU of human chorionic gonadotropin (hCG, Sigma-Aldrich, St. Louis, MO, USA) to induce ovulation of the oocytes contained in these follicles. Both injections were performed intraperitoneally with 27G gauge needle. After COS, females were mated with males (2 females: 1 male).

7. Sacrifice and sample collection

Seven mice per group were euthanized by cervical dislocation 36 h after hCG injection to collect ovaries and oviducts and analyze short-terms effects on fertility. The body weight of mice was recoded before sacrifice. The time-point for analysis was also established based on our previous studies with the injection of stem cells[145,146] in which fourteen days was shown to be the best time point to observe the highest regenerative effects in human ovarian tissue.

After sacrifice, the female reproductive system (ovaries, oviducts, and uterus) was removed in a Petri dish with PBS (Biowest, Nuaillé, France) on a hot plate at 37ºC. Under binocular loupe, the fat was removed from the ovaries-oviducts-uterus to avoid confusions with oocytes and embryos. The oviducts were separated from the ovaries and uterus with a scalpel, with care taken to avoid loss of any part of the oviduct.

The oviducts were transferred to a Petri dish collection medium (GCOL-100, CooperSurgical Fertility & Genomic Solutions, Denmark). The ovaries were weighed, and one was immediately fixed in neutral buffered formalin (PFA, Panreac Química S.A.U, Barcelona Spain) at 4% for immunohistochemistry, while the other was stored at -80º C for biomolecular analysis.

8. Short-term effects

8.1 Mouse Follicle count

8.1.1 Paraffin-embedding and histological sections

Ovaries fixed in PFA 4% were embedded in paraffin (Panreac Química S.A.U, Barcelona Spain), after dehydration, through successive passage in increasing concentrations of ethanol and xylol (Merck, Darmstadt, Germany), then paraffin, as shown in Table 3.

Table 3. Paraffin-embedding protocol.

Reagent	Time (min)
Ethanol 70%	60
Ethanol 96%	60
Ethanol 96% II	60
Ethanol 100% I	60
Ethanol 100% II	60
Ethanol 100 % III	60
Xylol I	20
Xylol II	20
Xylol III	20
Paraffin I	60
Paraffin II	60

Subsequently, serial 4 um slices were prepared using an HM-340E rotation microtome (ThermoFisher, Waltham, MA, USA). Sections were adhered onto SUPERFROST® PLUS slides (Thermo Scientific, Waltham, MA, USA).

8.1.2 Analysis of follicles

Every fifth section was stained with hematoxylin-eosin (H&E), as described below. This criterium was established to avoid double counting whilst still capturing as many follicles as possible, considering that the size of the primordial follicles in mice are approximately 20 μm.

First, the ovarian sections were deparaffinized by incubating the samples for 1 h at 60°C and performing successive passes through xylol. After, tissue sections were hydrated by performing successive passes through decreasing concentrations of ethanol. Subsequently, the sections were stained with hematoxylin (Sigma-Aldrich, St. Louis, MI) for 5 min and with eosin (Sigma-Aldrich, St. Louis, MI) for another 3 min. Finally, the slices were dehydrated and mounted with Eukit mounting medium (Sigma-Aldrich, St. Louis, MI).

To avoid double counting, only normal follicles with the oocyte nucleus present in the section were counted. Follicular subpopulations were identified under optical microscope as follows: primordial: oocyte surrounded by a layer of squamous granulosa cells; primary: oocyte surrounded by a layer of cuboidal granulosa cells; secondary: with two or three granulosa cell layers; late pre-antral: four or more granulosa cell layers but without an antrum; early antral: with one or more fluid-filled foci; and antral: with a larger centrally located antral cavity. Follicles were considered morphologically abnormal when degeneration and necrosis of granulosa cells and/or oocytes were observed, and these abnormal follicles were not included in counts.

8.2 Oocyte and embryo collection

Immediately after collection, the oviducts were placed in a small Petri dish with PBS (Biowest, Nuaillé, France). Oocytes and embryos were flushed from the oviducts using a 30G needle (Braun Vetcare, S.A., Barcelona, Spain) loaded with global collect medium (GCOL-100, CooperSurgical Fertility & Genomic Solutions, Denmark), as shown in Figure 21.

Figure 21. Collection of oocytes and embryos. After sacrifice, the oviducts were isolated. Under a binocular loupe and using a 30G needle, oocytes and embryos were flushed. Subsequently, they were classified and evaluated. Imagen created with biorender.com

The resulting oocytes and embryos were isolated, counted, and classified based on morphological criteria[212,213] under a binocular loupe with a warming stage.

The meiotic maturation of oocytes was evaluated by assessing germinal vesicle breakdown and extrusion of the first polar body. Embryos with two symmetrical, non-fragmented blastomeres and a proportionate zona pellucida were considered a morphologically normal embryo.

9. Long-term effects: Breeding performance

After COS and mating, breeding performance was assessed in four mice per group throughout the three months following the plasma treatments.

During this period, a total of three mating attempts were performed, and the pregnancy rate (number of spontaneously pregnant females/total number of females in the group), and litter sizes (the number of pups each female had) were recorded. Each mating attempt was maintained for a total of 7 days. Then, females were housed separately until delivery.

10. Mouse ovarian stroma status

Due to the relevance of the ovarian stroma for follicular development, and its alteration in DOR and POI profiles, its status was analyzed after administration of the plasmas.

10.1 Cell proliferation

To establish the status of the ovarian niche, proliferative stromal and follicle cells were quantified by Ki-67 immunostaining.

First, ovarian sections were deparaffinized and dehydrated with ethanol, as described above in section 8. Then, the samples were placed in a 10 mM sodium citrate solution, pH 6 (Dako, Denmark), at a pressure of 1.5 bar in microclave (J.P. Selecta) for 3 min (minutes). Once tempered, the samples were incubated for 15 min in a solution of Methanol: Hydrogen peroxide (29:1; Sigma-Aldrich, St. Louis, US) to block endogenous peroxidase activity. Following this, samples were incubated for 1 h in a solution containing 10% horse serum to reduce nonspecific labeling. After this blocking, they were incubated with the primary anti-Ki67 antibody (Abcam, U.K.; 1:500) for 18 h at 4°C. The samples were washed with tris-buffered saline with 0.1% Tween® 20 detergent (TBST, Dako, Denmark) and incubated at room temperature (R.T) for 1 h with a biotinylated anti-rabbit secondary antibody (Vector Laboratories, U.K.). Both antibodies (primary and secondary) were diluted in a 1% horse serum solution.

Horseradish peroxidase (HRP)-conjugated streptavidin was used for detection (LSAB method Dako Denmark A/S, Glostrup, Denmark) with the VIP substrate (Vector Laboratories, Burlingame, CA, USA). To contrast the VIP signal, Methyl green (Vector Laboratories, Burlingame, CA, USA) staining was used. The negative control was an isotype-matched rabbit immunoglobulin (Ig)G used at a 1:50 dilution (DakoCytomation). Proliferative endometrial sections were used as positive controls.

Finally, the sections were dehydrated with ethanol and xylol, and the samples were mounted using DePeX mounting medium (BDH Prolabo, VWR International, U.K.).

To quantify cell proliferation, four sections per sample were analyzed by light-field microscopy (Leica DMI 3000B, Leica Microsystems GmbH, Germany). For each section, high magnification images (20X) were obtained and analyzed using Image Pro-plus

software (Media Cybernetics, Carlsbad, CA, USA). Proliferation was quantified as the Ki-67 positive area measured as a percent of the total analyzed tissue area.

10.2 Microvessel density

Double immunofluorescence with isolectin B4 (IB4; FL-1201, Vector Laboratories, Burlingame, USA), which specifically labels endothelial cells, and with an antibody against α-smooth muscle actin (α-sma; Dako, Glostrup, Denmark), which stains mature vessels, was used to assess the microvessel density (MVD).

Briefly, ovarian sections were deparaffinized with xylol and dehydrated with ethanol as mentioned above. Antigenic unmasking was then performed using 10 mM sodium citrate solution (pH 9) (Dako, Denmark) in a microclave (J.P. Selecta) at a pressure of 1.5 bar for 3 min. Once tempered, the sections were incubated for 30 min at RT with a solution containing 1 mM $CaCl_2$, 1 mM $MgCl_2$, 1 mM $MnCl_2$, and 0.05% Tween at pH 7.4 (blocking solution). Next, the sections were incubated for 10 min with a 1% Bovine Serum Albumin (BSA) solution at RT and for another 20 min with blocking solution to avoid nonspecific signals. Then, sections were incubated with primary antibody IB4 (Vector Laboratories, USA) at a dilution of 1: 200 for 18 h at 4°C. Finally, the samples were incubated with a mouse monoclonal anti-α-SMA antibody conjugated to Alexa 594 (Sigma-Aldrich, USA; 1:200) for 30 min at RT, washed with TBST (Dako, Denmark) and directly mounted with 4',6-diamidino-2-fenilindol (DAPI) mounting medium (Abcam, U.K.). Antibodies were diluted in the blocking solution. A section incubated with α-SMA but not with IB4 was used as a negative control for labeling, and a mouse brain section was used as a positive control.

Four random ovarian sections per sample were assayed. High-magnification images (20X) were obtained using a bright-field microscope with a fluorescence module and a digital camera (LEICA DM4000B and DFC450C; Leica Microsystems GmbH, Germany), and analyzed using Image Pro-plus software (Media Cybernetics, Carlsbad, CA, USA). Lectin-positive areas were classified as vessels, and microvessel density was quantified as the lectin-positive area as a percent of the total area.

10.3 Apoptosis

Apoptosis was assessed by western blot probed for cleaved caspase-3. Ovarian tissue fragments were lysed using a radioimmunoprecipitation assay (RIPA) buffer (0.15M NaCl, 10 mM Tris-HCl [pH 7.4], 1% Nonidet P-40, 1% deoxycholate, 0.1% SDS, and 0.5% aprotinin) and incubated for 15 min at 4º C. Nuclear and cellular debris were removed by centrifugation at 14 000 g for 20 min at 4º C. Protein concentrations were determined with a Bradford protein assay (Bio-rad, Hercules, CA, USA).

Sodium dodecyl sulfate-polyacrylamide gel electrophoresis (SDS-PAGE) was performed under reducing conditions. Samples were diluted in 2X loading buffer (0.5M Tris-HCl at pH 6.8, 25% Glycerol, 10% SDS, 10% 2-Mercaptoethanol, Bromophenol 1%) and 20 µg of protein from each sample was separated on 12% acrylamide gels. Electrophoresis was carried out for 1 h at 30 mA. Proteins were then transferred to PVDF membranes, and the membranes blocked in 5% skim milk in TBST buffer (20 mM Tris-HCl, pH 7.6, 0.1369 M NaCl, 0.1% Triton X-100) at RT. for 1 h. After blocking, samples were incubated overnight at 4ºC with a rabbit antibody to Cleaved caspase-3 at 1:1000 (Cell Signaling Technology, Danvers, MA, USA). Anti-β-actin (1:2000; Abcam, Cambridge, UK) was used as a loading control. Blots were washed and incubated with secondary antibodies conjugated with alkaline phosphatase (1:2000; Sigma, St. Louis, MO, USA) for 1 h at RT. The membranes were washed with TBST, and the antigen-antibody complex revealed by chemiluminescence (ThermoFisher, Waltham, MA USA) using the LAS-3000 scanner (Fujifilm, Tokyo, Japan) and short exposure times (5 to 30 seconds).

The intensity of the protein bands was quantified with ImageJ[214], and the signal normalized to the intensity of the β-actin band.

11. Plasma proteome assessment

To characterize the proteomic profile of the different plasmas, a SWATH-MS analysis was performed.

11.1 Protein relative quantitation in plasma samples: SWATH-MS

11.1.1 Sample preparation

A total of six plasma samples pooled from each group (PB, aPB, BMDSC, aBMDSC, UCB and aUCB plasmas) were processed and analyzed as previously described[215].

First, 100 µL of every individual pooled sample was centrifuged for 15 min at 15 000 g and 5ºC, and 60 µL of the delipidated plasma was transferred to a new tube. Then, 60 µL of every individual sample were precipitated with 40% cold ethanol. Precipitates were incubated for 2 h at 5ºC, and then centrifuged for 1 h at 15 000 g and 5ºC. Supernatant was discarded and pellets were left to air dry. Pellets were dissolved with 120 µL of 2M urea, 1% SDS, 250 mM Triethylammonium bicarbonate (TEAB, pH 8) and the final solutions were quantified with the Machery Nagel Quantitation kit (ThermoFisher, Waltham, MA, USA) according to the manufacturer's protocol. After that, an appropriate volume of 4x Laemmli Sample Buffer with β-mercaptoethanol (Biorad, Hercules, CA, USA) was added to 20 ug of the samples, and samples were then denatured by heating at 95ºC for 5 min.

11.1.2 SWATH analysis of individual samples

For SWATH LC-MS/MS analysis, samples were loaded onto 2 successive columns, then eluted with a linear gradient. Peptides were then analyzed in a mass spectrometer microESI qQTOF (6600plus TripleTOF, ABSCIEX), and samples were ionized in a Source Type.

20 µg of each protein sample was loaded without resolving in one 1D PAGE. Electrophoresis was then performed at 200V for 10 min. Gels were fixed with 40% EtOH /10% acetic acid for 1 h, stained with colloidal Coomassie for 1 h, then destained with MilliQ H2O. Following this, samples were digested with sequencing-grade trypsin as

described elsewhere[216]. The digestion mixture was dried in a vacuum centrifuge, resuspended in 20 µL of 2% acetonitrile (ACN) and 0.1% trifluoroacetic acid (TFA). 5 µl of each sample was loaded onto a trap column and desalted with 0.1% TFA at 10 µl/min for 5 min. Peptides were then loaded onto an analytical column equilibrated in 3% ACN and 0.1% formic acid (FA). Elution was carried out with a linear gradient of 3% A to 35% B for 45 min (A: 0.1% FA; B: ACN, 0.1% FA) at a flow rate of 300 nl/min. Peptides were analyzed in a mass spectrometer microESI qQTOF. For that, samples were ionized in an Optiflow 1-50 uL Micro applying 4.5 kV to the spray emitter. Analysis was carried out in a data-dependent mode; survey MS1 scans were acquired from 400-1250 m/z for 250 ms. The total cycle time was 2.79 secs, and the quadrupole resolution was set to 'UNIT' for MS2 experiments, which were acquired from 100–1500 m/z for 25 ms in 'high sensitivity' mode.

11.1.3 Data analysis and protein quantification

For data analysis and protein quantitation, the Wiff files obtained from the SWATH experiment were analyzed by Peak View 2.1 with the UVEG 'pan serum library 2019'., according to the following workflow:

a. Target peptide assay (from shotgun identification library).
b. Extract target peptide assay.
c. Score target peptide assay (spectronaut raw score = 3.15).
d. Decoy peptide assay (pseudo-reversed sequence).
e. Extract decoy peptide assay.
f. Score decoy peptide assay (spectronaut score = -1.57).
g. Compare the distribution of targets and decoy scores (FDR estimation for a given score cutoff).

Retention times were aligned among the different samples using the main protein peptides. The processing settings used for the peptide selection were:

a. Number of peptides per protein: 20.
b. Number of transitions per peptide: 6.

c. Peptide confidence threshold % (0-99): 95.

d. False discovery rate threshold % (0-100): 1.0.

e. XIC extraction window (min): 20.

f. XIC width (ppm): 50.

The cycle time used in the MS-MS/MS acquisition allowed quantitation of each peptide area with more than 10 points.

The area data obtained with Peak View was then analyzed with Marker View (Sciex). The calculated protein areas were normalized to the sum of the areas of all quantified proteins.

11.2 SWATH-MS data analysis

Fold change (FC) values were calculated in three different types of comparison: 1) comparison of the BMDSC and UCB groups to the PB group, 2) comparison of the aBMDSC and aUCB groups to the aPB group, and 3) comparison of each activated sample to its respective non-activated fraction. We considered those proteins with a $Log_2(FC)$ above 1.5 to be upregulated and those with a $Log_2(FC)$ below 1.5 value to be downregulated.

Pathway analysis was performed using PantherDatabase[217], focusing on reactome pathway results[218]. We examined the number of up- or downregulated proteins specific to a given identified pathway in all three above comparisons.

12. *In vitro* analysis of DNA damage and repair in mouse ovarian tissue

We evaluated the effect of plasma treatments to promote DNA repair in a model of ChT-induced ovarian damage.

12.1 Culture of mouse ovaries

Fifteen CD1 mouse ovaries (12-weeks old) were isolated and cultured for 24 h on top of a membrane (Whatman® Nuclepore™ Track-Etched Membranes – 13 mm – 8.0um, ThermoFisher, Waltham, MA, USA) in 24-well culture plates containing Gibco™ Minimum

61

essential media-α,with no nucleosides (ThermoFisher, Waltham, MA, USA) supplemented with fetal bovine serum (FBS, 1X), penicillin and streptomycin (0.1 mg/mL), insulin-transferrin-sodium (ITS, 0.1mg/mL), and BSA (1 mg/mL) (obtained from Sigma-Aldrich, St. Louis, MO, USA). Ovaries were then randomized to the treatment groups (n = 6/group): ChT, PB, BMDSC, UCB and control, and cultured for 12 h or 24 h. Ovaries were harvested after 12 h or 24 h and pooled by group.

12.2 Analysis of markers for DNA damage and repair by immunoblotting

Western blots were used, as described previously at section 10, to analyze DNA damage and apoptosis. In this study, primary antibodies to *H2AX* (1:1000; Cell Signaling Technology, Danvers, MA, USA), *BAX1, Bcl2* (1:200 and 1:500, respectively, Santa Cruz Biotechnology, Dallas, Texas, USA), and *Cleaved caspase-3* (1:1000; Cell Signaling Technology, Danvers, MA, USA) were used followed by horseradish peroxidase-conjugated secondary anti-mouse or anti-rabbit antibodies (1:2000 and 1:5000; ThermoFisher, Waltham, MA, USA). An anti-β-actin antibody (1:2000; Abcam, Cambridge, UK) was used as a loading control.

12.3 RNA extraction and RT-qPCR for DNA repair genes

Total RNA was extracted using the RNeasy Mini Kit (Qiagen, Hilden, Germany) according to the manufacturer's instructions. RNA quantification was determined by absorbance at 260 nm by NanoDrop (ThermoFisher, Waltham, MA USA), and complementary cDNA was synthesized using the PrimeScript RT reagent kit (Takara, Kyoto, Japan). RT-qPCR was performed with the StepOnePlus System (Applied Biosystems, Foster City, CA, USA) using PowerUp SYBR Green (ThermoFisher, Waltham, MA USA) and specifically designed primers (Invitrogen, Carlsbad, CA, USA; Table 4). PCR reactions were performed in a 10 µL reaction containing 1 µL of cDNA (final concentration 100 ng/uL), 0.5 µL of each primer (300-800 nM) (Table 4), 5 µL of PowerUp SYBR Green Mastermix (Applied Biosystems, Foster City, CA, USA) and RNase-free water. The reactions consisted of UDG activation for 2 min at 50ºC, dual-lock DNA polymerase hot start for 2 min at 95 ° C, followed by 40 cycles of denaturation for 15 s at 95 ° C, and annealing and extension for 1 min at 60

º C. The relative expression was obtained by the comparative Ct method (ΔΔCt) using *18S ribosomal* RNA expression for normalization.

Table 4. Primer sequences for the amplification of DNA repair genes.

GENE	PRIMER SEQUENCES
ATM	F- CAGTCATCATGCAGACCTATC
	R- GCCTTCATCTGTCCATTTCT
P53	F- GACCTATCCTTACCATCATCAC
	R- CACAAACACGAACCTCAAAG
RAD51	F- GCAGCGATGTCCTAGATAATG
	R- CAGTGCATACCTGGATTCTAC
Alkbh2	F-TCCAGGTGTTCGGAAAGT
	R-TGTCAGGGTAAGACCAGAAA
Msh6	F-GCAGTGTTGGATGTCTTACT
	R-GAAGGGATGTGTGTCTTCTC
Apex1	F- CTCAAGATATGCTCCTGGAATG
	R- CTGGTGCTTCTTCCTTTACC

13. Statistical analysis

Necessary sample sizes were calculated using the TrialSize package under R version 3.6.1, based on effect sizes observed in previous studies[145].

Kruskal-Wallis tests followed by Mann-Whitney U-tests for two-by-two comparisons were performed for group comparisons. Analyses were performed using GraphPad Prism version 8.12 (GraphPad Software, San Diego, CA USA), and p values less than 0.05 were considered statistically significant. Data are represented as violin plots with median and quartile values, or bar charts with mean ± standard deviation (SD).

B) EVALUATION OF THE MOST BENEFICIAL PLASMA TREATMENT ON HUMAN OVARIAN TISSUE

1. Ethical approval

As in the previous section A, this study was approved and conducted according to the Institutional Review Board of Hospital Universitario y Politécnico La Fe, Valencia, Spain (2014/0147) and the Institutional Review Board and the Ethics Committee from University of Valencia, Valencia, Spain (A1510574679987). Before ovarian cortex donation, the patients received a written information sheet and signed an informed consent form, as required by the relevant biomedical research law.

2. Animal housing

Similarly, the animal experiments were carried out as described above, in the authorized animal house of the Faculty of Medicine of the University of Valencia, according to current regulations, and respecting the handling and euthanasia procedures recommended by the Spanish and European and Spanish legislation. Mice were housed in a specific pathogen-free area under constant temperature (23ºC) and humidity (60–70%), with a 12-h light/dark cycle and free access to standard rodent diet and water.

3. Experimental design

Due to the functional differences between murine and human ovaries, we evaluated the most efficient treatment in human ovarian tissue. Plasma combining factors secreted by stem cells and platelets (aBMDSC) was tested in human ovarian tissue from POR patients xenografted into immunodeficient mouse.

Six NOD/SCID ovariectomized females were xenografted with human ovarian cortex fragments from POR patients and a week later, when grafts were completely vascularized, animals were allocated into two experimental groups, receiving either saline (control group) or activated BMDSC plasma (aBMDSC group). Treatments were administered

every other day for 2 weeks following the protocol described above. Then, ovarian xenografts (n = 4 in control group; n = 6 in aBMDSC group) were recovered to assess the effects of aBMDSC plasma on human follicles and the ovarian niche from women with impaired ovarian reserve. A proteomic study of human xenografts was also performed after treatment to elucidate the mechanisms underlying the regenerative effects of aBMDSC plasma (Figure 22).
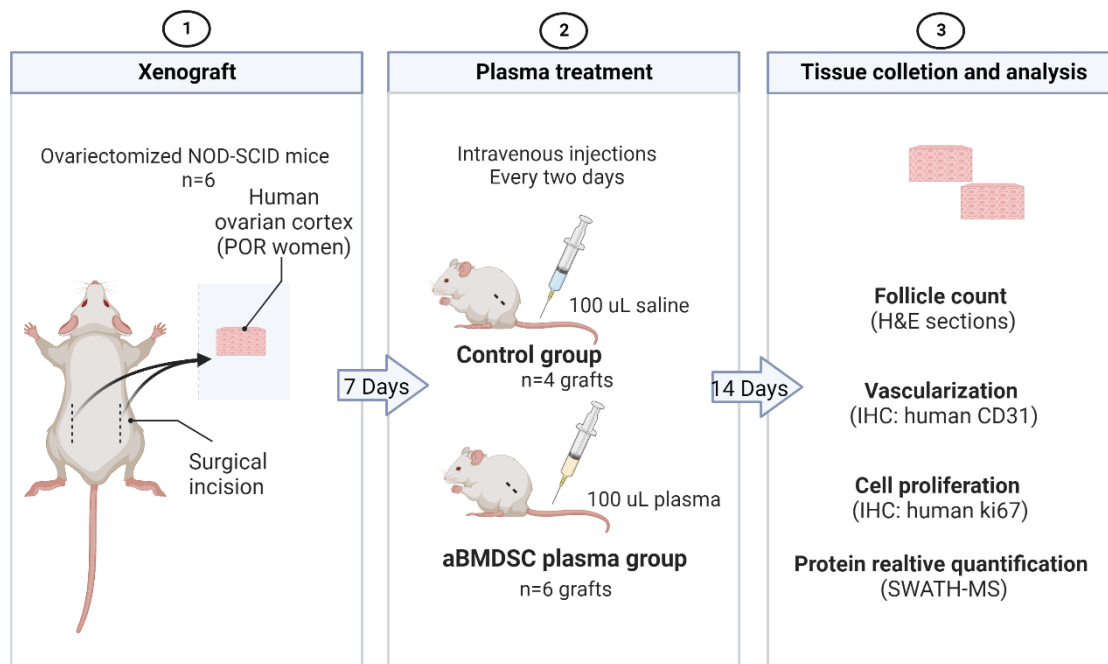
Figure 22. Experimental design to determine the effect of aBMDSC plasma on human ovarian tissue. The effect of activated plasma rich in bone marrow-derived stem cell secreted factors (aBMDSC plasma) was analyzed on ovarian cortex from poor ovarian responder patients (POR), xenotransplanted into immunosuppressed (NOD/SCID) mice. After two weeks of plasma administration, the grafts were harvested to evaluate the effects of plasma treatment. Image created with biorender.com

4. Plasma collection

aBMDSC plasma was obtained from POR patients after stem cell mobilization by G-CSF treatment, as described in phase A section 4. The activation of plasma was performed by a treatment with 5% $CaCl_2$ at 0.1 M prior to administration.

Material and Methods

5. Human ovarian tissue collection

After obtaining written informed consent, 10 ovarian cortex strips were obtained from five women (41 ± 13 years) undergoing fertility preservation or ovarian surgery for benign disease. Ovarian strips (5 x 5 mm approximately) were washed with serum-free M199 medium (Sigma, St. Louis MI), dissected by removing the medulla with a scalped blade and cryopreserved by slow-freezing until use. Briefly, the pieces of cortex were incubated for 15 min with M199 medium (Sigma, St. Louis MI) containing 5% Human serum albumin (HSA; Vitrolife, Sweden) and 5% DMSO (Sigma, St. Louis MI) at 4°C under agitation. The ovarian tissue samples were then incubated for another 15 min with M199 medium (Sigma, St. Louis MI) containing 5% HSA (Vitrolife, Sweden) and 10% DMSO (Sigma, St. Louis MI). After this incubation, the fragments were immersed in fresh medium as above and subjected to slow freezing at -1°C/min to -80°C using a Mr FrostyTM (ThermoFisher, Waltham, MA, USA). Finally, they were stored at -196ºC in a liquid nitrogen tank until use.

Before xenotransplantation, the human ovarian samples were thawed by immersing the cryovials for 2 min in a 37°C water bath with agitation. The DMSO was gradually removed by resuspending the tissue in fresh M199 medium (Sigma, St. Louis MI).

A small piece of each patient´s ovary was stored at -80ºC for building the human ovarian cortex spectral ion library needed for the SWATH proteomic assessment.

6. Xenograft surgery and plasma administration

Six adult NOD/SCID female mice (eight-weeks-old; Charles River, Écully, France) were randomly allocated to control or aBMDSC group. Animals were anaesthetized with isoflurane (Abbott Laboratories, Chicago, Illinois, USA; 5% for induction and 1-2% for maintenance), and ovariectomized by dorsal incision.

During the same surgery, two human ovarian cortex pieces were intraperitoneally grafted in the abdomen of each mouse with a Premilene 6-0 suture (B/Braun, Melsungen AG, Germany) by median laparotomy. Ovarian strips from the same patient were xenografted in both experimental groups to avoid patient-specific responses. Both the dorsal incisions

and the laparotomy were closed in two layers using Vicryl5-0 suture (Ethicon, New Brunswick, NJ, USA). After surgery, buprenorphine (0.1 mg/kg; Temgesic, Schering Plough) was administered every 8-12 h for 48-72 h.

One week later, mice in the control group received their first injection of 100 µl of saline, while mice in the aBMDSC group were treated with 100 µl of aBMDSC plasma. These administrations were performed every other day for two weeks via tail vein using a 27 - gauge needle, as previously described.

7. Sacrifice and tissue collection

Based on the previous study with DOR and POI models, we established 14 days of systemic administration of plasma as the optimum duration of treatment, after which animals were sacrificed by cervical dislocation. Then, the ovarian grafts were harvested (n = 4 in control and n = 6 in aBMDSC groups), and each cortex was divided into two parts. One part was fixed in 4% PFA (Panreac Quimica S.A.U, Barcelona, Spain) for histological and immunohistochemistry analyses. The other part was stored at -80°C for subsequent proteomic assessment.

8. Analysis of human follicle development

Ovarian formalin-fixed samples were paraffin-embedded and cut into 4-µm thick sections, as previously described in the first part of this thesis.

In this case, every tenth H&E section was used to perform follicular counts. This criterion was established to count all follicles present in the samples, considering that the size of human primordial follicles is approximately 40 µm.

Only morphologically normal follicles with the oocyte nucleus present were counted. Follicles were classified as: primordial follicle: oocyte surrounded by a layer of flattened GCs; primary follicle: oocyte surrounded by a complete layer of cuboidal GCs; secondary follicle: oocyte surrounded by two or more layers of cuboidal GCs; antral follicles: with an

antral cavity; and preovulatory follicles: with a large antrum and with the oocyte in one corner surrounded by cumulus cells.

The results were expressed as follicular density (number of follicles/mm^3 of ovarian tissue), to facilitate the analysis and comparison of the samples. In addition, the proportion of each follicular population for the total number of follicles in each graft was estimated.

9. Analysis of human ovarian stroma: proliferation and vascularization

For each analysis, ovarian sections (four representative sections per sample) were deparaffinized and hydrated, as detailed in phase A section 10. Subsequently, antigenic unmasking was performed in 10 mM sodium citrate solution pH 6.0 (Dako Denmark A/S, Glostrup, Germany) at 95ºC for 15 min in a water bath. Following this, the sections were incubated for 15 min at RT with Peroxidase-Blocking Solution (Dako Denmark A/S, Glostrup, Germany) to block endogenous peroxidase activity. The slides were then washed with TBST (Dako Denmark A/S, Glostrup, Germany) and incubated with the primary antibodies for 1 h at RT. A mouse monoclonal anti-human Ki-67 antibody (MIB-1, Dako Denmark A/S, Glostrup, Denmark; 1:100), or a mouse monoclonal anti-CD31 antibody (JC70A, Dako Denmark A/S, Glostrup, Denmark; 1:50) were employed to study proliferation and vascularization, respectively. The primary antibodies were diluted in ENVISION antibody diluent (Dako Denmark A/S, Glostrup, Denmark).

For the secondary antibody incubation, a biotin/streptavidin reaction was used (ENVISION method; Dako Denmark A/S, Glostrup, Denmark) according to the supplier's instructions, and staining was detected with 3,30-diaminobenzidine (DAB). After contrasting the DAB signal by gentle staining with hematoxylin, the samples were mounted with Eukit medium (Sigma-Aldrich St. Louis MI), after dehydration by ethanol and xylol passages. Negative controls with an isotype-matched mouse immunoglobulin (Ig)G at 1:50 dilution (Dako Denmark A/S, Glostrup, Denmark) were included. For positive controls, sections of proliferative human endometrium and human amygdala were utilized.

High-magnification images were obtained on a Leica DFC450C digital camera (Leica Microsystems GmbH, Germany) and analyzed using the Image Pro-plus software (Mediacybernetics; Carlsbad, CA). Proliferation was estimated as number of Ki-67 positive cells by tissue area, while microvessel density was determined as vessel positive area (CD31 immunostained) per section.

10. Proteomic analysis of human ovarian cortex: SWATH-MS

To understand the mechanisms underlying plasma treatments, a total of 15 ovarian cortex samples were processed and analyzed as described previously (in the plasma proteome assessment of phase A section 11) with minor modifications for protein library construction and sample preparation. The procedure was carried out in the same facilities and using the same equipment.

10. 1 Library construction

The five pre-xenotransplant ovarian samples were used for spectral library building.

10.1.1 Sample preparation and digestion

Different methods were employed for protein extraction. One of the ovarian pieces was treated with 100 μL of UTC (7 M Urea, 2 M Thiourea, 2% CHAPS) by sonication for 30 min and precipitated with TCA/acetone. Another two samples were treated in the same way with 100 μL of 2% SDS and 10 mM DTT. The protein concentration of the solutions was determined by Machery Nagel Quantitation (ThermoFisher, Waltham, MA, USA) assay, according to the manufacturers' instructions. Then, 50 μg of every sample were resolved in a 1D SDS-PAGE gel to determine the best conditions for sample preparation. An appropriate volume of 4x Laemmli Sample Buffer with β-mercaptoethanol (Biorad, Hercules, CA, USA) was added to 20 μg of each sample.

The samples were denatured at 95ºC for 5 min, and the electrophoresis was performed using an 12% precast gel (Biorad, Hercules, CA, USA) at 200V for 5 min. The gel was fixed with 40% ethanol/10% acetic acid for 1 h, stained with colloidal Coomassie ((Biorad, Hercules, CA, USA) and destained with MilliQ H_2O. The UTC extraction without

precipitation provides a completer and more balanced proteome. Then, the gel was digested to build the spectral library.

Every sample run was separated into 5 pieces and then digested with sequencing-grade trypsin (Promega, Madison, WI, USA), as described elsewhere[219]. 500 ng of trypsin was used for each sample, and digestion was set to 37 ºC for 20 min. The trypsin digestion was stopped with 10% TFA and the supernatant removed, and the library gel slides were dehydrated with pure ACN. The new peptide solutions were combined with the corresponding supernatant. The peptide mixtures were dried in a speed vacuum and re suspended with 15 μL of 2 % ACN and 0.1% TFA (20 μL).

For the last two samples, ThermoScientific EasyPep™ Mini MS Sample Prep Kit (ThermoFisher, Waltham, MA, USA) was used for sample preparation and digestion, according to the manufacturers' instructions. After digestion, the peptides were cleaned with the same kit. The peptide mixtures were dried in a speed vacuum and resuspended with 15 μL of 2 % ACN and 0.1% TFA (20 μL).

10.1.2 SWATH-MS analysis for library

5 μl of peptide mixture sample was loaded onto a trap column (3μ C18-CL, 350 μm x 0.5mm; Eksigent) and desalted with 0.1% TFA at 5 μl/min for 5 min.

The peptides were then loaded onto an analytical column (3μ C18-CL 120 Ǎ, 0.075 x 150 mm; Eksigent) equilibrated in 5% acetonitrile 0.1% FA. Elution was carried out with a linear gradient of 7% A to 40% B for 20 min for in-gel digested samples, or 120 min for in-solution digested samples (A: 0.1% FA; B: ACN, 0.1% FA, at a flow rate of 300 nL/min). Peptides were analyzed in a mass spectrometer nanoESI qQTOF (6600plus TripleTOF, ABSCIEX).

Samples were ionized in a Source Type Optiflow < 1 uL Nano applying 3.0 kV to the spray emitter at 200 ºC. Analysis was carried out in a data-dependent mode. Survey MS1 scans were acquired from 350–1400 m/z for 250 ms. The quadrupole resolution was set to 'LOW' for MS2 experiments, which were acquired 100–1500 m/z for 25 ms in 'high sensitivity' mode. The following switch criteria were used: charge: 2+ to 4+; minimum

intensity: 250 counts per second (cps). Up to 100 ions were selected for fragmentation after each survey scan. Dynamic exclusion was set to 15 s. The rolling collision energies equations were set, for all ions, as for 2+ ions according to the following equation: |CE|=(slope)x(m/z) + (intercept).

10.1.3 Protein identification

All the information was combined in a single search. ProteinPilot default parameters were used to generate a peak list directly from 6600 plus TripleTOF wiff files. The Paragon algorithm[220] of ProteinPilot v 5.0 was used to search the Swissprot_200601.fasta database with the following parameters: trypsin specificity, cys-alkylation, no taxonomy restriction (562246 proteins), and the search effort set to rapid with FDR analysis. 3010 proteins were identified as DEPs with an FDR ≤1%.

10.2 Sample preparation for SWATH-MS analysis

In this case, proteins from ovarian xenografts were extracted by using UTC (7 M Urea, 2 M Thiourea, 2% CHAPS), precipitated with TCA/acetone and digested as previously described for the library construction. The following SWATH-MS steps were carried out as described in phase A sections 11.1.2 and 11.1.3.

10.3 SWATH-MS data analysis

In this proteomic analysis, FC values were calculated using the normalized protein area values of the aBMDSC samples, relative to those of the control group. Also, a Welch´s t-test was performed, and the proteins presenting a p-value <0.05 were considered as statistically significant.

Finally, functional processes, in which the significant proteins were implicated, were studied using the NCBI database.

11. Statistical analysis

Kruskal-Wallis tests followed by Mann-Whitney U-tests for two-by-two comparisons were performed for comparisons between control and aBMDSC groups. Analyses were performed using GraphPad Prism version 8.12 (GraphPad Software, San Diego, CA USA) and p values <0.05 were considered statistically significant. Data are represented as violin plots with median and quartile values, or bar charts with mean ± SD.

C) DEVELOPMENT AND VALIDATION OF A MOUSE MODEL OF PHYSIOLOGICAL REPRODUCTIVE AGING

1. Ethical approval

Animal experiments were carried out following approval from the Ethics Committee of the University of Valencia (Valencia, Spain; A20200617081941).

2. Animal housing

As in the previous sections, the experiments were carried out in the authorized animal house of the Faculty of Medicine of the University of Valencia, following European and Spanish legislation. During the experiment, mice were housed in a specific pathogen-free area under constant temperature (23ºC) and humidity (60–70%), with a 12-h light/dark cycle and *ad libitum* access to sterilized standard rodent pellets and water.

3. Experimental Design

To properly evaluate the effects of novel therapeutic approaches for treating age-related infertility, preclinical studies in appropriate animal models are needed. Thus, we aimed to characterize a physiological reproductive aging mouse model displaying most of the ovarian characteristics of different stages during women's reproductive life.

Twelve NOD/SCID female mice of 8, 28, and 36-40-week-old were employed to mimic different human reproductive ovarian phenotypes: young (~18-20 years-old), Advanced Maternal Age (AMA, ~36-38 years-old), and old women (>45 years-old), respectively. Once animals reached the target age, they were stimulated, mated, and sacrificed to recover MII oocytes and 2-cell embryos. Then, ovulation rate, oocyte quality, and embryo development were assessed. Ovaries were also harvested to analyze follicular growth, stroma, mitochondrial function, and proteomic profile (Figure 23), keeping one ovary in PFA for immunohistology studies and the other at -80ºC for molecular analysis.

The different ages were established considering the characteristics of the NOD/SCID strain[189,221] and the equivalent age in the aging human[189].
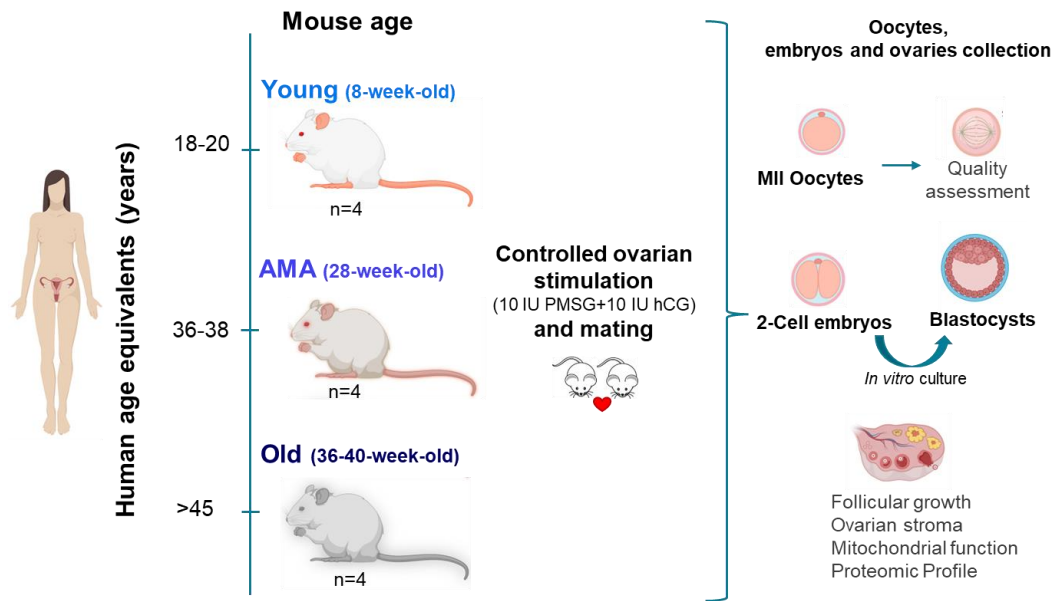
Figure 23. Experimental design to characterize a mouse model of physiological reproductive aging. Mice of different ages (8-, 28-, and 36–40-week-old) were employed to mimic different human reproductive ovarian phenotypes: young (~18-20 years-old), Advanced Maternal Age (AMA, ~36-38 years-old), and old women (>45 years-old), respectively. Animals underwent ovarian stimulation and were mated. Mice were sacrificed 36h after to recover metaphase-II (MII) oocytes and 2-cell embryos. Then, ovulation rate, oocyte quality, and embryo development were assessed. Ovaries were also harvested to analyze follicular growth, stroma, mitochondrial function, and proteomic profile Image created with biorender.com

4. Ovarian stimulation, sacrifice and sample collection.

Animals were stimulated with PMSG and hCG injections, mated and sacrificed as previously described in phase A sections 6 and 7, respectively.

Under a binocular loupe, the fat and the oviducts were removed and separated from the ovary and uterus by cutting with a scalpel. The oviducts were transferred to a Petri dish with collection medium (GCOL-100, CooperSurgical Fertility & Genomic Solutions, Denmark).

5. Fertility outcomes

5.1 Follicle count

Follicles were categorized and recorded as described in phase A section 8.1.2. In this study, the number of corpora lutea was also included in accordance with previous studies[222].

5.2 Follicle activation

FOXO3a immunostaining was performed to analyze the activation of dormant primordial follicles[223].

First, samples were deparaffinized and rehydrated in ethanol. Antigen retrieval pretreatment was carried out by boiling the sections in 0.01 M citrate buffer, pH 6.0, for 20 min and cooling slowly (15-20 min). Then, endogenous peroxidase activity was blocked by incubation in 3% peroxide in methanol (Sigma-Aldrich, St. Louis, US) for 10 min. After washing with TBST (Dako Denmark A/S, Glostrup, Germany), immunohistochemical analysis was performed by the ENVISION kit (Dako Denmark A/S, Glostrup, Denmark) using an antibody to FOXO3 (1:250; Cell Signaling Technology, Danvers, MA, USA) overnight at 4 °C. For some sections, primary antibodies were replaced with nonimmune rabbit IgG as negative controls. As a positive control human breast cancer tissue sections were employed.

The next day, samples were washed with TBST, and then incubated with an HRP-conjugated goat-anti-rabbit antibody at 1:500 (Vector Laboratories, Burlingame, CA, USA) for 1 h at RT. For the biotin/streptavidin reaction, the ENVISION method (Dako Denmark A/S, Glostrup, Denmark) was employed, according to the supplier's instructions, and staining was detected with DAB. After contrasting the DAB signal by gentle staining with hematoxylin, the samples were mounted with Eukit medium (Sigma-Aldrich St. Louis MI), after dehydration by ethanol and xylol passages.

As in previous reports[223], primordial follicles were considered activated when the FOXO3a nuclear extrusion was detected in the oocyte, thus, we calculated the percentage of primordial follicles with FOXO3a located in the ooplasm.

5.3 Oocyte and embryo collection

As in phase A section 8.2, oocytes and embryos were flushed from the oviducts (harvested at sacrifice) using a 30G needle (Braun Vetcare, S.A., Barcelona, Spain) loaded with global collect medium (GCOL-100, CooperSurgical Fertility & Genomic Solutions, Denmark). The obtained oocytes and embryos were isolated, counted, and classified under a binocular loupe with a warming stage. The meiotic maturation of oocytes was evaluated by assessing germinal vesicle breakdown and extrusion of the first polar body. Moreover, in this study, we considered oocytes with fragmented artifacts visible in the ooplasm as abnormal and of poor-quality.

5.4 Oocyte quality assessment

Oocytes that had achieved polar body extrusion were considered mature (MII oocytes), removed from the collection medium, and fixed in supplemented PHEM solution as detail in Table 5. Oocytes were incubated in this solution for 20-25 min at RT. Oocytes were then washed in PBS and blocked overnight, using PBS supplemented with various reagents (Table 5).

The next day, oocytes were incubated overnight at 4°C with anti-α-tubulin-FITC antibody (diluted 1:50 in the blocking solution) to label the microtubules of the spindle. Then, oocytes were washed in PBS with 0.1%Triton X-100, and chromosomes were labeled with Hoechst 33342 (20 μg/ml) for 20 min at RT. All reagents were obtained from Sigma-Aldrich (St. Louis, MO, USA).

Table 5. Composition of fixing and blocking solutions for oocyte quality assessment.

SOLUTION	COMPONENTS
Fixing solution	PHEM buffer (60 mM PIPES at pH 6.9, 25 mM HEPES, 10mM EGTA, 2mM $MgCl_2$)
	3.7% paraformaldehyde
	50% Deuterium oxide
	0.1%Triton X-100
	0.01% aprotinin
	1mM DTT
	1µM Taxol
Blocking solution	1X PBS
	1% BSA
	0.2% dried milk
	2% Fetal Bovine Serum
	0.1M Glicina
	0.2% sodium azide
	0.01% Triton x-100

Oocytes were transferred to micro-drops of PBS under mineral oil, in Ibidi µ-slide 8-well glass-bottom plates (Ibidi, Germany) for confocal imaging. Serial Z sections of fixed oocytes were captured by a confocal microscope (LEICA TCS-SP8) with an oil immersion objective (40X-63X) to span the entire region of the spindle. Oocytes with well-organized microtubules and aligned chromosomes on the metaphase plate were considered normal, and conversely, those with disordered spindles and/or chromosomes were considered abnormal. Spindle area and chromosome alignment were measured using ImageJ software[214].

5.5 *In vitro* embryo culture

All 2-cell embryos were cultured in GPS dishware with Sage 1-step medium (both from Cooper Surgical Fertility & Genomic Solutions, Denmark) at 37°C with 5% O_2, 6% CO_2 and 89% N_2 until the blastocyst stage. Blastocyst formation and hatching was evaluated on days 5 and 6 using an inverted microscope.

6. Ovarian stroma status: analysis of cell proliferation and microvessel density

Stroma and follicle cell proliferation and vascularization were analyzed to determine the effects of aging in the ovarian niche.

Proliferative stroma and follicle cells were studied by Ki-67 immunostaining, as previously described in phase A section 10.1. However, in this study, we also evaluated the proportion of proliferative follicles in each subpopulation.

The MVD was measured by double immunofluorescence, targeting isolectin B4 and α-smooth muscle actin, following our previous protocols in phase A section 10.2.

7. Mitochondrial function and oxidative damage

Because mitochondrial dysfunction and oxidative damage are a principal contributor to the ovarian aging process, we evaluated the mtDNA copy number, the lipid peroxidation, and the apoptosis.

7.1 mtDNA copy number

mtDNA copies in the ovarian samples were estimated using a RT-qPCR-based method.

Total DNA was isolated from half of each frozen ovary using the QIAamp kit (Qiagen, Germantown, MD, USA), following the manufacturer's instructions. Specific primers were designed to target the following mitochondrially-encoded genes: *ND1* (F:5´-CTAGCAGAAACAAACCGGGC-3'; R:5'-CCGGCTGCGTATTCTACGTT-3'), *COX3* (F:5´-TTTGCAGGATTCTTCTGAGC; R: 5´-TGAGCTCATGTAATTGAAACACC-3´) and *16SrRNA* (F:5'-CCGCAAGGGAAAGATGAAAGAC-3'; R:5'-TCGTTTGGTTTCGGGGTTTC-3'). The *18S*

gene was selected to represent nuclear DNA (F:5′-CCGCTAGAGGTGAAATTCTT-3′; R: 5′-CTCCGACTTTCGTTCTTGAT-3′). RT-qPCRs were performed using PowerUp SYBR Green on a StepOnePlus System (Applied Biosystems, Foster City, CA, USA), with the optimized cycling parameters: 50℃ for 2 min, dual-lock DNA polymerase for 2 min at 95℃, 40 cycles of denaturation at 95℃ for 15 s, followed by annealing and extension at 60℃ for 1min. Finally, the mtDNA/nuclear DNA (nDNA) ratio was calculated using the ΔΔCt method.

7.2 Assessment of oxidative stress

Immunohistochemical staining of the lipid peroxidation product 4-HNE was performed on ovarian sections, to localize oxidative damage.

Paraffin sections were dewaxed, and antigen retrieval was then performed in sodium citrate buffer (pH 6.0) at 95 – 100 °C for 20 min The sections were cooled to RT and washed with PBS (Biowest, Nuaillé, Francia) for 5 min three times. The samples were incubated with 3% hydrogen peroxide (Sigma-Aldrich, St. Louis, US) for 10 min, washed with PBS and blocked in a solution with 5% goat serum in 1× TBST buffer for 1 h at RT. After blocking, the slides were incubated overnight with the primary antibody 4-HNE at 1:500 (Abcam, Cambridge, UK) at 4ºC. The primary antibody was diluted in a solution with 2% goat serum. HRP-conjugated goat-anti-rabbit antibody (1:1000, Vector Laboratories, Burlingame, CA, USA) was employed for the secondary antibody incubation, and the staining was revealed with DAB peroxidase substrate kit (Dako Denmark A/S, Glostrup, Denmark). Sections were re-stained with methyl green (Vector Laboratories, Burlingame, CA, USA). For the negative control, the primary antibody was omitted. Human kidney sections were used as a positive control.

Sections were imaged by microscopy and analyzed with Image-Pro Plus software (Media Cybernetics, Carlsbad, CA, USA). Age-related oxidative damage was estimated by dividing the 4-HNE-positive area by the total area of ovarian tissue.

7.3 Analysis of cell death

Apoptosis was assessed by the terminal deoxyribonucleotidyl transferase-mediated dUTP nick-end labeling (TUNEL) assay using the TMR red In Situ Cell Death Detection Kit (Roche Diagnostics, Risch-Rotkreuz, Sweden). This technique detects DNA fragmentation due to apoptotic signaling cascades' activation, adding labeled dUTPs to the 3' ends generated because of DNA fragmentation.

In detail, after deparaffinizing and hydrating the ovarian sections as detailed above, antigenic unmasking was performed using a 10 mM sodium citrate solution at pH 6 and incubating at 850W for 5 min in a microwave. The slices were then incubated for 60 min at 37ºC in a dark and humid environment with the TUNEL mixture, consisting of a labeling solution (dUTPs labeled with the TMR fluorophore) and an enzyme solution (TdT enzyme).

After incubation, the samples were washed with PBS and mounted with the mounting medium DAPI ProLong Gold antifade reagent (Life Technologies, Carlsbad, CA) overnight at RT. Ovarian sections incubated after unmasking with 2000 U/mL DNAse I in 50mM Tris + 1mg/mL BSA at pH 7.5 for 10 min were employed as a positive control. Ovarian sections incubated after antigenic unmasking with the labeling solution alone (without the enzyme solution) were used as a negative control.

To quantify apoptotic cells, the proportion of TUNEL-positive cells was assessed in four sections per sample. High-magnification images were captured and analyzed using Image-Pro Plus (Media Cybernetics, Carlsbad, CA, USA). The TUNEL-positive (red) and DAPI-positive (blue) signal was quantified, and the percentage of apoptotic cells calculated as the positive TUNEL area relative to the positive DAPI area.

8. Proteomic profile analysis

8.1 SWATH-MS method

8.1.1 Sample preparation

Firstly, the mouse ovarian tissue samples were prepared and processed for SWATH-MS. In this study, the preparation of the samples differed from those used in phase A section 11.1.1 and phase B section 10.2. All samples were lysed using the Sample Grinding Kit (GE Healthcare) with 100 µL of Lysis Buffer (EasyPep™ Mini MS Sample Prep Kit, Thermo Scientific, Waltham, MA, USA) according to manufacturer's instructions. After centrifugation (15 min at 15,000 x g) to remove lipids, 1 µL of each sample was quantified using the Qubit protein quantitation kit (ThermoFisher, Waltham, MA, USA).) according to manufacturer´s instructions. Protein concentrations ranged from 4 to 9 µg/µL.

Then, the samples were digested. Specifically, 20 µg of each sample was digested using the EasyPep™ Mini MS Sample Prep Kit (Thermo Scientific, Waltham, MA, USA), according to the manufacturer's instructions. Cleaned peptide mixtures were dried in a speed vacuum and resuspended in 2% AN and 25 µL of 0.1% TA, to a final concentration of 0.8 µg/µL.

8.1.2 SWATH-MS analysis of individual samples

Every peptide mixture sample was analyzed as described above in phase B section 10.1.2, using a mass spectrometer nanoESI qQTOF (6600plus TripleTOF, ABSCIEX).

8.1.3 Data analysis and protein quantitation

The data obtained from SWATH experiments were examined by PeakView 2.1 software (Sciex) with a specific spectral library for mice, following the workflow described in phase A section 11.1.3.

The area data obtained with PeakView was subsequently analyzed with MarkerView (Sciex). Then, the protein areas were normalized to the total sum of the areas of all quantified proteins.

8.2 SWHAT-MS data analysis

A multiple regression model with ElasticNET penalty was performed using the miXOmics R package[224] (v.6.16.3) with the normalized area to obtain DEPs associated with each experimental group. Heatmap analysis was used to visualize the hierarchical clustering of the DEPs.

To analyze the functional implications of the affected genes on ovarian physiology, functional proteomic analysis was carried out using the Gene Ontology (GO) database from WGCNA package[225], focusing on biological processes, cellular components, and molecular functions enriched for each age group. For that, the DEPs obtained from the previous analysis were employed.

9. Statistical analysis

To determine the statistical differences between groups, we performed the Kruskal-Wallis test, followed by a Mann-Whitney U-test for two-by-two comparisons, in GraphPad Prism v.8.12 (GraphPad Software, San Diego, CA, USA). $P<0.05$ was considered statistically significant.

D) INTRAOVARIAN ADMINISTRATION OF THE MOST BENEFICIAL PLASMA TREATMENT IN A PHYSIOLOGICAL AGING MOUSE MODEL

1. Ethical approval

The use of human plasma samples was approved by the Institutional Review Board of the Hospital Universitario y Politécnico La Fe (Valencia, Spain; 2014/0147). All animal experiments were carried out according to approval by the Ethics Committee of the University of Valencia (Valencia, Spain; A20200617081941).

The intraovarian injection procedure and the volume administered were optimized in a previous pilot study (A20191203130113).

2. Animal housing

The experiments were carried out in the authorized animal house of the Faculty of Medicine of the University of Valencia, in accordance with European and Spanish legislations. During the experiment, all mice were fed a standard diet *ad libitum* and housed in the specific pathogen-free zone in a 12:12 h light: dark cycle.

3. Experimental design

To test if plasma rich in both BMDSC- and platelet-secreted factors can recover ovarian function in age-related infertility, we employed our aging mouse model mimicking three stages of women´s reproductive life: young, advanced maternal age (AMA) and old (Figure 24).

In this phase, we compared the effect of the most beneficial treatment (aBMDSC) versus aPRP, recently proposed as an alternative therapy in the rescue of ovarian function. Moreover, the plasmas were administered by a single intraovarian injection, to reflect treatment more closely in clinical practice.

Material and Methods

Young (8-week-old, n=12), AMA (28-week-old, n=12) and old (36-40-week-old, n=12) NOD/SCID females were randomized to receive a single intraovarian injection (10 µL/ovary) of saline solution (control group, n=4), activated PRP from peripheral blood (aPRP group, n=4), or activated plasma rich in BMDSC- and platelet-secreted factors (aBMDSC group, n=4). A week after treatments, animals underwent COS and mated. Then, animals were sacrificed by cervical dislocation 36 h after hCG injection to recover ovulated MII oocytes and 2-cell embryos from the oviduct. The ovaries were also harvested to analyze follicular growth, stroma, mitochondrial function, and proteomic profiles at different ages. One ovary was kept in PFA for immunohistology studies and the other at -80ºC for molecular analysis.
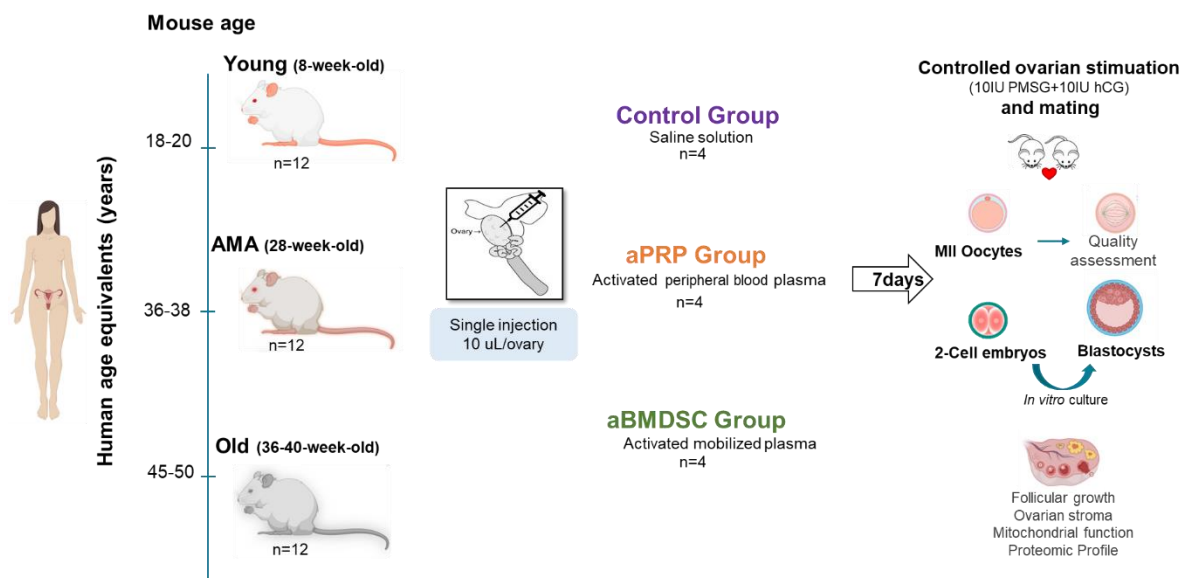
Figure 24. Experimental design to evaluate the intraovarian administration of plasmas in a physiological aging mouse model. Young, advanced maternal age (AMA) and old mice were employed in a physiological aging murine model to evaluate the effects of activated platelet-rich plasma (aPRP) and plasma rich in stem cell- and platelet-secreted factors (aBMDSC). The plasmas were administered by a single intraovarian administration. A week after, animals underwent ovarian stimulation, were mated, and then sacrificed to analyze the short-term effects on fertility.

4. Plasma collection

The plasma rich in bone marrow-derived stem cells (BMDSC plasma) was directly obtained via aphaeresis, from patients with POR who were undergoing bone marrow-derived stem cell mobilization using a 5-day long pharmacological treatment with G-CSF,

as previously described. Meanwhile, the standard plasma was obtained from peripheral blood from POR women without mobilization.

The apheresis and blood samples were collected in EDTAK2 BD Vacutainer tubes (BD Diagnostics, Madrid, Spain). Plasma fractions were isolated using centrifugation at 280 x g for 10 min at 4°C, followed by a second centrifugation at 400 x g for 15 min at 4°C to isolate the PRP, increasing the concentration of platelets. Finally, the BMDSC and PRP samples were activated using 5% $CaCl_2$ at 0.1 M (Sigma-Aldrich, St.Louis, US), forming aBMDSC and aPRP treatments, respectively.

5. Intraovarian plasma administration in the physiological aging mouse model

Thirty-six female NOD-SCID mice (Janvier-Lab, Le Genest-Saint-Isle, France) that were 8, 28, or 36-40 weeks old (n=12/age) were used to model the phenotypes of young (18-20 years old), AMA (~36-38 years old), and old women (>45 years old), respectively, as previously characterized.

The young, AMA, and old mice were randomly allocated (using the virtual tool random.org) to receive a single intraovarian injection of either saline solution (control group, n=4), activated PRP from human peripheral blood (aPRP group, n=4), or activated BMDSC from apheresis (aBMDSC group, n=4).

For the surgical procedure, animals were anesthetized with isoflurane (Abbott Laboratories, Chicago, Illinois, USA; 5% for induction and 1-2% for maintenance). A small dorsal incision of the skin and muscle was made on both sides to access the left and right ovaries. The ovarian injection was performed using an insulin syringe of 0.5 ml BD micro-fine plus 31G (BD Diagnostics, Madrid, Spain). The saline solution or plasmas were administered into the center of each ovary in a single dose (Figure 25). Then, the incisions were sutured and disinfected with a povidone-iodine solution. After surgery, buprenorphine (0.1 mg/kg; Temgesic, Schering Plough) was administered, and the animals were monitored daily. No leakage was observed after the procedure.

Intraovarian injection
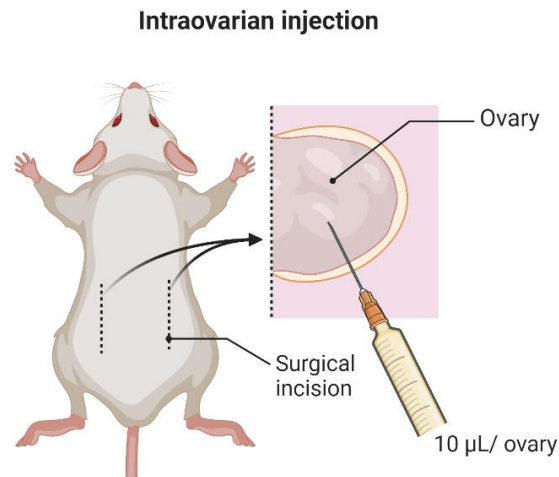
Figure 25. Intraovarian injection of plasma in mouse ovaries. The plasmas were administered into the center of each ovary in a single douse of 10 µL per ovary. Image created with biorender.com

6. Statistical analysis

Necessary sample sizes were calculated using the TrialSize package under R version 3.6.1, based on effect sizes observed in previous studies[145].

Kruskal-Wallis tests followed by Mann-Whitney U-tests for two-by-two comparisons, were performed in GraphPad Prism v.8.12 (GraphPad Software, San Diego, CA USA). P values <0.05 were considered statistically significant.

For proteomic analysis, a multiple regression model with ElasticNET penalty was performed using the miXOmics R package[224] (v.6.16.3).

V. RESULTS

V. RESULTS

A) REGENERATIVE EFFECT OF DIFFERENT PLASMA SOURCES, RICH IN GROWTH FACTORS, IN MOUSE MODELS OF OVARIAN DAMAGE INDUCED BY CHEMOTHERAPY

First, we evaluated different plasma sources rich in factors secreted by SCs, bone marrow-derived stem cells (BMDSC plasma), and umbilical cord stem cells (UCB plasma) to recover the ovarian function of chemotherapy-induced DOR and POI murine models by systemic administration.

In this phase, we also characterized the protein profile of different plasmas tested to uncover potential mechanisms underlying the observed regenerative effects. Based on these results, we assessed the role of plasmas in DNA repair, performing an additional in vitro experiment with mouse ovarian tissue exposed to chemotherapy.

1. Analysis of ovarian weight

The ovarian weight at death was recorded as an indicator of the number of large follicles responding to gonadotropin stimulation. All DOR treatment groups showed lower levels than the wild-type group, and plasma treatments did not induce any improvement (Figure 26).
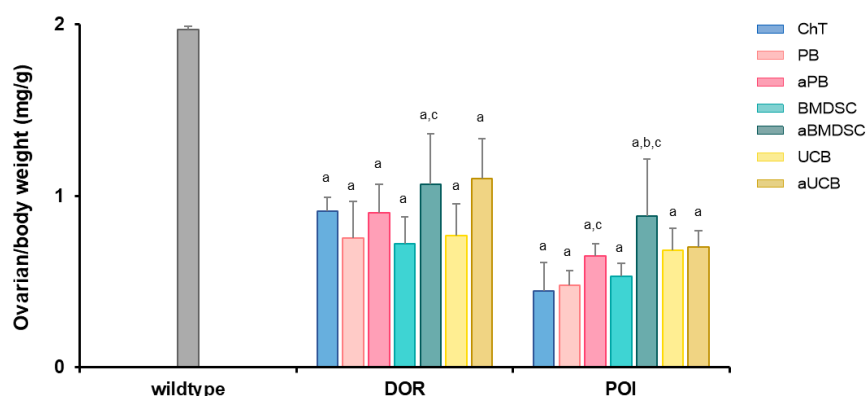
Figure 26. Ovarian weight after plasma administration in DOR and POI models. The ovarian weight on the day of sacrifice normalized to total body weight was recorded after two weeks of plasma administration (n=7 animals/group). Lowercase letters indicate statistical significance (p<0.05) with respect to wildtype (a), ChT group (b) and activated vs. non-activated plasma (c).

For POI mice, standard BMDSC and UCB plasma did not increase ovarian weight. Treatment with aBMDSC plasma did increase ovarian weight relative to other treatment groups (Figure 26; p = 0.021), but the treatment was not sufficient to restore ovarian weight to wild-type levels. Furthermore, aBMDSC plasma increased ovarian weight in both ovarian damage models when compared to its non-activated standard form (aBMDSC vs. BMDSC p = 0.03 and p = 0.01 in DOR and POI models, respectively).

2. Short-term effects

2.1 Analysis of ovarian reserve and follicular development

Follicular counts were performed in H&E-stained ovarian sections to evaluate the ovarian reserve and follicular development in all experimental conditions.

In the DOR model, ChT treatment reduced the total follicle number to 66.5% of wildtype levels. Treatment with PB, aPB, BMDSC, or UCB did not rescue this depletion (Figure 27). However, the use of aBMDSC and aUCB seemed to partially reduce the ChT-induced follicular depletion, recovering follicle numbers to 94% and 81.1% of the wild-type reference value, respectively.

This rescue appeared to be largely driven by restoration of primordial follicles in both the aBMDSC and aUCB groups, with values like those observed in the wild-type group (Figure 27B). Moreover, both activated plasmas increased the number of late pre-antral follicles above wild-type levels, but only aBMDSC restored the number of early antral follicles (Figure 27E-F).

In the POI model, ChT treatment reduced the ovarian reserve to 17.5% of wildtype levels and this was not rescued by PB, aPB, or BMDSC treatments. Interestingly, UCB-treated mice showed a higher number of total follicles when compared to ChT mice (p = 0.034, Figure 27A) mainly due to the primordial population (p = 0.019) (Figure 27B), although growing follicles, especially the late pre-antral population (p=0.032, Figure 27E), also increased. aBMDSC and aUCB were more potent than their non-activated forms at rescuing ChT-induced follicle loss, recovering values by increasing primordial, secondary,

and late-pre-antral populations. In fact, late preantral population values were like or even higher than wild-type values in both the aUCB and aBMDSC treated groups (Figure 27E). aBMDSC was also able to increase the number of antral stage follicles (Figure 27G).

A slight increase in primordial, secondary, and late pre-antral populations was also observed after aPB plasma treatment, although it was not as significant as that of the aBMDSC or aUCB effects.

The parallel analysis performed to understand how follicular depletion takes place after chemotherapy administration indicated that this process starts with an immediate first wave of follicular death, depleting 56.3% of the ovarian reserve by two days after exposure. Numbers then remained stable until day 7, when a second wave of death began, and lasted until day 21, decreasing the ovarian reserve to 2.5% of the starting value (Figure 28). These two main phases of follicular depletion indicate that plasma treatment administered on day 7 may act on the remaining primordial population that can benefit from the regenerative properties of the stem cell-secreted factors.
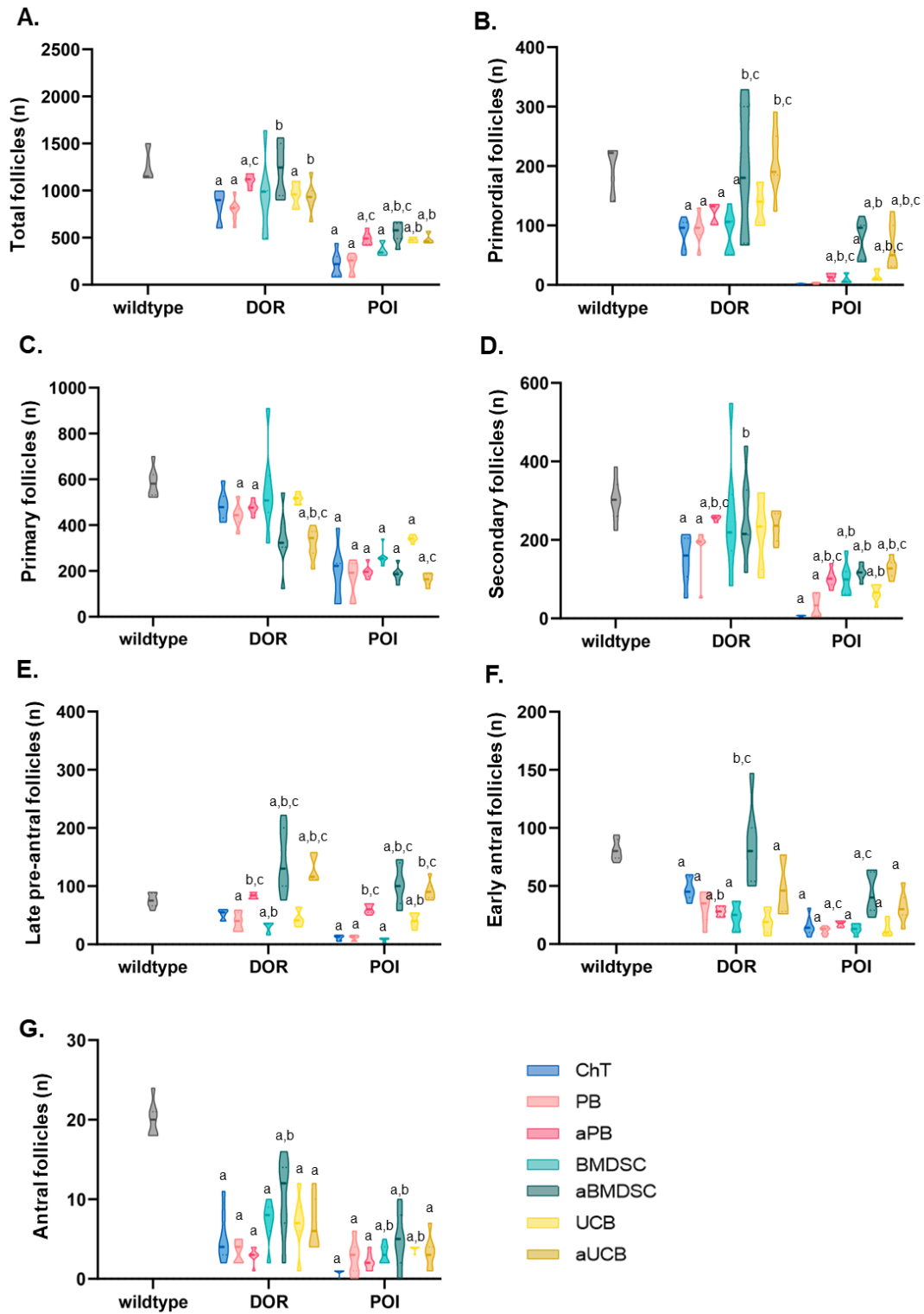
Figure 27. Ovarian reserve and follicle growth after plasma treatments in DOR and POI models. (A) Total number of follicles, (B) primordial, (C) primary, (D) secondary, (E) late pre-antral, (F) early antral and (G) antral follicles observed in DOR and POI mice after 2-weeks plasma treatment (n=7 animals/group). Lowercase letters indicate statistical significance (p<0.05) with respect to wildtype (a), ChT group (b) and activated vs. non-activated form (c).
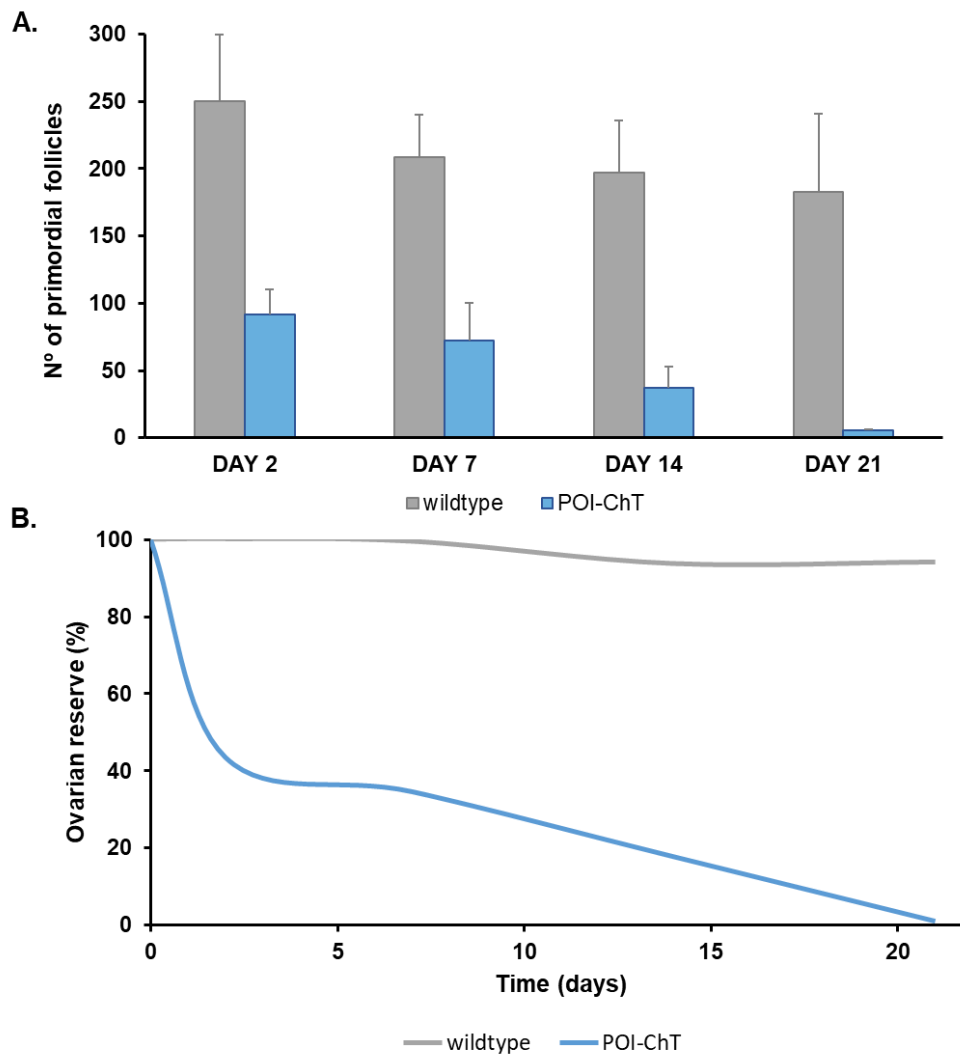
Figure 28. Dynamics of chemotherapy-induced follicular depletion. A) The number of primordial follicles was analyzed at two, seven, fourteen, and twenty-one days after ChT or vehicle (DMSO) administration. B) The ovarian reserve exhibited two waves of follicular depletion. Wildtype n=2 per group, POI-ChT n= 3 per group.

2.2 Analysis of MII oocytes and embryos

Following on from our main objective, and to further characterize the effects of plasma treatments on fertility, MII oocytes and embryos recovered from oviducts were evaluated.

Our experimental design and timing allowed the collection of MII oocytes and embryos derived from follicles at the primordial and early pre-antral stages at the time of ChT injury and treatment exposure[226]. In the DOR model, no differences in the number of MII oocytes and embryos were detected between the BMDSC/UCB and ChT groups.

Results

However, aBMDSC and aUCB treatments significantly improved both oocyte and embryo numbers. Specifically, aBMDSC-treated mice produced 10-fold and 7-fold more MII-oocytes and embryos, respectively, than ChT mice (p = 0.049 and p = NS, Figure 29A-B), and aUCB treated animals produced 11-fold and 10-fold more oocytes and embryos, respectively (p = 0.020 and p = 0.021).

In POI mice, administration of UCB, activated UCB, and activated BMDSC had positive effects on the number of MII oocytes (p = 0.049, p = 0.049 and p = 0.021, compared to ChT, respectively), and both aBMDSC and aUCB treatments increased the MII recovery rate to wild-type levels (Figure 29A).
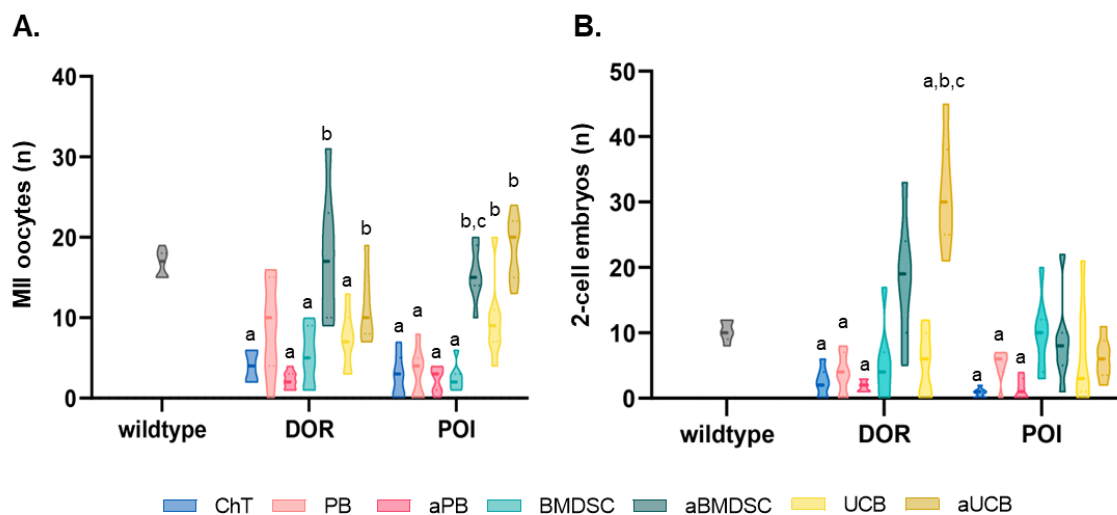
Figure 29. Oocytes and embryos recovered from DOR and POI mice after plasma injections. (A) Number of metaphase II (MII) oocytes and (B) 2-cell embryos recovered from mouse oviducts 36 h after human chorionic gonadotropin (hCG) injection in DOR- and POI-treated mice (n = 7 animals per group). Lowercase letters indicate statistical significance (p<0.05) with respect to wildtype (a), ChT group (b) and activated vs. non-activated form (c).

3. Evaluation of long-term reproductive potential

Breeding performance was assessed in four mice per group following our established treatment design in DOR and POI mice with continuous mating attempts for three months after plasma treatments.

BMDSC and UCB plasmas enhanced the long-term breeding performance of both DOR and POI mice. DOR females from all treatment groups achieved pregnancies and delivered pups at rates similar to those of ChT-treated females (Figure 30A). However, both UCB and BMDSC treatments increased litter sizes (Figure 30B; p = 0.015 and p = 0.002 compared to the ChT group, respectively). This increase was more significant when activated forms were used, especially for the aUCB group, where the litter size was similar to the wildtype value (10 ± 1 pups, Figure 30B).
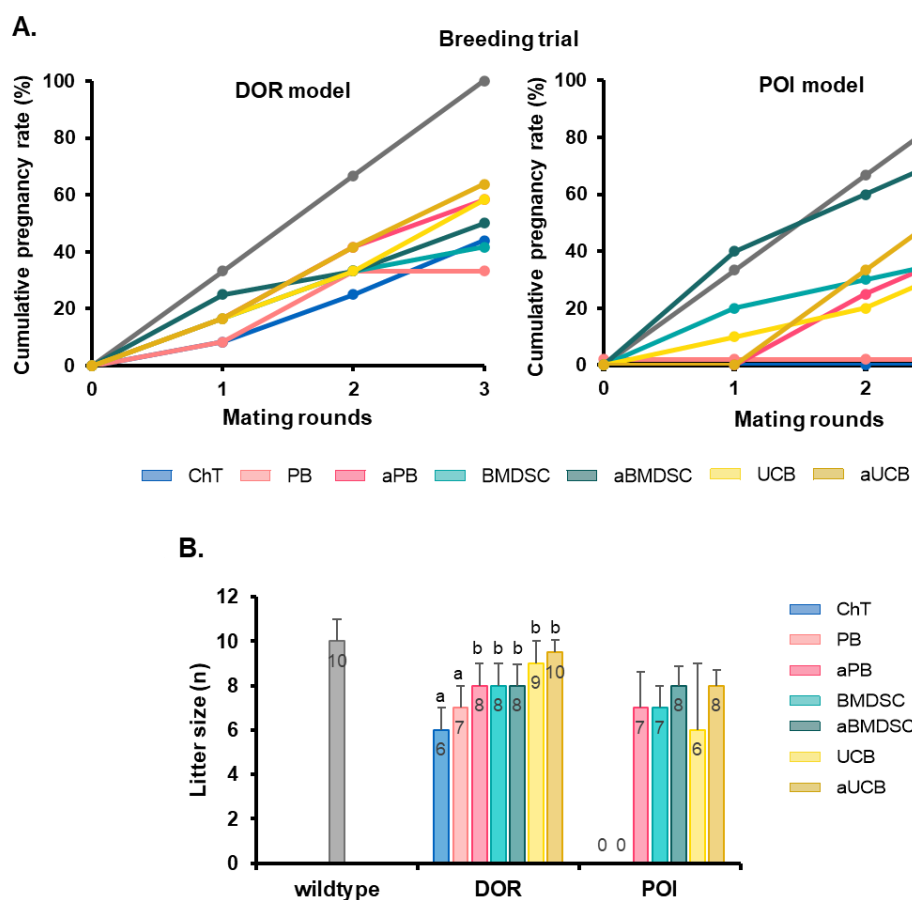
Figure 30. Breeding performance in DOR and POI models after plasma administrations. (A) Cumulative pregnancy rates from DOR- and POI- treated mice after 12 weeks and 3 mating attempts (n = 4 animals per group). (B) Number of healthy pups recorded after spontaneous pregnancies in each experimental group. Lowercase letters indicate statistical significance (p<0.05) with respect to wild-type (a), ChT group (b), and activated vs. non-activated form (c).

In the POI model, all animals in the ChT and PB plasma groups failed to achieve pregnancy after several mating attempts. Meanwhile, 40% of the BMDSC and UCB-treated mice obtained pregnancy and delivered healthy pups with average litter sizes of

7±1 and 6±3 pups, respectively (Figure 30A-B). Use of the activated forms (aBMDSC and aUCB) increased pregnancy rates to 80% and 67% respectively, with an average litter size of 8 ± 1 pups in both cases.

aPB plasma also restored pregnancies and the birth of healthy pups, although this improvement was much less than that observed for aBMDSC and aUCB.

4. Ovarian stroma status

The ovarian environment is important for promoting and maintaining follicle growth and maturation; thus, cell proliferation and ovarian local vascularization were examined by immunostaining in the ovarian samples harvested 21 days after injury and treatment.

4.1 Analysis of cell proliferation

BMDSC and UCB plasmas dramatically increased cell proliferation in ovarian tissue in both models of ovarian damage (DOR: BMDSC p = 0.0004, UCB p = 0.0024; POI: BMDSC p = NS , UCB p = 0.004, compared to the ChT group; Figure 31A-B), with the proliferative cells mainly identified as granulosa cells.

Activated BMDSC and UCB plasmas had more potent effects on proliferation than the non-activated forms in the DOR (aBMDSC vs. BMDSC p = 0.036; aUCB vs. UCB p = NS) and the POI (aBMDSC vs. BMDSC p = 0.006; aUCB vs. UCB p = 0.02) models. Interestingly, aPB plasma also increased cell proliferation in both models, but less dramatically than the aBMDSC and aUCB plasmas. In the activated plasma groups, both granulosa cells and ovarian stroma exhibited enhanced proliferation (Figure 31A).

4.2 Analysis of microvessel density

Compared to saline treatment, all plasma treatments stimulated a comparable increase in local MVD in DOR mice. However, in the POI condition, this increase ranged from a slight ~2-fold increase in the case of PB and aPB plasma to the almost 8 to 10-fold increases seen with the BMDSC, aBMDSC, UCB, and aUCB plasmas, which restored vasculature to wild-type levels (Figure 31C-D).
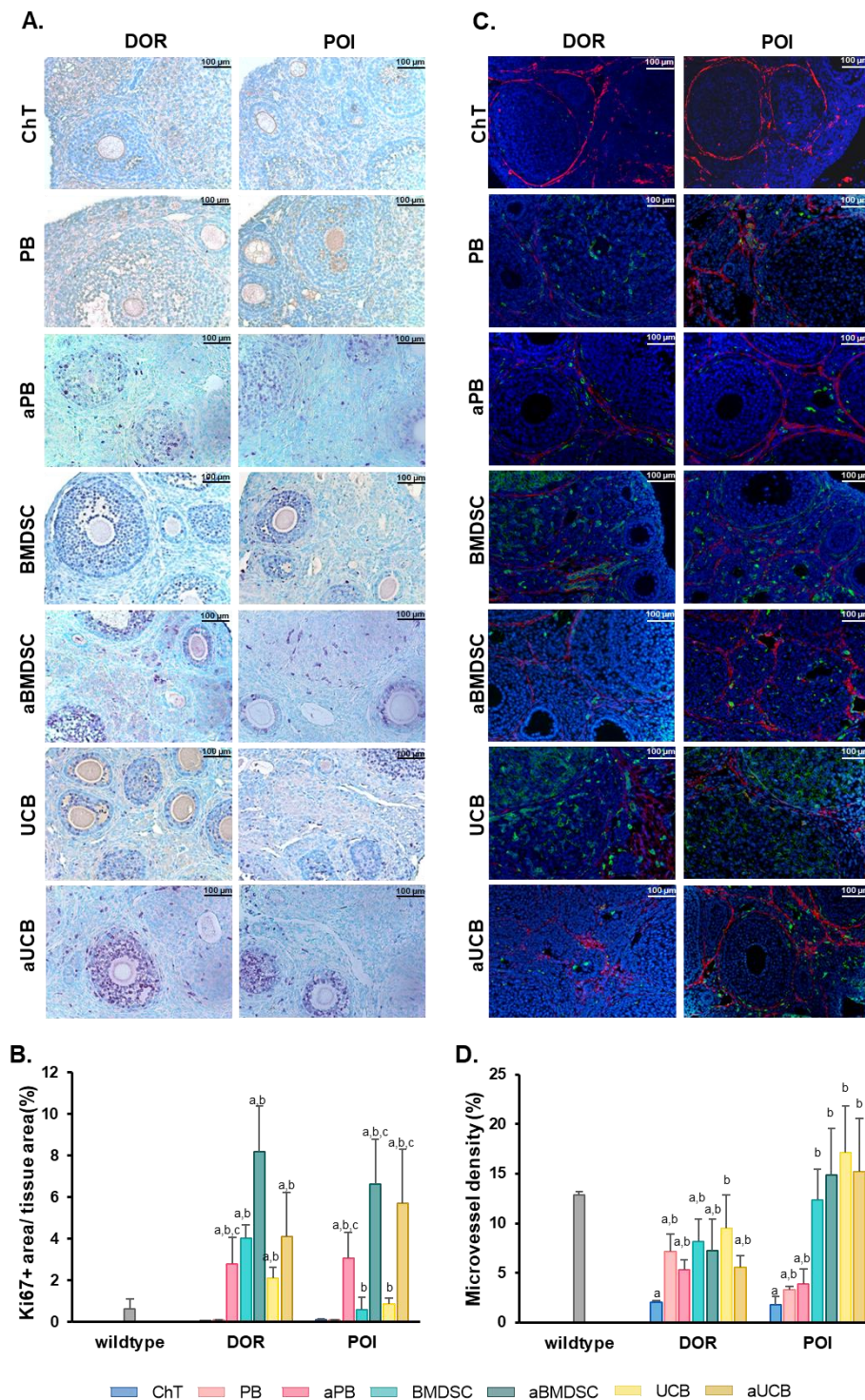
Figure 31. Analysis of cell proliferation and microvessel density in DOR and POI ovaries after 2-weeks of plasma treatments. (A) Ki-67 immunostained sections showing proliferative cells (purple) after plasma treatments in DOR and POI mice. Black scale bar = 200 μm. (B) Cell proliferation (n = 4 animals per group) measured as the Ki-67 positive area by total analyzed ovarian tissue area. (D) Ovarian vascularization imaged by immunostaining after plasma treatments in DOR and POI mice. Isolectin B4 (IB4) is in green, α-smooth muscle actin (a-SMA) in red, and nuclei stained with diamidino-2-phenylindole (DAPI) in blue. White scale

Results

bar = 200 µm. (E) Microvessel density (n = 4 animals per group), measured as the lectin-positive area by total analyzed ovarian tissue area. Lowercase letters indicate statistical significance (p<0.05) with respect to wildtype (a), ChT group (b), and activated vs. non-activated form (c).

4.3 Apoptosis

Apoptosis, the main effect of chemotherapy on ovaries, was also assessed by immunoblotting.

In DOR mice, BMDSC plasma was the only treatment that decreased cleaved caspase 3 protein levels (Figure 32, p = 0.02). In the POI model, the relative amount of cleaved caspase 3 in the BMDSC, aBMDSC, UCB and aUCB groups was reduced, although this difference was only statistically significant for the aBMDSC (p = 0.034) and UCB (p = 0.018) plasmas. In these four groups, the levels of this apoptotic effector did not differ from those observed in wild-type mice. In contrast, the PB-based treatments did not suppress the apoptosis induced by chemotherapy.
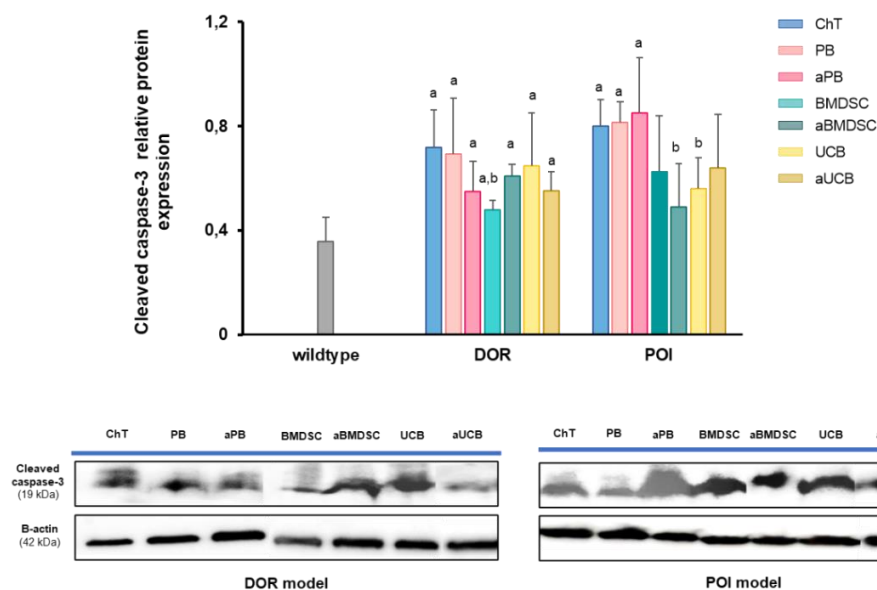
Figure 32. Cleaved caspase-3 levels in ovaries from control and plasma-treated DOR and POI mice. Immunoblotting analysis of the levels of the apoptotic marker cleaved caspase-3 after plasma treatments in DOR and POI models. N = 4 animals per group. Two-by-two comparisons were performed by the Mann-Whitney U-test. Lowercase letters indicate statistical significance (p<0.05) with respect to wildtype (a), ChT group (b), and activated vs. non-activated form (c).

5. Study of the proteomic profile of plasmas

To further elucidate possible mechanisms and effectors of the observed ovarian rescue, the proteome of all assayed plasma sources was established by SWATH-MS. A total of 293 proteins (FDR < 1%) were quantified in the six plasma samples to identify up- and down-regulated proteins associated with plasma type and/or activation status (Figure 33A-B).

A.

NON-ACTIVATED PLASMAS

ACTIVATED PLASMAS

NON-ACTIVATED PLASMAS	UP-REGULATED PROTEINS	DOWN-REGULATED PROTEINS	INVARIABLE PROTEINS
BMDSC	42	15	236
UCB	47	36	210

ACTIVATED PLASMAS	UP-REGULATED PROTEINS	DOWN-REGULATED PROTEINS	INVARIABLE PROTEINS
aBMDSC	39	30	224
aUCB	45	30	218

B.

ACTIVATED PLASMAS	UP-REGULATED PROTEINS	DOWN-REGULATED PROTEINS	INVARIABLE PROTEINS
aPB	18	22	253
aBMDSC	16	23	255
aUCB	25	16	253

Figure 33. DEPs of the proposed human plasma therapies obtained by SWATH-MS. (A) Table showing a global view of the differentially expressed proteins (DEPs) in non-activated and activated fractions. BMDSC and UCB samples were compared to the PB plasma, and aBMDSC and aUCB compared to the aPB. (B) Table showing a global view of the DEPs in activated compared to non-activated cognate fractions.

Comparison of BMDSC and UCB samples to PB plasma yielded DEPs, with the BMDSC sample exhibiting a higher percentage involved in the cell cycle, gene expression, developmental biology, DNA repair, chromatin organization, and metabolism than the UCB sample. The upregulated proteins in the UCB serum were mainly related to

metabolism, hemostasis, vesicle-mediated transport, and extracellular matrix organization (Figure 34). When signal transduction pathways were examined, the BMDSC DEPs were enriched in pathways related to RhoGTPases, death receptors, HIPPO, and nuclear receptors, while the UCB DEPs mostly affected signaling by GPCRs, integrins, and the MAPK family.

Activated fractions were then compared to PBa and the aBMDSC fraction showed a higher percentage of upregulated proteins acting in gene expression, DNA repair, and chromatin organization pathways. Surprisingly, proteins in the aUCB fraction were involved in the same processes enriched in the non-activated fraction (Figure 34A-B), indicating that activation has much less effect on this specific type of plasma. An in-depth analysis of the signal transduction pathways revealed that the aBMDSC DEPs were associated with signaling by RhoGTPases, nuclear receptors, NOTCH, PDGF, and WNT, while aUCB-upregulated DEPs were highly involved in MAPK signaling cascades. Remarkably, both fractions presented upregulated proteins implicated in AKT signaling activated by PIP3, VEGF, and HIPPO. Changes in proteins involved in DNA repair were also detected (Figure 34A-B). The BMDSC fraction DEPs were involved in DNA double-strand break repair (greater in aBMDSC than BMDSC), and DEPs in both the BMDSC and UCB (activated and non-activated) plasmas were associated with nucleotide excision repair.

Finally, activated plasmas were compared to their related non-activated plasmas. The UCB and aUCB samples shared several pathways, unlike the BMDSC samples, where activation resulted in the greatest number of changes (Figure 34B).
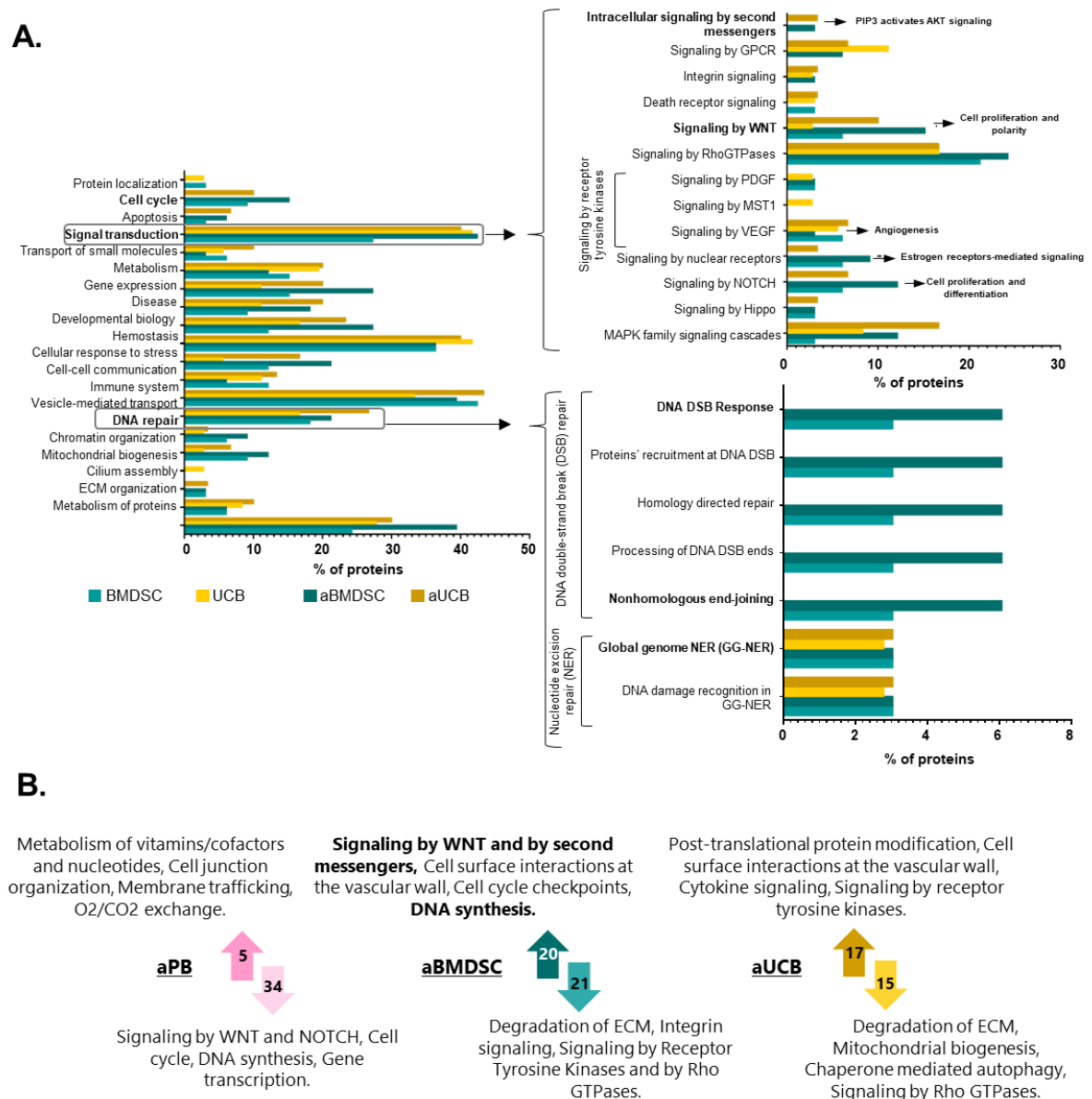
Figure 34. Functional analysis of DEPs from human plasmas. (A) The percentage of upregulated DEPs from BMDSC, UCB, aBMDSC, and aUCB fractions involved in different reactome pathways and DEPs specifically involved in signal transduction and DNA repair processes. (B) Diagrams showing the number of up- and down-regulated reactome pathways in each plasma fraction following activation.

6. Analysis of plasma effects on DNA damage and repair

Based on the proteomic data, an additional *in vitro* experiment with mouse tissue damaged by ChT was performed to establish the role of plasma treatments on DNA damage and repair.

Results

The expression of both DNA damage recognition (*Atm* and *p53*) and repair (*Rad51*, *Albkh2*, and *Apex1*) genes were increased by BMDSC plasma and less dramatically by UCB treatment at 12 h after exposure (Figure 35A). The activation of these signaling pathways correlated with a decrease in the pro-apoptotic *BAX/Bcl2* ratio (Figure 35B), and by 24 h, both the BMDSC and UCB groups exhibited reduced expression of the DNA damage marker *H2AX*, the pro-apoptotic *BAX/Bcl2* ratio, and cleaved caspase-3 (Figure 35C).
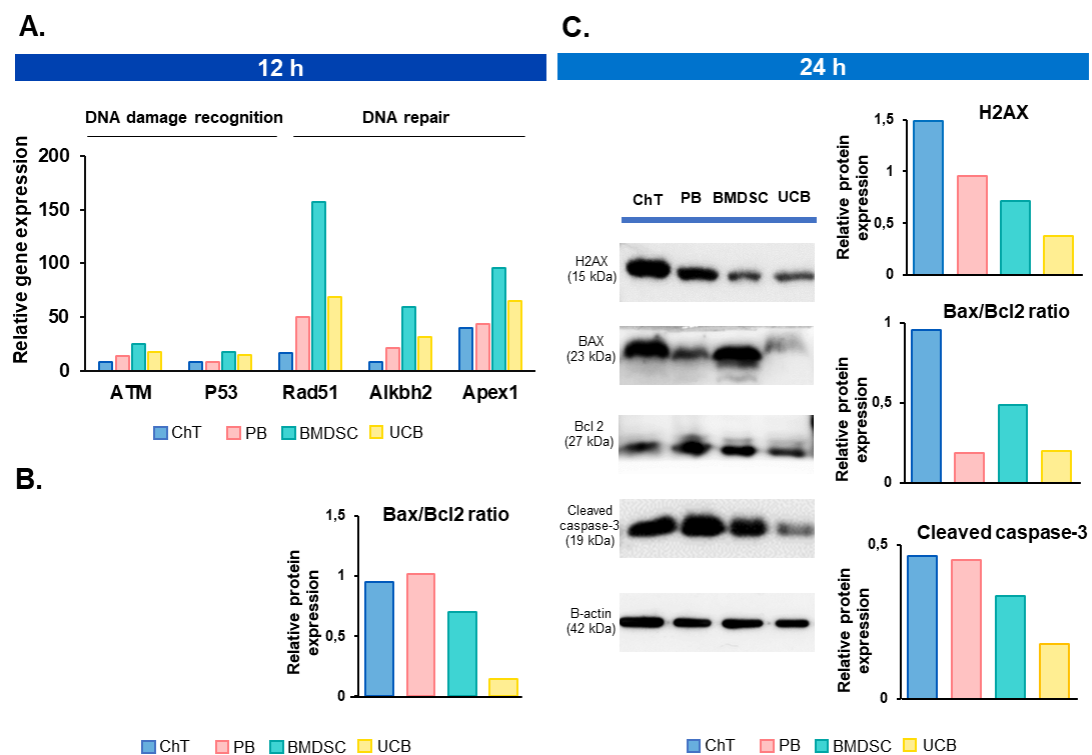
Figure 35. *In vitro* study to analyze DNA damage and repair after plasma treatments. (A) Relative expression of DNA damage recognition and repair genes, assessed by quantitative PCR, 12 h after chemotherapy and PB, BMDSC, or UCB *in vitro* treatments (n=3 mouse ovaries/group). (B) Immunoblotting analysis for the apoptotic regulators Bax and Bcl2 at 12 h (left panel). Quantitation of relative protein amounts at 12 h (n=3 mouse ovaries/group, pooled), showing a reduction in the pro-apoptotic Bax/Bcl2 ratio in G-CSF and UCB treated groups (right panel). (C) Immunoblotting analysis for the DNA damage marker H2AX and the apoptotic regulators Bax, Bcl2, and Cleaved caspase-3 at 24 h (left panel). Quantitation of relative protein amounts at 24 h (n=3/ group, pooled; right panel).

Similarly, at 24 h, the expression of DNA damage recognition and repair genes was lower in the BMDSC and UCB-treated groups than in the ChT group (Table 6). Interestingly, PB plasma also seemed to have a slight positive effect on the expression of DNA repair factors, although this did not correspond to alterations in H2AX or caspase-3 gene expression.

Table 6. Relative expression of DNA damage recognition and repair genes in ovaries 24 h after ChT and plasma treatments *in vitro*.

	Gene/protein	24h			
		ChT	PB plasma	BMDSC plasma	UCB plasma
Relative gene expression (fold change)	*ATM*	1.0	7x10-3	0.2	0.2
	p53	1.0	7x10-3	2x10-3	5x10-3
	Rad51	1.0	7x10-3	2x10-3	4x10-3
	Alkbh2	1.0	8x10-3	2x10-3	3x10-3
	Apex1	1.0	9x10-3	3x10-3	4x10-3

B) EFFECT OF THE MOST BENEFICIAL PLASMA TREATMENT ON HUMAN OVARIAN TISSUE

Based on the promising results obtained in our preclinical mouse model, the aBMDSC plasma was the most effective, and therefore most promising treatment, which we sought to validate in human ovarian tissue.

1. Analysis of ovarian reserve and follicular development

When follicular density and total follicle counts were compared, differences were not detected (Figure 36A), highlighting the homogeneity of the samples included in both groups. Nevertheless, a decrease in primordial (Figure 36B), together with an increase in primary (p=0.036; Figure 36C) and secondary populations (Figure 36D), was observed in aBMDSC treated grafts, indicating a promotion of follicular growth. Indeed, secondary follicles were only detected in human xenografts receiving aBMDSC plasma, where the percentage of growing follicles increased to 50.5%, compared to 19.9% in controls.
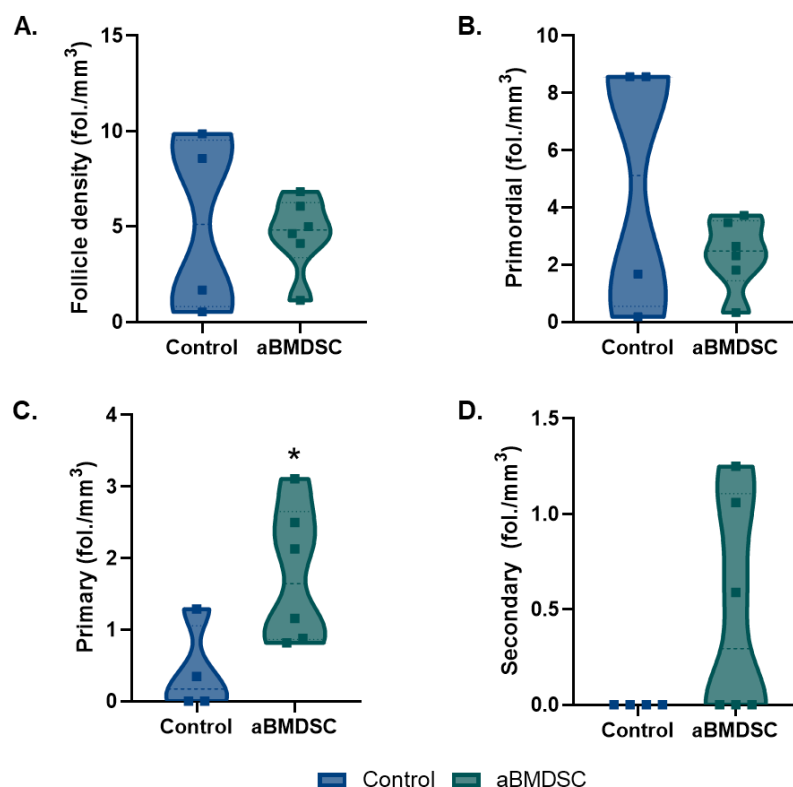
Figure 36. Human follicle development after aBMDSC treatment. (A) Total, (B) primordial, (C) primary and (D) secondary follicular densities in control (n=4) and aBMDSC treated (n=6) xenografts from poor ovarian response patients. $p < 0.05$ (*) was considered statistically significant.

2. Analysis of the human ovarian stroma

aBMDSC treatment induced a 4.6-fold improvement in stromal cell proliferation (p = 0.011; Figure 37A-B) and a 4-fold increase in microvessel density when compared to controls (p=ns; Figure 37C-D). Taken together, these findings confirm the regenerative properties of aBMDSC in human ovarian tissue, by promoting follicular growth, local vascularization, and cell proliferation.
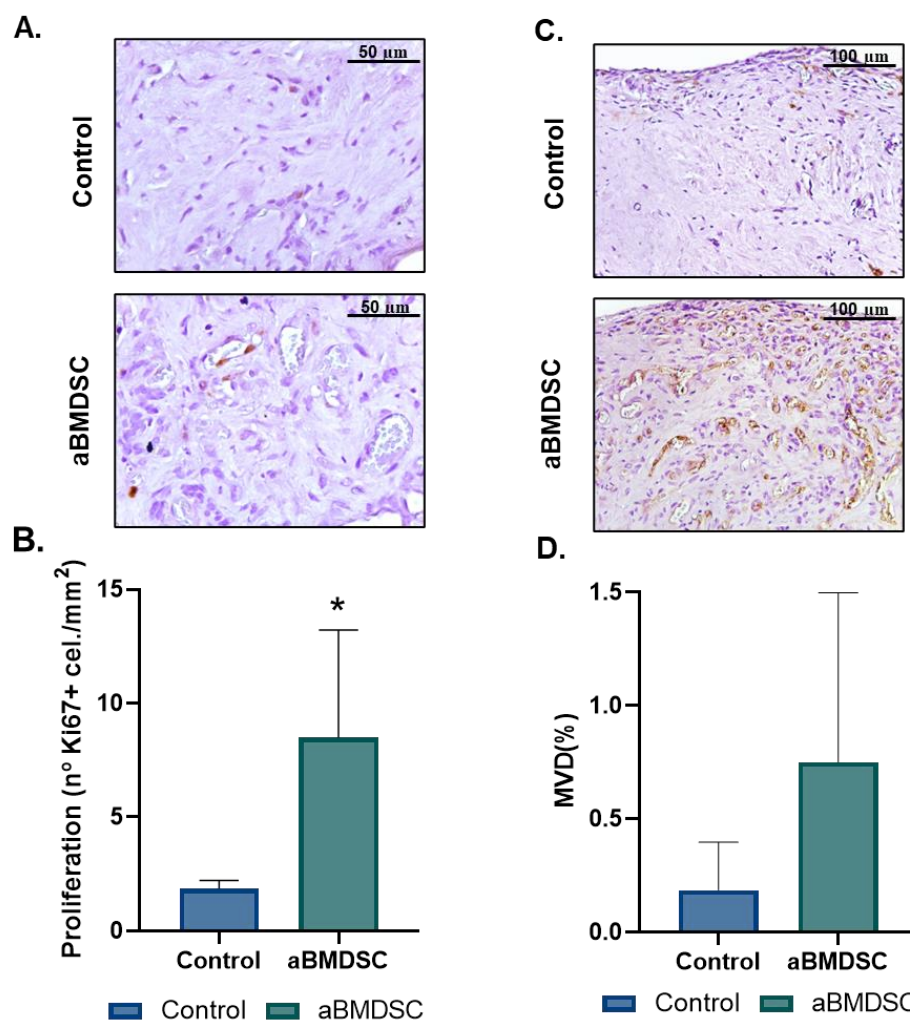
Figure 37. Human ovarian stroma status after aBMDSC injections. (A) Representative images and (B) quantification of the Ki-67 immunostaining (brown nuclei) after saline (control) and aBMDSC treatment in xenografts from poor ovarian response patients. Scale bar=50 µm. (C) Representative images of immunohistochemistry performed against the endothelial marker CD31 (brown). Scale bar = 100 µm. (D) Microvessel density measured as the CD31 positive area by total analyzed tissue area. $p < 0.05$ (*) was considered statistically significant.

3. Proteomic analysis of human ovarian tissue after plasma treatment.

To further establish an in-depth analysis of the beneficial effects of aBMDSC plasma in human ovarian tissue, the proteomic profiles of both control and aBMDSC-treated xenografts were established by SWATH.

A total of 1,224 proteins were quantified (FDR <1 %) in the xenografts, with 17 of these differentially expressed in the aBMDSC group, compared to controls. A brief functional description of these proteins (based on NCBI database information) and their specific role in the ovary are included in Table 7.

Thirty-five percent of these DEPs were involved in protein synthesis and processing in the endoplasmic reticulum, 24% in autophagy and 18% in angiogenesis. Moreover, several of the most upregulated proteins were linked to a specific function in the ovary, such as ANXA3, PGBM and RPS7, which have a key role in folliculogenesis, and ACSL1 and CATS, which are involved in follicular atresia. Additionally, three of the DEPs (PGK1, ANXA3 and PGBM) have been described as markers of oocyte quality (Table 7).

Table 7. SWATH-MS xenograft results: DEPs in aBMDSC human samples compared to controls. Protein description, fold regulation values and protein involvement in different biological processes, with a focus on those occurring in ovarian tissue, are included. Biological analysis was based on NCBI database information.

Protein ID	Protein Name	Fold-regulation	Functional description	Specific role in ovarian tissue
P33121	Long-chain-fatty-acid--CoA ligase 1 (ACSL1)	8.76	Isozyme involved in lipid biosynthesis and fatty acid degradation.	Regulator of follicular atresia[227].
P00558	Phosphoglycerate kinase 1 (PGK1)	8.16	Glycolytic enzyme with a role in angiogenesis.	Marker of oocyte quality[228].
P43307	Translocon-associated protein subunit alpha (SSR1)	5.02	Glycoylated endoplasmic reticulum membrane receptor associated with protein processing in this organelle.	Downregulated in follicles during aging[229].
P12429	Annexin 3 (ANXA3)	3.94	Calcium-dependent phospholipid-binding protein with a role in the regulation of cellular growth and signal transduction pathways.	Regulator of follicular development[230] /Marker of oocyte quality[231].
P38646	Stress-70 protein, mitochondrial (GRP75)	3.80	Mitochondrial protein with a role in cell proliferation, stress response and maintenance of the mitochondria.	Protection against apoptosis during follicular development[232,233].
Q9BPW8	Protein NipSnap homolog 1 (NIPSNAP1)	3.71	Protein involved in vesicular transport and mitophagy events.	-
Q02818	Nucleobindin-1	3.52	Component of calcium-binding EF-hand protein family, which has a key role in Golgi calcium homeostasis and Ca^{2+}-regulated signal transduction events.	-
O60256	60S ribosomal protein L5 (RPL5)	3.31	Ribosome subunit involved in protein synthesis.	-
P23918	Thymidylate kinase	3.30	Kinase involved in cell cycle progression and cell growth stages.	-
P62081	40S ribosomal protein (RPS7)	3.05	Ribosome subunit involved in protein synthesis.	Regulator of follicular development through the PI3K/AKT signaling pathway[234].

Protein ID	Protein Name	Fold-regulation	Functional description	Specific role in ovarian tissue
P98160	Basement membrane-specific heparan sulfate proteoglycan core protein (PGBM)	2.53	Proteoglycan that binds and cross-links many extracellular matrix components, regulating endothelial growth and re-generation.	Marker of oocyte quality[235] / Follicle-ECM interaction and regulator of follicle development[236].
Q99627	COP9 signalosome complex subunit 8 (CSN8)	2.22	Component of a protein complex, involved in the ubiquitin-proteasome pathway and, consequently, in autophagy and DNA repair mechanisms.	-
P51149	Calnexin (CALX)	1.91	Chaperone associated with protein processing in endoplasmic reticulum.	Folding of rLHR and rFSHR receptors[237,238].
P51149	Ras-related protein Rab-7A (RAB7A)	1.86	RAS-related GTP-binding protein involved in endo-lysosomal trafficking, endoplasmic reticulum processes and autophagy.	-
P25774	Cathepsin S (CATS)	-2.78	Thiol protease involved in antigen presentation, ECM degradation and autophagy.	Regulator of follicular atresia[239].
O43852	Calumenin (CALU)	-5.88	Calcium-binding protein associated with protein processing in endoplasmic reticulum.	Maintenance of the homeostasis induced by hypoxia during late follicular development[240,241].

C) DEVELOPMENT AND VALIDATION OF A MOUSE MODEL OF PHYSIOLOGICAL REPRODUCTIVE AGING

In this section, we aimed to validate a feasible animal model mimicking human ovarian physiological aging, to understand and test new strategies to delay or reverse ovarian aging effects.

1. Fertility outcomes

1.1 Ovarian reserve and follicle growth

To characterize how this depletion takes place in mice, follicular counts were performed at different ages.

Our model mimicked depletion of the ovarian reserve with advanced age. We observed significant reductions in the number of primordial and primary follicles in old mice compared to young and AMA groups ($p < 0.05$, Figure 38A). The activation of primordial follicles by FOXO3 extraction was also reduced in AMA and old mice compared to young mice (young: 53 ± 5%; AMA: 43 ± 3%, old: 22 ± 7%; young vs. AMA $p = 0.049$, young vs. old $p = 0.003$; Figure 38B). We also observed a reduced number of growing follicles at different developmental stages (secondary, late pre-antral and early antral follicles) in old mice compared to young and AMA mice ($p < 0.05$, Figure 38A).

The decrease in the follicle subpopulations was mirrored in the total number of follicles (young vs. old $p = 0.0078$; AMA vs. old $p = 0.03$; Figure 38C). Accordingly, the number of corpora lutea was lower in the ovaries of old mice (young vs. old $p = 0.013$; AMA vs. old $p = 0.044$; Figure 38D).
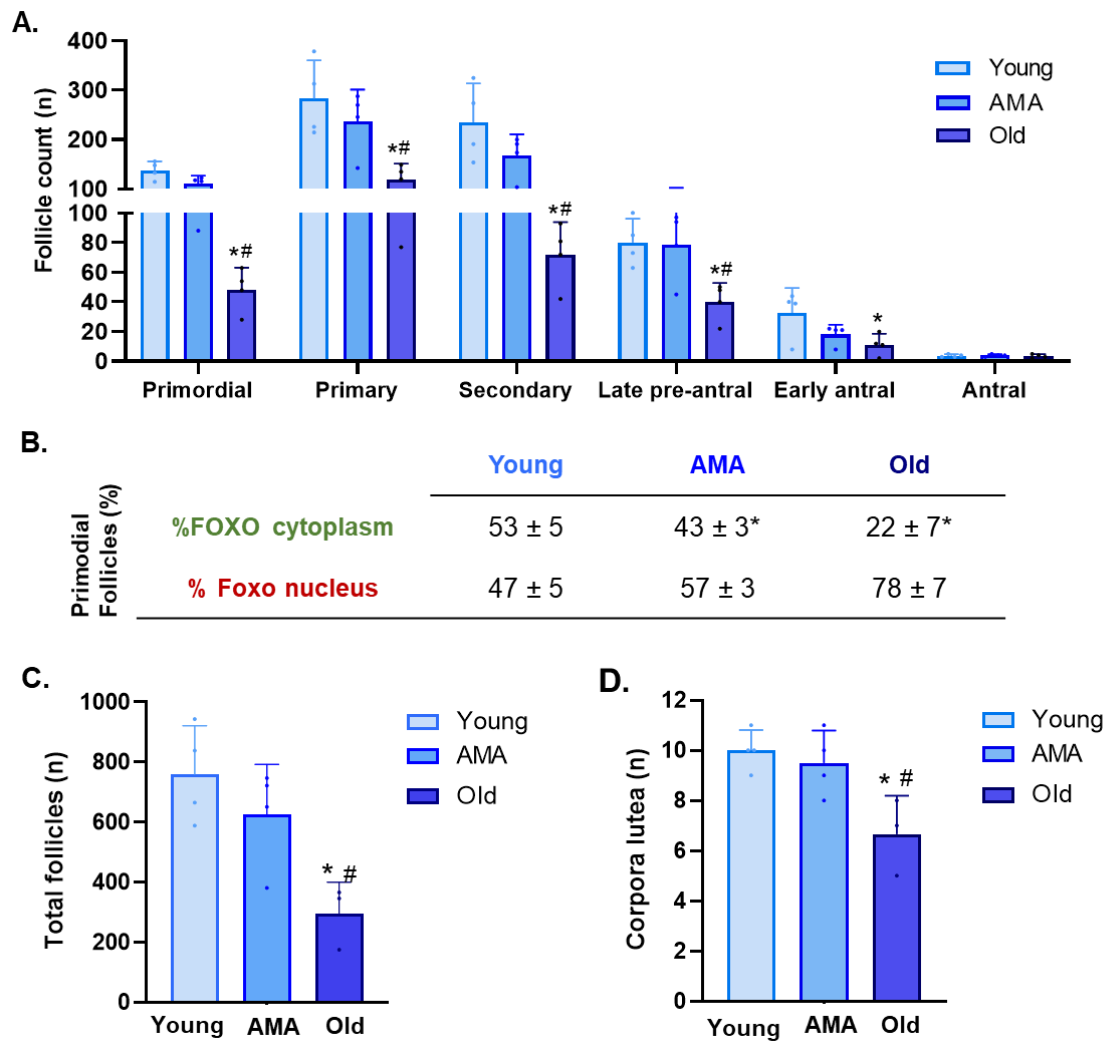
Figure 38. Ovarian reserve and follicle development in a physiological aging model. (A) The number of primordial, primary, secondary, late pre-antral, early antral, and antral follicles in young, AMA, and old mice. (B) The percentage of primordial follicles with FOXO3 located in cytoplasm (activated follicles) and nucleus (non-activated) in young, advanced maternal age (AMA), and old mice. (C) The total number of follicles, and (D) the corpora lutea in the physiological aging model *p < 0.05 AMA and old vs. young, #p < 0.05 Old vs. AMA.

1.2 Number and quality of MII oocytes

Because the quantity and quality of oocytes decrease with age, these parameters were studied in animals of different ages.

Following COS, less MII oocytes were recovered from the AMA mice than young mice (young: 24 ± 9, AMA: 13 ± 5; p = NS). Notably, this trend was significantly enhanced with

the old mice (young: 24 ± 9, old: 5 ± 5; p = 0.014, Figure 39A), who had 67.5% of oocytes with fragmented intracellular contents as a consequence of reduced quality (Figure 39B).
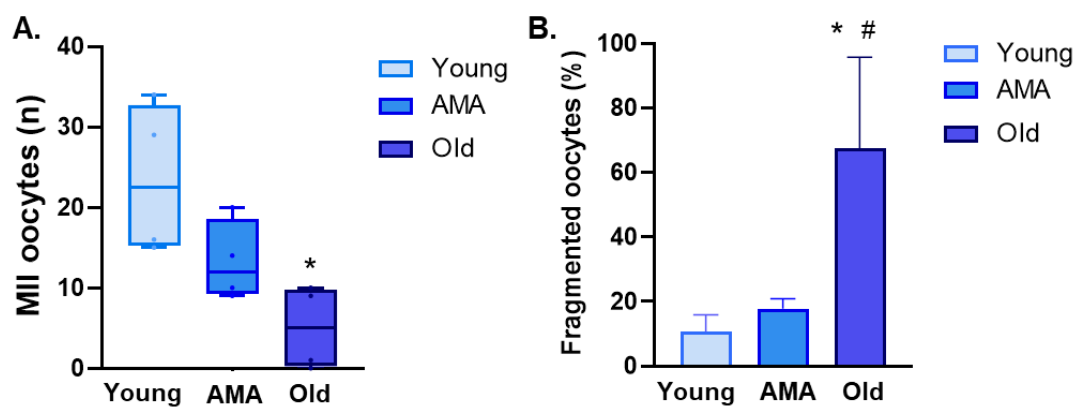
Figure 39. Oocyte number in a physiological aging mouse model. The number of metaphase-II (MII) oocytes (A) and percentage of fragmented oocytes (B) recovered from young, advanced maternal age (AMA), and old mice, following controlled ovarian stimulation (COS). *p < 0.05 AMA and Old vs. Young; #p < 0.05 Old vs. AMA.

In-depth immunofluorescence-based assessment of oocyte quality (Figure 40A) showed significantly decreased spindle area (Figure 40B) and abnormal spindle assembly (Figure 40B) in both the oocytes of AMA and old mice compared to the young group (p<0.05). Accordingly, we found a higher proportion of MII oocytes with chromosomal misalignments in AMA and old groups compared to young mice (79% and 100% vs. 40%, respectively; Figure 40D).

Results
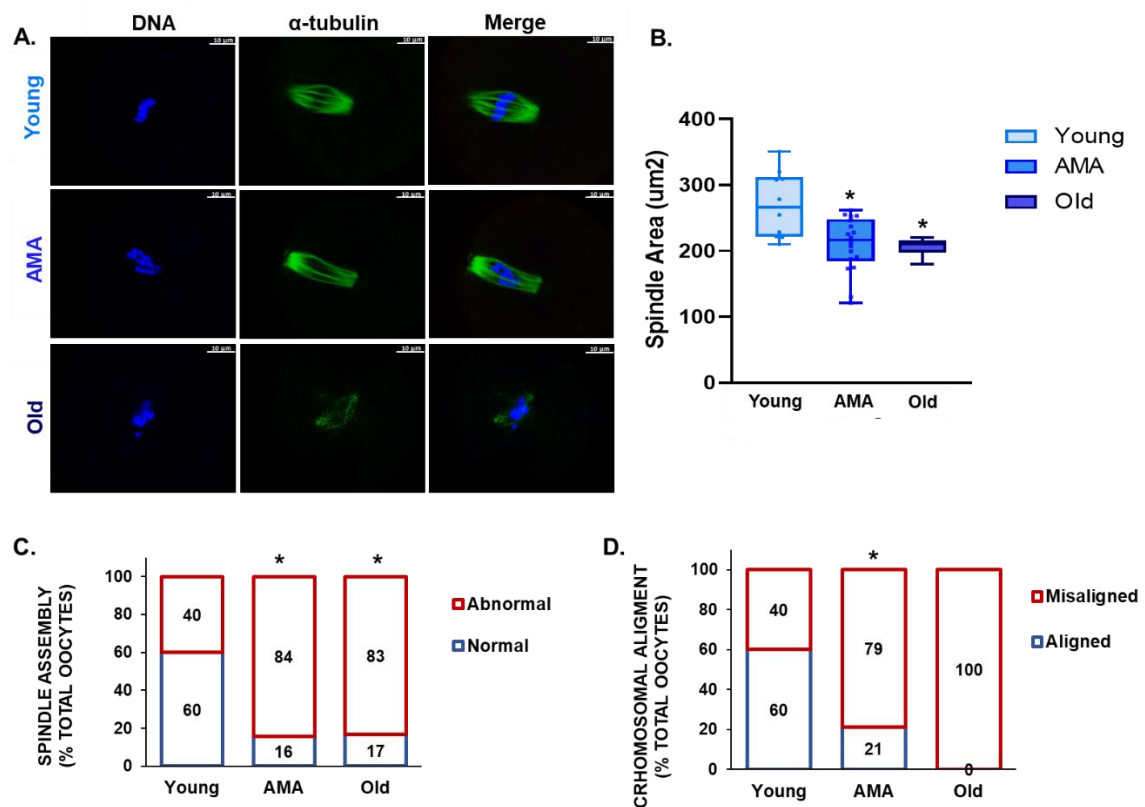
Figure 40. Oocyte quality assessment in a physiological aging mouse model. (A) Representative immunofluorescence images of spindle oocytes of young, AMA and old oocytes, showing alpha-tubulin (green) and Hoechst (blue). White scale bar = 10 μm. (B) Spindle area measurement of metaphase (MII) oocytes from young, advanced maternal age (AMA), and old experimental groups. C) Percentage of MII oocytes with normal or abnormal spindle assembly, and (D) percentage of oocytes with aligned/misaligned chromosomes from young, AMA, and old oocytes. *p < 0.05 AMA and Old vs. Young; #p < 0.05 Old vs. AMA.

1.3 Number of 2-cell embryos and further *in vitro* culture

At the time of collection, the 2-cell embryos were recovered to analyze the effects of age on the number and further embryo development to the blastocyst stage.

In a similar manner, the number of harvested 2-cell embryos was lower in AMA mice compared to young mice (young: 9 ± 5, AMA: 5 ± 3; p = NS, Figure 41A), and subsequent *in vitro* embryo culture revealed impaired blastocyst formation rates from 86% in young mice to 67% in AMA (Figure 41B). Age also affected the percentage of hatching

blastocysts (Young: 69%; AMA: 47%). Notably, no viable embryos were recovered from old mice, substantiating the significant implications of age on reproductive function.

	Young	AMA	Old
Blastocyst formation rate (%)	86 ± 24	67 ± 7	0 ± 0*#
Hatching blastocyst rate (%)	69 ±29	47 ± 6	0 ± 0*#
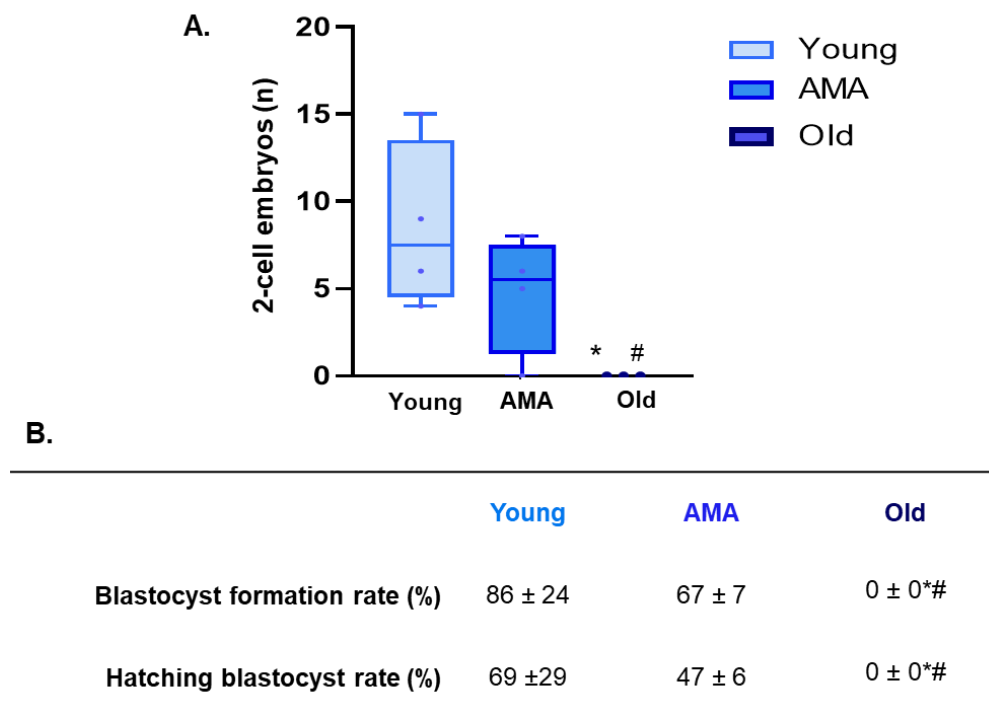
Figure 41. Number of 2-cell embryos from a physiological aging mouse model and subsequent *in vitro* culture. (A) The number of 2-cell embryos after COS from young, advanced maternal age (AMA), and old mice. (B) Blastocyst formation and hatching rates after embryo *in vitro* culture evaluated at day 5 and 6 of embryo development. $*p < 0.05$ AMA and Old vs. Young; $\#p < 0.05$ Old vs. AMA.

2. Ovarian stroma status: cell proliferation and vascularization

As previously mentioned, the ovarian stroma is essential for follicular growth and development and is affected by age in humans. Therefore, the proliferation status and MVD were studied in the ovaries of AMA and old mice, compared with young animals.

Age-related deficiencies were also observed in ovarian stroma, with cell proliferation significantly decreased in AMA ($p < 0.01$) and old ovaries ($p < 0.01$), compared to young mice (Figure 42A-B). Particularly, the percentage of proliferative primary (young: 47%, AMA: 25%, old: 28%) and secondary follicles (young: 80%, AMA: 71%, old: 37%) gradually decreased with age, was lower in the AMA and old groups, corresponding with the trend

for reduced microvessel density in older mice, although this did not reach statistical significance (p = NS, Figure 42A-C).
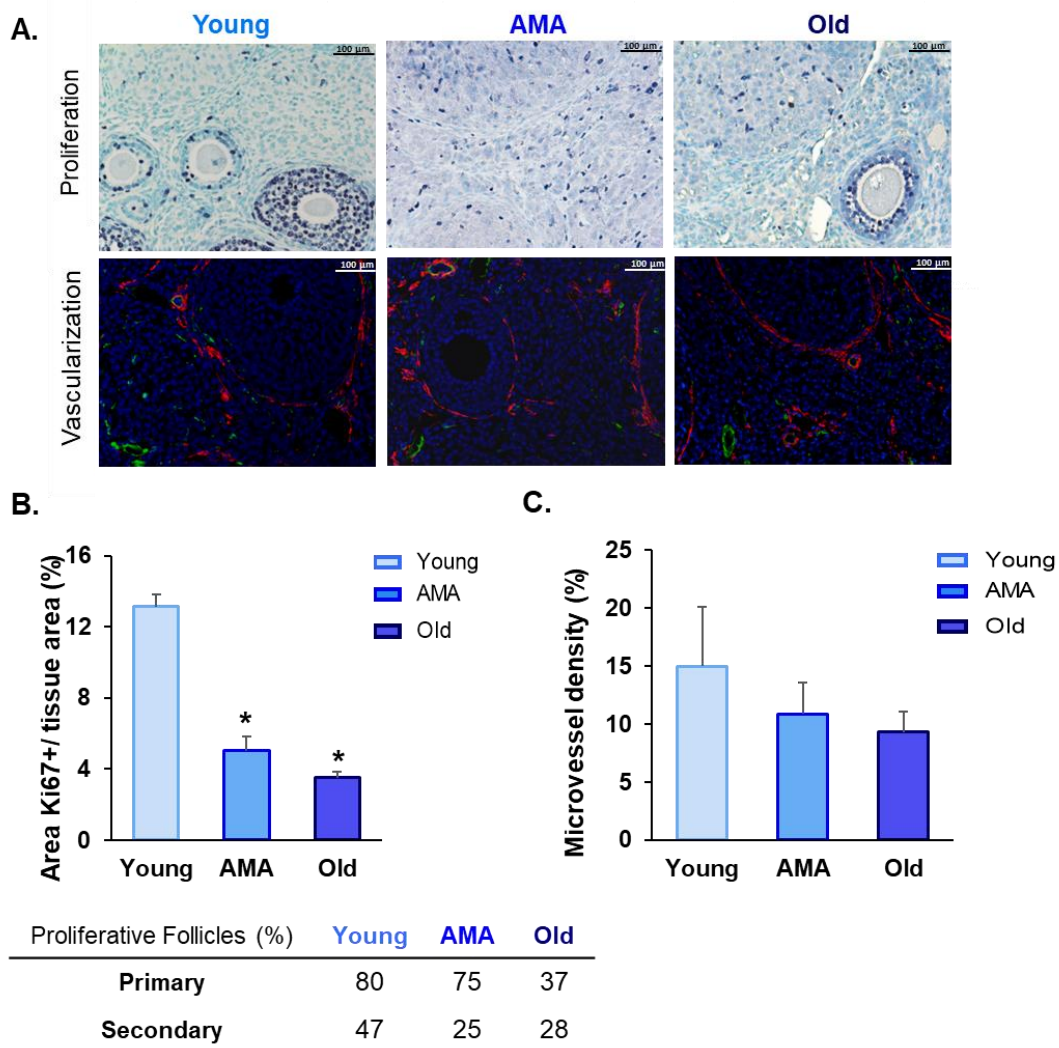
Figure 42. Analysis of ovarian stroma in a physiological aging mouse model. (A) Immuno-stained sections from ovarian stroma analysis in young, advanced maternal age (AMA) and old mice. Ki67-positive proliferative cells in purple (top row), isolectin-B4-positive endothelial cells in green and a-smooth muscle actin in red (bottom row). Black and white scale bars = 100 μm. (B) Quantification of total proliferation and percentage of proliferative primary and secondary follicles. Total cell proliferation was measured by dividing the Ki-67 positive area by total analyzed ovarian tissue area. (C) Quantification of vascularization. The microvessel density was measured by dividing the lectin-positive area by total analyzed ovarian tissue area. *p < 0.05 AMA and old vs. young, #p < 0.05 old vs. AMA.

3. Mitochondrial function and oxidative damage

Due to the association between ovarian aging, mitochondrial dysfunction, and oxidative damage, we evaluated the impact of these mechanisms on the fertility outcomes observed in ovarian aging.

First, the mtDNA copy number was employed as a marker of mitochondrial dysfunction. We noticed a decreasing mtDNA copy number in AMA and old ovaries compared to the young group (Figure 43) when mitochondrial genes, belonging to the stable part of mtDNA, were analyzed. The ND1 and COX3 mtDNA/nDNA ratio decreased in the AMA and old groups (p < 0.05).
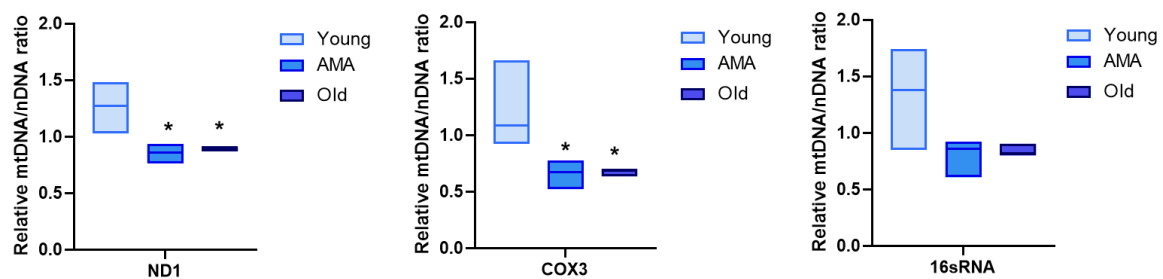
Figure 43. Analysis of mitochondrial DNA copy number in a physiological aging mouse model. (A) Relative mitochondrial/nuclear DNA (mtDNA/nDNA) ratio in the ovarian tissue of young, advanced maternal age (AMA), and old mice based on the RT-qPCR amplification of *ND1*, *COX3* and *16sRNA* mitochondrial genes (belonging to the stable part of mtDNA) normalized to the nuclear *18S* gene. *p < 0.05 AMA and old vs. young, #p < 0.05 old vs. AMA.

The reduced mitochondrial copies were associated with an increased level of 4-HNE, a marker of lipid peroxidation and oxidative damage, in AMA and old ovaries, compared to young (young vs. AMA p=0.012; young vs. old p =0.001; Figure 44A-B).

Corroborating this, TUNEL analysis showed a higher number of apoptotic cells (p = 0.028, Figure 44A-C) in the older mice, suggesting increased cell death in aged ovaries. Moreover, the analysis of apoptotic follicles revealed an increase in AMA and old mice, compared to the young group (young: 23%, AMA:52%, old: 64%; Figure 44D).

A.

B.

C.

D.

	Young	AMA	Old
Tunel (-)	77	48	36
Tunel (+)	23	52	64
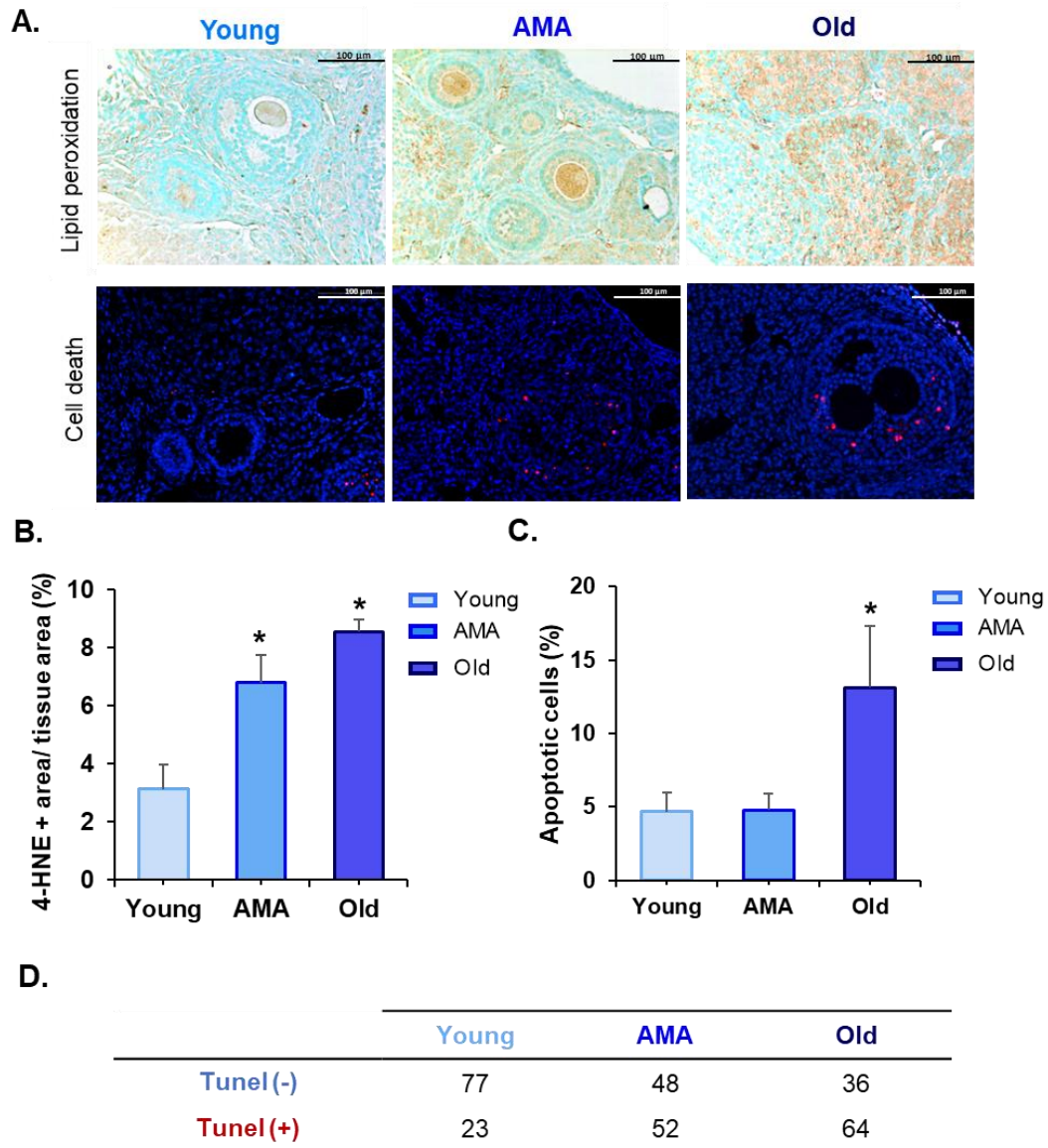
Figure 44. Analysis of lipid peroxidation and cell death in a physiological aging mouse model. (A) Photomicrograph of ovarian sections showing the oxidative damage-related peroxidative lipid product 4-hydroxynonenal (4-HNE; brown, top row), and cell death assessed by TUNEL (red, bottom row) in young, advanced maternal age (AMA) and old ovaries. (B) Corresponding quantification of the damaged tissue, estimated by dividing 4-HNE-positive area by the total area of ovarian tissue. (C) Quantification of apoptotic cells and percentage of apoptotic follicles at different ages. Black and white scale bars = 100 μm. *p < 0.05 AMA and old vs. young, #p < 0.05 old vs. AMA.

4. Proteomic profile of ovarian tissue at different ages

To corroborate the observed effects on reproductive potential and ovarian stroma, a SWATH analysis was carried out to study age-related modifications at the proteomic level.

A total of 1,834 proteins were quantified among the ovaries of young, AMA, and old mice. ElasticNet regression analysis identified 30 DEPs that were analyzed using a heatmap. Hierarchical clustering divided these DEPs into two main categories: one consisting of the old group, and the other including both the young and AMA groups, which in turn were classified into two distinct sub-clusters (Figure 45A).
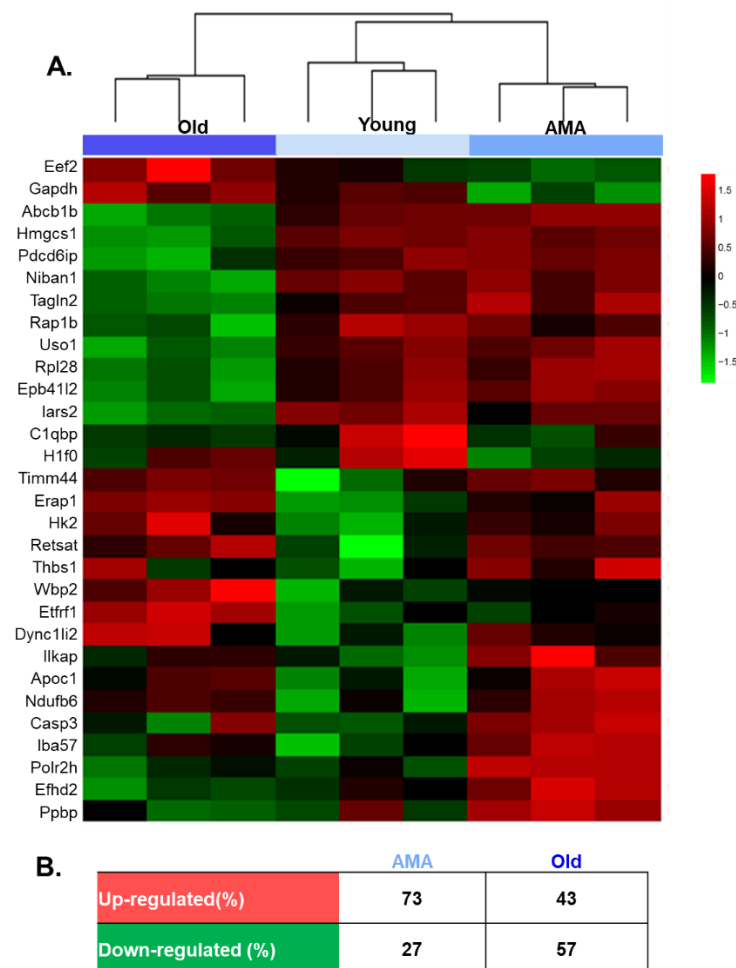
Figure 45. Proteomic characterization of a physiological aging mouse model by SWATH-MS technique. (A) Hierarchical clustering based on the expression of the top 30 significantly differentially expressed proteins (DEPs) between young, advanced maternal age (AMA) and old mice identified by ElasticNet regression analysis. The table beneath the heatmap shows an overview of the DEPs from the AMA and old mice, with respect to the young mice.

Remarkably, we observed a global downregulation of proteins in the old and AMA mice, with respect to the young mice, 57% and 27%, respectively (Figure 45B).

Then, the pathways regulated by the DEPs were studied by performing a GO analysis to understand more about the underlying biological processes, molecular function, and cellular components.

The GO enrichment revealed biological processes related to the regulation of metabolic processes, gene expression, lipid transport, and angiogenesis, in addition to pathways involved in mitochondrial activity, such as response to stress, ATP metabolic processes, or respiratory electron transport chain. Cellular components of the reticulum, mitochondrial matrix, intercellular transport, polymerase complexes, and DNA binding proteins were also enriched. Regarding molecular functions, the enrichment analysis highlighted the tumor necrosis factor receptor superfamily, chromatin DNA and death receptor, and complement component C1q complex (Figure 46A)

Finally, GOchord plot analysis highlighted genes such as *Casp3, C1q, Thbs1,* and *Gapdh,* among the top ten enriched biological processes (Figure 46B).
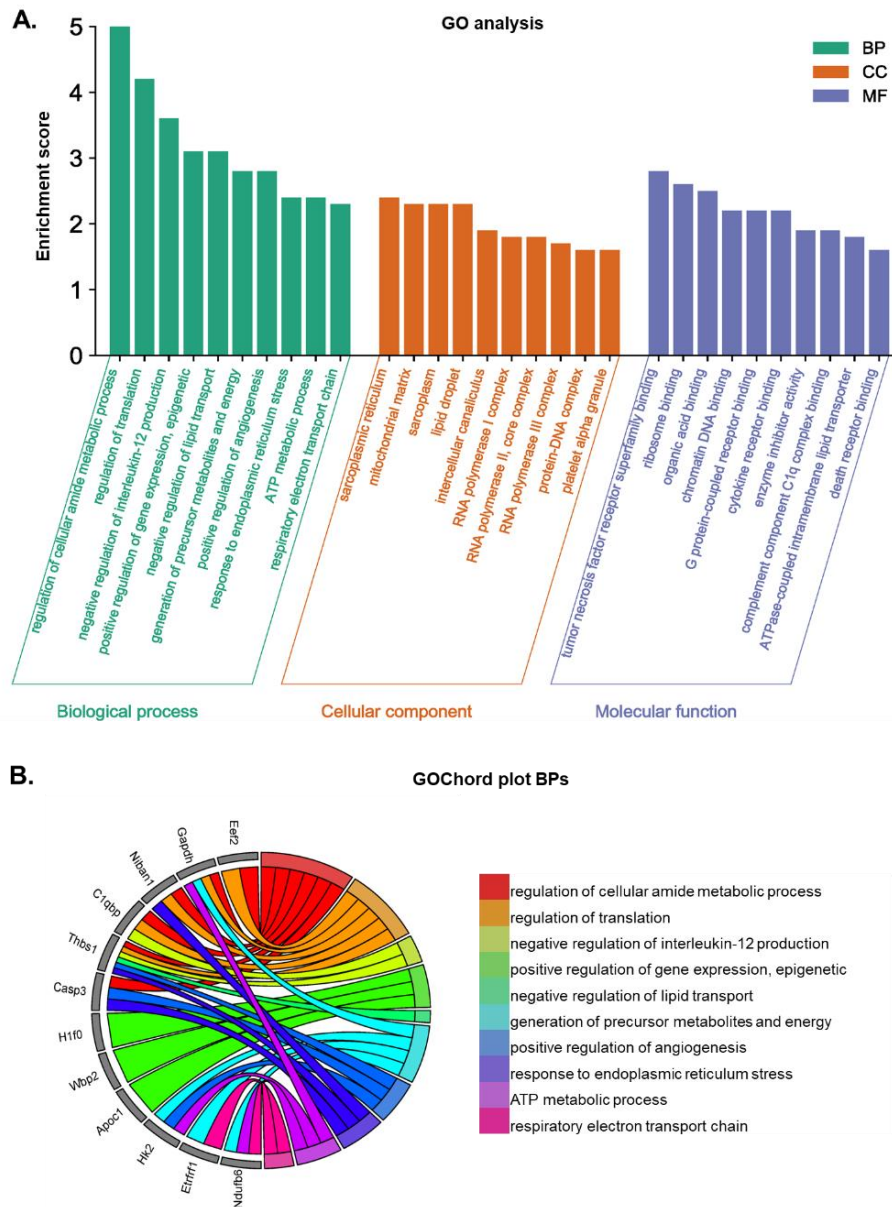
Figure 46. Functional analysis of DEPs from a physiological aging mouse model. (A) Significantly enriched Gene Ontology (GO) biological processes (BPs), cellular components (CCs), and molecular functions (MFs) (FDR < 0.05) associated with the DEPs identified in advanced maternal age (AMA) and old mice. (B) GOChord plot graph of the top ten BPs for each group young, showing the relationship between pathways and the most relevant genes between them.

D) INTRAOVARIAN ADMINISTRATION OF THE MOST BENEFICIAL PLASMA TREATMENT IN A PHYSIOLOGICAL AGING MOUSE MODEL

After characterizing the physiological aging model, we aimed to evaluate whether combining bone marrow-derived stem cell-secreted and platelet-enclosed factors (aBMDSC) could improve fertility through a single intraovarian injection, improving the effects of standard activated platelet-rich plasma (aPRP).

1. Effects on fertility outcomes

1.1 Follicle growth activation and dynamics

A single intraovarian injection of aBMDSC activated dormant follicles in all age groups, as indicated by the increased percentage of primordial follicles with FOXO3 nuclear extrusion, compared to control and aPRP treatment groups (Figure 47).
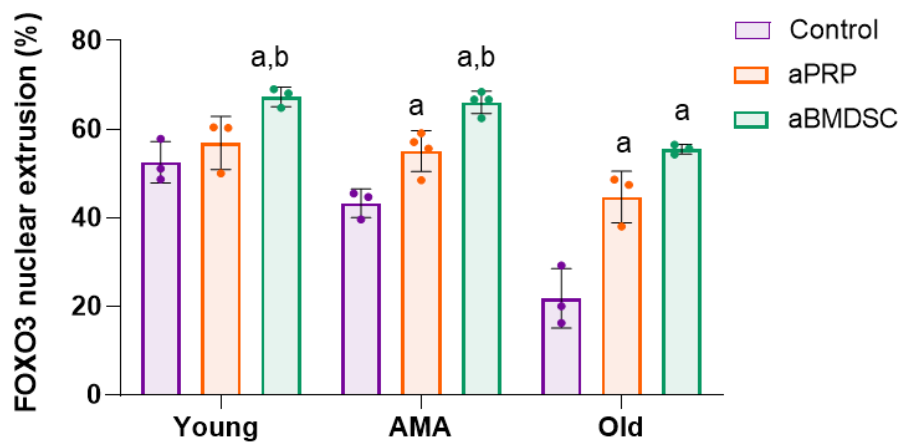
Figure 47. Follicular activation after intraovarian plasma administration in a physiological aging mouse model. Percentage of primordial follicles with FOXO3 nuclear extrusion in young, AMA, and old mice after a single intraovarian injection of saline solution, aPRP, or aBMDSC. Lowercase letters indicate statistical significance (p<0.05) with respect to control (a) or aPRP treatments (b).

Follicular activation was also confirmed by a significant reduction of primordial follicles in both the young and AMA mice (Figure 48A). These changes in follicular dynamics were associated with increased numbers of growing populations (statistically significant for primary and antral follicles) in the young, AMA, and to a lesser extent, in the old mice

(Figure 48B-F-H). Notably, only primary follicles were significantly increased in old mice that received aBMDSC (p=0.0006).

Moreover, the aBMDSC protected against global follicular depletion by 40% in the AMA and old mice compared to control-treated mice, however, statistically significant differences were not detected between any of the experimental groups (Figure 48G).

We also observed more corpora lutea in AMA mice, compared to control group (Figure 48H). These results, together with the previously noted effects of aBMDSC plasma on primordial follicles, could suggest the end of a follicular-growth wave and the initiation of a new one occurs even in aging ovaries.

Finally, aPRP treatment also produced positive effects on primordial activation and primary follicle numbers in both the AMA and old mice (Figure 48A-B).
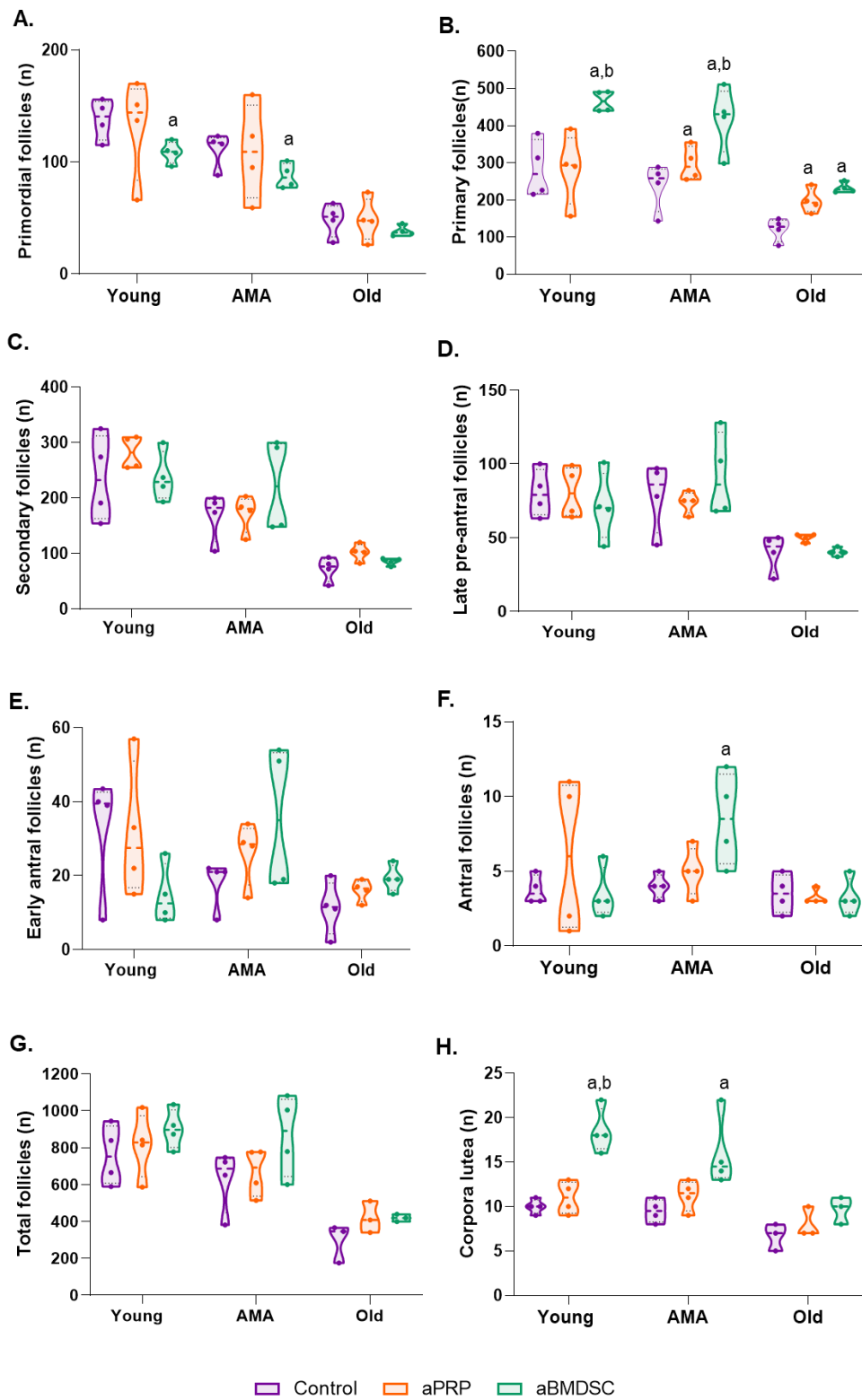
Figure 48. Follicle growth activation and dynamics after intraovarian plasma injections in a physiological aging mouse model. The number of (A) primordial, (B) primary, (C) secondary, (D) late pre-antral, (E) early antral, (F) antral, (G) total follicles, and (H) corpora lutea observed in young, AMA, and old mice after a single intraovarian injection of saline solution, aPRP or aBMDSC (n=4 animals per group). Lowercase letters indicate statistical significance (p<0.05) with respect to control (a) or aPRP treatments (b).

1.2 Number and quality of MII oocytes

Following COS, we recovered significantly more MII oocytes from the young mice treated with aBMDSC rather than control (Figure 49A). We observed no differences in the percentage of fragmented MII oocytes (Figure 49B), suggesting aBMDSC injection did not cause any deleterious effects on oocytes when injected into healthy ovaries.
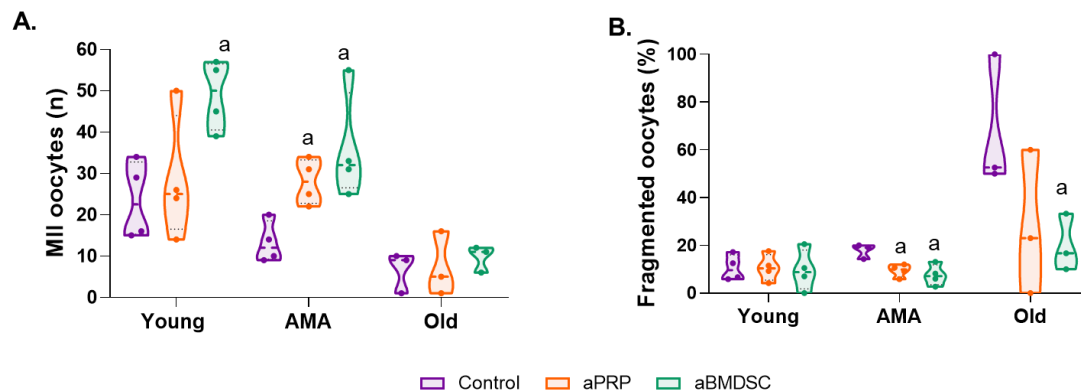
Figure 49. Oocytes recovered after intraovarian plasma injections in a physiological aging mouse model. The number of metaphase II (MII) oocytes (A), and percentage of fragmented oocytes (B) recovered from young, AMA and old treated mice 36 h after human chorionic gonadotropin (hCG) administration (n = 4 animals per group). Lowercase letters indicate statistical significance (p<0.05) with respect to control (a) or aPRP treatments (b).

In the AMA group, aBMDSC significantly augmented the quantity of MII oocytes (p=0.017, Figure 49A) and reduced the percentage of fragmented oocytes (p=0.018, Figure 49B) to a level comparable to young mice. Evaluating the oocyte quality of AMA mice, we observed that aBMDSC increased spindle area (p=0.027), improved spindle assembly (p=0.04), and reduced chromosomal misalignment (p=NS) (Figure 50 and Figure 51A-B). Despite old mice exhibiting the worst baseline outcomes, the benefits of aBMDSC treatment were evidenced with an increased yield of MII oocytes (p=NS, Figure 49A), significantly reduced oocyte fragmentation (p=0.05, Figure 49B), and improved chromosomal alignment (p=NS) (Figure 51B).

The benefits of standard aPRP treatment were also evident in the AMA model, with the improvement in quantity and quality of MII oocytes, though to a lesser extent than the improvements in old mice (Figure 49-51).
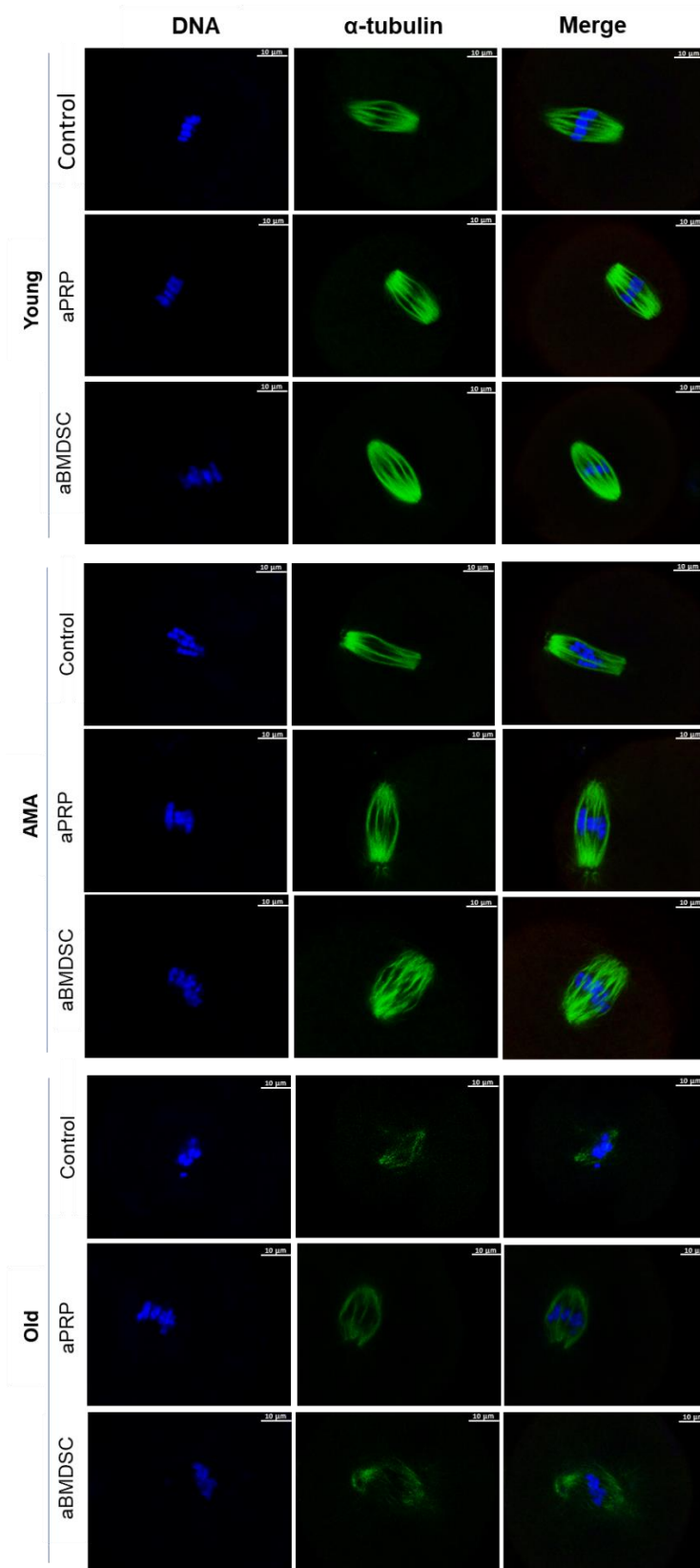
Figure 50. Immunofluorescence to analyze oocyte quality after intraovarian plasma injections in a physiological aging mouse model. Representative confocal immunofluorescent images of the meiotic spindles from each group used to analyze oocyte quality. Alpha-tubulin (microtubules) stained green, and chromosomes stained with Hoescht in blue. Scale bars are set to 10 μm.
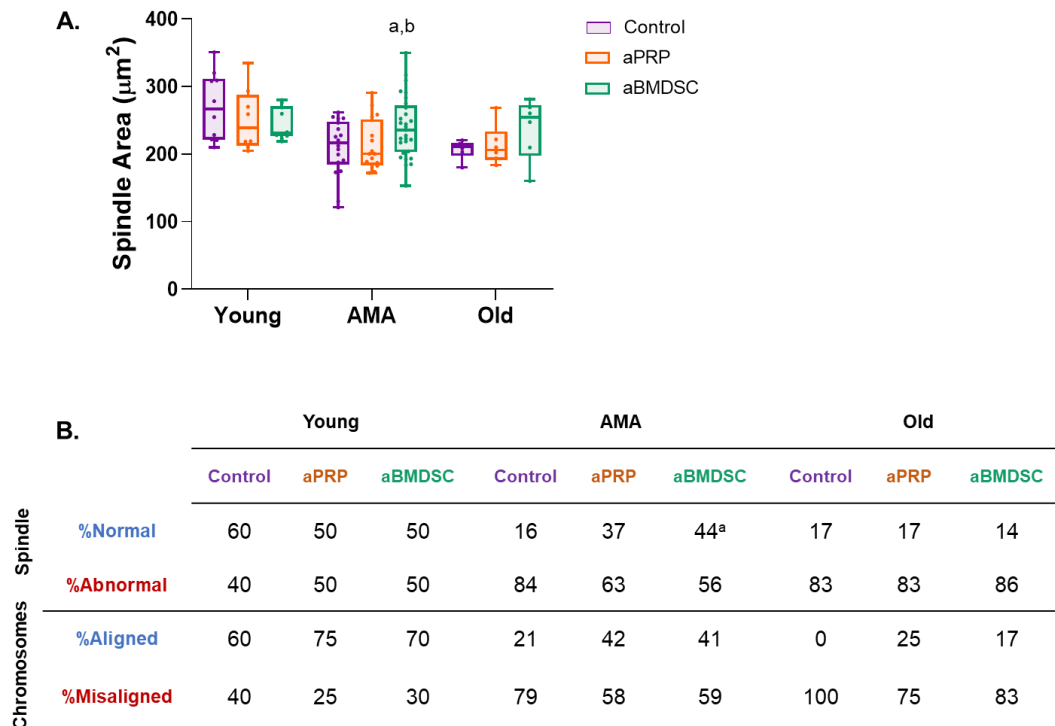
Figure 51. Assessment of oocyte quality after intraovarian plasma injections in a physiological aging mouse model. (A) Measurement of spindle area of oocytes from young, AMA and old mice after a single intraovarian injection of saline solution, aPRP or aBMDSC, using immunofluorescent images. (B) Proportions of normal/abnormal spindle assembly and chromosomal alignments in young, AMA, and old oocytes (n=12-30 oocytes per group). Lowercase letters indicate statistical significance (p<0.05) with respect to control (a) or aPRP treatments (b).

1.3 Number of 2-cell embryos and further *in vitro* culture

At sacrifice, a greater number of 2-cell embryos were harvested from young, AMA, and old mice treated with aBMDSC than control treatment (p=0.040, p=0.046, and p=NS, respectively; Figure 52A). Indeed, mice who received the control treatment were not able to generate embryos.

125
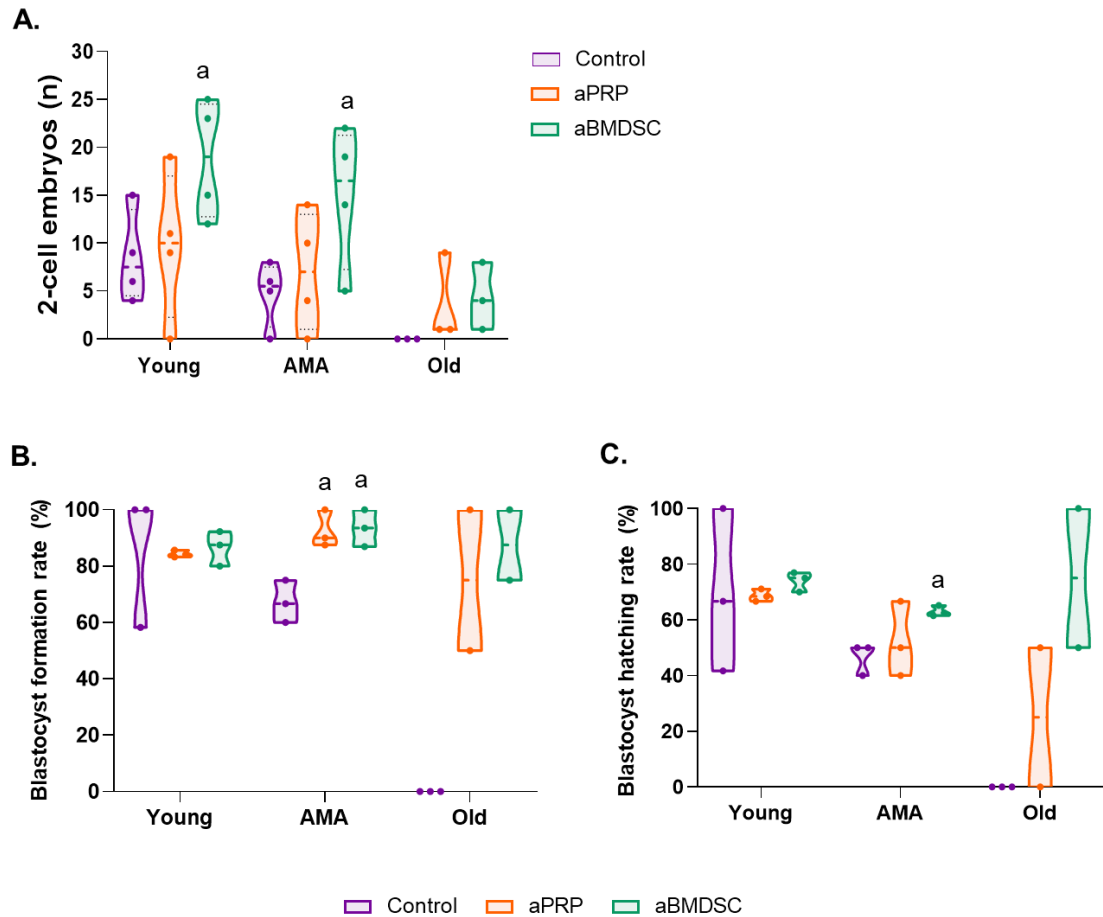
Figure 52. 2-cell embryos recovered after intraovarian plasma injections in a physiological aging mouse model and further *in vitro* culture. (A) Number of 2-cell embryos collected from mouse oviducts 36 h after hCG administration in young, AMA, and old mice (n=4 per group). Blastocyst formation (B) and hatching rates (C) achieved after *in vitro* culture of the collected 2-cell embryos. Lowercase letters indicate statistical significance (p<0.05) with respect to control (a) or aPRP treatments (b).

Subsequent *in vitro* embryo culture revealed that aBMDSC treatment supported blastocyst formation (Figure 52B) and the ability to reach hatching (Figure 52C), especially in the AMA and old mice.

aPRP also improved the blastocyst formation rate in the AMA condition (p=0.011) and enabled the generation of embryos in the old mice. However, this treatment did not significantly improve embryo cleavage or blastocyst hatching rates in any of the age groups.

2. Ovarian stroma status

2.1 Analysis of cell proliferation

aBMDSC treatment increased cell proliferation compared to controls in the young, AMA and old conditions, while there was no effect in the old mice with aPRP only (Figure 53A-B). Proliferative cells were identified in both the stroma and follicles (Figure 53A).

Indeed, the analysis of follicles at each specific stage showed an increase in the number of primordial, primary, and secondary follicles in a proliferative state following plasma treatments (Figure 54A-B-C). This effect was especially relevant after aBMDSC injection in the AMA and old groups, particularly in the secondary follicles, where 90% of follicles were proliferating (Figure 54C).

2.2 Analysis of microvessel density

When ovarian vascularization was assessed, no differences were noticed in the young model depending on the plasma treatment. However, we found that MVD was improved after aBMDSC injection in the AMA and old conditions compared to controls, reaching levels similar to those observed in young mice (Figure 55A-B), especially in the AMA condition.

After aPRP treatment, MVD was only increased from control levels within the old group, whilst aPRP did not increase MVD in young or AMA mice.
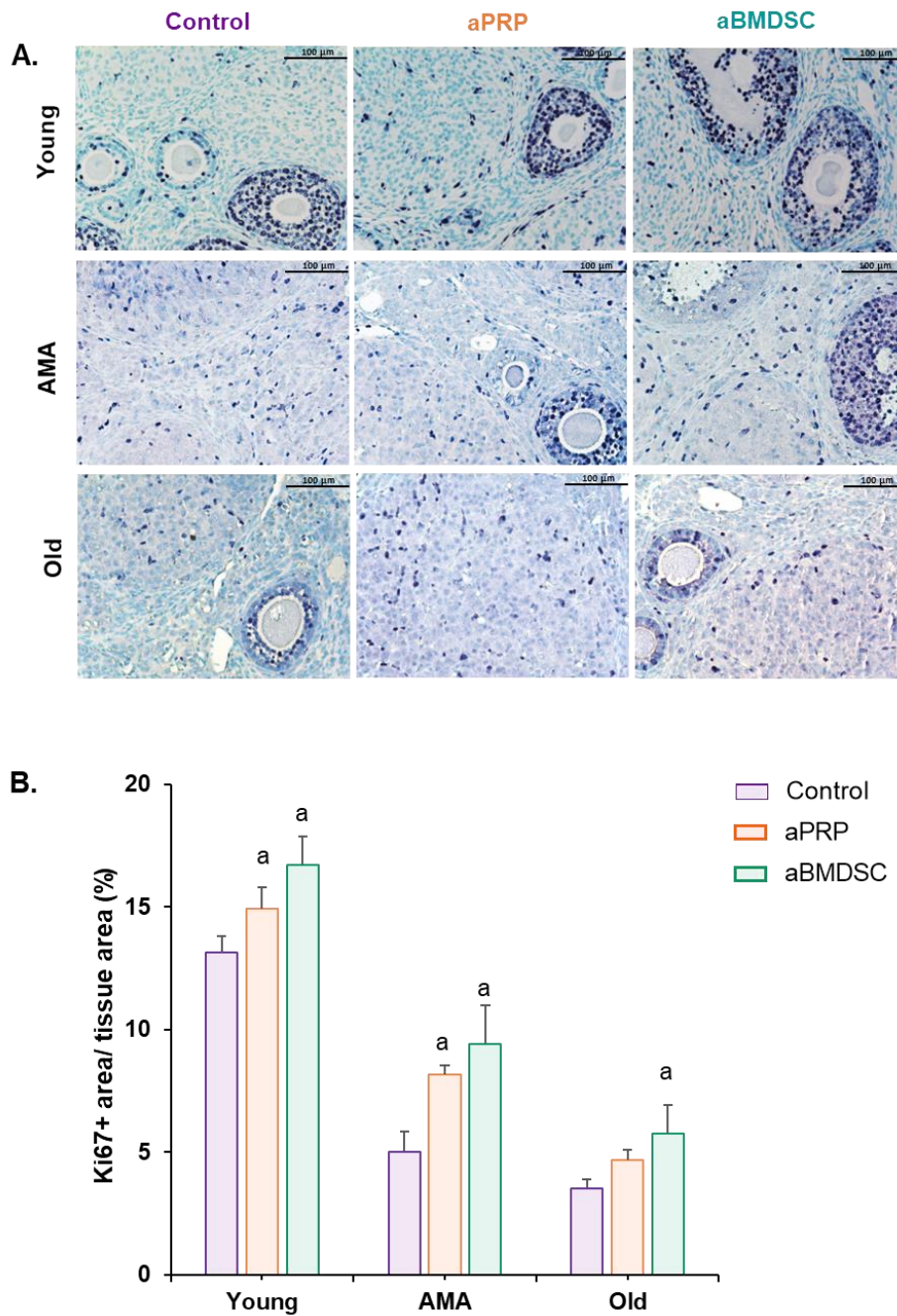
Figure 53. Analysis of cell proliferation after intraovarian plasma injections in a physiological aging mouse model. (A) Ki-67 immunostained sections showing proliferative cells (purple) after a single intraovarian injection of saline solution, aPRP or aBMDSC treatments in young, AMA and old mice. Scale bars are set to 100 µm. (B) Cell proliferation (n = 4 animals per group) was measured by dividing the Ki-67 positive area by the total area of ovarian tissue in the section. Lowercase letters indicate statistical significance (p<0.05) with respect to control (a) or aPRP (b).

A.

B.

C.
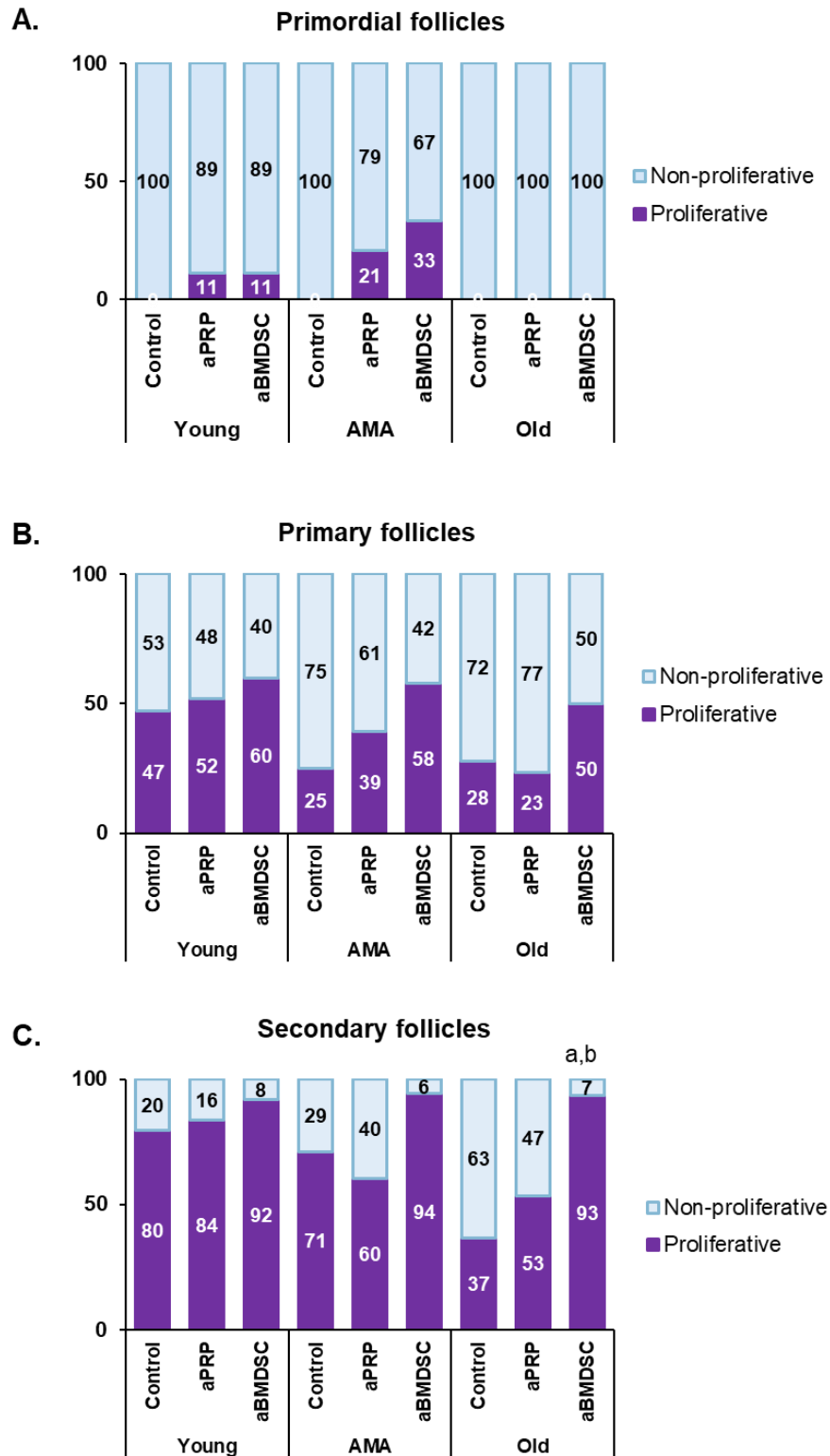
Figure 54. Analysis of proliferative follicles after intraovarian plasma injections in a physiological aging mouse model. Proportions of proliferative (A) primordial, (B) primary, and (C) secondary follicles after a single intraovarian injection of saline solution, aPRP or aBMDSC treatments in young, AMA and old mice (n = 4 animals per group). Lowercase letters indicate statistical significance (p<0.05) with respect to control (a) or aPRP (b).
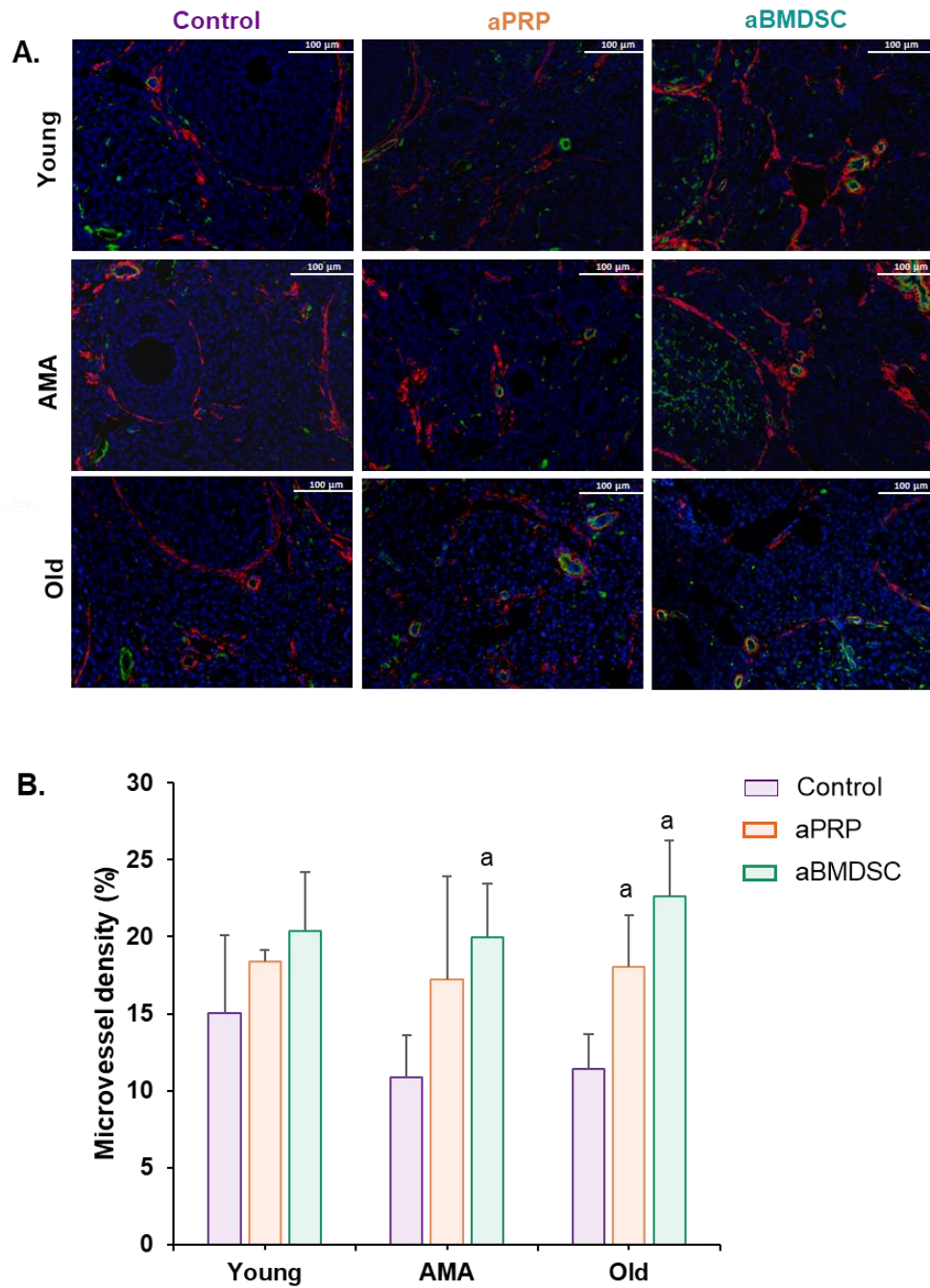
Figure 55. Microvessel density analysis after intraovarian plasma injections in a physiological aging mouse model. (A) Immunofluorescent images of ovarian vascularization after a single intraovarian injection of saline solution, aPRP or aBMDSC treatments in young, AMA and old mice. Isolectin B4 (IB4) is green, α-smooth muscle actin (a-SMA) is stained red, and nuclei are stained blue with diamidino-2-phenylindole (DAPI). Scale bars are set to 100 μm. (B) Microvessel density (n = 4 animals per group) was calculated by dividing the lectin-positive area by the total area of ovarian tissue in the section. Lowercase letters indicate statistical significance (p<0.05) with respect to control (a) or aPRP (b).

3. Mitochondrial function and oxidative damage

The mtDNA copy numbers were analyzed after plasma treatments as a marker of mitochondrial function. The treatments made no difference in the young mice (Figure 56). However, aBMDSC increased mtDNA copies in the AMA and old groups, as highlighted by the increased ratio of mitochondrial to nuclear DNA with respect to control-treated mice. This finding was especially evident in the old mice, where the mtDNA copies were augmented by up to 75% by aBMDSC treatment. This effect could be observed when analyzing the three mitochondrial genes, *ND1*, *COX3*, and *16S rRNA*, which belong to stable regions of the mitochondrial genome (Figure 56).

aPRP produced a positive effect only in old mice, which are affected by age, by increasing mtDNA copies by 41% relative to control-treated old mice.
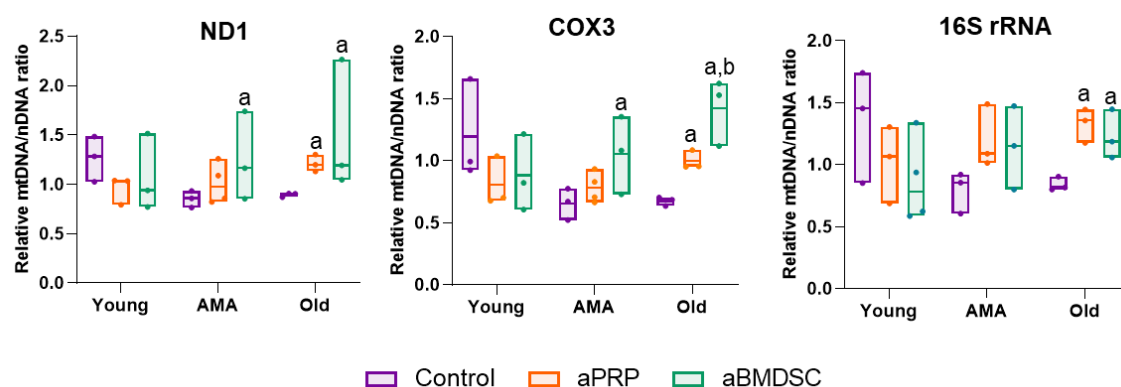
Figure 56. Analysis of mitochondrial DNA copy number after intraovarian plasma injections in a physiological aging mouse model. Relative mitochondrial DNA (mtDNA) levels in young, AMA, and old mice after a single intraovarian injection of saline solution, aPRP or aBMDSC. mtDNA copies were assessed via quantitative PCR analysis of *ND1*, *COX3* and *16S rRNA* gene expression (belonging to the stable part of mtDNA), normalized to 18S nuclear gene (nDNA) (n = 4 animals per group). Lowercase letters indicate statistical significance (p<0.05) with respect to control (a) or aPRP (b).

Overall, our treatments reduced the levels of oxidative damage, as detected by the lipid peroxidation product 4-HNE, with statistically significant differences in the aBMDSC-treated old mice when compared to their respective control and aPRP groups (Figure 57A-B).
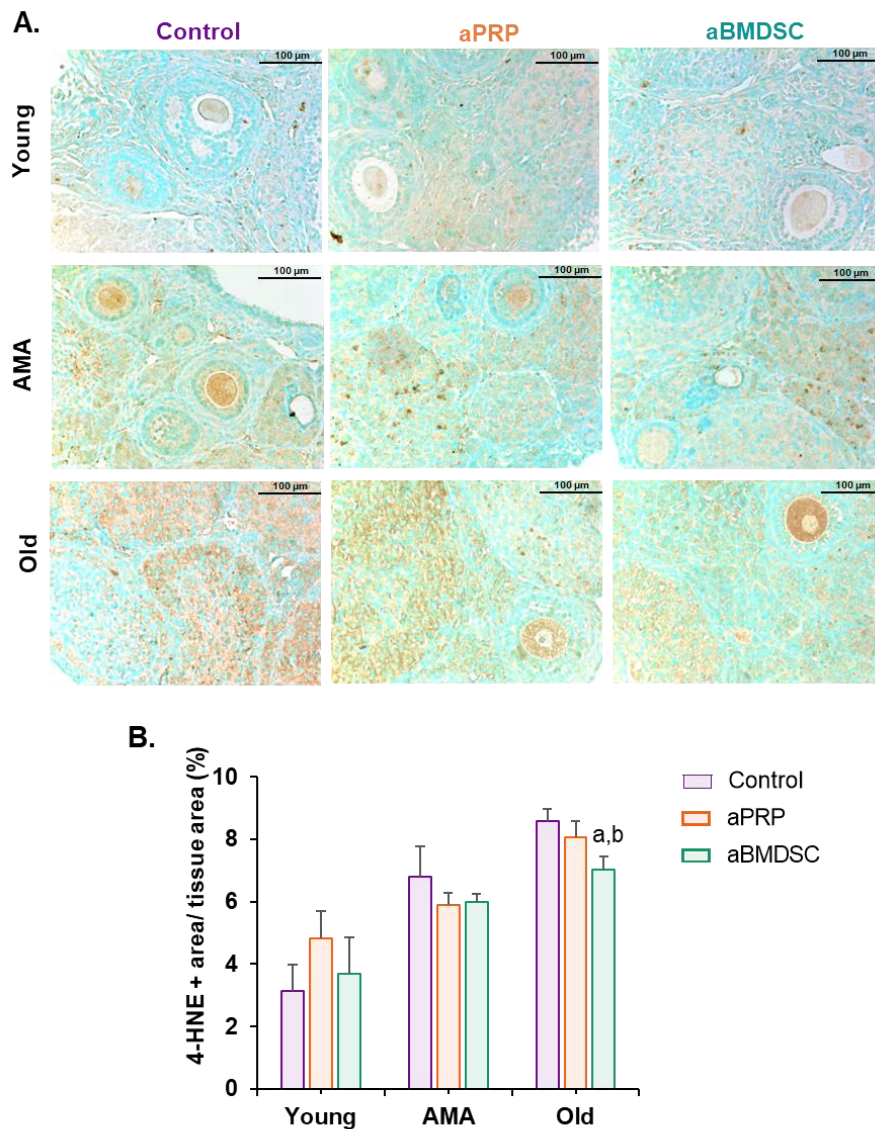
Figure 57. Analysis of lipid peroxidation after intraovarian plasma injections in a physiological aging mouse model. Representative photomicrographs of oxidative damage (brown) visualized with staining of the peroxidative lipid product 4-hydroxynonenal (4-HNE) in young, AMA and old mice after a single intraovarian injection of saline solution, aPRP or aBMDSC treatments. (B) The quantification of peroxidation was estimated by dividing 4-HNE+ area by the total tissue area (n= 4 animals per group). Scale bars are set to 100 μm. Lowercase letters indicate statistical significance ($p<0.05$) with respect to control (a) or aPRP (b).

aBMDSC additionally reduced the proportion of apoptotic stromal and follicular cells (Figure 58A-B) in the older mice. When we specifically studied the percentage of apoptotic follicles (Figure 58C), we observed a decrease in AMA mice after treatment with aBMDSC (control: 52%; aBMDSC: 39%), and an even more significant decrease in the case of old mice (control: 64%; aBMDSC: 19%).

Interestingly, aPRP also reduced apoptosis in the old mice compared to their control, resulting in a lower percentage of apoptotic follicles.
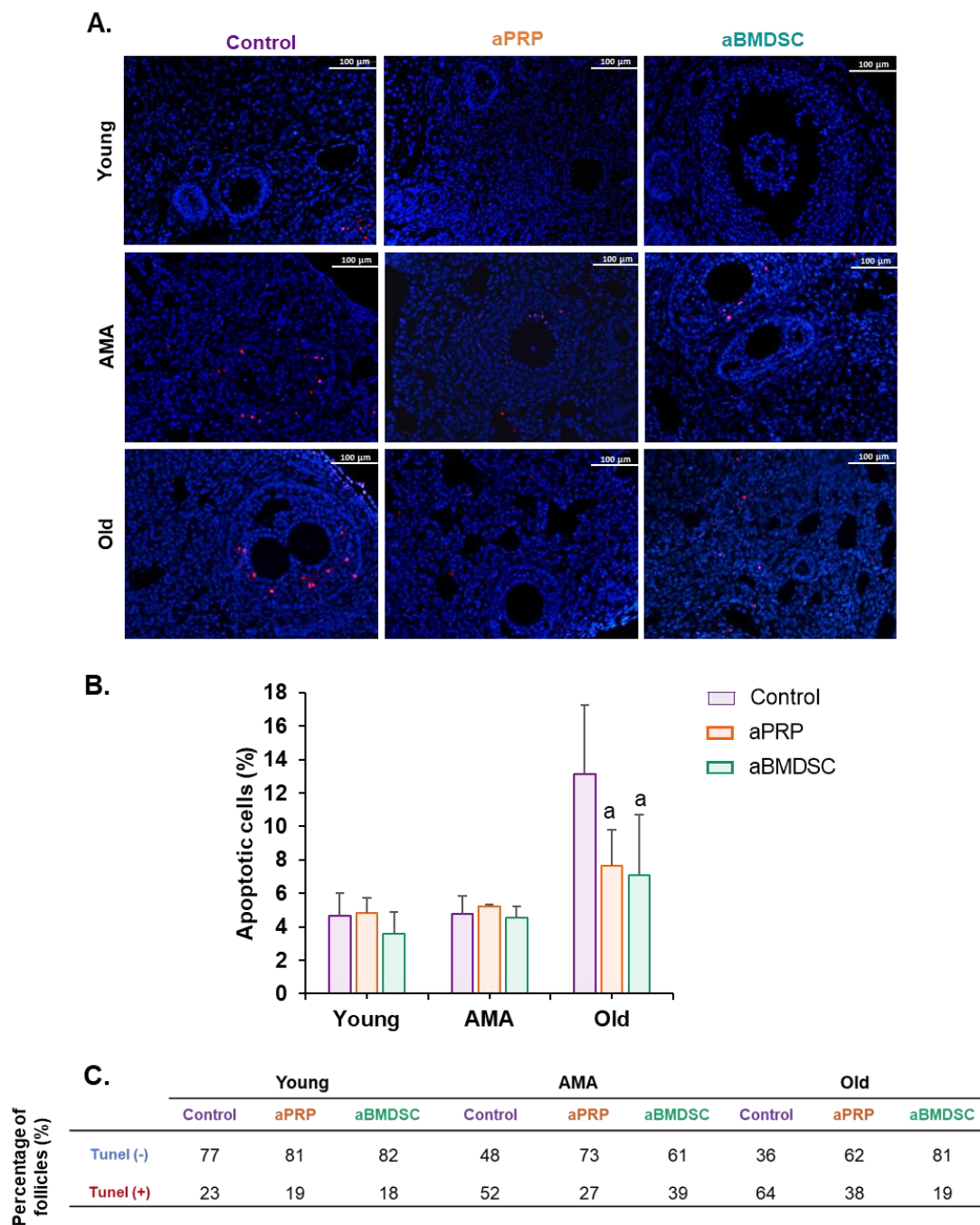
Figure 58. Analysis of cell death by TUNEL after intraovarian plasma injections in a physiological aging mouse model. (A) Representative immunofluorescent images of cell death (red signal) in young, AMA and old mice after a single intraovarian injection of saline solution, aPRP or aBMDSC treatments, labeled with a TUNEL kit. (B) The quantification of apoptotic cells was estimated by dividing red signal by total tissue area (n=4 animals per group). Scale bars are set to 100 μm. (C) Comparison of apoptotic follicles after plasma-based treatment in young, AMA, and old mice. Lowercase letters indicate statistical significance (p<0.05) with respect to control (a) or aPRP (b).

Results

## 4. Proteomic profile of ovarian tissue after plasma treatment

The ElasticNet regression analysis identified a total of 1834 proteins. In the ovaries of young mice there were 26 differentially expressed proteins (DEPs), which were then represented using a heatmap (Figure 59A). Hierarchical clustering divided these DEPs into two main categories: one comprised of the control group, and the other included both the aPRP and aBMDSC groups. aPRP and aBMDSC samples had 77% and 65% of their DEPs, respectively, upregulated with respect to the control group (Figure 59A).

We similarly identified 30 DEPs in AMA mice, and 27 DEPs in old mice (Figure 59B-C). However, these DEPs exhibited remarkably different proteomic profiles in older mice. In these cases, the hierarchical clustering classified and distinguished the aBMDSC-treated samples from a cluster composed of both the PRP and control groups.

Additionally, we found that 90% and 63% of the DEPs were downregulated in the aBMDSC-treated AMA and old groups, respectively, compared to their corresponding control groups (Figure 59B-C).
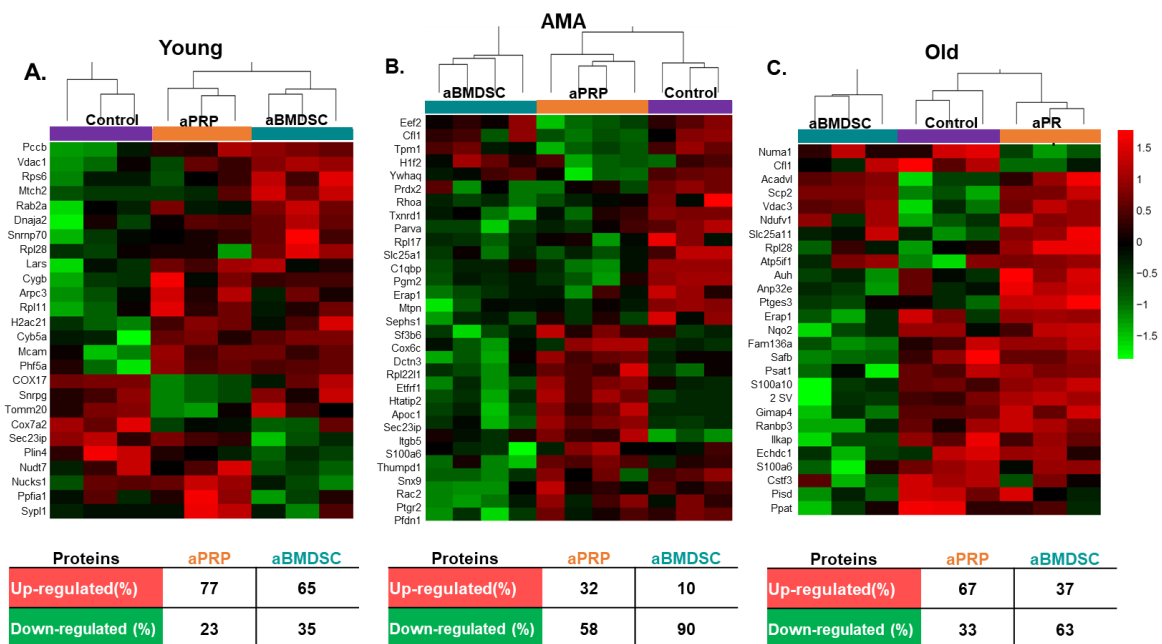
Figure 59. Proteomic characterization of ovarian tissue after plasma treatments by SWATH-MS technique. (A-C) Heatmap analysis and hierarchical clustering of significantly differentially expressed proteins (DEPs) between control, aPRP and aBMDSC samples in young, AMA, and old mice after ElasticNet regression analysis. The tables beneath the heatmaps present an overview of the DEPs in aPRP and aBMDSC treatment groups with respect to control.

We next studied the pathways regulated by the DEPs, by performing a GO analysis, which revealed the biological processes, cellular components, and molecular functions enriched for each age group following treatments.

In young mice, the DEPs were mainly associated with enriched mitochondrial-related pathways, including mitochondrion organization, protein localization to the mitochondrion, and oxidative phosphorylation. Accordingly, the enriched DEP functions were located in the spliceosomes and mitochondrial membrane and affected molecular functions including electron transfer and oxygen carrier activities (Figure 60A). Finally, GOchord plot analysis identified the mitochondrial genes *COX7a2*, *Tom20*, and *Mtch2* among the top ten enriched biological process-related genes (Figure 60B).

Alternatively, in AMA mice, we identified enriched pathways related to the regulation, organization, and proliferation of actin, in addition to reactive oxygen species (ROS) metabolic processes, positive regulation of growth, and regulation of angiogenesis (Figure 60C). Enriched molecular functions were associated with electron transfer, oxidoreductase, and antioxidant, and the GOchord plot analysis highlighted *Cf11*, *Tpm1*, *Rhoa*, and *Prdx2* genes, among others (Figure 60D).

Lastly, in the old group, functional analysis identified enriched biological processes related to oxidation, metabolism, and lipid modification (Figure 60E), however, we also note that mitochondrial electron transport and regulation of spindle assembly were significantly affected. The DEPs from this group had enriched functions localized in the mitochondria and spindle structure, and affected molecular functions included acetyl-CoA binding and oxidoreductase activity. GOchord plot analysis distinguished genes including *Acadvl1*, *Scp2*, *Ptges3*, *Numa1*, and *Ndufv1* (Figure 60F).

Results
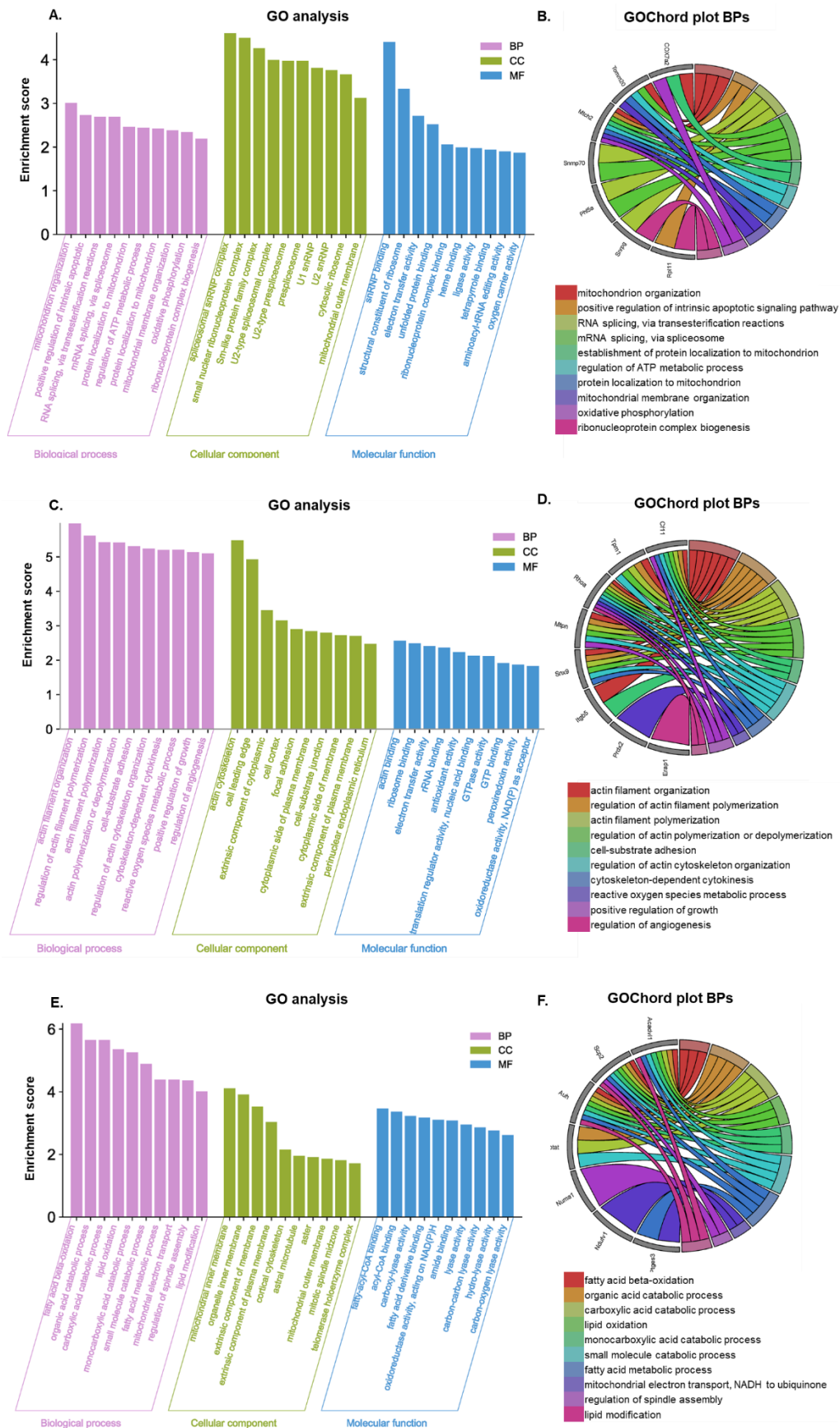
Figure 60. Functional analysis of DEPs after intraovarian plasma injections in a physiological aging mouse model. Significantly enriched Gene Ontology (GO) biological processes (BPs), cellular components

136

(CCs), and molecular functions (MFs) (FDR<0.05) associated with the DEPs identified in young (A), AMA (B) and old (C) mice. The top ten results of each analysis are presented. GOChord plots of the top ten BPs for young (B), AMA (D) and old (F) mice, depicting the relationships between the pathways (illustrated by the different coloured chords) and the most relevant genes they have in common (labeled on the outside of the plots).

Results

VI. DISCUSSION

VI. DISCUSSION

Regenerative effect of different plasma sources, rich in growth factors, in mouse models of ovarian damage induced by chemotherapy

We assessed the systemic administration of different sources of human plasma enriched in stem cell-soluble factors (plasma rich in BMDSC-secreted factors and UCB plasma) to rescue fertility in DOR and POI models. We also assessed their activated forms. Moreover, to elucidate possible mechanisms and effectors of the observed ovarian rescue, we examined the proteomes of the plasmas and validated proteome-predicted pathways affected by the proposed therapies, using an *in vitro* system. We showed that BMDSC and UCB treatments, and especially their activated forms, increased vascularization and cell proliferation, and inhibited apoptosis, ultimately improving pregnancy rates and increasing litter sizes in mouse models of ovarian damage.

We found that the activated aBMDSC and aUCB fractions preserved primordial and growing follicles in both DOR and POI models. aBMDSC had the strongest effects, yielding follicle numbers similar to those observed in wild-type reference ovaries and restoring ovarian weight in ovaries 21 days after ovarian damage. This period corresponds to that required for primordial follicles to reach the preovulatory stage in mice[226], and allowed us to evaluate the effects of treatments on the primordial and early growing follicles at the time of exposure. Some of the positive effects induced by the activated fractions were also observed in the non-activated forms. The superior activity of the activated plasmas demonstrates that the activation procedure, which releases platelet-derived and associated growth factors, likely increases the expression of soluble factors better able to stimulate ovarian repair[242].

Because the follicular reserve is limited and non-renewable[17], we hypothesized that the plasma treatment rescues damaged primordial follicles before they undergo atresia. Indeed, one week after chemotherapy, some partially damaged primordial follicles remain[243], which are susceptible to be repair and rescue by plasma-secreted soluble factors. Considering that the cyclophosphamide and busulfan act to induce DNA-damage, plasma treatment may rescue primordial follicles, in part, by promoting DNA repair machinery. Indeed, we detected DEPs involved in DNA repair in both BMDSC and UCB plasmas (whether activated or inactivated) and determined that both increased the

expression of DNA repair markers in cultured ovarian fragments. A DNA repair response was particularly notable after BMDSC treatment, with increased expression of molecules such as Rad51, which has a specific key role in repair of double-strand breaks, the most common DNA damage induced by both aging and cancer treatment with alkylating agents[207] in ovarian tissue. These findings could be part of the mechanism behind the observed protection, especially induced by aBMDSC, of the primordial population, which might otherwise be cleared in a secondary wave of apoptosis[243].

Both aUCB and aBMDSC treatment also increased the number of growing follicles. In our proteomic analysis, we noted DEPs associated with signaling processes, including RhoGTPases, known to affect primordial follicle activation by regulating PI3K-Akt signaling[244]. These factors were upregulated in BMDSC, UCB, aUCB, and, most dramatically, in aBMDSC plasma. Proteomic characterization highlighted a possible role for HIPPO and PIP3 pathways in follicle activation and growth[122,223], providing a mechanism by which aBMDSC and aUCB could, in a later phase, induce the promotion of late pre-antral and antral follicles, and ultimately allow for ovulation of competent MII oocytes. Moreover, these plasmas provided molecules related to relevant processes such as cell cycle, apoptosis, gene expression, protein metabolism, cell-to-cell communication, signal transduction, and cell response to stress. These findings may be relevant to age-induced ovarian damage in addition to acute ChT insult, since a link between reduced oxidative stress response, cell communication, metabolism of proteins, and ovarian aging was recently described[53].

Regarding the long-term effects on fertility, and despite the known low pregnancy rate of the NOD/SCID strain[245], activated and non-activated BMDSC and UCB treatments had a positive effect on the number of pregnancies and average litter sizes. In the DOR model, pregnancies and live births were recorded in all experimental groups, including the ChT and PB control groups, but litter sizes were larger in the BMDSC and UCB groups. In the POI model, as seen for infertile patients with POI, ChT mice failed to achieve pregnancies despite successive matting attempts, but aBMDSC and aUCB had a dramatic effect, increasing pregnancy rates to 70-80%. This aspect represents one of the most clinically relevant findings of our study and opens new avenues of research for developing

treatment for women with POI, who have a spontaneous pregnancy rate lower than 5%[246], and for whom oocyte donation is the only current clinical option.

One factor that may be important for longer-term regeneration is the ovarian stroma, which supports follicular growth and development[247] and is seriously impaired in women with ovarian aging, DOR, and POI patients[248], and in our mouse models of ovarian damage[200]. Thus, we examined the regenerative properties of plasma treatments on the stromal microenvironment. We found that animals treated with BMDSC and UCB activated and non-activated plasmas showed increased microvascular density, in both DOR and POI models, with the density in the POI model restored to wild-type values. Treatment with PB plasma, particularly the activated form, also caused a limited but noticeable improvement in vascularization which could be explained by platelet-secreted factors present in regular peripheral blood. This finding demonstrates that the proposed therapies promote the formation of new vessels, which are essential for maintaining follicular growth[249] and ovulation, contributing to enhanced future breeding performance. In fact, proteomic analysis showed that BMDSC and UCB plasmas and their activated forms contained several factors/proteins, such as THBS1 and others, involved in regulating the formation of new vessels through VEGF and PDGF signaling pathways, and with crucial roles in neoangiogenesis[250,251]. Notably, the levels of THBS1, a BMDSC-secreted paracrine factor, were positively correlated with ovarian reserve biomarkers after ASCOT in women with POR[146]. Plasma-derived treatments also improved the viability and function of ovarian stroma by reducing apoptosis, the main effect of chemotherapy on rapidly dividing ovarian support cells[252,253], and increasing cell proliferation, primarily of granulosa cells, as previously observed with mesenchymal BMDSC-secreted factors[254]. Further, activated plasmas had the greatest positive effects on the ovarian stroma. This indicates that the granulosa cell layers were in a growth and expansion phase, which correlates with the observed increase of growing follicles. Further, the greatest effects of activated plasmas in ovarian stroma might be due to additional platelet-released factors controlling proliferation and migration of specific cells essential for tissue repair[255], which also explains some of the beneficial but limited effects of aPB plasma. This is relevant as ovarian injection of PRP is being offered to women worldwide but without proper

evaluation of ovarian effects relative to controls and, to date, with limited supporting experimental studies.

Our findings, together with previous studies demonstrating the safety of blood plasma administration in patients[167–173], suggest that non-cellular components of SCs and platelet-derived growth factor approaches could be an effective treatment for DOR and POI patients. In fact, the combined but not sequential use of SCs with platelet-rich plasma had an additive and accelerated restorative effect on ovarian function in a cyclophosphamide-induced POI rat model[256]. Thus, rather than use single treatments with positive but limited effects, we propose to combine the benefits of both stem cell treatment and platelet-secreted growth factors to design effective therapies for women with impaired ovarian function able to use their own oocytes.

To this end, it is encouraging that activated BMDSC plasma appears more effective than UCB and aUCB, as this allows for harvesting an autologous source using safe and well-established mobilization protocols, which will facilitate worldwide application without requiring specialized facilities.

Evaluation of the most beneficial plasma treatment in human ovarian tissue

After testing different plasma sources in animal models of ovarian damage, highlighting the promising benefits of stem cell-secreted factors in the ovaries of DOR and POI mice, we decided to evaluate the most effective treatment, aBMDSC plasma, in human ovarian tissue. This study was required to confirm our findings prior to clinical implementation.

In this part of the thesis, we evaluated the effect of plasma aBMDSC to promote follicular development and regenerate ovarian stroma. In addition, a proteomic study was carried out to elucidate possible underlying mechanisms of aBMDSC plasma in humans.

First, we analyzed the follicle populations and observed that aBMDSC increased the number of primary and secondary follicles, promoting human follicular development, as previously described in DOR and POI animal models. Moreover, we also observed a regeneration of ovarian stroma, increasing vascularization and promoting cell

proliferation. A relationship could therefore be established between the enhancement of ovarian stroma in human tissue and the promotion of follicular development.

Indeed, the proteomic analysis of human treated samples revealed an upregulation of specific proteins related to the regulation of both follicular development and angiogenesis, such as *PGK1*, *ANXA3*, *RPS7*, and *PGBM*[228,230,234,236] . Thus, this over expression could contribute to follicular growth and ovarian niche regeneration induced by aBMDSC. Additionally, the analysis of human samples showed that relevant biological processes related to ovarian function, such as protein processing in endoplasmic reticulum and autophagy, were regulated by these factors. Recent reports suggest an involvement of endoplasmic reticulum stress and unfolded protein response in physiological follicle development[257] and the maintenance of GC proliferation[258]. Besides, autophagy also plays a key role in follicular development and atresia, given that its regulated genes and proteins are downregulated in GCs during gonadotropin-dependent follicular growth[259].

The results obtained in the xenograft model were reassuring to confirm the feasibility of aBMDSC plasma for ovarian rescue by promoting human follicle development and ovarian niche regeneration. Moreover, this validation step in human ovarian tissue brings the use of aBMDSC plasma closer to clinical application.

Development and validation of a mouse model of physiological reproductive aging

After employing animal models of ovarian damage induced solely by ChT in previous studies, we decided to characterize an animal model of physiological ovarian aging due to the need to understand the process of ovarian aging and find therapies to slow or reverse the effects of aging. In our study, we employed animals of different ages to mimic the ovarian phenotypes of young, AMA, and old women, allowing us to assess the histological and proteomic changes associated with physiological ovarian aging, and begin to reveal the underlying mechanisms. Furthermore, by using immunodeficient mice, our model has the potential to become a valuable tool to test human-origin anti-aging treatments, such as SCs or plasmas[146,242,260,261], which may be used to treat the growing number of patients with age-related ovarian infertility.

Discussion

This study characterized the reproductive outcomes of young, AMA and old mice modeling the physiological ovarian aging of humans. Older mice presented with reduced ovarian reserves, follicular activation, and growth, deteriorated ovarian stroma, and decreased quantity and quality of harvested oocytes and embryos following COS. Based on histological analyses, we established associations between progressive ovarian aging and a reduced number of mitochondrial copies, oxidative damage, and apoptosis, and these age-related changes were corroborated at the proteomic level.

To our knowledge, our mouse model is the first to recapitulate processes of physiological and progressive ovarian aging, compared to models currently in use, which are established by chemotherapeutic agents or gene deletion to damage the ovarian reserve, and represent aging in genetic conditions without a natural progression [200,262–268].

Comparing the ovarian reserve across the three groups, we found a significantly reduced number of primordial and primary follicles in old mice. Moreover, the analysis of activated and growing follicular populations revealed an impairment of folliculogenesis in aged ones, respectively corresponding with the decline in ovarian reserve and reduced efficiency of COS reported for older women[269]. Accordingly, the age-related effects were also evident in the ovarian stroma of AMA and old mice, with reduced proliferation and vascularization. As established in previous studies[270,271], cellular senescence increases with biological age, limiting cellular proliferation. Moreover, ovaries from older individuals have fewer blood vessels, hindering the delivery of oxygen and nutrients to growing follicles [272,273]. Altogether, these results establish a link between the age-associated deficiencies of the ovarian stroma, follicular development, and, ultimately, ovarian function.

Following COS, we recovered fewer oocytes, of poorer quality, from older mice. This poor oocyte quality was also reflected by the reduced number, or absence, of 2-cell embryos recovered in the AMA and old groups, respectively. As observed in patients over the age of 35 who experience age-related fertility problems, the limited quantity and compromised quality of oocytes is significant[274], and leads to a marked reduction in fertilization and pregnancy rates[269,270] . Accordingly, we found embryo development to the blastocyst stage was impaired in the AMA and old groups compared with young embryos. Poor oocyte quality in aged women[275] occurs due to oocyte spindle dysfunction

and meiotic errors [276,277], and has been described as one of the reasons for depressed blastocyst development.

Mitochondrial dysfunction is a principal contributor to the aging process [278,279], and result in increased levels of ROS that damage the ovarian tissue. The mtDNA copy number is a promising biomarker, correlated in different studies with a lower oocyte quality[280–283]. Notably, lipid peroxidation and the electrophilic product 4-HNE are responsible for the oxidative damage affecting folliculogenesis and oocyte meiosis[284,285], contributing to the accumulation of spindle assembly defects and chromosome misalignments [286]. Our study showed lower mtDNA copy numbers in the AMA and old ovaries compared to young ones. In addition, higher lipid peroxidation and apoptosis were detected in older mice, supporting previous reports of age-related decreases of mtDNA levels, increased ROS, oxidative damage, and apoptosis, that altogether have adverse effects on oocyte quality [285,287].

Remarkably, our histological findings were all supported at the proteomic level, showing distinct expression profiles for the ovaries of young, AMA, and old mice. Functional analysis of the DEPs revealed ovarian aging was associated with the stress response, respiratory electron transport chain, death receptor binding, complement component 1q binding, and chromatin DNA binding, supporting the above-mentioned age-related effects. In addition, older mice overexpressed pro-apoptotic and age-related cell death genes, such as Casp3, and repressed genes associated with damage prevention, vascularization, and cell survival such as *C1qbp* [288], *Thbs1* [289], and *Gapdh* [290], respectively.

Our study confirms that immunodeficient NOD/SCID mice of established ages can be employed to model the physiological aging of human ovaries. Indeed, our murine model mimicked the ovarian phenotypes of young, AMA, and old women, highlighting the histological and proteomic characteristics of each stage. As such, we put forth this commonly used laboratory mouse strain as a preclinical model that may feasibly be employed to further decipher the complexities of ovarian aging, or test novel and alternative anti-aging treatments to prolong women's fertility.

Discussion

Intraovarian administration of the most beneficial plasma treatment in a physiological aging mouse model

In the first part of this doctoral thesis, we found that aBMDSC plasma had the strongest effects, increasing the number of MII-mature oocytes and embryos, by regenerating the ovarian stroma and restoring long-term fertility in mouse models of ovarian damage. Then, these positive effects were also validated in human ovarian tissue from poor responders, where aBMDSC promoted human follicle development and regenerated the ovarian stroma.

Nevertheless, these experiments were conducted using animal models of ChT-induced DOR and POI, where the ovarian function is severely impaired by alkylating agents, the ovarian reserve is depleted, and the oocyte quality is compromised. However, due to the increasing number of patients affected by age-related fertility, there also exists an urgent clinical need to analyze the effect of plasma treatments in models of physiological aging. Moreover, previously the plasma treatments were tested by systemic administration through the animal's tail vein for two weeks, a treatment regimen which would be challenging to apply in a future clinical setting. Therefore, in the last part of this thesis, we aimed to evaluate if a single intraovarian injection of plasma combining bone marrow stem-cell secreted and platelet-enclosed growth factors (aBMDSC) could improve ovarian function in a mouse model of physiological human aging, which we previously characterized mimicking the three stages of women´s reproductive lifespan: young, AMA, and old.

In this phase of the thesis, we determined that a single intraovarian injection of aBMDSC, which combines the paracrine actions of stem cell- and platelet-secreted factors, improves reproductive outcomes following COS, by increasing the quantity and quality of MII oocytes, promoting early embryo development, and providing substrates for a long-lasting ovarian reactivation that supports follicle development in a mouse model of physiological human aging. We further report a positive association between reproductive outcomes and mitochondrial function after aBMDSC treatment, with increased mitochondrial mass, along with reduced oxidative damage and cell death.

This study showcased that aBMDSC promotes the activation and complete development of dormant follicles in young, AMA, and old mice. This phenomenon could be explained by the presence in aBMDSC of proteins involved in follicular activation and growth processes, particularly those associated with the HIPPO and PI3K/PTEN/AKT signaling pathways, as revealed by the previous characterization of plasma treatments. Consistent with previous studies describing that PRP contains growth factors necessary for folliculogenesis, such as FGF and HGF [291], standard aPRP also facilitated some positive improvements, though it activated follicles less efficiently than aBMDSC.

Further, aBMDSC rescues fertility and restores response to COS, enhancing the quantity and quality of ovulated MII oocytes, which are compromised by aging in old women and in our physiological aging mouse model. This result is consistent with recent reports of PRP-based therapy efficiently improving oocyte quality in POR patients[172]. Nevertheless, in this study, the effects on oocyte yield and quality were higher after aBMDSC treatment, showing the supplemental benefits of the soluble stem cell factors. This result also supported our previous findings that stem cell-secreted factors increased the expression of proteins that regulate oocyte quality, and systemically act to promote maturation in human ovarian tissue.

Based on the premise that the accumulation of meiotic errors during aging compromises embryo development[60,276], we assessed embryo development to the blastocyst stage, and further confirmed that the morphological improvements observed in oocytes following aBMDSC treatment were mirrored in improved embryo quality, with increased blastocyst formation and hatching blastocyst rates in AMA mice.

Of the multiple and complex mechanisms underlying aging, mitochondrial dysfunction[53,279,292] and production of ROS[67,293] are crucial in ovarian tissue. Reductions in mtDNA copies is associated with aging[76,294], and considered a negative predictor of oocyte quality and embryo viability[75,82,282,283]. Alternatively, ROS increase with age, inducing apoptosis, associated with follicular atresia and a decline in oocyte quality[84]. Moreover, as we described above, the lipid peroxidation, and its electrophilic product 4-HNE, are also among the factors responsible for the oxidative damage affecting folliculogenesis and oocyte meiosis[88,284], contributing to the accumulation of spindle assembly defects, chromosome misalignments, and aneuploidy[89]. Our physiological

Discussion

aging model demonstrates that aging is associated with less mtDNA copies and increased oxidative damage, apoptosis, and lower oocyte quality. However, aBMDSC treatment mitigated these impairments in aged mice, by increasing mtDNA while reducing 4-HNE and cell death, suggesting aBMDSC mediates the improvements in oocyte quality and developmental competence through mitochondrial action and anti-oxidative factors.

The ovarian niche is essential for follicle growth and oocyte quality[272,273]. In POI models, stem cell factors and PRP treatment modulated angiogenesis and regenerated the ovary[145,186], whereas in our mouse model of DOR and POI, and in the ovarian cortex of POR patients, treatment with a combination of stem cell-secreted and platelet-enclosed factors promoted stromal vascularization and folliculogenesis. In agreement with these results, a single intraovarian injection of aBMDSC improved local vascularization in AMA and old mice, and this effect is likely mediated by the angiogenesis-related soluble factors from SCs and platelets, such as FGF-2 and THSP-1[154,242,295]. Moreover, our mouse model recapitulated phenotypical hallmarks of aging, evidenced by reduced ovarian cell proliferation with age[271]. Treatment with aBMDSC reversed this phenomenon, by tripling actively dividing cells in the ovarian stroma and follicles in old mice (90% vs 30-40% proliferative secondary follicles in control).

All the above-mentioned ovarian regenerative effects of aBMDSC were reflected by changes in the proteomic profile of treated ovarian tissue. Functional analysis of the DEPs identified in aBMDSC-treated ovaries showed enrichment in pathways related to spindle reorganization, regulation of stromal proliferation and vascularization, and mitochondrial function. In addition, we detected upregulation of Cox7a2, Mtch2 (which plays an important role in mitochondrial function[296,297]), and Ptges3 proteins (involved in human ovulation and oocyte maturation[298]), along with a downregulation of Prdx2 (a peroxiredoxin family member involved in ROS reduction[299]) and Numa1 (involved in spindle reorganization and DNA repair by homologous recombination[300,301]) proteins.

aBMDSC induced follicular rescue in aged ovaries with a single intraovarian injection, which has a safe and well-established application in human clinical trials evaluating plasma-based treatments and avoids repeated systemic administration. Moreover, the

150

absence of deleterious effects in the ovaries of young healthy mice supports the safety of this novel approach.

In this study, we have presented a treatment based on the combination of stem cell-secreted- and platelet-enclosed growth factors that reverses the effects of ovarian aging in a mouse model of physiological human aging. We focused on fertility outcomes after COS, ovarian stromal regeneration, and underlying aging mechanisms, particularly mitochondrial function. Further analysis of the long-term effects on breeding performance and detailed molecular studies of the mitochondria of isolated oocytes should be considered. Moreover, further preclinical studies with human samples are required to confirm our findings prior to clinical implementation.

Clinical implications

This doctoral thesis showed the regenerative properties of different sources of plasmas enriched in stem cell-secreted factors in mouse models of DOR and POI induced by ChT. Thus, it raises the possibility of a paracrine signaling-based alternative to overcome impaired ovarian reserve, a key issue in reproductive medicine, and offers new alternatives for those patients seeking to use their own oocytes.

Moreover, our findings, together with previous studies demonstrating the safety of blood plasma administration in patients, suggest that to combine the benefits of both non-cellular components of SCs and platelet-derived growth factor approaches could be a more effective treatment for patients than using either individually. Specifically, the most beneficial treatment was the combination of factors secreted by marrow stem cells and factors released from platelets. To that end, we also evaluated the regenerative effects of this plasma on human ovarian tissue from POR women, bringing the treatment more closely towards clinical practice. Moreover, due to the increasing number of patients affected by age-related fertility, we decided to characterize a physiological aging mouse model and test this effective treatment for patients with age-related infertility. We also decided to test the local effect through intraovarian plasma administration, improving its clinical application and avoiding repeated systemic administration.

Discussion

Due to the autologous nature of the non-cellular components of BMDSCs collected by non-invasive mobilization protocols and PRP, along with the synergistic benefits provided by the combination of their soluble factors, we propose this treatment as a promising autologous treatment to improve the reproductive potential of aged, DOR and POI patients. Nevertheless, human studies and well-designed controlled randomized clinical trials in patients are required prior to clinical application.

VII. CONCLUSIONS

VII. CONCLUSIONS

The following conclusions can be drawn from this thesis:

1. Systemic administration of human plasma enriched in stem cell-secreted factors (BMDSC and UCB plasmas) rescue follicular development and fertility, inducing microvessel formation and cell proliferation, and reducing apoptosis in mouse models of DOR and POI.

2. Plasma activation for both BMDSC and UCB plasmas enhanced the positive effects on fertility in chemotherapy-induced mouse models of ovarian damage.

3. Proteomic and *in vitro* analyses indicate that plasma effects may be mediated by soluble factors related to cell cycle/apoptosis, gene expression, signal transduction, cell communication, response to stress, and DNA repair.

4. The most effective treatment, aBMDSC plasma, promoted human follicle development and regenerated the ovarian stroma in human ovarian tissue in POR women, supporting the effects observed in the DOR and POI models.

5. BMDSC and UCB plasmas could be effective treatments to increase reproductive outcomes in women with impaired ovarian function due to several causes. However, combining the benefits of both stem cell-secreted and platelet-enclosed growth factors could improve and accelerate the regenerative effects on ovaries. Thus, activated BMDSC plasma is the most promising treatment due to its potent restorative effects.

6. We established a feasible mouse model of physiological aging, representing different women's fertility profiles, such as advanced maternal and old age. This model represents a tool to decipher the process of ovarian aging and to test future potential treatments to slow down or reverse the effects of aging on fertility.

7. A single intraovarian injection combining bone marrow-derived stem cell- and platelet-secreted factors (aBMDSC) improves reproductive outcomes in a mouse model of human physiological aging, promoting follicle activation and development, and regenerating the ovarian stroma.

Conclusions

8. The positive effects of aBMDSC on fertility outcomes were positively associated with mitochondrial function, with treatment increasing mitochondrial DNA copy numbers and reducing oxidative damage and apoptosis.

9. The improvement in reproductive potential after aBMDSC injection was accompanied by changes at the proteomic level, with proteins involved in mechanisms of oocyte spindle reorganization, regulation of proliferation and apoptosis, and mitochondrial functions.

10. A single intraovarian injection of aBMDSC appears to be a promising treatment with the potential to improve the reproductive outcomes of women with age-related infertility.

VIII. BIBLIOGRAPHY

VIII. BIBLIOGRAPHY

1. Richards, J. S. & Pangas, S. A. The ovary: basic biology and clinical implications. *J Clin Invest* **120**, 963 (2010).

2. Jorge, S., Chang, S., Barzilai, J. J., Leppert, P. & Segars, J. H. Mechanical signaling in reproductive tissues: mechanisms and importance. *Reprod Sci* **21**, 1093–1107 (2014).

3. Hornick, J. E., Duncan, F. E., Shea, L. D. & Woodruff, T. K. Isolated primate primordial follicles require a rigid physical environment to survive and grow in vitro. *Hum Reprod* **27**, 1801–1810 (2012).

4. Pereda, J., Zorn, T. & Soto-Suazo, M. Migration of human and mouse primordial germ cells and colonization of the developing ovary: an ultrastructural and cytochemical study. *Microsc Res Tech* **69**, 386–395 (2006).

5. Mamsen, L. S., Brøchner, C. B., Byskov, A. G. & Møllgard, K. The migration and loss of human primordial germ stem cells from the hind gut epithelium towards the gonadal ridge. *Int J Dev Biol* **56**, 771–778 (2012).

6. Kerr, J. B., Myers, M. & Anderson, R. A. The dynamics of the primordial follicle reserve. *Reproduction* **146**, (2013).

7. Forabosco, A. & Sforza, C. Establishment of ovarian reserve: a quantitative morphometric study of the developing human ovary. *Fertil Steril* **88**, 675–683 (2007).

8. Hansen, K. R. *et al.* A new model of reproductive aging: the decline in ovarian non-growing follicle number from birth to menopause. *Hum Reprod* **23**, 699–708 (2008).

9. Broekmans, F. J., Knauff, E. A. H., te Velde, E. R., Macklon, N. S. & Fauser, B. C. Female reproductive ageing: current knowledge and future trends. *Trends Endocrinol Metab* **18**, 58–65 (2007).

10. Maheshwari, A. & Fowler, P. A. Primordial follicular assembly in humans--revisited. *Zygote* **16**, 285–296 (2008).

11. BLOCK, E. A quantitative morphological investigation of the follicular system in newborn female infants. *Acta Anat (Basel)* **17**, 201–206 (1953).

12. Stringer, J. M. & Western, P. S. A step toward making human oocytes. *Nature Biotechnology 2019 37:1* **37**, 24–25 (2019).

13. de Pol, A., Vaccina, F., Forabosco, A., Cavazzuti, E. & Marzona, L. Apoptosis of germ cells during human prenatal oogenesis. *Hum Reprod* **12**, 2235–2241 (1997).

14. Pepling, M. E. & Spradling, A. C. Mouse ovarian germ cell cysts undergo programmed breakdown to form primordial follicles. *Dev Biol* **234**, 339–351 (2001).

15. Greenwald, G. S. Of eggs and follicles. *Am J Anat* **135**, 1–3 (1972).

16. Tingen, C. M. *et al.* Prepubertal primordial follicle loss in mice is not due to classical apoptotic pathways. *Biol Reprod* **81**, 16–25 (2009).

17. McGee, E. A. & Hsueh, A. J. W. Initial and cyclic recruitment of ovarian follicles. *Endocr Rev* **21**, 200–214 (2000).

18. Vanderhyden, B. Molecular basis of ovarian development and function. *Front Biosci* **7**, (2002).

19. Matzuk, M. M., Burns, K. H., Viveiros, M. M. & Eppig, J. J. Intercellular communication in the mammalian ovary: oocytes carry the conversation. *Science* **296**, 2178–2180 (2002).

20. Williams, C. J. & Erickson, G. F. Morphology and Physiology of the Ovary. *Endotext* (2012).

21. Young, J. M. & McNeilly, A. S. Theca: the forgotten cell of the ovarian follicle. *Reproduction* **140**, 489–504 (2010).

22. Hirshfield, A. N. Granulosa cell proliferation in very small follicles of cycling rats studied by long-term continuous tritiated-thymidine infusion. *Biol Reprod* **41**, 309–316 (1989).

23. Sternlicht, A. L. & Schultz, R. M. Biochemical studies of mammalian oogenesis: kinetics of accumulation of total and poly(A)-containing RNA during growth of the mouse oocyte. *J Exp Zool* **215**, 191–200 (1981).

24. Schultz, R. M., Letourneau, G. E. & Wassarman, P. M. Program of early development in the mammal: changes in the patterns and absolute rates of tubulin and total protein synthesis during oocyte growth in the mouse. *Dev Biol* **73**, 120–133 (1979).

25. Peters, H. The development of the mouse ovary from birth to maturity. *Acta Endocrinol (Copenh)* **62**, 98–116 (1969).

26. Jünger, M. A. *et al.* The Drosophila forkhead transcription factor FOXO mediates the reduction in cell number associated with reduced insulin signaling. *J Biol* **2**, (2003).

27. Fan, H. Y., Liu, Z., Cahill, N. & Richards, J. A. S. Targeted Disruption of Pten in Ovarian Granulosa Cells Enhances Ovulation and Extends the Life Span of Luteal Cells. *Molecular Endocrinology* **22**, 2128 (2008).

28. Castrillon, D. H., Miao, L., Kollipara, R., Horner, J. W. & DePinho, R. A. Suppression of ovarian follicle activation in mice by the transcription factor Foxo3a. *Science* **301**, 215–218 (2003).

29. Holt, J. E. *et al.* CXCR4/SDF1 interaction inhibits the primordial to primary follicle transition in the neonatal mouse ovary. *Dev Biol* **293**, 449–460 (2006).

30. Bachvarova, R. *et al.* Amounts and modulation of actin mRNAs in mouse oocytes and embryos. *Development* **106**, 561–565 (1989).

31. Choi, Y. & Rajkovic, A. Characterization of NOBOX DNA Binding Specificity and Its Regulation of Gdf9 and Pou5f1 Promoters. *Journal of Biological Chemistry* **281**, 35747–35756 (2006).

32. Joshi, S., Davies, H., Sims, L. P., Levy, S. E. & Dean, J. Ovarian gene expression in the absence of FIGLA, an oocyte-specific transcription factor. *BMC Dev Biol* **7**, 1–13 (2007).

33. Shimasaki, S., Moore, R. K., Otsuka, F. & Erickson, G. F. The bone morphogenetic protein system in mammalian reproduction. *Endocr Rev* **25**, 72–101 (2004).

34. Packer, A. I., Hsu, Y. C., Besmer, P. & Bachvarova, R. F. The ligand of the c-kit receptor promotes oocyte growth. *Dev Biol* **161**, 194–205 (1994).

35. Erickson, G. F., Magoffin, D. A., Dyer, C. A. & Hofeditz, C. The ovarian androgen producing cells: a review of structure/function relationships. *Endocr Rev* **6**, 371–399 (1985).

36. Hillier, S. G. Current concepts of the roles of follicle stimulating hormone and luteinizing hormone in folliculogenesis. *Hum Reprod* **9**, 188–191 (1994).

37. Farookhi, R. & Desjardins, J. Luteinizing hormone receptor induction in dispersed granulosa cells requires estrogen. *Mol Cell Endocrinol* **47**, 13–24 (1986).

38. Filicori, M. The role of luteinizing hormone in folliculogenesis and ovulation induction. *Fertil Steril* **71**, 405–414 (1999).

39. Gervásio, C. G., Bernuci, M. P., Silva-de-Sá, M. F. & Rosa-e-Silva, A. C. J. de S. The role of androgen hormones in early follicular development. *ISRN Obstet Gynecol* **2014**, 1–11 (2014).

40. Gougeon, A. Human ovarian follicular development: from activation of resting follicles to preovulatory maturation. *Ann Endocrinol (Paris)* **71**, 132–143 (2010).

41. Harman, D. The aging process. *Proc Natl Acad Sci U S A* **78**, 7124 (1981).

42. López-Otín, C., Blasco, M. A., Partridge, L., Serrano, M. & Kroemer, G. The Hallmarks of Aging. *Cell* **153**, 1194 (2013).

43. Fontana, L., Kennedy, B. K. & Longo, V. D. Medical research: treat ageing. *Nature* **511**, 405–406 (2014).

44. Broekmans, F. J., Soules, M. R. & Fauser, B. C. Ovarian aging: mechanisms and clinical consequences. *Endocr Rev* **30**, 465–493 (2009).

45. Mills, M., Rindfuss, R. R., McDonald, P. & te Velde, E. Why do people postpone parenthood? Reasons and social policy incentives. *Hum Reprod Update* **17**, 848–860 (2011).

46.   Richardson, S. J., Senikas, V. & Nelson, J. F. Follicular depletion during the menopausal transition: evidence for accelerated loss and ultimate exhaustion. *J Clin Endocrinol Metab* **65**, 1231–1237 (1987).

47.   Faddy, M. J. Follicle dynamics during ovarian ageing. *Mol Cell Endocrinol* **163**, 43–48 (2000).

48.   Faddy, M. J. & Gosden, R. G. A model conforming the decline in follicle numbers to the age of menopause in women. *Hum Reprod* **11**, 1484–1486 (1996).

49.   Li, Q. *et al.* Current understanding of ovarian aging. *Science China Life Sciences 2012 55:8* **55**, 659–669 (2012).

50.   Frick, A. P. Advanced maternal age and adverse pregnancy outcomes. *Best Pract Res Clin Obstet Gynaecol* **70**, 92–100 (2021).

51.   Navot, D. *et al.* Poor oocyte quality rather than implantation failure as a cause of age-related decline in female fertility. *Lancet* **337**, 1375–1377 (1991).

52.   O'Connor, K. A., Holman, D. J. & Wood, J. W. Menstrual cycle variability and the perimenopause. *American Journal of Human Biology* **13**, 465–478 (2001).

53.   Wang, S. *et al.* Single-Cell Transcriptomic Atlas of Primate Ovarian Aging. *Cell* **180**, 585-600.e19 (2020).

54.   Ruth, K. S. *et al.* Genetic insights into biological mechanisms governing human ovarian ageing. *Nature 2021 596:7872* **596**, 393–397 (2021).

55.   Nakagawa, S. & FitzHarris, G. Intrinsically Defective Microtubule Dynamics Contribute to Age-Related Chromosome Segregation Errors in Mouse Oocyte Meiosis-I. *Curr Biol* **27**, 1040–1047 (2017).

56.   Webster, A. & Schuh, M. Mechanisms of Aneuploidy in Human Eggs. *Trends Cell Biol* **27**, 55–68 (2017).

57.   Zielinska, A. P. *et al.* Meiotic Kinetochores Fragment into Multiple Lobes upon Cohesin Loss in Aging Eggs. *Curr Biol* **29**, 3749-3765.e7 (2019).

58.   Duncan, F. E. *et al.* Chromosome cohesion decreases in human eggs with advanced maternal age. *Aging Cell* **11**, 1121–1124 (2012).

59.   Chiang, T., Duncan, F. E., Schindler, K., Schultz, R. M. & Lampson, M. A. Evidence that weakened centromere cohesion is a leading cause of age-related aneuploidy in oocytes. *Curr Biol* **20**, 1522–1528 (2010).

60.   Chiang, T., Schultz, R. M. & Lampson, M. A. Meiotic origins of maternal age-related aneuploidy. *Biol Reprod* **86**, 3–4 (2012).

61.   Schon, E. A., Dimauro, S. & Hirano, M. Human mitochondrial DNA: roles of inherited and somatic mutations. *Nat Rev Genet* **13**, 878–890 (2012).

62.   Bogenhagen, D. F. Mitochondrial DNA nucleoid structure. *Biochim Biophys Acta* **1819**, 914–920 (2012).

63.   Jansen, R. P. S. & de Boer, K. The bottleneck: mitochondrial imperatives in oogenesis and ovarian follicular fate. *Mol Cell Endocrinol* **145**, 81–88 (1998).

64.   Barritt, J. A., Kokot, M., Cohen, J., Steuerwald, N. & Brenner, C. A. Quantification of human ooplasmic mitochondria. *Reprod Biomed Online* **4**, 243–247 (2002).

65.   van Blerkom, J. Mitochondrial function in the human oocyte and embryo and their role in developmental competence. *Mitochondrion* **11**, 797–813 (2011).

66.   Babayev, E. & Seli, E. Oocyte mitochondrial function and reproduction. *Curr Opin Obstet Gynecol* **27**, 175 (2015).

67.   Zhang, X., Wu, X. Q., Lu, S., Guo, Y. L. & Ma, X. Deficit of mitochondria-derived ATP during oxidative stress impairs mouse MII oocyte spindles. *Cell Res* **16**, 841–850 (2006).

68.   El-Hattab, A. W. & Scaglia, F. Mitochondrial DNA depletion syndromes: review and updates of genetic basis, manifestations, and therapeutic options. *Neurotherapeutics* **10**, 186–198 (2013).

69.   Lynch, M., Koskella, B. & Schaack, S. Mutation pressure and the evolution of organelle genomic architecture. *Science* **311**, 1727–1730 (2006).

70.   Kujoth, C. C. *et al.* Mitochondrial DNA mutations, oxidative stress, and apoptosis in mammalian aging. *Science* **309**, 481–484 (2005).

71.   Bratic, A. & Larsson, N. G. The role of mitochondria in aging. *J Clin Invest* **123**, 951 (2013).

72.   Gomez-Cabrera, M. C. *et al.* Mitochondria as sources and targets of damage in cellular aging. *Clin Chem Lab Med* **50**, 1287–1295 (2012).

73.   Kennedy, S. R., Loeb, L. A. & Herr, A. J. Somatic mutations in aging, cancer and neurodegeneration. *Mech Ageing Dev* **133**, 118–126 (2012).

74.   Kazachkova, N. *et al.* Patterns of mitochondrial DNA damage in blood and brain tissues of a transgenic mouse model of Machado-Joseph disease. *Neurodegener Dis* **11**, 206–214 (2013).

75.   Ravichandran, K. *et al.* Mitochondrial DNA quantification as a tool for embryo viability assessment: retrospective analysis of data from single euploid blastocyst transfers. *Hum Reprod* **32**, 1282–1292 (2017).

76.   Kushnir, V. A. *et al.* Reproductive aging is associated with decreased mitochondrial abundance and altered structure in murine oocytes. *J Assist Reprod Genet* **29**, 637–642 (2012).

77. Cecchino, G. N. & Garcia-Velasco, J. A. Mitochondrial DNA copy number as a predictor of embryo viability. *Fertil Steril* **111**, 205–211 (2019).

78. Wang, T. *et al.* Mitochondrial unfolded protein response gene Clpp is required to maintain ovarian follicular reserve during aging, for oocyte competence, and development of pre-implantation embryos. *Aging Cell* **17**, (2018).

79. Zhang, M. *et al.* Mitofusin 2 plays a role in oocyte and follicle development, and is required to maintain ovarian follicular reserve during reproductive aging. *Aging (Albany NY)* **11**, 3919 (2019).

80. Dan Dunn, J., Alvarez, L. A. J., Zhang, X. & Soldati, T. Reactive oxygen species and mitochondria: A nexus of cellular homeostasis. *Redox Biol* **6**, 472–485 (2015).

81. Forman, H. J. Reactive oxygen species and alpha,beta-unsaturated aldehydes as second messengers in signal transduction. *Ann N Y Acad Sci* **1203**, 35–44 (2010).

82. Simon, H. U., Haj-Yehia, A. & Levi-Schaffer, F. Role of reactive oxygen species (ROS) in apoptosis induction. *Apoptosis* **5**, 415–418 (2000).

83. Shi, L. *et al.* Long-Term Moderate Oxidative Stress Decreased Ovarian Reproductive Function by Reducing Follicle Quality and Progesterone Production. *PLoS One* **11**, (2016).

84. Sasaki, H. *et al.* Impact of Oxidative Stress on Age-Associated Decline in Oocyte Developmental Competence. *Front Endocrinol (Lausanne)* **10**, (2019).

85. Liou, G. Y. & Storz, P. Detecting Reactive Oxygen Species by Immunohistochemistry. *Methods Mol Biol* **1292**, 97 (2015).

86. Dalleau, S., Baradat, M., Guéraud, F. & Huc, L. Cell death and diseases related to oxidative stress: 4-hydroxynonenal (HNE) in the balance. *Cell Death Differ* **20**, 1615–1630 (2013).

87. Breitzig, M., Bhimineni, C., Lockey, R. & Kolliputi, N. 4-Hydroxy-2-nonenal: a critical target in oxidative stress? *Am J Physiol Cell Physiol* **311**, C537 (2016).

88. Yang, L. *et al.* The Role of Oxidative Stress and Natural Antioxidants in Ovarian Aging. *Front Pharmacol* **11**, 2364 (2021).

89. Mihalas, B. P., de Iuliis, G. N., Redgrove, K. A., McLaughlin, E. A. & Nixon, B. The lipid peroxidation product 4-hydroxynonenal contributes to oxidative stress-mediated deterioration of the ageing oocyte. *Sci Rep* **7**, (2017).

90. Branzei, D. & Foiani, M. Regulation of DNA repair throughout the cell cycle. *Nature Reviews Molecular Cell Biology 2008 9:4* **9**, 297–308 (2008).

91. Wang, Q. & Sun, Q. Y. Evaluation of oocyte quality: morphological, cellular and molecular predictors. *Reprod Fertil Dev* **19**, 1–12 (2007).

92.   Gorbunova, V., Seluanov, A., Mao, Z. & Hine, C. Changes in DNA repair during aging. *Nucleic Acids Res* **35**, 7466–7474 (2007).

93.   Govindaraj, V., Keralapura Basavaraju, R. & Rao, A. J. Changes in the expression of DNA double strand break repair genes in primordial follicles from immature and aged rats. *Reprod Biomed Online* **30**, 303–310 (2015).

94.   Stringer, J. M., Winship, A., Zerafa, N., Wakefield, M. & Hutt, K. Oocytes can efficiently repair DNA double-strand breaks to restore genetic integrity and protect offspring health. *Proc Natl Acad Sci U S A* **117**, 11513–11522 (2020).

95.   Chatterjee, N. & Walker, G. C. Mechanisms of DNA damage, repair, and mutagenesis. *Environ Mol Mutagen* **58**, 235–263 (2017).

96.   Ménézo, Y., Dale, B. & Cohen, M. DNA damage and repair in human oocytes and embryos: a review. *Zygote* **18**, 357–365 (2010).

97.   Krejci, L., Altmannova, V., Spirek, M. & Zhao, X. Homologous recombination and its regulation. *Nucleic Acids Res* **40**, 5795–5818 (2012).

98.   Maidarti, M., Anderson, R. A. & Telfer, E. E. Crosstalk between PTEN/PI3K/Akt Signalling and DNA Damage in the Oocyte: Implications for Primordial Follicle Activation, Oocyte Quality and Ageing. *Cells* **9**, (2020).

99.   Kerr, J. B. *et al.* DNA damage-induced primordial follicle oocyte apoptosis and loss of fertility require TAp63-mediated induction of Puma and Noxa. *Mol Cell* **48**, 343 (2012).

100.   Nowsheen, S. & Yang, E. S. THE INTERSECTION BETWEEN DNA DAMAGE RESPONSE AND CELL DEATH PATHWAYS. *Exp Oncol* **34**, 243 (2012).

101.   Mara, J. N. *et al.* Ovulation and ovarian wound healing are impaired with advanced reproductive age. *Aging (Albany NY)* **12**, 9686 (2020).

102.   Amargant, F. *et al.* Ovarian stiffness increases with age in the mammalian ovary and depends on collagen and hyaluronan matrices. *Aging Cell* **19**, (2020).

103.   Dipali, S. S., Ferreira, C. R., Zhou, L. T., Pritchard, M. T. & Duncan, F. E. Histologic analysis and lipid profiling reveal reproductive age-associated changes in peri-ovarian adipose tissue. *Reproductive Biology and Endocrinology* **17**, 1–13 (2019).

104.   Poulsen, P., Esteller, M., Vaag, A. & Fraga, M. F. The Epigenetic Basis of Twin Discordance in Age-Related Diseases. *Pediatric Research 2007 61:7* **61**, 38–42 (2007).

105.   Keefe, D. L. Telomeres, Reproductive Aging, and Genomic Instability During Early Development. *Reprod Sci* **23**, 1612–1615 (2016).

106.   Kalmbach, K. H. *et al.* Telomeres and human reproduction. *Fertil Steril* **99**, 23–29 (2013).

107. Garcia, J. E., Jones, G. S., Acosta, A. A. & Wright, G. Human menopausal gonadotropin/human chorionic gonadotropin follicular maturation for oocyte aspiration: phase II, 1981. *Fertil Steril* **39**, 174–179 (1983).

108. Pellicer, A. *et al.* Aetiological factors involved in the low response to gonadotrophins in infertile women with normal basal serum follicle stimulating hormone levels. *Hum Reprod* **9**, 806–811 (1994).

109. Polyzos, N. P. *et al.* Live birth rates in Bologna poor responders treated with ovarian stimulation for IVF/ICSI. *Reprod Biomed Online* **28**, 469–474 (2014).

110. Beck-Peccoz, P. & Persani, L. Premature ovarian failure. *Orphanet J Rare Dis* **1**, 9 (2006).

111. Coulam, C. B., Adamson, S. C. & Annegers, J. F. Incidence of premature ovarian failure. *Obstetrics and Gynecology* **67**, 604–606 (1986).

112. Goswami, D. & Conway, G. S. Premature ovarian failure. *Horm Res* **68**, 196–202 (2007).

113. Bidet, M. *et al.* Resumption of ovarian function and pregnancies in 358 patients with premature ovarian failure. *J Clin Endocrinol Metab* **96**, 3864–3872 (2011).

114. Visser, J. A., Schipper, I., Laven, J. S. E. & Themmen, A. P. N. Anti-Müllerian hormone: an ovarian reserve marker in primary ovarian insufficiency. *Nat Rev Endocrinol* **8**, 331–341 (2012).

115. Munné, S., Cohen, J. & Sable, D. Preimplantation genetic diagnosis for advanced maternal age and other indications. *Fertil Steril* **78**, 234–236 (2002).

116. Kyrou, D. *et al.* How to improve the probability of pregnancy in poor responders undergoing in vitro fertilization: a systematic review and meta-analysis. *Fertil Steril* **91**, 749–766 (2009).

117. Pandian, Z., McTavish, A. R., Aucott, L., Hamilton, M. P. & Bhattacharya, S. Interventions for 'poor responders' to controlled ovarian hyper stimulation (COH) in in-vitro fertilisation (IVF). *Cochrane Database Syst Rev* (2010) doi:10.1002/14651858.CD004379.PUB3.

118. Rosen, G. F., Stone, S. C. & Yee, B. Ovulation induction in women with premature ovarian failure: a prospective, crossover study. *Fertil Steril* **57**, 448–449 (1992).

119. Surrey, E. S. & Cedars, M. I. The effect of gonadotropin suppression on the induction of ovulation in premature ovarian failure patients. *Fertil Steril* **52**, 36–41 (1989).

120. van Kasteren, Y. M. & Schoemaker, J. Premature ovarian failure: a systematic review on therapeutic interventions to restore ovarian function and achieve pregnancy. *Hum Reprod Update* **5**, 483–492 (1999).

121. Kawamura, K., Kawamura, N. & Hsueh, A. J. W. Activation of dormant follicles: a new treatment for premature ovarian failure? *Curr Opin Obstet Gynecol* **28**, 217–222 (2016).

122. Kawamura, K. *et al.* Hippo signaling disruption and Akt stimulation of ovarian follicles for infertility treatment. *Proc Natl Acad Sci U S A* **110**, 17474–17479 (2013).

123. Zhai, J. *et al.* In Vitro Activation of Follicles and Fresh Tissue Auto-transplantation in Primary Ovarian Insufficiency Patients. *J Clin Endocrinol Metab* **101**, 4405–4412 (2016).

124. Lunding, S. A. *et al.* Biopsying, fragmentation and autotransplantation of fresh ovarian cortical tissue in infertile women with diminished ovarian reserve. *Human Reproduction* **34**, 1924–1936 (2019).

125. Smith, A. A glossary for stem-cell biology. *Nature 2006 441:7097* **441**, 1060–1060 (2006).

126. Zakrzewski, W., Dobrzyński, M., Szymonowicz, M. & Rybak, Z. Stem cells: Past, present, and future. *Stem Cell Res Ther* **10**, 1–22 (2019).

127. Veitia, R. A., Gluckman, E., Fellous, M. & Soulier, J. Recovery of female fertility after chemotherapy, irradiation, and bone marrow allograft: further evidence against massive oocyte regeneration by bone marrow-derived germline stem cells. *Stem Cells* **25**, 1334–1335 (2007).

128. Hershlag, A. & Schuster, M. W. Return of fertility after autologous stem cell transplantation. *Fertil Steril* **77**, 419–421 (2002).

129. Salooja, N. *et al.* Pregnancy outcomes after peripheral blood or bone marrow transplantation: A retrospective survey. *Lancet* **358**, 271–276 (2001).

130. Sanders, J. E. *et al.* Pregnancies following high-dose cyclophosphamide with or without high-dose busulfan or total-body irradiation and bone marrow transplantation. *Blood* **87**, 3045–3052 (1996).

131. Salooja, N. *et al.* Successful pregnancies in women following single autotransplant for acute myeloid leukemia with a chemotherapy ablation protocol. *Bone Marrow Transplant* **13**, 431–435 (1994).

132. Astori, G. *et al.* Bone marrow derived stem cells in regenerative medicine as Advanced Therapy Medicinal Products. *Am J Transl Res* **2**, 285 (2010).

133. Friedenstein, A. J., Petrakova, K. V., Kurolesova, A. I. & Frolova, G. P. Heterotopic of bone marrow. Analysis of precursor cells for osteogenic and hematopoietic tissues. *Transplantation* **6**, 230–247 (1968).

134. Koç, O. N. *et al.* Rapid hematopoietic recovery after coinfusion of autologous-blood stem cells and culture-expanded marrow mesenchymal stem cells in

advanced breast cancer patients receiving high-dose chemotherapy. *J Clin Oncol* **18**, 307–316 (2000).

135. Ringdén, O. *et al.* Mesenchymal stem cells for treatment of therapy-resistant graft-versus-host disease. *Transplantation* **81**, 1390–1397 (2006).

136. Hoggatt, J. & Pelus, L. M. Mobilization of hematopoietic stem cells from the bone marrow niche to the blood compartment. *Stem Cell Res Ther* **2**, 1–8 (2011).

137. Cashen, A. F., Lazarus, H. M. & Devine, S. M. Mobilizing stem cells from normal donors: is it possible to improve upon G-CSF? *Bone Marrow Transplant* **39**, 577–588 (2007).

138. Demetri, G. D. & Griffin, J. D. Granulocyte colony-stimulating factor and its receptor. *Blood* **78**, 2791–2808 (1991).

139. Böyum, A. Isolation of mononuclear cells and granulocytes from human blood. Isolation of monuclear cells by one centrifugation, and of granulocytes by combining centrifugation and sedimentation at 1 g. *Scand J Clin Lab Invest Suppl* **97**, 77–89 (1968).

140. Liu, J. *et al.* Homing and restorative effects of bone marrow-derived mesenchymal stem cells on cisplatin injured ovaries in rats. *Mol Cells* **37**, 865–872 (2014).

141. Mohamed, S. A. *et al.* Human Mesenchymal Stem Cells Partially Reverse Infertility in Chemotherapy-Induced Ovarian Failure. *Reprod Sci* **25**, 51–63 (2018).

142. Lee, H. J. *et al.* Bone marrow transplantation generates immature oocytes and rescues long-term fertility in a preclinical mouse model of chemotherapy-induced premature ovarian failure. *J Clin Oncol* **25**, 3198–3204 (2007).

143. Ghadami, M. *et al.* Bone marrow transplantation restores follicular maturation and steroid hormones production in a mouse model for primary ovarian failure. *PLoS One* **7**, (2012).

144. Bao, R. *et al.* Bone marrow derived mesenchymal stem cells transplantation rescues premature ovarian insufficiency induced by chemotherapy. *Gynecol Endocrinol* **34**, 320–326 (2018).

145. Herraiz, S. *et al.* Fertility rescue and ovarian follicle growth promotion by bone marrow stem cell infusion. *Fertil Steril* **109**, 908-918.e2 (2018).

146. Herraiz, S. *et al.* Autologous stem cell ovarian transplantation to increase reproductive potential in patients who are poor responders. *Fertil Steril* **110**, 496-505.e1 (2018).

147. Kawamoto, A. *et al.* Therapeutic potential of ex vivo expanded endothelial progenitor cells for myocardial ischemia. *Circulation* **103**, 634–637 (2001).

148. Gnecchi, M. *et al.* Paracrine action accounts for marked protection of ischemic heart by Akt-modified mesenchymal stem cells. *Nat Med* **11**, 367–368 (2005).

149. Gnecchi, M. *et al.* Evidence supporting paracrine hypothesis for Akt-modified mesenchymal stem cell-mediated cardiac protection and functional improvement. *FASEB J* **20**, 661–669 (2006).

150. Gnecchi, M., Zhang, Z., Ni, A. & Dzau, V. J. Paracrine mechanisms in adult stem cell signaling and therapy. *Circ Res* **103**, 1204–1219 (2008).

151. Santamaria, X. *et al.* Autologous cell therapy with CD133+ bone marrow-derived stem cells for refractory Asherman's syndrome and endometrial atrophy: a pilot cohort study. *Hum Reprod* **31**, 1087–1096 (2016).

152. He, Y. *et al.* The therapeutic potential of bone marrow mesenchymal stem cells in premature ovarian failure. *Stem Cell Res Ther* **9**, 1–7 (2018).

153. Cervelló, I. *et al.* Human CD133(+) bone marrow-derived stem cells promote endometrial proliferation in a murine model of Asherman syndrome. *Fertil Steril* **104**, 1552-1560.e3 (2015).

154. Takahashi, M. *et al.* Cytokines produced by bone marrow cells can contribute to functional improvement of the infarcted heart by protecting cardiomyocytes from ischemic injury. *Am J Physiol Heart Circ Physiol* **291**, (2006).

155. Khanmohammadi, N. *et al.* Effect of Transplantation of Bone Marrow Stromal Cell-Conditioned Medium on Ovarian Function, Morphology and Cell Death in Cyclophosphamide-Treated Rats. *Cell J* **20**, 10–18 (2018).

156. Zhu, S. F. *et al.* Human umbilical cord mesenchymal stem cell transplantation restores damaged ovaries. *J Cell Mol Med* **19**, 2108–2117 (2015).

157. Wang, S. *et al.* The therapeutic potential of umbilical cord mesenchymal stem cells in mice premature ovarian failure. *Biomed Res Int* **2013**, (2013).

158. Li, H. *et al.* Human Umbilical Cord Mesenchymal Stem Cells Therapy in Cyclophosphamide-Induced Premature Ovarian Failure Rat Model. *Biomed Res Int* **2016**, (2016).

159. Li, J. *et al.* Human umbilical cord mesenchymal stem cells improve the reserve function of perimenopausal ovary via a paracrine mechanism. *Stem Cell Res Ther* **8**, (2017).

160. Castellano, J. M., Kirby, E. D. & Wyss-Coray, T. Blood-Borne Revitalization of the Aged Brain. *JAMA Neurol* **72**, 1191–1194 (2015).

161. Castellano, J. M. *et al.* Human umbilical cord plasma proteins revitalize hippocampal function in aged mice. *Nature* **544**, 488–492 (2017).

162. Villeda, S. A. *et al.* Young blood reverses age-related impairments in cognitive function and synaptic plasticity in mice. *Nat Med* **20**, 659–663 (2014).

163. Ehrhart, J., Sanberg, P. R. & Garbuzova-Davis, S. Plasma derived from human umbilical cord blood: Potential cell-additive or cell-substitute therapeutic for neurodegenerative diseases. *J Cell Mol Med* **22**, 6157 (2018).

164. Romanov, Y. A., Vtorushina, V. v., Dugina, T. N., Romanov, A. Y. & Petrova, N. v. Human Umbilical Cord Blood Serum/Plasma: Cytokine Profile and Prospective Application in Regenerative Medicine. *Bull Exp Biol Med* **168**, 173–177 (2019).

165. Mussano, F. *et al.* Cytokine, chemokine, and growth factor profile of platelet-rich plasma. *https://doi.org/10.3109/09537104.2016.1143922* **27**, 467–471 (2016).

166. Callejo, J. *et al.* Live birth in a woman without ovaries after autograft of frozen-thawed ovarian tissue combined with growth factors. *J Ovarian Res* **6**, (2013).

167. Cakiroglu, Y. *et al.* Effects of intraovarian injection of autologous platelet rich plasma on ovarian reserve and IVF outcome parameters in women with primary ovarian insufficiency. *Aging* **12**, 10211–10222 (2020).

168. Jackman, J. M. *et al.* INTRAOVARIAN INJECTION OF AUTOLOGOUS PLATELET RICH PLASMA (PRP) ENHANCES OVARIAN FOLLICULOGENESIS. *Fertil Steril* **114**, e167–e168 (2020).

169. Melo, P., Navarro, C., Jones, C., Coward, K. & Coleman, L. The use of autologous platelet-rich plasma (PRP) versus no intervention in women with low ovarian reserve undergoing fertility treatment: a non-randomized interventional study. *J Assist Reprod Genet* **37**, 855–863 (2020).

170. Sfakianoudis, K. *et al.* Reactivating Ovarian Function through Autologous Platelet-Rich Plasma Intraovarian Infusion: Pilot Data on Premature Ovarian Insufficiency, Perimenopausal, Menopausal, and Poor Responder Women. *J Clin Med* **9**, 1–25 (2020).

171. Sills, E. S. *et al.* Regenerative Effect of Intraovarian Injection of Activated Autologous Platelet Rich Plasma: Serum Anti-Mullerian Hormone Levels Measured Among Poor-Prognosis In Vitro Fertilization Patients. *International Journal of Regenerative Medicine* **2020**, 1–5 (2020).

172. Parvanov, D. *et al.* Autologous ovarian platelet rich plasma treatment improves oocyte and embryo quality: a before-after prospective study. *http://mc.manuscriptcentral.com/tbeq* **36**, 425–432 (2022).

173. Cakiroglu, Y. *et al.* Ovarian reserve parameters and IVF outcomes in 510 women with poor ovarian response (POR) treated with intraovarian injection of autologous platelet rich plasma (PRP). *Aging* **14**, 2513–2523 (2022).

174. Sills, E. S., Rickers, N. S., Li, X. & Palermo, G. D. First data on in vitro fertilization and blastocyst formation after intraovarian injection of calcium gluconate-activated autologous platelet rich plasma. *Gynecol Endocrinol* **34**, 756–760 (2018).

175. Hsu, C. C., Hsu, L., Hsu, I., Chiu, Y. J. & Dorjee, S. Live Birth in Woman With Premature Ovarian Insufficiency Receiving Ovarian Administration of Platelet-Rich Plasma (PRP) in Combination With Gonadotropin: A Case Report. *Front Endocrinol (Lausanne)* **11**, (2020).

176. Fréchette, J. P., Martineau, I. & Gagnon, G. Platelet-rich plasmas: Growth factor content and roles in wound healing. *J Dent Res* **84**, 434–439 (2005).

177. Farimani, M., Heshmati, S., Poorolajal, J. & Bahmanzadeh, M. A report on three live births in women with poor ovarian response following intra-ovarian injection of platelet-rich plasma (PRP). *Mol Biol Rep* **46**, 1611–1616 (2019).

178. Pantos, K. *et al.* A Case Series on Natural Conceptions Resulting in Ongoing Pregnancies in Menopausal and Prematurely Menopausal Women Following Platelet-Rich Plasma Treatment. *Cell Transplant* **28**, 1333–1340 (2019).

179. Li, Z., Delaney, M. K., O'Brien, K. A. & Du, X. Signaling during platelet adhesion and activation. *Arterioscler Thromb Vasc Biol* **30**, 2341–2349 (2010).

180. Lopez-Vilchez, I., Diaz-Ricart, M., White, J. G., Escolar, G. & Galan, A. M. Serotonin enhances platelet procoagulant properties and their activation induced during platelet tissue factor uptake. *Cardiovasc Res* **84**, 309–316 (2009).

181. Wraith, K. S. *et al.* Oxidized low-density lipoproteins induce rapid platelet activation and shape change through tyrosine kinase and Rho kinase-signaling pathways. *Blood* **122**, 580–589 (2013).

182. Shen, J. *et al.* Coordination of platelet agonist signaling during the hemostatic response in vivo. *Blood Adv* **1**, 2767–2775 (2017).

183. Irmak, G., Demirtaş, T. T. & Gümüşderelioğlu, M. Sustained release of growth factors from photoactivated platelet rich plasma (PRP). *European Journal of Pharmaceutics and Biopharmaceutics* **148**, 67–76 (2020).

184. Atkinson, L., Martin, F. & Sturmey, R. G. Intraovarian injection of platelet-rich plasma in assisted reproduction: too much too soon? *Hum Reprod* **36**, 1737 (2021).

185. Bakacak, M. *et al.* Protective Effect of Platelet Rich Plasma on Experimental Ischemia/Reperfusion Injury in Rat Ovary. *Gynecol Obstet Invest* **81**, 225–231 (2016).

186. Ahmadian, S. *et al.* Intra-ovarian injection of platelet-rich plasma into ovarian tissue promoted rejuvenation in the rat model of premature ovarian insufficiency and restored ovulation rate via angiogenesis modulation. *Reproductive Biology and Endocrinology* **18**, (2020).

187. Cremonesi, F., Bonfanti, S., Idda, A. & Anna, L. C. Improvement of Embryo Recovery in Holstein Cows Treated by Intra-Ovarian Platelet Rich Plasma before Superovulation. *Vet Sci* **7**, (2020).

188. Cozzolino, M., Herraiz, S. & Seli, E. EFFECTS OF INTRAOVARIAN INJECTION OF PLATELET RICH PLASMA (PRP) ON A PRIMARY OVARIAN INSUFFICIENCY (POI) MOUSE MODEL. *Fertil Steril* **116**, e43 (2021).

189. Flurkey, K., Currer, J. M. & Harrison, D. E. Mouse Models in Aging Research. *The Mouse in Biomedical Research* **3**, 637–672 (2007).

190. Tecott, L. H. The genes and brains of mice and men. *Am J Psychiatry* **160**, 646–656 (2003).

191. Bronson, F. H. The reproductive ecology of the house mouse. *Q Rev Biol* **54**, 265–299 (1979).

192. Lu, H. *et al.* Current Animal Model Systems for Ovarian Aging Research. *Aging Dis* **13**, 1183–1195 (2022).

193. Miao, Y. *et al.* BRCA2 deficiency is a potential driver for human primary ovarian insufficiency. *Cell Death Dis* **10**, (2019).

194. Abel, M. H. *et al.* The effect of a null mutation in the follicle-stimulating hormone receptor gene on mouse reproduction. *Endocrinology* **141**, 1795–1803 (2000).

195. Li, X. hui *et al.* Loss of pigment epithelium-derived factor leads to ovarian oxidative damage accompanied by diminished ovarian reserve in mice. *Life Sci* **216**, 129–139 (2019).

196. Kalich-Philosoph, L. *et al.* Cyclophosphamide triggers follicle activation and 'burnout'; AS101 prevents follicle loss and preserves fertility. *Sci Transl Med* **5**, (2013).

197. Sonmezer, M. & Oktay, K. Fertility preservation in young women undergoing breast cancer therapy. *Oncologist* **11**, 422–434 (2006).

198. Ben-Aharon, I. *et al.* Doxorubicin-induced ovarian toxicity. *Reprod Biol Endocrinol* **8**, 20 (2010).

199. Spears, N. *et al.* Ovarian damage from chemotherapy and current approaches to its protection. *Hum Reprod Update* **25**, 673–693 (2019).

200. Buigues, A., Marchante, M., Herraiz, S. & Pellicer, A. Diminished Ovarian Reserve Chemotherapy-Induced Mouse Model: A Tool for the Preclinical Assessment of New Therapies for Ovarian Damage. *Reprod Sci* (2019) doi:10.1177/1933719119831784.

201. Soleimani, R., Heytens, E., Darzynkiewicz, Z. & Oktay, K. Mechanisms of chemotherapy-induced human ovarian aging: double strand DNA breaks and microvascular compromise. *Aging* **3**, 782–793 (2011).

202. Petrillo, S. K., Desmeules, P., Truong, T. Q. & Devine, P. J. Detection of DNA damage in oocytes of small ovarian follicles following phosphoramide mustard exposures of cultured rodent ovaries in vitro. *Toxicol Appl Pharmacol* **253**, 94–102 (2011).

203. Chen, X. *et al.* Heat shock pretreatment of mesenchymal stem cells for inhibiting the apoptosis of ovarian granulosa cells enhanced the repair effect on chemotherapy-induced premature ovarian failure. *Stem Cell Res Ther* **9**, 240 (2018).

204. Morgan, S., Anderson, R. A., Gourley, C., Wallace, W. H. & Spears, N. How do chemotherapeutic agents damage the ovary? *Hum Reprod Update* **18**, 525–535 (2012).

205. Stolk, L. *et al.* Meta-analyses identify 13 loci associated with age at menopause and highlight DNA repair and immune pathways. *Nat Genet* **44**, 260–268 (2012).

206. Stringer, J. M., Winship, A., Liew, S. H. & Hutt, K. The capacity of oocytes for DNA repair. *Cell Mol Life Sci* **75**, 2777–2792 (2018).

207. Winship, A. L., Stringer, J. M., Liew, S. H. & Hutt, K. J. The importance of DNA repair for maintaining oocyte quality in response to anti-cancer treatments, environmental toxins and maternal ageing. *Hum Reprod Update* **24**, 119–134 (2018).

208. Rubia, J. de la. Basal CD34(+) cell count predicts peripheral blood progenitor cell mobilization and collection in healthy donors after administration of granulocyte colony-stimulating factor. *Haematologica* (2004).

209. Brydøy, M., Fosså, S. D., Dahl, O. & Bjøro, T. Gonadal dysfunction and fertility problems in cancer survivors. *Acta Oncol* **46**, 480–489 (2007).

210. Yoo, J. *et al.* Therapeutic effects of umbilical cord blood plasma in a rat model of acute ischemic stroke. *Oncotarget* **7**, 79131–79140 (2016).

211. Dehghani, F., Aboutalebi, H., Esmaeilpour, T., Panjehshahin, M. R. & Bordbar, H. Effect of platelet-rich plasma (PRP) on ovarian structures in cyclophosphamide-induced ovarian failure in female rats: a stereological study. *Toxicol Mech Methods* **28**, 653–659 (2018).

212. Ozturk, S. Selection of competent oocytes by morphological criteria for assisted reproductive technologies. *Mol Reprod Dev* **87**, 1021–1036 (2020).

213. MacHtinger, R. & Racowsky, C. Morphological systems of human embryo assessment and clinical evidence. *Reprod Biomed Online* **26**, 210–221 (2013).

214. Schneider, C. A., Rasband, W. S. & Eliceiri, K. W. NIH Image to ImageJ: 25 years of image analysis. *Nature Methods 2012 9:7* **9**, 671–675 (2012).

215. Perez-Patiño, C. *et al.* Characterization of the porcine seminal plasma proteome comparing ejaculate portions. *J Proteomics* **142**, 15–23 (2016).

216. Shevchenko, A. *et al.* Linking genome and proteome by mass spectrometry: large-scale identification of yeast proteins from two dimensional gels. *Proc Natl Acad Sci U S A* **93**, 14440–14445 (1996).

217.   Mi, H., Muruganujan, A., Ebert, D., Huang, X. & Thomas, P. D. PANTHER version 14: more genomes, a new PANTHER GO-slim and improvements in enrichment analysis tools. *Nucleic Acids Res* **47**, D419–D426 (2019).

218.   Jassal, B. *et al.* The reactome pathway knowledgebase. *Nucleic Acids Res* **48**, D498–D503 (2020).

219.   Shevchenko, A. *et al.* Linking genome and proteome by mass spectrometry: large-scale identification of yeast proteins from two dimensional gels. *Proc Natl Acad Sci U S A* **93**, 14440–14445 (1996).

220.   Shilov, I. v. *et al.* The Paragon Algorithm, a next generation search engine that uses sequence temperature values and feature probabilities to identify peptides from tandem mass spectra. *Mol Cell Proteomics* **6**, 1638–1655 (2007).

221.   Santagostino, S. F., Arbona, R. J. R., Nashat, M. A., White, J. R. & Monette, S. Pathology of Aging in NOD scid gamma Female Mice. *Vet Pathol* **54**, 855–869 (2017).

222.   Sandrock, M. *et al.* Reduction in corpora lutea number in obese melanocortin-4-receptor-deficient mice. *Reprod Biol Endocrinol* **7**, 24 (2009).

223.   Li, J. *et al.* Activation of dormant ovarian follicles to generate mature eggs. *Proc Natl Acad Sci U S A* **107**, 10280–10284 (2010).

224.   Rohart, F., Gautier, B., Singh, A. & Lê Cao, K. A. mixOmics: An R package for 'omics feature selection and multiple data integration. *PLoS Comput Biol* **13**, (2017).

225.   Langfelder, P. & Horvath, S. WGCNA: An R package for weighted correlation network analysis. *BMC Bioinformatics* **9**, 1–13 (2008).

226.   Pedersen, T. & Peters, H. Proposal for a classification of oocytes and follicles in the mouse ovary. *J Reprod Fertil* **17**, 555–557 (1968).

227.   Zhang, J. *et al.* Initiation of follicular atresia: gene networks during early atresia in pig ovaries. *Reproduction* **156**, 23–33 (2018).

228.   Hamel, M. *et al.* Identification of follicular marker genes as pregnancy predictors for human IVF: new evidence for the involvement of luteinization process. *Mol Hum Reprod* **16**, 548–556 (2010).

229.   Duncan, F. E. *et al.* Age-associated dysregulation of protein metabolism in the mammalian oocyte. *Aging Cell* **16**, 1381–1393 (2017).

230.   Nivet, A. L., Léveillé, M. C., Leader, A. & Sirard, M. A. Transcriptional characteristics of different sized follicles in relation to embryo transferability: potential role of hepatocyte growth factor signalling. *Mol Hum Reprod* **22**, 475–484 (2016).

231.   Brazert, M., Kranc, W., Jopek, K., Kempisty, B. & Pawelczyk, L. New markers of human cumulus oophorus cells cultured in vitro-transcriptomic profile. *Medical Journal of Cell Biology* **8**, 60–72 (2020).

232. Colella, M. *et al.* Thyroid Hormones and Functional Ovarian Reserve: Systemic vs. Peripheral Dysfunctions. *J Clin Med* **9**, (2020).

233. Govindaraj, V., Krishnagiri, H., Chauhan, M. S. & Rao, A. J. BRCA-1 Gene Expression and Comparative Proteomic Profile of Primordial Follicles from Young and Adult Buffalo (Bubalus bubalis) Ovaries. *Anim Biotechnol* **28**, 94–103 (2017).

234. Bonnet, A. *et al.* In vivo gene expression in granulosa cells during pig terminal follicular development. *Reproduction* **136**, 211–224 (2008).

235. Ma, Y. *et al.* ADAMTS1 and HSPG2 mRNA levels in cumulus cells are related to human oocyte quality and controlled ovarian hyperstimulation outcomes. *J Assist Reprod Genet* **37**, 657–667 (2020).

236. Ambekar, A. S. *et al.* Proteomics of follicular fluid from women with polycystic ovary syndrome suggests molecular defects in follicular development. *J Clin Endocrinol Metab* **100**, 744–753 (2015).

237. Rozell, T. G., Davis, D. P., Chai, Y. & Segaloff, D. L. Association of gonadotropin receptor precursors with the protein folding chaperone calnexin. *Endocrinology* **139**, 1588–1593 (1998).

238. Turathum, B. & Sroyraya, M. Protein Profile Involved in Mammalian Oocyte Maturation, Fertilization and Early Embryogenesis (Pre-Implantation). *Cell Dev Biol* **06**, (2017).

239. Oksjoki, S., Söderström, M., Vuorio, E. & Anttila, L. Differential expression patterns of cathepsins B, H, K, L and S in the mouse ovary. *Mol Hum Reprod* **7**, 27–34 (2001).

240. Gershon, E. & Dekel, N. Newly Identified Regulators of Ovarian Folliculogenesis and Ovulation. *Int J Mol Sci* **21**, 1–18 (2020).

241. Likszo, P., Skarzynski, D. J. & Moza Jalali, B. Proteomic Analysis of Porcine Pre-ovulatory Follicle Differentiation Into Corpus Luteum. *Front Endocrinol (Lausanne)* **10**, (2019).

242. Scott Sills, E. & Wood, S. H. Autologous activated platelet-rich plasma injection into adult human ovary tissue: Molecular mechanism, analysis, and discussion of reproductive response. *Biosci Rep* **39**, (2019).

243. Johnson, J., Canning, J., Kaneko, T., Pru, J. K. & Tilly, J. L. Germline stem cells and follicular renewal in the postnatal mammalian ovary. *Nature* **428**, 145–150 (2004).

244. Yan, H. *et al.* CDC42 controls the activation of primordial follicles by regulating PI3K signaling in mouse oocytes. *BMC Biol* **16**, 1–16 (2018).

245. Kumagai, K. *et al.* Generation of transgenic mice on an NOD/SCID background using the conventional microinjection technique. *Biol Reprod* **84**, 682–688 (2011).

246. van Kasteren, Y. M. & Schoemaker, J. Premature ovarian failure: a systematic review on therapeutic interventions to restore ovarian function and achieve pregnancy. *Hum Reprod Update* **5**, 483–492 (1999).

247. Niikura, Y., Niikura, T. & Tilly, J. L. Aged mouse ovaries possess rare premeiotic germ cells that can generate oocytes following transplantation into a young host environment. *Aging* **1**, 971–978 (2009).

248. Richardson, R. B., Allan, D. S. & Le, Y. Greater organ involution in highly proliferative tissues associated with the early onset and acceleration of ageing in humans. *Exp Gerontol* **55**, 80–91 (2014).

249. Fraser, H. M. Regulation of the ovarian follicular vasculature. *Reprod Biol Endocrinol* **4**, (2006).

250. Garside, S. A., Harlow, C. R., Hillier, S. G., Fraser, H. M. & Thomas, F. H. Thrombospondin-1 inhibits angiogenesis and promotes follicular atresia in a novel in vitro angiogenesis assay. *Endocrinology* **151**, 1280–1289 (2010).

251. Osz, K., Ross, M. & Petrik, J. The thrombospondin-1 receptor CD36 is an important mediator of ovarian angiogenesis and folliculogenesis. *Reprod Biol Endocrinol* **12**, (2014).

252. Lopez, S. G. & Luderer, U. Effects of cyclophosphamide and buthionine sulfoximine on ovarian glutathione and apoptosis. *Free Radic Biol Med* **36**, 1366–1377 (2004).

253. Plowchalk, D. R. & Mattison, D. R. Reproductive toxicity of cyclophosphamide in the C57BL/6N mouse: 1. Effects on ovarian structure and function. *Reprod Toxicol* **6**, 411–421 (1992).

254. Xia, J. *et al.* Bone marrow mesenchymal stem cells stimulate proliferation and neuronal differentiation of retinal progenitor cells. *PLoS One* **8**, (2013).

255. Crowley, S. T., Dempsey, E. C., Horwitz, K. B. & Horwitz, L. D. Platelet-induced vascular smooth muscle cell proliferation is modulated by the growth amplification factors serotonin and adenosine diphosphate. *Circulation* **90**, 1908–1918 (1994).

256. Huang, Q. *et al.* G-CSF-mobilized peripheral blood mononuclear cells combined with platelet-rich plasma accelerate restoration of ovarian function in cyclophosphamide-induced POI rats†. *Biol Reprod* **101**, 91–101 (2019).

257. Huang, N., Yu, Y. & Qiao, J. Dual role for the unfolded protein response in the ovary: adaption and apoptosis. *Protein Cell* **8**, 14 (2017).

258. Harada, M. *et al.* Evidence of the activation of unfolded protein response in granulosa and cumulus cells during follicular growth and maturation. *http://dx.doi.org/10.3109/09513590.2015.1062862* **31**, 783–787 (2015).

259. Choi, J. Y., Jo, M. W., Lee, E. Y., Yoon, B. K. & Choi, D. S. The role of autophagy in follicular development and atresia in rat granulosa cells. *Fertil Steril* **93**, 2532–2537 (2010).

260. Cakiroglu, Y. *et al.* Effects of intraovarian injection of autologous platelet rich plasma on ovarian reserve and IVF outcome parameters in women with primary ovarian insufficiency. *Aging* **12**, 10211–10222 (2020).

261. Everts, P., Onishi, K., Jayaram, P., Lana, J. F. & Mautner, K. Platelet-rich plasma: New performance understandings and therapeutic considerations in 2020. *Int J Mol Sci* **21**, 1–36 (2020).

262. Ben-Aharon, I. *et al.* Doxorubicin-induced ovarian toxicity. *Reprod Biol Endocrinol* **8**, 20 (2010).

263. Goldman, K. N. *et al.* mTORC1/2 inhibition preserves ovarian function and fertility during genotoxic chemotherapy. *Proc Natl Acad Sci U S A* **114**, 3186–3191 (2017).

264. Spears, N. *et al.* Ovarian damage from chemotherapy and current approaches to its protection. *Hum Reprod Update* **25**, 673–693 (2019).

265. Wang, T. *et al.* Mitochondrial unfolded protein response gene Clpp is required to maintain ovarian follicular reserve during aging, for oocyte competence, and development of pre-implantation embryos. *Aging Cell* **17**, (2018).

266. Abel, M. H. *et al.* The effect of a null mutation in the follicle-stimulating hormone receptor gene on mouse reproduction. *Endocrinology* **141**, 1795–1803 (2000).

267. Li, X. hui *et al.* Loss of pigment epithelium-derived factor leads to ovarian oxidative damage accompanied by diminished ovarian reserve in mice. *Life Sci* **216**, 129–139 (2019).

268. Britt, K. L. *et al.* An age-related ovarian phenotype in mice with targeted disruption of the Cyp 19 (aromatase) gene. *Endocrinology* **141**, 2614–2623 (2000).

269. Takahashi, T. A. & Johnson, K. M. Menopause. *Medical Clinics of North America* **99**, 521–534 (2015).

270. Lebrasseur, N. K., Tchkonia, T. & Kirkland, J. L. Cellular Senescence and the Biology of Aging, Disease, and Frailty. *Nestle Nutr Inst Workshop Ser* **83**, 11–18 (2015).

271. Tomasetti, C. *et al.* Cell division rates decrease with age, providing a potential explanation for the age-dependent deceleration in cancer incidence. *Proc Natl Acad Sci U S A* **116**, 20482–20488 (2019).

272. Robinson, R. S. *et al.* Angiogenesis and vascular function in the ovary. *Reproduction* **138**, 869–881 (2009).

273. Brown, H. M. & Russell, D. L. Blood and lymphatic vasculature in the ovary: Development, function and disease. *Hum Reprod Update* **20**, 29–39 (2014).

274. Frick, A. P. Advanced maternal age and adverse pregnancy outcomes. *Best Pract Res Clin Obstet Gynaecol* **70**, 92–100 (2021).

275. Grøndahl, M. L. *et al.* Effect of women's age on embryo morphology, cleavage rate and competence - A multicenter cohort study. *PLoS One* **12**, (2017).

276. Herbert, M., Kalleas, D., Cooney, D., Lamb, M. & Lister, L. Meiosis and maternal aging: Insights from aneuploid oocytes and trisomy births. *Cold Spring Harb Perspect Biol* **7**, (2015).

277. Chiang, T., Schultz, R. M. & Lampson, M. A. Meiotic origins of maternal age-related aneuploidy. *Biol Reprod* **86**, (2012).

278. Wang, S. *et al.* Single-Cell Transcriptomic Atlas of Primate Ovarian Aging. *Cell* **180**, 585-600.e19 (2020).

279. Wang, T., Zhang, M., Jiang, Z. & Seli, E. Mitochondrial dysfunction and ovarian aging. *American Journal of Reproductive Immunology* **77**, e12651 (2017).

280. Zhang, X., Wu, X. Q., Lu, S., Guo, Y. L. & Ma, X. Deficit of mitochondria-derived ATP during oxidative stress impairs mouse MII oocyte spindles. *Cell Res* **16**, 841–850 (2006).

281. Kushnir, V. A. *et al.* Reproductive aging is associated with decreased mitochondrial abundance and altered structure in murine oocytes. *J Assist Reprod Genet* **29**, 637 (2012).

282. Cecchino, G. N. & Garcia-Velasco, J. A. Mitochondrial DNA copy number as a predictor of embryo viability. *Fertil Steril* **111**, 205–211 (2019).

283. Ravichandran, K. *et al.* Mitochondrial DNA quantification as a tool for embryo viability assessment: retrospective analysis of data from single euploid blastocyst transfers. *Human Reproduction* **32**, 1282–1292 (2017).

284. Maclaran, K. & Nikolaou, D. Early ovarian ageing. *The Obstetrician & Gynaecologist* **21**, 107–116 (2019).

285. Yang, L. *et al.* The Role of Oxidative Stress and Natural Antioxidants in Ovarian Aging. *Front Pharmacol* **11**, (2021).

286. Mihalas, B. P., de Iuliis, G. N., Redgrove, K. A., McLaughlin, E. A. & Nixon, B. The lipid peroxidation product 4-hydroxynonenal contributes to oxidative stress-mediated deterioration of the ageing oocyte. *Sci Rep* **7**, (2017).

287. Sasaki, H. *et al.* Impact of Oxidative Stress on Age-Associated Decline in Oocyte Developmental Competence. *Front Endocrinol (Lausanne)* **10**, (2019).

288. Son, M., Diamond, B. & Santiago-Schwarz, F. Fundamental role of C1q in autoimmunity and inflammation. *Immunol Res* **63**, 101 (2015).

289. Bender, H. R., Campbell, G. E., Aytoda, P., Mathiesen, A. H. & Duffy, D. M. Thrombospondin 1 (THBS1) Promotes Follicular Angiogenesis, Luteinization, and Ovulation in Primates. *Front Endocrinol (Lausanne)* **10**, (2019).

290. Vigelsø, A. *et al.* GAPDH and β-actin protein decreases with aging, making Stain-Free technology a superior loading control in Western blotting of human skeletal muscle. *J Appl Physiol (1985)* **118**, 386–394 (2015).

291. Seckin, S., Ramadan, H., Mouanness, M., Kohansieh, M. & Merhi, Z. Ovarian response to intraovarian platelet-rich plasma (PRP) administration: hypotheses and potential mechanisms of action. *J Assist Reprod Genet* **39**, 37–61 (2022).

292. May-Panloup, P. *et al.* Ovarian ageing: The role of mitochondria in oocytes and follicles. *Hum Reprod Update* **22**, 725–743 (2016).

293. Liochev, S. I. Reactive oxygen species and the free radical theory of aging. *Free Radic Biol Med* **60**, 1–4 (2013).

294. Chiang, J. L. *et al.* Mitochondria in Ovarian Aging and Reproductive Longevity. *Ageing Res Rev* **63**, (2020).

295. Kinnaird, T. *et al.* Marrow-Derived Stromal Cells Express Genes Encoding a Broad Spectrum of Arteriogenic Cytokines and Promote In Vitro and In Vivo Arteriogenesis Through Paracrine Mechanisms. *Circ Res* **94**, 678–685 (2004).

296. Galati, D. *et al.* Role of nuclear-encoded subunit Vb in the assembly and stability of cytochrome c oxidase complex: Implications in mitochondrial dysfunction and ROS production. *Biochemical Journal* **420**, 439–449 (2009).

297. Maryanovich, M. *et al.* An MTCH2 pathway repressing mitochondria metabolism regulates haematopoietic stem cell fate. *Nat Commun* **6**, (2015).

298. Lussier, J. G., Diouf, M. N., Lévesque, V., Sirois, J. & Ndiaye, K. Gene expression profiling of upregulated mRNAs in granulosa cells of bovine ovulatory follicles following stimulation with hCG. *Reproductive Biology and Endocrinology* **15**, (2017).

299. Rhee, S. G. Overview on Peroxiredoxin. *Mol Cells* **39**, 1–5 (2016).

300. Siller, K. H. & Doe, C. Q. Spindle orientation during asymmetric cell division. *Nat Cell Biol* **11**, 365–374 (2009).

301. Vidi, P. A. *et al.* NuMA promotes homologous recombination repair by regulating the accumulation of the ISWI ATPase SNF2h at DNA breaks. *Nucleic Acids Res* **42**, 6365–6379 (2014).

Bibliography

IX. ANNEXES

IX. ANNEXES

ANNEXE I

Proteome composition of the assayed plasmas established by SWATH-MS. For each plasma, the normalized area of each quantified protein is shown. There are also included all the specific Log2(FC) values obtained after performing different comparison approaches (BMDSC and UCB groups vs. PB; aBMDSC, and aUCB groups vs. aPB; each activated sample to its respective non-activated fraction); keratins were not considered for these comparisons. In each of the comparison approaches, those proteins that revealed as up- (Log2(FC)>1.5) or down- regulated (Log2(FC)<-1.5) are marked in colored cells.

Available at: Annexe_I.xlsx

ANNEXE II

Proteomic composition of the human ovarian tissue samples after control or aBMDSC plasma treatments. For each sample, the normalized area of each quantified protein is shown. There are also included the FC and Log2(FC) values calculated using the normalized protein area values of the aBMDSC samples, relative to those of the control group. Moreover, a Welch t-test was performed and the proteins presenting a p-value <0.05 were considered as statistically significant for the functional analysis.

Available at: Annexe_II.xlsx

ANNEXE II

Proteomic composition of the ovarian samples from young, AMA and old mice, established by SWATH-MS. For each sample, the normalized area of each quantified protein is shown. There are included the ElastiNEC and GO analysis for each group age,

showing the DEPs after plasma treatments and the GO information (ID, GOterm, subgroup, Enrichment score, FDR, gene count and gene name).

Available at: Annexe_III.xlsx

ANNEXE III

Proteomic characterization of aPRP- and aBMDSC-treated ovarian samples by SWATH-MS. The normalized area of each quantified protein is presented for each sample. There are included the ElastiNEC and GO analysis for each group age, showing the DEPs after plasma treatments and the GO information (ID, GOterm, subgroup, Enrichment score, FDR, gene count and gene name).

Available at: Annexe_IV.xlsx

ANNEXE V. SCIENTIFIC PRODUCTION

1. International scientific publications

-Buigues A*, **Marchante M***, Herraiz S, Pellicer A. Diminished Ovarian Reserve Chemotherapy-Induced Mouse Model: A Tool for the Preclinical Assessment of New Therapies for Ovarian Damage. *Reprod Sci* (2019) doi:10.1177/1933719119831784. *Authorship.

-Buigues A*, **Marchante M***, de Miguel-Gómez L, Martinez J, Cervelló I, Pellicer A, Herraiz S. Stem cell-secreted factor therapy regenerates ovarian niche and rescues follicles. *Am J Obstet Gynecol* 2021;**225**:65.e1-65.e14. *Authorship.

-**Marchante M**, Ramirez-Martin N, Buigues A, Martinez J, Pellicer N, Pellicer A, Herraiz S. Physiological reproductive aging: a mouse model to represent different human clinical fertility phenotypes. Submitted to BJOG: an International Journal of Obstetrics & Gynaecology.

-**Marchante M**, Buigues A, Ramirez-Martin N, Martinez J, Pellicer N, Pellicer A, Herraiz S. Single intraovarian dose of stem cell- and platelet-secreted factors mitigates age-related ovarian infertility in a murine model. Accepted for publication in American Journal of Obstetrics & Gynecology.

2. Works submitted to international conferences directly related with the present Ph.D. thesis

2.1 Oral communications

-G-CSF mobilized plasma regenerate ovarian stroma and restore ovarian function. Buigues A*, **Marchante M***, Herraiz S, Pellicer A. 67th Annual Meeting of the Society for Reproductive Investigation. Vancouver, (Canada), 2020. *Authorship.

-Plasma Enriched in Stem Cell Secreted Factors Improves Ovarian Function in a Mouse Model of Advanced Maternal Aged. **Marchante M**, Buigues A, Martinez J, Pellicer A, Herraiz S. 68th Annual Meeting of the Society for Reproductive Investigation. Boston, Massachusetts (USA), 2021.

-*Plenary session.* Combination of Stem Cell Secreted and Platelet Enclosed Growth Factors Restores Ovarian Function in an Aging Mouse Model. **Marchante M**, Martinez J, Pellicer A, Herraiz S. 69th Annual Meeting of the Society for Reproductive Investigation. Denver, Colorado (USA), 2022.

2.2 Poster presentation

-Stem Cell Secreted Factors-Enriched Plasma Promotes DNA Repair and Protects Against Chemotherapy-Induced Cell Death in Ovarian Tissue. **Marchante M***, Buigues A*, Pellicer A, Herraiz S. 67th Annual Meeting of the Society for Reproductive Investigation. Vancouver (Canada), 2020. *Authorship.

-Reproductive Aging Mouse Model: A Physiological Tool for the Preclinical Assessment of Ovarian Therapies. **Marchante M**, Ramirez N, Pellicer A, Herraiz S. 69th Annual Meeting of the Society for Reproductive Investigation. Denver, Colorado (USA), 2022

-Mitochondrial function and oocyte quality improved in an aging model by intraovarian administration of a combination of stem cell-secreted- and platelet-enclosed growth factors. **Marchante M**, Martinez J, Buigues A, Ramirez N, Pellicer A and Herraiz S. American Society for Reproductive Medicine. Anaheim, California (USA), 2022.

3. Works submitted to international conferences not related with the present Ph.D. thesis.

3.1 Oral communications

-Fertility Rescue by Bone Marrow Derived Stem Cell Infusion. Buigues A, Herraiz S, **Marchante M**, Hsueh J, Pellicer A. 65th Annual Meeting of the Society for Reproductive Investigation. San Diego, California (USA), 2018.

3.2 Poster presentations

-LH *in vitro* treatment promotes DNA repair of mouse apoptotic follicles damaged by alkylating agents. Castillo LM, Buigues A, **Marchante M**, Rossi V, Martinez J, Klinger FG, Herraiz S, Pellicer A. 35th Annual Meeting of the European Society of Human Reproduction and Embryology. Viena, Austria, 2019

-Potential Molecules and Pathways Involved in Ovarian Rescue by Bone Marrow Derived Stem Cells in Human Ovarian Tissue. Buigues A, **Marchante M**, Díaz-Gimeno P, Martinez J, Pellicer A, Herraiz S. 68th Annual Meeting of the Society for Reproductive Investigation. Boston (USA), 2021.

-Contribution of the D19S884 allele 8 of the FBN3 gene and the Hippo signaling to the reproductive and metabolic phenotype of PCOS patients. Ramírez N, Romeu M, Martinez J, Peinado I, Buigues A, **Marchante M**, Pellicer A, Herraiz S. 38th Annual Meeting of the European Society of Human Reproduction and Embryology, Milan, (Italy), 2022.

-Thrombospondin-1 depletion suppressed follicular growth induced by stem cell secreted factors-enriched plasma on chemotherapy-damaged mouse ovaries. Buigues A,

Ramírez N, Martinez J, **Marchante M**, Pellicer A, Herraiz S. American Society for Reproductive Medicine. Anaheim, California (USA), 2022.

-Nicotinamide mononucleotide (NMN) in vitro supplementation improves deficiencies in nuclear and cytoplasmic competence of germinal vesicle oocytes. Galbete A, **Marchante M**, Mifsud A, Pellicer A, Herraiz S, Escriba MJ. American Society for Reproductive Medicine. Anaheim, California (USA), 2022.

4. Awards

-Pfizer Award SRI 2018 "Fertility Rescue by Bone Marrow Derived Stem Cell Infusion" awarded by the Society for Reproductive Investigation (SRI) in 2018 as one of the 25 best papers submitted.

-Pfizer Award SRI 2020 "G-CSF mobilized plasma regenerate ovarian stroma and restore ovarian function" awarded by the Society for Reproductive Investigation (SRI) in 2020 as one of the 25 best papers submitted.

-President's Plenary Awards SRI 2022 "Combination of Stem Cell Secreted and Platelet Enclosed Growth Factors Restores Ovarian Function in an Aging Mouse Model". Recognizes the four highest ranked abstracts chosen for presentation at the President's New Investigator Plenary. These awards are supported by the Society for Reproductive Investigation Past Presidents' Fund in 2022.

ANNEXES